SAPIENZA
UNIVERSITÀ DI ROMA

Use of cell wall degrading enzymes for the recovery of lipids from microalgae

Faculty of Civil and Industrial Engineering
Chemical, Material and Environmental Engineering Department
PhD Course in Chemical Engineering

PhD Candidate
Gianluca Maffei

Supervisor
Prof. Roberto Lavecchia

XXIX Cycle

Index

Chapter 3 – Enzymatic degradation of microalgae cell wall

Chapter 4 – Enzyme-assisted lipid extraction from *Nannochloropsis* sp.

Chapter 5 – Characterization of untreated and enzymatically treated microalgae

List of Figures

List of Tables

Introduction

Nowadays, nearly 80% of world energy demand is satisfied by the use of fossil fuels, which provoke the increasing accumulation of CO_2 in atmosphere. Thus, the capture of this gas and the prevention of its release will play a key role to prevent climate changes, which are causing adverse effects. Great efforts have been focused on the production of biodiesel, bioethanol, or biogas. The use of biofuels does not contribute to an increase in the atmospheric CO_2 concentration, since the carbon released has previously been taken from atmosphere by photosynthesis. In this scenario, the utilization of microalgae cultures can contribute to CO_2 capture and storage, converting it into a biomass rich in valuable products, such as carotenoids, aminoacids and lipids for biodiesel production. Another advantage is that the conversion efficiency of solar energy into biomass for algal cultures and the productivity per hectare are much greater than those obtainable with traditional crops. Moreover, algal cultures do not compete for fertile land, do not require pesticides and can be grown in seawaters or wastewater from where microalgae take nutrients that they transform in biomass.

One of the factors hindering the large-scale use of microalgae as a lipid source is the high energy consumption associated with the recovery of lipids. In fact, in most microalgal species, lipids are located inside the cell, which must be disrupted to allow their extraction. The hardness of algal walls and their organization into a complex multi-layered structure make disruption an energy-intensive process. Common methods of cell disruption involve the use of mechanical (e.g., ultrasonication, high-pressure homogenization, bead beating) or chemical (e.g., alkali, acid, detergent) means. In addition to their request for a large consumption of energy or chemicals, these treatments may cause damage to the most easily degradable algal components, such as proteins and carotenoids, which could be co-extracted with lipids in a biorefinery perspective.

In this context, the primary objective of this doctoral thesis was the development of an enzyme-assisted lipid extraction method using unpurified low cost industrial enzyme preparations.

Enzymatic treatment of microalgae is an attractive, but still little explored method of cell wall disruption. It is based on the selective degradation of cell wall components by specific enzymes. This method has the potential to facilitate the recovery of lipids or the post-extraction use of the algal biomass and to preserve the most labile compounds. However, the choice of suitable enzymes is strictly related to the characteristics of the algal wall which, in turn, depend on the microalgae species, the growth conditions and the harvesting and dewatering steps. Unfortunately, microalgal cell walls are still poorly characterized.

The first part of the work focused on the selection and the screening of enzyme preparations on the basis of the characteristics of the cell wall of *Nannochloropsis* sp., the microalga that was used as model organism. This microalga is of great industrial interest because of its ability to accumulate large amounts of lipids and other valuable components, such as the carotenoids astaxanthin and zeaxanthin and the omega-3 polyunsaturated fatty acid EPA. However, it shows unusual resistance towards mechanical and chemical treatments, which seems to be at least partly due to the presence in the outer cell layer of the aliphatic biopolymer algaenan. This makes the extraction of intracellular algal components a challenging and energy-consuming process.

Subsequently, an enzyme-assisted extraction processes based on the development of optimized cell wall-degrading enzyme cocktail was developed by the use of the statistical methodology of *mixture design*.

The influence of the most important process parameters (pretreatment time, enzymes to biomass ratio, pH and temperature of pre-treatment) on the yield of lipid extraction was then analyzed using the pretreatment mixture of optimized composition. A *factorial design* has been identified with the purpose to analyze their effect on the yield of lipid extraction. Numerical optimization of the obtained model allowed identifying the optimal pretreatment conditions, in terms of extraction yield and cost of the pretreatment.

The recovery of the enzyme pre-treatment solution for the re-use in subsequent cycles was also evaluated to lower the operating cost.

Moreover, a characterization of the untreated and enzymatically treated biomass was performed through the use of instrumental methods, such as Fourier transform infrared spectroscopy (FTIR), X-ray diffraction spectrometry (XRD), thermogravimetry (TGA/DTG) and scanning and transmission electron microscopy (SEM and TEM) in order to understand the action of each enzyme and, consequently, to properly design the process.

Finally, the exhausted algal biomass after lipid extraction process has been studied to assess its implementation as a low cost absorbent material for textile azo-dyes, in order to find new application that could allow a further decrease of the cost of the entire biodiesel production chain from microalgae.

CHAPTER 1

Microalgae

In this chapter, a general introduction on microalgae and their use is described. In particular, a focus on the classification of various known species is done, highlighting the main features of each class, with particular attention to the cell wall composition. At the end of the chapter, a list of the potential and the most important industrial application of microalgae will be highlighted. Special attention will be put on the biorefinery concept. According to this context, each component of the microalgal biomass is converted or utilized in a manner to hence sustainability to the plant, maximizing the value derived from the biomass feedstock.

1.1 Background

The microphytes or microalgae are microscopic algae, typically found in fresh and sea water. They are single-celled organisms able to live alone or in colonies. Their size varies from a few to 100 micrometers, depending on the species.
Unlike higher plants, microalgae do not have roots, stems and leaves, but they are essential for life on Earth, as they are part of biodiversity, which helps for environmental balance. In fact, they are directly responsible for almost 50% of photosynthesis, producing about half of the atmospheric oxygen. Moreover, they use carbon dioxide for photoautotrophic growth: approximately 1.83 kg of CO_2 is fixed per kg (dry weight) of microalgal biomass produced. They constitute a very diverse

group of microorganisms that can be either photosynthetic or heterotrophic, with extraordinary potential in energy production.
The biodiversity of microalgae is enormous and represents an almost untapped resource. It is estimated that there are about 200,000 to 800,000 species, but only 50,000 have been classified. Over 15,000 compounds originating from microalgae biomass have been determined chemically.

The importance of studying the cultivation of microalgae is motivated by the fact that they are very efficient at converting light, water and carbon dioxide into biomass in systems that do not require agricultural land. Their cultivation nutrients may also come from wastewater. Microalgae can be grown in dedicated systems, allowing better control of cultivation conditions and then the subsequent quality of the desired products. Algae can contain extremely high percentages of lipids or carbohydrates which are easily converted into a whole range of biofuels, including biodiesel or bioethanol. Although biofuels are still more expensive than fossil fuels, their production is increasing worldwide. Biodiesel is synthesized from vegetable oils or animal fats. Among the various possibilities currently being investigated and implemented at pilot scale concerning potential feedstocks, the more interesting ones are microalgae, because of their properties mentioned before (Mata et al., 2010).
Furthermore, the remaining biomass, mostly composed of proteins and carbohydrates, can be transformed into many other products such as food, chemical products, medicines, mineral, animal feed, fertilizers, pigments, ingredients for salad dressings, ice cream, puddings and cosmetics. Algae-based products can serve as an alternative to a wide range of compounds that are currently produced from fossil sources or agriculture, without requiring high quality land and, in some cases, without the need of freshwater, with CO_2 as the sole carbon source.

The major obstacles for the possible applications in wide scale are their high production costs. These are mainly related to the cultivation systems and to the extraction of the desired metabolites. This problem is due to the high resistance of the cell wall, which leads to the necessity of a pretreatment step in order to facilitate the release of valuable compounds. A solution to this issue could be an extension of application fields, coupling the production of fuel to high value-added compounds that could be co-extracted. This co-production is an important option to break though the barrier of economic viability. Some algae also represent a new source of protein for humans, livestock and aquaculture. The high nutritional value of algal protein has been known for decades and could solve some problems related to malnutrition in poor and developing countries.
In particular, the Integrated Food and Energy Systems (IFES) are designed to produce energy, food, feed, bio-chemicals and fertilizers simultaneously, through sustainable management of terrestrial and aquatic zones, transforming the byproducts of a production system in the raw material for another one.

1.2 Algae classification

1.2.1 Macroalgae and microalgae

The term "algae" has no taxonomic significance, but it stands for a group of rather primitive plants that, apart from some common characteristics, are very different from a morphological, ecological, physiological and biochemical point of view.
Algae include the microscopic (microalgae) and macroscopic forms (macroalgae), the latter consist mainly of seaweeds. In terms of dimensions, algae range from the size of a few micrometers in diameter to giant kelps with fronds up to 60 m in length (Barsanti and Gualtieri, 2006). The number of species of algae has been estimated to be one to ten million, most of which are microalgae.
Algae most commonly occur in water, be it fresh, marine, or brackish water. However, they can also be found in almost every other environment on earth, including extreme ones, such as snow and glaciers in the Arctic and Antarctic, desert soils, tree trunks and hot springs. Some of them are symbionts of plants or animals, while some others are even parasitic.
The algae are thallophytes (plants lacking roots, stems, and leaves) as well as bacteria, fungi and lichens. All of these are characterized by the lack of distinction between the root, stem and leaves (thallus).
In modern classification schemes based on molecular phylogenetic systems, algae are not classified under the Kingdom of Plantae, although they undoubtedly resemble of higher plants (Graham, 2000).
A well as plants (which belong to the group of *Cormophytes*), they perform photosynthesis through particles called chloroplasts that contain chlorophyll “a”. They possess other corpuscles containing various pigments that, besides giving color to the cells, allow the algae to exploit different kinds of light radiation, depending on the habitat in which they live and on its depth. For this reason, the green algae live only in bright environments, considering that they primarily absorb red radiation, which hardly manages to penetrate deeply into the water, while red algae, thanks to their red pigment, can absorb blue and green radiation, and, consequently, can live at greater depths. Brown algae can absorb all the radiation and are able to live at different depths.
Together with fungi and lichens, they are the most ancient and primitive organisms capable to reproduce both in a sexual way, with the junction of the gametes, and asexual, for fission or budding. The two methods are alternated according to environmental factors and the presence or absence of partners. This capability, combined with the ease of adaptation (a lot more than plants), makes them the precursors of life in hostile environments and a vital resource for all creatures of the earth, including humans. Algae are the main producers of oxygen in the seas and lakes, and can produce more oxygen than all the equatorial forests of the world.
Unlike plants, algae lack of cellular specialization, so that all the cells are exactly alike. As a consequence, there are no tissues or organs and therefore the whole body of the alga is nothing but a more or less defined cluster of cells. Cells constitute only

an endless series of perfectly identical pieces, united only for evolutionary convenience.

1.2.2 Taxonomy

The classification of every living organism must be exhaustive and unambiguous. The hierarchical level in descending order is defined as follows:

1) Domain (eg. *Eukaryotes*);
2) Kingdom (eg. *Protozoa*);
3) Phylum or Division (-phyta, eg. *Chlorophyta*);
4) Class (-phyceae, eg. *Trebouxiophyceae*);
5) Order (-ales, eg. *Chlorellales*);
6) Family (-aceae, eg. *Chlorellaceae*);
7) Genus (a Latin name, eg. *Chrorella*);
8) Species (often a Latin name, eg. *Vulgaris* adjective). The species is always indicated by two words (binary nomenclature), eg. *Chlorella vulgaris*.

The classification of algae is very complex and can follow different criteria. According to Lee, algae may be classified following the evolution of the chloroplast (Lee, 2008).

According to this criterion, algae can be grouped into 4 groups (Table 1.1):
1) Prokaryotes, *Cyanophyta* (Cyanobacteria) and *Prochlorophyta* characterized by prokaryotic cell organization.
2) Eukaryotic algae, with chloroplasts surrounded by the two membranes of the chloroplast envelope. It is believed that the chloroplast results from the capture of a cyanobacterium by an aerobic phagocytic protozoan, containing mitochondria and peroxisomes. The cyanobacterium, for still unknown reasons, was not digested, but remained as a symbiont; the symbiosis was beneficial to both: the protozoan received the photosynthesis products and the cyanobacterium continued to live in a safe environment. *Glaucophyta*, *Rhodophyta* (red algae) and *Chlorophyta* (green algae) belong to this group. The *Glaucophyta* represent an intermediate stage in the process as the endosymbiont did not evolved into the chloroplast.
3) Eukaryotic algae with the chloroplast surrounded by one membrane of chloroplast endoplasmic reticulum. They resulted from ingestion by a phagocytic protozoan of a chloroplast of a eukaryotic alga. The chloroplast was not digested and remained with two membranes surrounded by the endoplasmic reticulum. *Euglenophyta* (*Euglenae*) and *Dinophyta* (*Dinoflagellates*) belong to this group.
4) Eukaryotic algae with the chloroplast surrounded by two membranes of chloroplast endoplasmic reticulum. They resulted from a secondary endosymbiosis: a phagocytic protozoan ingested a photosynthetic eukaryote algae and this remained undigested inside a digestive vacuole whose membrane merged with the

endoplasmic reticulum of the host protozoan bringing ribosomes on the outer face of the membrane that became the outer membrane of the endoplasmic reticulum in the chloroplast with 4 membranes. *Cryptophyta* (*Criptoficeae*), *Chrisophyta* (*Crisoficeae*), *Prymnesiophyta* (*Aptoficeae*) and *Heterokontophytae* belong to this group.

Table 1.1 – Algal classification.

DOMAIN	KINGDOM	GROUP	PHYLUM
Prokaryotes	*Bacteria*	1	*Cyanophyta*
			Prochlorophyta
Eukaryotes	*Protozoa*	2	*Glaucophyta*
			Rhodophyta
			Chlorophyta
		3	*Euglenophyta*
			Dinophyta
		4	*Cryptophyta*
			Prymnesiophyta
			Heterokontophyta

Another classification gathers all the algae, unicellular and multicellular, in the kingdom of Protists (cells with very primitive structural organization) and unicellular eukaryotes (organisms with eukaryotic cells with the nucleus enclosed by the nuclear envelope). Photosynthetic prokaryotes, formerly known as blue-green algae, are now more properly called cyanobacteria and are classified precisely in the kingdom of prokaryotes (with a simple cellular organization without nucleus membrane). Cyanobacteria were the first colonizers on Earth. They are distinguished from other bacteria as they carry out oxygenic photosynthesis, which was enabled other life forms to live on this planet (Chu, 2012).

1.3 Characteristics of algae

1.3.1 Prokaryotic algae

The *Cyanophyceae* or blue-green algae are usually referred to as cyanobacteria (blue-green bacteria). The term “cyanobacteria” acknowledges that these prokaryotic algae are more closely related to the prokaryotic bacteria than to eukaryotic algae.

The major components of the photosynthetic light-harvesting system of the cyanobacteria are chlorophyll “a” in the thylakoid membrane, and the phycobiliproteins, which are water-soluble chromoproteins assembled into macromolecular aggregates (phycobilisomes) attached to the outer surface of the thylakoid membranes. Some cyanobacteria contain chlorophyll b and d. Cyanobacteria use glycogen (α-1,4-linked glucan) as a storage product and their cell walls contains aminosugars and aminoacids. The carotenoids of the cyanobacteria differ from those of the eukaryotic algae (echineone and myxoxanthophyll) with higher proportions of β-carotene, while they lack in lutein, the major xanthophyll of chloroplasts. The *Cyanophyceae* have four phycobiliproteins: C-phycocyanin, allophycocyanin, C-phycoerythrin and phycoerythrocyanin. All cyanobacteria contain the first two, whereas C-phycoerythrin and phycoerythrocyanin occur only in some species. The phycobiliproteins of the cyanobacteria change in concentration in response to light quality and growth conditions. Many cyanobacteria have the ability to photosynthesize under aerobic or anaerobic conditions.
The *Prochlorophytae* have chlorophyll a and b, but are devoid of phycobiliproteins.
Cyanobacteria and Prochlorophytes have a four-layered cell wall, which is of the Gram-negative type; the structural part consists of a murein (peptidoglycan) layer, outside which there is a lipopolysaccharide layer. The high digestibility of cyanobacteria cells, due to the lack of cellulose, unlike the majority of algae, facilitates their use for human consumption (e.g. *Spirulina* – health food). Mucilaginous envelopes may surround the cell wall (sheaths, glycocalix, capsule or slime). The cell wall may be perforated by small pores and may also have appendages such as fimbriae and pili (Tomaselli, 2004).

1.3.2 Eukaryotic algae

The cells of the organisms belonging to this kingdom possess a nucleus and well compartmentalized cellular organelles.
Some species only have the cell membrane and in many divisions the membrane presents different modifications, although it cannot be considered a true cell wall.
Plastids are very rare in algae, but the chloroplast is always present. The shape can be very diverse (lobata, tape, star, disc etc.), as well as the arrangement of the thylakoids and the composition of the pigments: chlorophyll a is always present with chlorophyll b or c, phycobilins and carotenoids.
A microfibrillar layer of cellulose, surrounded by an amorphous layer, generally composes the algal cell wall. The cell wall is secreted by the Golgi apparatus. It may be silicified or calcified and strengthened with plates and scales. Some species do not have the cell wall. Outside the outer amorphous layer there may occur a laminated polysaccharide investment. The nature of the outer cell wall layers supports polysaccharide production (alginates, agar and carragaenans) from various macroalgae. The cytoplasm contains the nucleus and different kinds of organelles and compartments. Among the organelles, there are chloroplast, Golgi apparatus,

endoplasmic reticulum, ribosomes, mitochondria, vacuoles, contractile vacuoles, plastids, lipid globules, flagella, and microtubules. Chloroplast and cytoplasmic lipids represent an important source of polyunsaturated fatty acids, such as eicosapentaenoic, docosahexaenoic and arachidonic acids. The nucleus is bounded by a double nuclear membrane and it contains several DNA molecules distributed among the chromosomes and undergoes division by mitosis (Tomaselli, 2004).

Among the eukaryotic algae, they are particularly interesting ones belonging to *Rhodophytae* (Red algae), *Chlorophytae* (Green algae) and *Eustigmatophytae*. *Rhodophyceae* (Fig. 1.1) includes multicellular and filamentous forms, whereas unicellular species are less represented. These algae lack flagellate cells and have chlorophyll a and d, phycobiliproteins (phycoerythrin and phycocyanin), and floridean starch (α-1,4-linked glucan) as storage products accumulated in the cytoplasm outside the chloroplast. Cell wall is composed of a microfibrillar layer of cellulose or xylan and amorphous polysaccharidic mucilages (agar or carrageenans). Thylakoids are contained in chloroplasts. The green of chlorophyll is masked by the red of phycoerythrin, which is the dominant pigment in most species. The phycobiliproteins are water soluble and when the algae die becomes green because the phycoerythrin comes out while chlorophyll remains in the plastid (Tomaselli, 2004).

Figure 1.1 – Specimen of *Rhodophyta*.

Red algae are predominantly marine algae: among the 4000 species, only 200 live in freshwater. They are mainly multicellular, (less than a dozen of species are unicellular). They represent the highest number of large algae, distributed in all the seas and oceans with a clear majority in the warm seas. They can live up to 200 m deep, thanks to their special accessory photosynthetic pigments.
Commercial utilization of red algae concerns the polysaccharidic mucilage of the cell wall, agar and carrageenan. The red microalga *Porphyridium* is an important source

of sulphated polysaccharides, phycobiliproteins and polyunsaturated fatty acids, such as arachidonic acid.

Chlorophytae gather a large group of organisms with a great morphological variability, ranging from microscopic to macroscopic forms. They have chlorophyll a and b and several carotenoids, which may be synthesized and accumulated outside the chloroplast under particular conditions, such as nitrogen deficiency, coloring the alga orange or red. The storage product is starch (α-1,4-linked glucan), composed of amylose and amylopectin. Cell walls generally contain cellulose. Most species have flagellate stages with the flagella apically inserted into the cell, the flagellar root system anchored with four sets of crucially arranged microtubules. The green algae live primarily in freshwater, but a great number grow in marine, terrestrial and subaerial habitats. Some species occur in symbiotic associations, mostly with lichens.
Commercial exploitation of microscopic green algae comprises relatively few chlorophycean genera among which there are *Chlorella*, *Dunaliella* and *Haematococcus*. Moreover, *Botryococcus braunii* was proposed and cultivated as a renewable source of liquid fuel, owing to the high hydrocarbon content. *Dunaliella* spp. From hypersaline environments have been extensively studied, cultivated and commercialized as a source of natural β-carotene (Tomaselli, 2004).

The class of *Eustigmatophyceae* includes unicellular and coccoid organisms that can live in seas, freshwaters and soil. The chloroplasts have chlorophyll “a”, while violaxanthin is the major light-harvesting carotenoid pigment. The cell wall is polysaccharidic. Cytoplasm and photosynthetic lamella lipids of many species are promising sources of fatty acid, like eicosapentaenoic acid in microalga *Nannochloropsis*. This alga is a picoplanktonic genus of marine environment. The cells are small (2–4 mm in diameter), spherical to slightly ovoid, non-flagellate. They have one single chloroplast with a continuous endoplasmic reticulum with the nuclear envelope. *Nannochloropsis* has polysaccharide cell walls, but do not accumulate starch; it uses in fact lipids as storage products (Tomaselli, 2004).
Among the *Heterokontophytae*, *Laminariales*, also called Kelp (Fig. 1.2), are undoubtedly important from an economic point of view. At first, they were used only when turned to ashes in porcelain and glass, until the discovery of new production methods. In 1811, a substantial amount of iodine was discovered in these algae, thanks to which they were employed in the treatment of thyroid disorders. So far, the most important use is for the extraction of alginate, which is employed in the preparation of ice creams to prevent the formation of ice crystals. Alginate is also used in the preparation of other foods, in the rubber and paint industry, where it is added to avoid visible brush marks, and in the pharmaceutical industry to prepare suspensions. *Laminaria* is used in different branches of medicine as surgery, gynecology, ophthalmology because of its ability to rehydrate, when dried, and get to ten times its volume thus opening fistulas, lachrymal canals etc.
It is also employed as a fertilizer for the soil and as food for humans and animals.

Figure 1.2 – Specimen of *Laminariales* (Kelp).

In Table 1.2 the main features of each class of algae are summarized, giving particular attention to their cellular structure, the reserve substances and pigments.

Table 1.2 – Summary of the characteristics of the algae.

Phylum	Organism	Environment	Photosynthetic pigment	Cell wall structure	Storage products
Rhodophyta **(red algae)**	Mainly multicellular	Especially marine water	Chlorophyll a and d, carotenoids (α and β-carotene, zeaxanthin), phycobilins, xanthophylls	Mainly cellulose and other polysaccharides (agar, carragenin)	Starch
Chlorophyta **(green algae)**	Unicellular and multicellular	Especially freshwater	Chlorophyll a and b, carotenoids (α e β-carotene, lycopene), xanthophylls (lutein)	Cellulose, glycoproteins and sporopollenin	Starch and fructans
Euglenophyta	Unicellular	Especially freshwater	Chlorophyll a and b, carotenoids, xanthophylls	Proteins, lipids and some polysaccharides	Paramilon (glucan)
Dinophyta	Unicellular	Especially marine water	Chlorophyll a and c2, carotenoids (β-carotene, peridinin, neoperididnin), xanthophylls (dinoxanthin)	Cellulose, sporopollenin	Starch and lipids
Cryptophyta	Multicellular	Marine and freshwater	Chlorophyll a and c2, carotenoids (α e β-carotene)	Absent	Starch
Heterokonphyta **(Diatoms)**	Unicellular	Marine and freshwater	Chlorophyll a and c2, β-carotene, fucoxanthin	Cellulose, silicon or absent	Lipids and Chrisolaminarine
Heterokonphyta **(brown algae)**	Multicellular	Especially marine water	Chlorophyll a and c2, carotenoids (α e β-carotene), xanthophylls (fucoxanthin, violaxanthin)	Cellulose, polysaccharides, alginic acid, fucoidin	Lipids, Laminarine and mannithol

1.4 Microalgal cell wall

A general formulation for microalgae fraction distribution would reach up to 25–30 % cellulose, 15–25 % hemicellulose, 35 % pectin and 5–10 % glycoprotein. On the contrary, Cyanobacteria, such as *Spirulina*, present a cell envelope typical of gram-negative bacteria. In this context, the cell wall exhibits a peptidoglycan outer membrane surrounding the cytoplasmic membrane (González-Fernández et al., 2012).
As well as higher plants, the cell wall of algae and microalgae is generally made up of two components:

- the fibrillar component, which forms the skeleton of the wall;
- the amorphous component, which forms a matrix within which the fibrillar component is embedded (Lee, 2008).

In marine algae, cellulose accounts for a smaller and more variable proportion than in higher plants and in some species it can be lacking. Moreover, in algal cell, there is a prevalence of polyanionic polysaccharides rather than neutral sugars.
In both red and brown algae, the cellulose content is rather low. Mostly, green algae have a cellulosic wall, with cellulose content ranging up to 70% of the dry weight, such as in *Chladophorales* and *Ulvales*. Furthermore, algal cellulose is rarely a pure ß-1,4 glucan; more frequently it contains sugars other than glucose, commonly xylose and mannose (Baldan et al., 2001).

1.4.1 Cellulose and hemicelluloses

Skeletal cellulose is composed of chains with 8000 to 12000 units of 1,4 linked β-D-glucose. This polymer could make a compact crystalline structure with all-parallel chains, which is known as cellulose I. Cellulose I is mainly present in *Siphonocladales* and *Cladophorales*. However, in most microalgae the glucose molecules are organized in anti-parallel chains, forming Cellulose II, which represents a lower free energy organization.
The X-ray diffractograms of microalgal cellulose is often weakened, or even modified, by the presence of other amorphous wall components, such as alginates or carrageenans. These polymers reinforce the cell wall, making it more difficult to penetrate.
Like cellulose, the skeletal xylans are linear high molecular weight polysaccharides of 1,3 linked β-D-xylose. Each chain contains about 10,000 monomers. These chains are left-handed helix with six xyloses per turn or right-handed with three xyloses per turn, forming a hexagonal compact crystalline network.
Skeletal mannans are linear homopolymers of 1,4 linked β-D-mannose. Mannan chains adopt a conformation similar to cellulose with a two-fold symmetry (Kloareg and Quatrano, 1988).

Such fibrillar layers do usually alternate with layers of the amorphous material. Matrix polysaccharides are generally known as mucilage. They consist mainly of hemicelluloses and, in some cases, pectins.
Unlike cellulose, the hemicelluloses are amorphous, non-fibrous and branched. They are distinguished according to the last sugar that forms the backbone chain.
Some illustrative structures are summarized in Fig. 1.3.

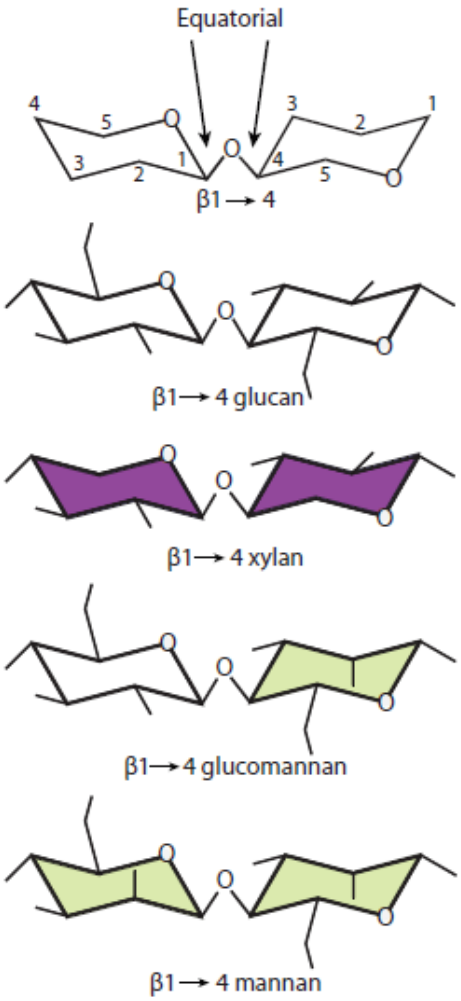

Figure 1.3 – Hemicelluloses structures

Hemicelluloses are polysaccharides contained in plant cell walls that have β – 1,4 linked backbones with an equatorial configuration. Hemicelluloses include xyloglucans, glucoronoarabinoxylans, xylans, mannans, galactomannans, glucomannans and 1,3 and 1,4 linked β-glucans (Table 1.3). The detailed structure of the hemicelluloses and their abundance vary widely between different species and cell types. The most important biological role of hemicelluloses is their contribution to strengthening the cell wall interacting with cellulose (Scheller and Ulvskov, 2010).

Table 1.3 –Hemicelluloses nomenclature.

Hemicellulose	Structure
Xyloglucans	Glucose chains with ramifications of a xylose molecule to which, rarely, galactose and fucose are added.
Glucoronoarabinoxylans	Linear chain of xylose, with ramifications of arabinose and, rarely, other sugars.
Xylans	Linear chain of xylose, with a few more added sugars in the ramifications.
β-glucans	Non-linear chain articulated in "sine wave" with the presence of β-glucose bonds between carbons 1-4 and 1-3.
Glucomannans	Linear chain formed by glucose and mannose in alternating groups according to the glucose-glucose-mannose-mannose scheme.
Mannans	Linear chain formed by mannose
Galactomannans	Linear chain formed by β 1-4 glucose and galactose as lateral residues.

1.4.2 Other cell wall components

Alginic acid and its salts, the alginates, are important components of the walls of microalgae, in particular brown algae. They are singular in many aspects. They consist exclusively of uronic acids: mannuronic acid and beta-L-glucuronic acid. The alginates of brown algae can be found both within the cell wall and in the intercellular substance. They can constitute up to 40 per cent of the dry matter. They have a high affinity for divalent cations (calcium, strontium, barium, magnesium) and the tendency to gel. The main portion of the magnesium ions isolated from brown algae stem from the alginic acid fraction.

The presence of sulfonated polysaccharides is typical in most microalgae. These polysaccharides are esterized to sulfuric acid residues and are partially methylated; these reactions occur partially in the cell wall itself and in the intercellular substance. Sulfonated galactanes are typical of many red algae. According to their origin, they are called agarose, carrageenan, porphyran, furcelleran, ulvans and funoran. L- and D-galactose, which are linked by β 1–3 or α 1–4 glycosidic bonds form the basic pattern of agarose and porphyran. In the latter, glycosidic bonds could be alternated to L- and D-galactosyl residues. Carrageenan and furcelleran contain exclusively D-compounds. Ulvans are water soluble starch polysaccharides which

consist of molecules of sulphated uronic acid that cannot be degraded by digestive enzymes. Just like in alginates, one of the most important physical properties of this family of molecules is the formation of gelatine. The peculiar binding types of agarose and carrageenan lead to specific tertiary structures.

The resistance of microalgae cell walls is attributed to the formation of polymers of difficult biodegradation. Two polymers, namely sporopollenin and algaenan, are, in particular, associated with biodegradation resistency. Sporopollenin is a very stable compound that can appear as an oxygenated aromatic building block or as an aliphatic biopolymer, depending on the oxidative polymerization of lipids. Sporopollenin is an isoprene derivative, which is a component of pollen cell walls, but was also detected in the walls of some green algae (*Chlorella*, *Scenedesmus*, etc.). Likewise, algaenans are aliphatic molecules resistant to acid or alkali treatments. Cell walls containing algaenans have shown to be an effective barrier for extracellular enzymes (González-Fernández et al., 2012).

Arabinogalactan proteins (AGPS) are another group of cell wall components that seems to have ancient origin. AGPS are a group of proteoglycans that exhibit considerable structural and functional diversity. Their presence was detected in green algae especially in *Chlorophytae* (McCann et al., 2007).

1.4.3 Cell wall evolution and composition

Popper and Tuohy (2010) attempted to study the evolutionary scenario of the cell walls of algae. According to them, the best examined cell wall biosynthetic genes are members of the cellulose synthase superfamily, which appears to have diversified within the land plant lineage to give nine cellulose synthase-like families and one cellulose synthase (CesA) family.
Cellulose is synthesized by CesA genes in the *Chlorophyta* and red and brown algae, whose origin predates that of the plant-specific CesA genes; their products form linear terminal complexes. Mannans and glucomannans are synthesized by CslAs. While CslAs appears to be absent from green algae, these algae contain a specific Csl family, that is most homologous to land plant CslA and CslC families. Since mannans are known to occur in green algae, the products of CslA/CslC could be responsible for mannan synthesis. CslA/CslC appears to be absent from brown and red algae, suggesting that an absence of reports for mannans in brown algae (Table 4) could be due to a lack of the required biosynthetic machinery. However, some red algae have been reported to contain mannans. The genes responsible for mannan synthesis in red algae may not be CslAs.

Table 1.4 – Occurrence of cell wall components in algal cell walls.

+ Component is likely to be present; ± component may be present; – component is likely to be absent

Plant group	Cellulose	Xylan	Mannan	Xyloglucan	(1,3), (1,4)-β-D-glucan	AGPs	Lignin	Silica
Brown algae	+				±	±	–	–
Diatoms	+	+	+		±			+
Rhodophyte (red algae)	+	+	+		–	±	+	–
Chlorophyte (green algae)	+	+	+		+	+	–	–
Charophycean (green algae)	+	+	+	±	–	+	–	–

In a subsequent study Popper et al. (2011) have tried to investigate the evolution of the cell wall, from algae to plants. Fig. 1.4 and Table 1.5 show the major lineages of phylogeny of cell wall components.

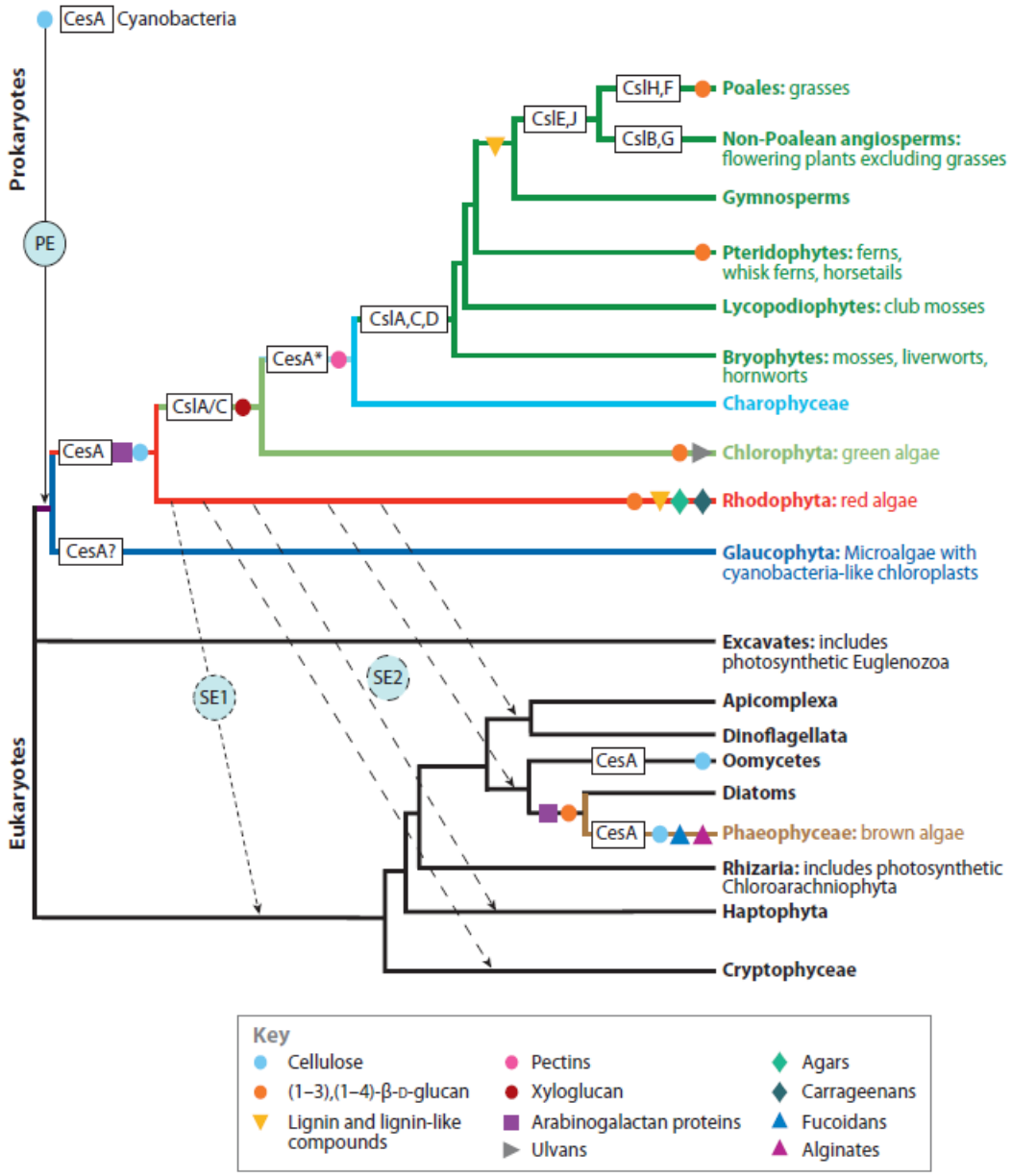

Figure 1.4 – Simplified Eukaryote phylogeny highlighting the occurrence of major wall components. The identification of specific wall components within lineages is symbolized as shown in the key.

Table 1.5 – Major cell-wall polymers present in different algal taxa.

Polysaccharides	***Chloroplastida***			***Rhodophyta***	***Phaeophyceae***
	Embryophyceae	*Charophyceae*	*Chlorophyta*		
Crystalline polysaccharides	Cellulose	Cellulose	Cellulose		
Hemicelluloses	Xyloglucan, Mannan, Xylan, MLG, (1,3)-β-glucan	Xyloglucan, Mannan, Xylan, MLG, (1,3)-β-glucan	Xyloglucan, Mannan, Glucuronate, (1,3)-β-glucan	Glucomannan, MLG sulphatate, (1,3),(1,4)-β-D-xylan	Xylofucoglucan sulphonate, xylofucoglucoronate sulphonate, (1,3)-β-glucan
Carboxylic polysaccharides	Pectins	Pectins	Ulvans	_	Alginate
Sulphonate polysaccharides	_	_	Ulvans	Agar, Carrageenan, Porphyrinate	Omofucan

1.5 Potential and application of microalgae

Microalgae have peculiar properties that lead to numerous advantages, among which the capability of accumulating high amounts of starch and lipids. The potential of these microorganisms reside also in the possibility of being employed in other sectors, such as biofixation of CO_2 or the phyto-purification of water. In addition to carbohydrates and lipids, they contain high value-added products highly demanded in the food, cosmetic and pharmaceutical industries, such as fatty acids, carotenoids and proteins. The potential industrial applications of microalgae are summarized in Table 1.6.

Table 1.6 – Microalgae application.

Application	Status
Human consumption	Commercial
Food supplements	Commercial
Animal feed	Commercial
Carotenoids	Commercial
Phycobiliproteins	Commercial
Fluorescent compounds	Commercial
Stable isotopes	Commercial
Polysaccharides	Research
Bio-fertilizers	Research
Bio-pesticides	Research
Drugs	Research
Cosmetics	Research
Probiotics	Research
Biosensors	Research
Phytoremediation	Research
CO_2 biofixation	Research
Heavy metals biofixation	Research
Biodiesel production	Research
Bioethanol production	Research
Biohydrogen production	Research

One of the most interesting aspects of microalgae is that they can accumulate significant quantities of lipids (fats and oils) whose composition is similar to that of traditional vegetable oils. Some microalgae are capable of producing oils in greater quantities, compared to the best oil crops and for that reason they may constitute a renewable source of oil for biodiesel synthesis.
Microalgae have been proposed as "feedstock" for third-generation biofuels. They have, in fact, a number of advantages compared to terrestrial plants:

- Microalgae grow quickly and, potentially, all over the year;
- Microalgae can be grown on marginal or desert soils;
- Microalgae need much less water per kg of biomass produced than terrestrial crops;
- Many strains can be grown in sea or brackish water;
- Microalgae are capable of sequestering CO_2 from fuel gas of industrial installations;
- Certain strains accumulate large amounts (up to 50% of the dry weight) of triglycerides, suitable for the production of biodiesel, while others accumulate starch, suitable for the production of bioethanol;
- Microalgae do not require the application of herbicides or pesticides;
- Some strains can be used for bioremediation purposes.

Furthermore, the solar energy conversion efficiency into biomass of the algal cultures, and thus the productivity per hectare, is much greater than the one obtainable with traditional crops. For example, one hectare of sunflower or rapeseed can produce 700-1000 kg of oil per year, while the algal cultures, if grown in suitable reactors in closed systems or "photobioreactors", can overcome 20 tons of oil per hectare per year in central and southern regions of Italy and have a potential of more than 30 tons in tropical countries.

Despite these advantages and considering that many start-up companies are based on algae biofuels industry, a commercial supply chain for this production has not born yet. The main reason is that the cost for the production of algal biomass and for the extraction of the desired compounds is still too high. Current commercial applications of microalgae are mainly in the areas of food supplements, food industry and cosmetics (Table 1.7).
However, it is important to emphasize, that, at the moment, the production of microalgae for energy production only occurs in pilot plants (in tanks from 10 m up to installations of 2 ha), while the production of algae destined to niche sectors (health and diet foods, pharmaceuticals, cosmetics) is about of ten thousand tons per year.

Table 1.7 – Commercial production of microalgae.

Microalga	Annual production	Producers	Products and applications	Price (€)
Spirulina	3000 t dw	China, India, USA, Myanmar, Japan	Human consumption, animal feed, cosmetics and Phycobiliproteins	36 kg^{-1} 11 mg^{-1}
Chlorella	2000 t dw	Taiwan, Germany, Japan	Human consumption, cosmetics, Aquaculture	36 kg^{-1} 50 L^{-1}
Dunaliella salina	1200 t dw	Australia, Israel, USA, Japan	Human consumption, cosmetics, β-carotene	215-2150 kg^{-1}
Aphanizomenon flos-aquae	500 t dw	USA	Human consumption	
Haematococcus pluvialis	300 t dw	USA, India, Israel	Aquaculture, Astaxanthin	50 L^{-1} 7150 kg^{-1}
Crypthecodinium cohnii	240 t DHA	USA	DHA	43 g^{-1}
Shizochytrium	10 t DHA	USA	DHA	43 g^{-1}

It is still to be demonstrated that the amount of energy produced by a large-scale algal culture is higher than the amount that it consumes. Furthermore, the amount of energy required to keep the culture under the proper stirring conditions, separate the biomass, dry the algal cells and extract the oil or the fraction of fuel is very high.

To overcome these obstacles and to bring to a greater scale production, it could be recommended to:

- manage the sources carefully;
- employ the CO_2 derived from combustion as carbon source;
- use wastewater as feed for microalgae;
- adopt very low cost construction methods and skilled management techniques to handle reactors per unit area;
- carefully evaluate all the constituents of residual biomass after extraction of oil.

Moreover, the co-production of bioactive molecules with high value added, such as antibiotics, anti-cancer drugs, antivirals, antioxidants and immunostimulants, could be a very interesting solution to make the large-scale application sustainable.

1.5.1 Biorefinery

Recently, there has been a severe rise in oil prices and consumers started to prefer products that do not cause harm for the health and environment; furthermore, the population growth does not match the limited reserves of non-renewable resources. For all these reasons, the need of substituting non-renewable sources with biofuels has become more urgent and therefore industries got interest in investing in their production.
One of the key institutions to promote this transition is the IEA Bioenergy Agreement Implementation. Within IEA Bioenergy, Task 42 is focused on particular on Biorefineries.
The concept of a biorefinery is similar to that of an oil refinery. In an oil refinery, the raw material (crude oil) is converted into fuels and by-products such as fertilizers and plastics. A biorefinery is made of processes that employ renewable biological sources to obtain zero-waste end product; each component of the renewable biological or bio-based source is converted or utilized in a manner to add value, and hence sustainability to the plant. The biorefinery takes advantage of the various components contained in biomass and their intermediates therefore maximizing the value derived from the biomass feedstock (Khan and Rashmi, 2010).
The objective of a biorefinery is to use the most the "noble" parts of biomass, such as starch, oil, cellulose, proteins and minor components, to produce chemical compounds of high added value for the industry by subsequent chemical-physical or enzymatic transformations and / or organic synthesis. These compounds are, in particular: plastic, lubricants, solvents, fibers, dyes, pesticides, fertilizers, etc., or chemical molecules such as glycerin, lactic, propionic, levulinic and gallic acids, etc. The residual biomass obtined from these processes, oscillating indicatively between 10% and 40% of initial biomass, can be used for energy production necessary for the operation of the plant itself, or can be placed on the market in the form of electric energy or heat.

In the case of microalgae, the main driving force for the development and implementation of algal biorefinery is the transport sector. A promising approach to reduce the production costs of biofuels is to use the bio-refineries for the co-production of high value-added products in an efficiently integrated process. Algal biorefineries could produce one or more low volume chemical or nutraceutical products with high value and a low value, but high volume liquid transportation fuel such as biodiesel or bioethanol. At the same time, the process generates electricity and process heat, through combined heat and power (CHP) technology, for its own use and, possibly, in a sufficient amount to sell it as electric energy to the local utility (Khan and Rashmi, 2010).
This way, the production costs of biofuels may be reduced by about 30%, compared to individual non-integrated production processes.
At present, scientific research and the industrial application of bio-refineries are still in an embryonic state: economic sustainability and up-scale industrial level are still to prove.

1.5.2 Microalgae as energetic source

The microalgae can be used to produce biomethanol, bioethanol and biodiesel. Furthermore, they can be grown to produce hydrogen or for the production of biomass, which can be burned to obtain heat and electricity.

Biofuel

The biofuel is made of photosynthetic reduction products of carbon dioxide, whose generation and use can stabilize the level of accumulation of carbon dioxide in the atmosphere. The advantage of biofuels is that it has no negative influence on the environment.
Biofuel can be produced by pyrolysis, thermo-mechanical liquefaction, gasification or by direct combustion (Varfolomeev and Wasserman, 2011).
The pyrolysis of microalgae has been carried out for the first time in 1986 in Germany. Currently, it is one of the most promising methods for the production of biofuel. The catalytic pyrolysis allows obtaining gasoline with high aromatic content and high octane number. The biomass in the pyrolysis process is degraded in the absence of oxygen at high temperature and allows producing biofuel, synthesis gas and pyrolysis oil. The latter is a mixture of organic compounds in its composition close to that of fossil oil. The pyrolysis of microalgae occurs at relatively low temperatures, with high quality pyrolysis oils. Microalgae, in fact, contain high amounts of lipids, water-soluble polysaccharides, and proteins that, as a result of the heat treatment, are easily converted into pyrolysis oils and synthetic gas. The main disadvantage of this method is that the biomass must first be dehydrated (Peng and Wu, 2000).

The thermo-mechanical liquefaction, instead, allows producing biofuel from microalgae biomass that have not been previously dried. Some studies have shown that the biomass of *Dunaliella tereiolata* with a water content of 78.2%, exposed to thermo-mechanical liquefaction at a temperature of 300 ° C and pressure of 10 MPa using a catalyst based on sodium carbonate, is converted effectively into biooil with similar characteristics to those of fossil oil with a yield of 37%. The microalgae *Botryococcus braunii* can have even higher yields, with a production of oil up to 57-64% of the dry biomass (Minowa et al., 1995).
The gasification process takes place via biomass oxidation in the presence of oxygen and water at high temperatures (800-1000 °C) to obtain syngas, which is a mixture of highly flammable gas. The gases composing syngas are hydrogen, nitrogen, methane, carbon monoxide and carbon dioxide with relatively low calorific value (4-6 MJ/m^3). This gas can be used as fuel for gas turbines and machines. Turbines can also work with gases obtained by direct combustion of the microalgal biomass at a temperature of 800 °C. This process uses biomass with a moisture content of less than 50% (Tran et al., 2010).

Biohydrogen

Biohydrogen from microalgae was first produced in 1942 using *Scenedesmus obliquus*. This species, in fact, starts to release hydrogen once adapted to a dark under anaerobic conditions. Currently, biohydrogen is produced from green microalgae *Chlamydomonas reinhardtii*, which is grown through an aerobic-anaerobic cycle. These microalgae are often used as model systems to study photosynthesis. The production of biohydrogen comprises two phases. During the first one, under the influence of sunlight, water is converted into hydrogen and oxygen. The first reaction takes place in all photosynthetic organisms, which use these products to synthesize ATP and NADPH-oxidase. The second reaction takes place in anaerobic conditions, if the medium in which microalgae are grown contains iron. This condition constitutes a limitation on the strains of microalgae that can be used for this purpose (Kruse et al., 2005).
The main advantage of the production of biohydrogen from microalgae, compared to vegetable biomass, is that hydrogen is rapidly released into the gas phase, because of the physicochemical properties of the culture.
At present, the possibilities of increasing the efficiency of the production of biohydrogen from microalgae are being investigated. New species of microalgae, genetically modified with a greater content of reserve starch, have been taken into account.
Moreover, some blue-green algae with both hydrogenase and nitrogenase activities are of great interest for the production of hydrogen.

Biomethane

The biomethane (biogas) is produced under anaerobic conditions. There are several methods for the production of biogas from agrotechnical cultures, but the important limiting factor of these processes is their low productivity (2000-4500 m^3/ha). When using microalgae, productivity is 5-30 times higher, due to the relatively high content of lipids, starch and proteins, in addition to the absence of lignin, which is difficult to ferment. The content of lipids is important for the production of bio-methane, being lipids much more easily converted into biogas respect to proteins and polysaccharides (Schenk et al., 2008).

Bioethanol

Bioethanol can be produced from microalgae through a fermentation process. In the first stage, the starch is separated from the cells with the help of degradative enzymes. Then, yeast of *Saccharomyces cerevisiae* is added to the biomass to begin the fermentation process.
Bioethanol can be used either as pure fuel or in mixture. In Europe it could be used with a maximum permissible concentration of 10% (E10), while in the United States, the ethanol content could be up to 85%. Bioethanol can also be employed as fuel in power plants. The energy value of ethanol is 31.1 MJ kg^{-1}, with an octane number of 129 (Amin, 2009).

Biodiesel

Biodiesel is the mixture of alkylene ethers of fatty acids obtained as a result of the transesterification of lipids. These lipids contain a lot of triglycerides (90–98%), some mono- and diglycerides, and free fatty acids (1–5%), as well as trace quantities of phospholipids, phosphatides, carotins, tocopherols, sulphur compounds and water remains (Bozbas, 2008). The production of biodiesel from microalgae is promising because of the following reasons:

- many microalgae species contain many lipids and triglycerides of fatty acids (up to 70% of the mass);
- microalgae quickly propagate under optimal conditions;
- injection of carbon dioxide allows intensifying the growth of microalgae;
- genetic engineering allows modifying microalgae, in order to increase photosynthetic and triglyceride production activities;
- microalgae can be cultivated in soils unfit for raising crops (in deserts, semideserts, and open water spaces, with the use of seawater or industrial and public service wastewater).

Microalgal biodiesel must not be qualitatively worse than biodiesel derived from plant materials. It must be also economically competitive with petroleum fuel. Unfortunately, the cost of this biofuel is still too high. Therefore, biofuel from microalgae has great potential, but further development of its production techniques is needed to make it less expensive (Varfolomeev and Wasserman, 2011).
A more detailed description of the potential and the production of microalgal biodiesel will be discussed extensively in Chapter 2.

1.5.3 Human consumption and animal feed

Some microalgae are currently used as dietary supplements because of the following important features (Chu, 2012):

- they are rich in proteins, which contain all the essential aminoacids that are involved in metabolic processes, such as the production of energy and enzymes;
- they contain high amounts of simple and complex carbohydrates that provide a source of additional fuel to the organism (in particular, they have complexes sulfated carbohydrates useful in improving the regulatory response of the immune system);
- they contain a wide profile of fatty acids, including Omega 3 and Omega 6, which are essential for energy production;
- they are rich in vitamins, minerals and trace elements.

In particular, the microalga *Spirulina* has been frequently used as food supplements because of its excellent nutritional compounds and its digestibility, due to the small amount of carbohydrates. *Spirulina* is a unique source of nutrients including vitamin B complex, minerals, proteins, gamma-linolenic acid and antioxidants (such as beta-carotene, vitamin E, trace elements). Compared to other microorganisms, *Spirulina* sp. can be grown in salt and alkaline waters, allowing obtaining animal feed with beneficial characteristics (Kulshreshtha et al., 2008).
The mass production of certain microalgae rich in proteins has been considered as a solution to close the "protein gap". Nutritional studies have demonstrated that these algal proteins are of high quality, comparable to conventional vegetable protein. However, due to high production costs and technical difficulties to incorporate the algal material in appetizing food preparations, the development of algal proteins is still far from industrial production.
The application in the food sector is more developed. Microalgae are an essential source of food in the breeding of many marine bivalve mollusks (clams, oysters and scallops), some marine gastropods (abalone, shell), larvae of several species of marine fish, shrimp and zooplankton (Yaacob et al., 2014).
The microalgal proteins can be used also as poultry feed. Several research groups have investigated the role of *Porphyridium* sp. as a food supplement. It was found that the cholesterol of the egg yolk has been reduced by about 10% and the color has become

darker. This is an indication of a higher production of carotenoids. The partial replacement of conventional proteins with those algae can be performed up to 5-10 %. Higher replacement can cause adverse effects (Ginzberg et al., 2000).

1.5.4 High added value compounds

Physiologically active nutraceuticals from microalgae include value-added food and, dietary supplements, as well as non-food products such as tablets, soft gel capsules, etc. The increasing use of algal biomass for nutraceuticals purposes should provide an attractive revenue stream for producers of algae (Ghosh et al., 2015).
One of the advantages of microalgae is that they can be used for the direct extraction of nutraceuticals free from mercury contamination, when produced under controlled conditions. Moreover, such products are also suitable for vegans. The best known nutraceutical compounds that can be obtained from microalgae are shown in Fig. 1.5, among which:

- ω-3 fatty acids required for the production of paracrine factors;
- ω-6 acids (gamma linolenic acid), essential fats in the diet;
- phycocyanins, useful for the defense against free radicals;
- carotenoids
  - beta-carotene, astaxanthin, canthaxanthin for antioxidant defense;
  - lutein and zeaxanthin for eye health.

The global nutraceutical market is expected to witness strong growth with predictions that reach 187 billion dollars in sales and an annual growth of 7%. Algae as *Nannochloropsis* and *Chlorella vulgaris* have a price of about $ 18,000 to 36,000 per ton and the market in the sports nutrition industry exceeds $ 27 billion. Particular attention should be given to production of carotenoids such as lutein and zeaxanthin, whose markets are expanding exponentially.
Despite their biochemical composition, only a few strains are commercially available for consumption, including *Chlorella*, *Dunaliella*, *Arthrospira*, *Nostoc* and *Aphanizomenon* (the last two species have limited availability). A list of key phytochemicals that can be produced from various species is listed in Table 1.8.

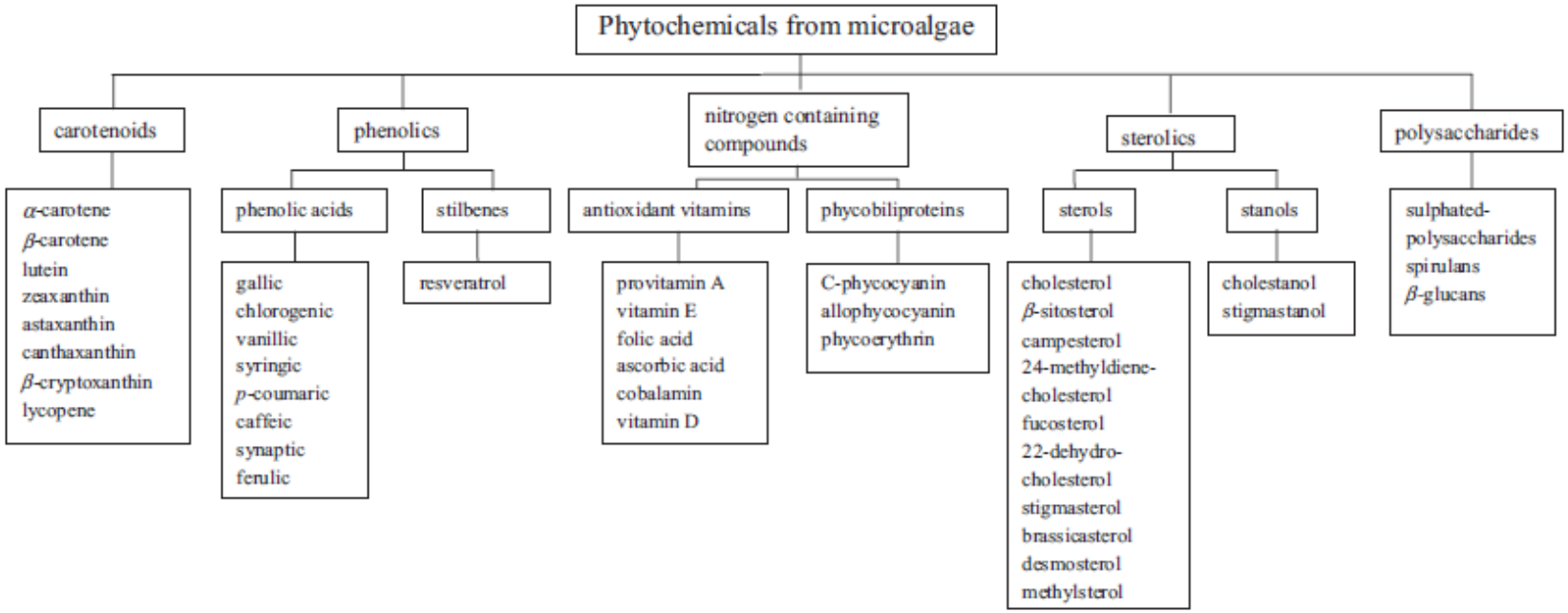

Figure 1.5 – Phytochemicals from microalgae.

Table 1.8 – Phytochemicals produced from microalgal strains.

Phytochemicals	Microalgae	Concentrtion	References
Carotenoids			
β-carotene	*Dunaliella salina*	10–13% dw	El-Baz et al. (2002)
	Chlorella zofingiensis	50% total carotenoids	Bar et al. (1995)
	Arthrospira	80% total carotenoids	Patel et al. (2005); Miranda et al. (1998)
Astaxanthin	*H. pluvialis*	Up to 4% dw	Steinbrenner and Hartmut (2001)
	Arthrospira		El-Baky et al. (2003)
Canthaxanthin	*C. zofingiensis*	25% total carotenoids	Bar et al. (1995)
Lutein	*Arthrospira*		El Baky et al. (2003)
Phycobiliproteins			
C- phycocyanin	*Arthrospira*	Up to 20% dw	Patel et al. (2005)
Phycoerythrin	*Porphyridium*	80% total phycobiliproteins	Rebolloso-Fuentes et al. (2000)
Phenolic acids			
Sinapic	*Arthrospira*		Miranda et al. (1998)
Gallic	*Phaeodactylum,*		Goiris et al. (2012)
Trans-Cinnamic	*Tetraselmis,*		
Chlorogenic	*Chlorella,*		
Quimic	*Neochloris, Isochrysis,*		
Caffeic	*Botryococcus*		

Phytochemicals	Microalgae	Concentrtion	References
Vitamins			
Vitamin E (α-tocopherol)	*Dunaliella*	12.1 mg/L	El-Baz et al. (2002)
	Haslea, Chlorella	116 mg/kg dw	Miranda et al. (1998)
	D. tertiolecta	442 mg/kg dw	Fabregas and Herrero (1990)
	T. suecica		
	Arthrospira		Miranda et al. (1998)
	P. cruentum		Sarrobert and Dermoun (1991);
Vitamin C (ascorbic acid)	*Isochrysis*	885 mg/kg dw	Bandarra et al. (2003)
	Dunaliella	24.6 mg/L	El-Baz et al. (2002)
	P. cruentum		Sarrobert and Dermoun (1991)
	D. tertiolecta	163.2 mg/kg	Fabregas and Herrero (1990)
	T. suecica	191 mg/kg dw	
Provitamin A	*P. cruentum*		Sarrobert and Dermoun (1991)
	D. salina		El-Baz et al. (2002)
Thiamin, riboflavin, piridoxin, folic acid.	*Dunaliella, Chlorella*		Fabregas and Herrero (1990)

Carotenoids

Carotenoids belongs to the class of terpenoid pigments, derived from a polyene chain of 40 carbon atoms, with important chemical properties including light-absorption characteristics that are essential for photosynthesis and for life in the presence of oxygen.

It is possible to make a distinction between primary and secondary carotenoids. Primary carotenoids (xanthophylls) are structural and functional components of the photosynthetic apparatus of the cell, while the secondary carotenoids are produced by microalgae only after exposure to specific environmental stimuli.

The xanthophylls are relatively hydrophobic molecules, typically associated to the membranes of the thylakoids and/or involved in specific non-covalent bonds with proteins. The secondary carotenoids, instead, are localized in lipid vesicles, in the stroma or in the intracellular fluid.

All xanthophylls synthesized by higher plants, such as violaxanthin, antheraxanthin, zeaxanthin, neoxanthin and lutein can be synthesized by green microalgae. Microalgae possess also additional xanthophylls, such as loroxanthin, astaxanthin and canthaxanthin. Diatoxanthin, diadinoxanthin and fucoxanthin can be produced from brown algae or diatoms.

The carotenoids perform different functions in the microalgae: they are involved in the collection of light, stabilization of the structure, scavenging of reactive oxygen species and in the dissipation of the excess energy. The inherent antioxidant activity of carotenoids is the basis for their protective action against oxidative stress (Raposo et al., 2015).

Chemically synthesized carotenoids dominate the market but the sales of naturally extracted carotenoids are growing because of the increasing demand from consumers. Natural carotenoids can be extracted from tomatoes, seaweed and mushrooms.

Among all existing natural carotenoids, five can be considered as the most important in economic terms (β-carotene, astaxanthin, cantaxanthin, lycopene and lutein).

β-carotene is a precursor of vitamin A, as several other carotenoids. It has antioxidant properties and a large number of studies have confirmed its health benefits. In particular, it reduces the risk of degenerative diseases and cancer especially in the elder age.

In human beings, oxidation reactions guided by reactive oxygen species can lead to damage proteins and DNA. This can lead to various syndromes, such as cardiovascular diseases, certain types of cancer, degenerative diseases and aging in general. As powerful biological antioxidants, carotenoids are able to absorb the energy of excitation of oxygen radicals, protecting the tissues from chemical damage. An example is the decline of cognitive abilities that accompanies Alzheimer's disease, which, apparently, is caused by persistent oxidative stress in the brain. Feeding transgenic mice with *Chlorella* sp. extracts containing β-carotene and lutein, scientists have shown a significant prevention of cognitive impairment. Other researchers have used *Chlorella* extracts containing 2-4 mg/g_{dw} of lutein and reported a reduction in the incidence of cancer, as well as the prevention of macular degeneration. Similarly, the carotenoids in

particular extracts from *Chlorella vulgaris* and *Chlorella ellipsoidea* showed inhibitory effects against the development of colon cancer (Vilchez et al., 2011).

Carotenoids also have the ability to stimulate the immune system, so they can potentially be involved in the fight against more than 60 serious diseases, including various forms of cancer, coronary heart disease, premature aging and arthritis. This is, in particular, the case of canthaxanthin and astaxanthin, and other non-provitamin A carotenoids from *Chlorella*. Some epidemiological studies on β-carotene from *Dunalliela* sp. provided evidence of a lower incidence of several types of cancer and degenerative diseases (Vilchez et al., 2011).

The species of microalgae source of carotenoids are *Chlorella*, *Chlamydomonas*, *Dunaliella*, *Haematococcus* and *Muriellopsis*, which belongs to the family of the *Chlorophyceae*. Among these, the microalga *Dunaliella* possesses the highest amount of 9-cis β-carotene, with levels of up to 100 g/kg_{dw}. Powder of β-carotene extracted from *Dunaliella* is commercially available in many countries since 1980. Although many microalgae can produce xanthophylls, *Haematococcus pluvialis* is that which accumulates them at higher levels (in particular astaxanthin), for which it is now cultivated on a large scale by different companies. Microalgae *Muriellopsis* sp. contains the higher content of lutein (up to 35 mg/L). Finally, *Chlorella ellipsoidea* was reported for the production of violaxanthin, along with two other minor xanthophylls, antheraxanthin and zeaxanthin (Raposo et al., 2015).

As mentioned before, in recent years, the production of carotenoids has become one of the most successful activities in the field of biotechnology based on microalgae, because of the strong increase in demand for carotenoids obtained from natural sources. This has promoted important efforts to improve the production of carotenoids from biological sources. The global market for all commercial carotenoids in 2008 was of $ 766 million and it reached $ 919 million in 2015. In particular, the market volume of β-carotene in 2007 was $ 247 million and $ 285 million in 2015. The astaxanthin derived from aquaculture reached a market value in 2009 of $ 260 million and a price of about $ 2500 kg^{-1}. In addition, among all the carotenoids, lutein has the fastest growth in sales, with a market value in 2010 of about $ 190 million. Therefore, microalgal carotenoids have many applications in a wide range of commercial activities (Table 1.9). As a result, the production of microalgae is dramatically becoming an attractive business (Vilchez et al., 2011).

Table 1.9 – Main commercial applications of microalgal carotenoids.

Microalga	Application	Product	Price
Chorella vulgaris	Aquaculture, cosmetics, nutraceutics, food supplements	Powder, tablets	\$30–100 kg^{-1}
Isochrysis galbana	Aquaculture, cosmetics, nutraceutics	Paste, powder	\$100–400 kg^{-1}
Nannochloropsis gaditana	Aquaculture, cosmetics	Paste, powder	\$300 kg^{-1}
Pavlova lutheri	Aquaculture	Paste, powder	>\$300 kg^{-1}
Phaeodactylum tricornutum	Aquaculture, nutraceutics	Paste, powder	>\$200 kg^{-1}
Tetraselmis	Aquaculture	Paste, powder	\$600–800 kg^{-1}
Thalassiosira weissflogii	Aquaculture	Paste, powder	>\$300 kg^{-1}
Arthrospira	Aquaculture, nutraceutics	Paste, powder	>\$200 kg^{-1}
Haematococcus pluvialis	Aquaculture, nutraceutics	Powder	>\$600 kg^{-1}
Dunaliella salina	Nutraceutics, food supplements	Powder, tablets	\$100–400 kg^{-1}

Phenolic compounds and vitamins

Phenolic compounds are another type of phytochemical found in microalgae that contribute to their antioxidant properties. The flavonoids, as well as other types of phenolic compounds, are potent scavengers of different types of reactive oxygen species (ROS) and lipid peroxy radicals, a feature that allows them to inhibit the oxidation of lipids. They also act as chelating agents of metals and inhibit the lipoxygenase enzyme.
The chlorogenic and caffeic acids from *Arthrospira* have antioxidant activity greater than that of other phenolic acids, and some studies have shown that their synergistic effect with the 13-cis-retinoic acid can prevent the lipid peroxidation and cause a regression of some cancer types in hamsters.
Botryococcus, *Chlorella*, *Isochrysis*, *Neochloris* and *Phaeodactylum* possess powerful antioxidant capacity, due to the combined action of carotenoids and polyphenols (Safafar et al., 2015). However, in spite of current knowledge in the field of microalgae

composition, there are only a few clinical studies on supplementation of phenolic compounds deriving from microalgae origin in humans.
Microalgae are also excellent sources of vitamins with antioxidant properties. Literature studies have shown the role of vitamin C and E in preventing cancer and cardiovascular diseases (Safafar et al., 2015).

Polyunsaturated fatty acids (PUFAs)

Polyunsaturated fatty acids (PUFAs) include docosahexaenoic acid (DHA), eicosapentaenoic acid (EPA), arachidonic acid (AA) and γ-linolenic acid (GLA). They have been widely recognized as beneficial compounds for human health. The market of naturally produced fatty acids was estimated at $ 7.2 billion in 2011. The total market value of fatty acids is expected to reach 13 billion in 2017. PUFAs, especially ω-3 and ω-6 of marine origin, such as EPA, DHA and GLA, are all present in microalgae. A recent study showed that daily intake of PUFAs (450 mg daily) is not introduced by the diet in the majority of the population; the current average intake of PUFAs by adults is estimated to be about 282 mg per day (EPA and DHA contribute to about 244 mg per day). Microalgae can be an alternative natural source for PUFAs. In fact, PUFAs in fish actually come from microalgae of which they feed. However, DHA is the only PUFA from microalgae commercially available. This ω-3 has a structural role in the gray matter of the brain (Bradbury, 2011). DHA is, therefore, important for the proper development of the brain and the eye in newborns and has been shown as the protector of cardiovascular health in adults. Recent studies, in fact, have explored the important role of PUFAs in the immune system and the positive effects of ω-3 PUFA on allergic diseases and in the treatment of eosinophilic disorders.
Marine microalgae have significantly higher content of DHA than those of fresh water, in particular, the marine dinoflagellates, such as *Crypthecodinium cohnii*. Nearly 30-50% of its constituent fatty acids are ω-6, while other PUFAs do not represent more than 1%. Therefore, it is easy to separate DHA from the mixtures of fatty acids. For this reason, *Crypthecodinium cohnii* represents a promising source for the commercial production of DHA. Some strains of heterotrophic algae that contain high amounts of DHA are *Schizochytrium mangroves* (33-39% of the total fatty acids), *Thrautocytrium aureum* and *Amphidium caryerea*, which contain up to 16% and 17%, respectively.

The strain *Nannochloropsis* sp. has been proposed as a source of PUFAs due to its high content of EPA. Diatoms *Phaeodactylum tricornutum* and *Nitzschia laevis* are also sources of EPA. *Chaetoceros muelleri* var. *subsalsum* and *Isochrysis galbana* have the higher percentages simultaneously of DHA and EPA and have the maximum yield of EPA, 3.5% and 4.8% on a dry basis, respectively (Zamora and Richmond, 2004). The EPA is a ω-3, which plays an important role in the regulation of biological functions, the prevention and the treatment of a number of human diseases, such as those related to the heart and inflammatory diseases. AA and EPA compounds are precursors of eicosanoids, such as prostaglandins, thromboxanes and leukotrienes.

The *Porphyridium cruentum* microalga has been used for massive production of PUFAs. The *Arthrospira* sp. is known to be the richest source of GLA among algae. The GLA is an important ingredient for foods for infants and has the potential to lower the rate of low-density lipoproteins in hypercholesterolemic patients, relieve premenstrual syndrome and treat atopic eczema. The GLA may also reduce the signs and symptoms of inflammatory diseases such as atopic dermatitis and rheumatoid arthritis (Yaakob et al., 2014).

Sterols

Phytosterols and phytostanols are another group of chemical substances which have shown the ability to reduce the risk of cardiovascular disease and stroke by lowering the levels of total lipids, cholesterol and LDL in plasma serum in hypercholesterolemic patients. β-sitosterol and β-sitosterol glucoside also show anti-inflammatory properties and protection against platelet aggregation. Other common sterols include campesterol and stigmasterol. Such as esters, sterols are fat-soluble and are easily incorporated into yogurt, margarine and salad dressings. The sterols are present not only in higher plants, but also in some types of microalgae, such as *Isochrysis galbana*, *Nannochloropis gaditana*, *Nannochloropsis* sp. and *Phaeodactylum tricornutum* (Luo et al., 2015).

Polysaccharides

Microalgae are an excellent source of polysaccharides (PS), which are associated to different biological activity and potential health benefits. Their properties have been recently studied. Particular attention was dedicated to the sulfated polysaccharides, as these compounds are found mainly in marine microalgae, mostly, *rhodophyte*, *phaeophyte* and *chlorophyte*. The microalgal polysaccharides contribute to their antioxidant activity, correlated directly with the content of sulfate groups. The ability of these polysaccharides to act as anti-inflammatory and immunomodulatory agents and lower the levels of LDL, VLDL and triglycerides in the serum has been highlighted in the literature.

The polysaccharides (or biomass) of *Porphyridium* have an important anticholesterolemic activities. Some types of PS from microalgae show anticoagulant capacity, making them promising heparin substitutes. They also offer the advantage of being free from contaminants such as prions or viruses (Arad and Levy-Ontman, 2010). Among the PS, an important role is played by β-1,3-glucans. These sugars are considered to be responsible for initiating the defense reactions in response to pathogens. *Chlorella* sp. is a major source of β-1,3-glucan (Iwamoto, 2004). The β-1,3-glucans have also shown a significant effect in the prophylactic treatment to reduce the anthrax infection in mice. Positive effects were also found in patients after

cardiopulmonary bypass. Moreover, β-1,3-glucans are commonly used in patients for immunotherapy in case of tumors. The use of β-1,3-glucan is of particular interest for cancer patients undergoing chemotherapy and/or radiation therapy, since they have shown a remarkable ability to accelerate hematopoietic recovery.

Phycobiliproteins

The phycobiliproteins are water-soluble proteins present in cyanobacteria and certain algae (*rhodophytes*, *Cryptomonads*, *glaucocystophytes*) that capture the energy of light, which is then transmitted to chlorophyll during photosynthesis. They are formed by a linkage between proteins and phycobilins via a covalent bond. Phycobilins act as chromophores. Phycobiliproteins have been used commercially as natural dyes and have a wide variety of applications in the pharmaceutical industry. They are classified as phycocyanin (blue pigment), phycoerythrin (red pigment) and allophycocyanin (pale blue pigment). The annual market of phycocyanin is about 5-10 million Euros. The cyanobacterium *Spirulina* is a source of phycocyanins and allophycocyanins.
Another type of microalgae that can be a source of phycobiliproteins is the species *Aphanizomenon flos-aquae*. Phycocyanin acts as an antioxidant against free radicals and selenium and possesses potent cancer chemopreventive properties (Yaakob et al., 2014).
Among phycobiliproteins, B-phycoerythrin has particular interest for biotechnological applications in food, immunodiagnostics therapy, cosmetics and cell labeling in the analysis. The microalgae *P. cruentum* is an important source of B-phycoerythrin. Thus, an eyeshadow resistant to heat and pH using phycobiliproteins has already been formulated. The pink and purple colors in cosmetics are often extracted from various red microalgae (Cuellar-Bermudez et al., 2014).

Cosmetic applications

Thanks to their composition, microalgae extracts have been used in the formulation of cosmetic products and skin care (anti-aging creams, products for refreshing or regenerating the skin, antioxidants and emollient products). For example, microalgae contain ω-3 that helps to reduce the appearance of wrinkles, prevent dryness and to fight skin problems such as eczema and acne. In addition, carotenoids and microalgal phenols have antioxidant properties, which help to fight against free radicals and to produce collagen and elastin, which are essential for a firmer skin.
Arthrospira sp. and *Chlorella* sp. are used in skin care products. A number of cosmetics companies have also invested in its own production of microalgae, such as LVMH (Paris, France) and Danial Jouvance (Carnac, France).

Examples of commercially available products are:

- an extract from *Arthrospira* sp. rich in proteins that repairs the signs of premature aging of the skin, has a firming effect and prevents the formation of wrinkles (Protulines, Exsymol SAM, Monaco);
- an extract of *Chlorella vulgaris*, which stimulates the synthesis of collagen in the skin, thus supporting tissue regeneration and wrinkle reduction (Dermochlorella, Codif, St. Malo, France);
- a compound of *Nannochloropsis oculata*, which is used for its excellent skin stretching properties (short and long term effects) (Pepha-Tight Pentapharm, Basel, Switzerland);
- one ingredient from *D. salina*, known to have the ability to stimulate cell proliferation and to positively influence the skin's energy metabolism (Pephactive, Pentapharm Basle, Switzerland);
- a product based on liposomes containing photolyases from blue-green microalgae *Anacystis nidulans*, produced by AGI Dermatics (Wang et al., 2015).

CHAPTER 2

Microalgal lipids and biodiesel production

This chapter describes the principles involved in biodiesel production from microalgal lipids.
After an economic analysis of the entire process, the upstream will be described, underlining the types of growing conditions for microalgae and the lipid synthesis pathway. Afterwards, the downstream processing step in the production of microalgal biodiesel will be analyzed, with a special insight on the harvesting, cell disruption and lipid extraction methods. The limitations and advantages of each of these techniques will be discussed.

2.1 Biodiesel

Several researchers are exploring alternative, renewable, economical and environmentally friendly fuel sources, since fossil fuels are exhausting quickly. Biodiesel refers to any diesel biofuel made from renewable biological materials. It can be used in pure form or blended with diesel derived from petroleum in any proportion.
Biodiesel obtained from crops, such as corn and soybeans, is one of these alternatives, but they are in competition with food and the amount needed to produce a gallon of oil is too high.
As mentioned in Chapter 1, one of the aspects of important practical interest concerning microalgae is their high lipid content. Moreover, microalgal lipid profile is similar to that of traditional vegetal oils. Some strains are capable of producing

higher amounts of lipids compared to the best crop oil and, for this reason, they may constitute a renewable source of oil for biodiesel synthesis.
The use of microalgae to produce biodiesel has been widely discussed by experts in petroleum and environmental industry. The content of lipids, in fact, can vary depending on the species and not all lipids can be used for the production of biodiesel. Table 2.1 shows data on lipid content, productivity of lipids and biomass for various species of microalgae (Mata et al., 2010).

Table 2.1 – Lipid content, productivity of lipids and biomass for various species of microalgae.

Microalga	Lipid content (%dw)	Lipid productivity (mg/L/day)	Biomass productivity (g/L/day)
Botryococcus braunii	25.0–75.0	–	0.07
Chaetoceros muelleri	33.6	21.8	0.07
Chaetoceros calcitrans	14.6–39.8	17.6	0.04
Chlorella emersonii	25.0–63.0	10.3–50.0	0.036–0.041
Chlorella protothecoides	14.6–57.8	12.14	2.00–7.70
Chlorella sorokiniana	19.0–22.0	44.7	0.23–1.47
Chlorella vulgaris	5.0–58.0	11.2–40.0	0.02–0.20
Chlorella sp.	10.0–48.0	42.1	0.02–2.5
Chlorococcum sp.	19.3	53.7	0.28
Crypthecodinium cohnii	20.0–51.1	–	10.0
Dunaliella salina	6.0–25.0	116.0	0.22–0.34
Dunaliella tertiolecta	16.7–71.0	–	0.12
Dunaliella sp.	17.5–67.0	33.5	–
Elipsoidion sp.	27.4	–	7.70
Euglena gracilis	14.0–22.0	–	0.05–0.06
Isochrysis galbana	7.0–40.0	–	0.32–1.60
Monallanthus salina	20.0–22.0	–	0.08
Nannochloris sp.	20.0–56.0	60.9–76.5	0.17–0.51
Nannochloropsis sp.	12.0–53.0	37.6–90.0	0.17–0.43
Pavlova lutheri	35.5	40.2	0.14
Phaeodactylum tricornutum	18.0–57.0	44.8	0.003–1.9
Porphyridium cruentum	9.0–60.7	34.8	0.36–1.50
Scenedesmus obliquus	11.0–55.0	–	0.004–0.74
Scenedesmus quadricauda	1.9–18.4	35.1	0.19
Skeletonema sp.	13.3–31.8	27.3	0.09
Skeletonema costatum	13.5–51.3	17.4	0.08
Spirulina platensis	4.0–16.0	–	0.06–4.3
Thalassiosira pseudonana	20.6	17.4	0.08
Tetraselmis sp.	12.6–14.7	43.4	0.30

It might be noted that some species of microalgae have high lipid content, accompanied, however, by low production of biomass (e.g. *Botryococcus braunii*). Other species, however, (*Chlorella*, *Chlorococcum*, *Dunaliella*, *Nannochloris*, *Phaeodactylum*, *Scenedesmus*) are characterized by a fairly high content of lipids (from 20 to 50%) and a good productivity of biomass. The strain *Nannochloropsis,* in particular, is one of the most promising.

The oil extracted from microalgae is called 'green crude', which has a profile similar to that of crude oil. The lipids present in the crude oil mainly contain triglycerides (90-98%), some mono- and di- glycerides and free fatty acids (1-5%), as well as traces of phospholipids, phosphatides, tocopherols, sulfur compounds, and aqueous residues (Bozbas, 2008). The characteristics of biodiesel are significantly influenced by the content of fatty acids. Table 2.2 provides data on the average composition of some fatty acids in microalgae. They are mainly unsaturated fatty acids: palmitoleic acid, oleic acid, linoleic acid, linolenic acid. However, there is a small amount of saturated fatty acids, such as palmitic acid, stearic acid (Hu et al., 2008).

Table 2.2 – Lipid profile of 'green crude'.

Fatty acids	Chain lenght: number of double bond	Content, % of total lipids
Palmitic	C16:0	12–21
Palmitoleic	C16:1	55–57
Stearic	C18:0	1–2
Oleic	C18:1	58–60
Linoleic	C18:2	4–20
Linolenic	C18:3	14–30

Crude oil is further processed into biodiesel through a process called 'transesterification'. In this process 'green crude' is mixed with a catalyst, typically sodium hydroxide, and an alcohol, such as methanol. The transesterification reaction is a multi-step process in which triglycerides are firstly converted to diglycerides; then, these are converted to monoglycerides, which are transformed to glycerol and fatty acid ethyl ethers (biodiesel). The mixture is then purified removing glycerol. Generally, the reaction is carried out under a triglyceride to alcohol ratio of 1: 6. It can be considered that it is necessary to 1 kg of oil is to produce 1 kg of biodiesel.
The reaction scheme of triglyceride transesterification is proposed in Fig. 2.1 (Varfolomeev and Wasserman, 2011).

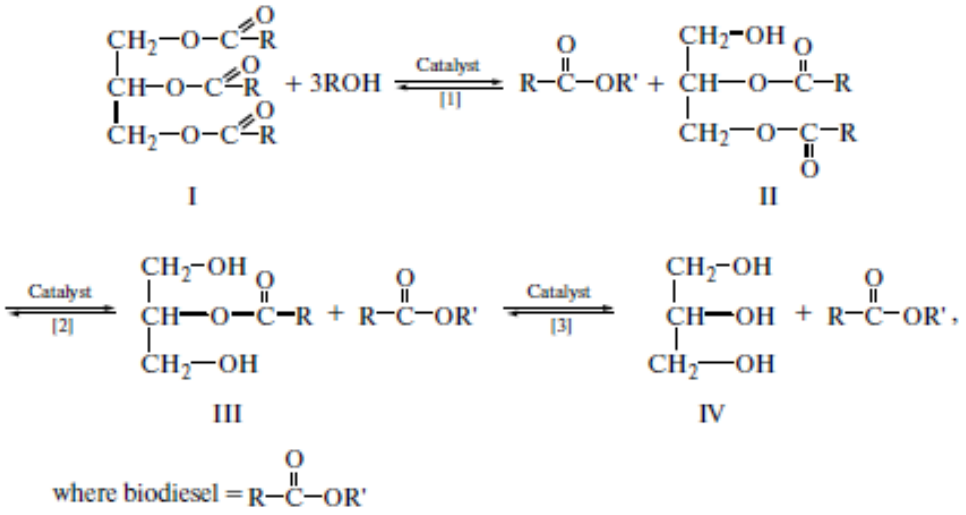

Figure 2.1 – Reaction scheme of triglyceride transesterification.

Homogeneous or heterogeneous acid or basic catalysts may be used to increase the rate of transesterification reaction. The homogeneous alkaline catalysis (hydroxides of sodium and potassium) is typically used for the industrial production of biodiesel. With this process, the reaction rate and the degree of conversion of the substrate are 4000 times higher than those that could be achieved using an acid catalyst. In addition to glycerin, co-products of the reaction are sodium salts of fatty acids (soaps) and water. Water can cause the hydrolysis of biodiesel with the formation of fatty acids and methanol. When fatty acid content is higher than 5%, soaps inhibit the separation of ethers from glycerol and cause the formation of an emulsion. Therefore, in order to reduce the content of free fatty acids, it is necessary to convert the methyl ether in the first phase. It is recommended to have less than 0.5% of fatty acids in the reaction system.
Di- and mono- glycerides are separated and recirculated into the reactor. However, free fatty acids, water and the unreacted catalyst remain in the reaction products. Therefore, it is necessary to purify the biodiesel in order to have a product in compliance with European standards. An alternative can be represented by the use of immobilized enzyme (lipase) as catalysts for the transesterification reaction, because lipases operate at low temperatures and at atmospheric pressure and are not aggressive towards metals that constitute the equipment. However, the main problem related to their use is that they are much more expensive than alkaline catalysts (Varfolomeev and Wasserman, 2011).

Glycerin, the main co-product of the transesterification reaction, can be used in pharmaceutical and cosmetics industry after refining. The acid-catalyzed condensation of glycerin with carbonyl compounds allows obtaining cyclic ketals. These are a new class of biologically active additives for fuels containing alcohol,

which are quite compatible with hydrocarbon fuels and can significantly increase the octane number and stabilize fuel phase homogeneity in a wide temperature range. A high yield (up to 90%) in ketals can be achieved with catalysts which act as proton donors (Varfolomeev and Wasserman, 2011).

Microalgal oil is richer in polyunsaturated fatty acids compared to that derived by plants. In particular it contains acids with four or more double bonds, such as eicosapentaenoic acid ($C_{20}H_{30}O_2$, five double bonds) and docosahexaenoic acid ($C_{22}H_{32}O_2$, six double bonds). These compounds are easily oxidized during their storage. This makes them less favorable for the production of biodiesel. In Europe, there are legalized restrictions on the ether of linolenic acid content in biodiesel (not more than 12%). The oil unsaturation, which determines low oxidation stability, is characterized by the number of iodine. For 100 g of fossil fuel, iodine number must not exceed 120 g, while the limit is 130 g for 100 g of biodiesel. Furthermore, according to European standards, the content of methyl ethers of fatty acids in the fuel should not exceed 1%. Depending on the number and position of double bonds, the unsaturated compounds are oxidized with different rates. The degree of unsaturation of microalgae oils can be reduced by a partial catalytic hydrogenation process. However, this operation increases the production costs of biodiesel. At the same time, the high content of eicosanoic acids in oils creates combustion problems at low temperatures, not allowing the use of this biofuel in cold regions. Table 2.3 compares the characteristics of biodiesel produced from microalgae and petroleum, which seem to be very similar (Amin, 2009).

Table 2.3 – Characteristics of microalgal biodiesel and petrodiesel.

Properties	Microalgal biodiesel	Petrodiesel
Density, kg L^{-1}	0.864	0.838
Viscosity at 40°C, mm^2 c^{-1}	5.2	1.9–4.1
Ignition temperature, °C	115	75
Hardening temperature, °C	–12	–50/10
Cold filter occlusion temperature, °C	–11	–3.0/–6.7
Acid number, mg KOH g^{-1}	0.374	0.5
Combustion heat, MJ kg^{-1}	41	40–45

Biodiesel produced from microalgal oil has important advantages. In fact, it does not contain sulfur and is characterized by a smaller amount of combustion products (carbon monoxide, hydrocarbons, oxides of sulfur) than diesel derived from fossil oil. However, the release of nitrogen oxides can be higher in some types of fuel.

2.2 Economic evaluation of microalgal biodiesel

Biodiesel from microalgae must not be worse than that coming from vegetable oils both in terms of quality and costs. For example, biodiesel and cane ethanol have only minor differences, but bio-ethanol contains only 64% of the energy that it is possible to get with biodiesel. This is the main reason why biodiesel from microalgae is the best alternative to fossil fuels compared to ethanol. Moreover, the growth per hectare of the cane under the same energy and solar radiation is less effective than the microalgal biomass production. In addition, as said earlier, microalgae can be grown in soils which are unsuitable for harvesting crops (in deserts, semi-deserts, with the use of sea water or industrial and waste water). Another significant aspect is that the productivity of microalgae can be increased employing genetically engineered strain. This allows an intensification of photosynthetic efficiency, an increment in the biomass yield per unit of solar energy used, in the biomass growth rate and in the content of oil. In addition, it is possible to create microorganisms, which are resistant to high temperatures by decreasing the demand for refrigerated water.
However, the main problem related to biodiesel from microalgae remains its cost, which must be reduced by at least 3-4 times to make it competitive with respect to a barrel of bioethanol or other biofuels of vegetable origin.

This biodiesel must also be economically competitive compared to petroleum diesel fuel. The cost of algal biofuel is proportional to the biomass cost. Therefore, it is reasonable to compare the maximum unit price of microalgae biomass with the product of fossil origin with the same potential energy. If a barrel of oil costs $ 100, one ton of biomass of microalgae should not cost more than $ 340. Literature data state that the cost of one ton of biomass produced in bioreactors or in open pounds varies between $ 2,955 and $ 3,800. With an annual increase in production of microalgae to 10,000 t, one ton of biomass will cost between $ 470 and $ 600. Considering a biomass with 30% of oil, the price of 1 ton of oil will be approximately $ 1400 (photobioreactor) and $ 1800 (open ponds). Therefore, the price of diesel produced by this biomass will be $ 2.8/L. To make biodiesel competitive, its cost should reach about $ 0.48/L. This may occur if they are used genetically engineered strains. Therefore, the microalgal biofuel is of great potential, but a further development of the production techniques is necessary to make it less expensive (Christi, 2008).

Fig. 2.2 shows schematically the production of biodiesel from microalgae (Halim et al., 2012).

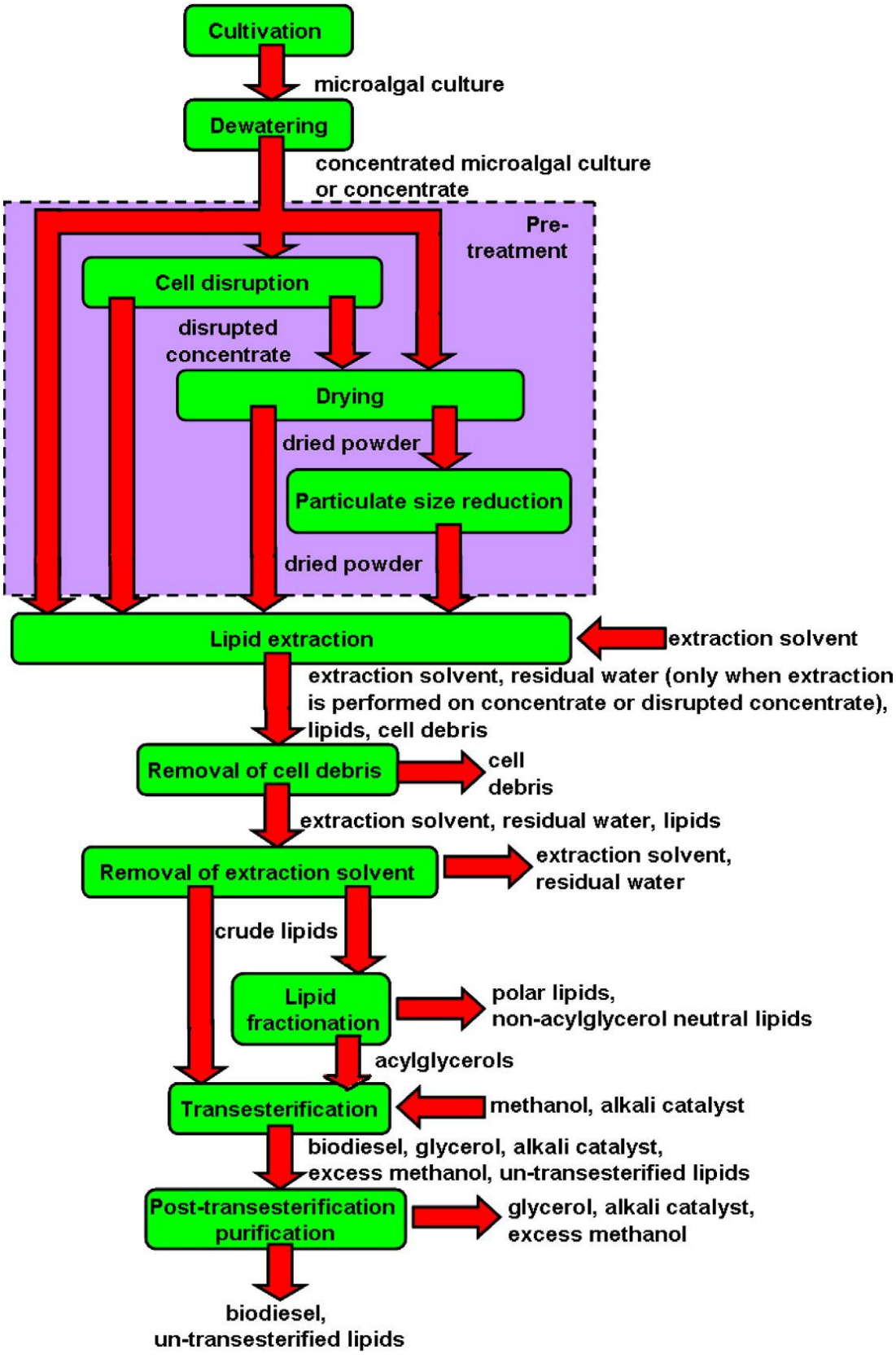

Figure 2.2 – Scheme of the production process of biodiesel from microalgae.

Another reason for the high cost of microalgal biodiesel, probably the most relevant one, is represented by the energy needed to extract lipids (Rios et al., 2013). This is due to the fact that microalgae have thick and highly resistant cell walls, which must be broken to allow the recovery of lipids. High pressure homogenization, mechanical crushing, ultrasound and microwaves are the most common methods of cell breakage. These pretreatments allow a good lipid recovery but require a high consumption of energy and expose the non-lipid components potentially extractable with high added value to risk of damaging (Gerardo et al., 2015).
An alternative is the use of an enzymatic pre-treatment. This is based on the use of enzymes capable of degrading the cell walls of microalgae, thus promoting the extraction and recovery of the lipids. Compared to other types of treatment, enzymatic methods allow operating in mild conditions and have a high specificity and efficiency. An enzyme, in fact, may selectively act on a specific chemical bond or a particular functional group, in contrast to mechanical treatments, which destroy almost all cellular components, and of the chemical treatments, which often lead to undesired transformations of compounds of interest (Kim et al., 2013).
In fact, a viable way to make the production of biodiesel from microalgae competitive is the possibility to recover these bioactive compounds present in them. Therefore, the approach to the biorefinery concept explained in Chapter 1 is crucial.
Although the production of biomolecules from algae requires a sufficiently thorough knowledge of available technology, the demands and the market value of these biomolecules are such as to justify the great interest around these compounds. Their production can make sustainable the use of microalgae on an industrial scale for the production of biodiesel and the entire supply chain in the medium term.

2.3 Biomass and lipid metabolism

2.3.1 Microalgal growth

The growth of microalgae in a suitable culture medium and under appropriate conditions has the typical pattern shown in Fig. 2.3 (Concas et al., 2014). This curve takes the name of growth curve, where growth stands for the increase in the number of cells and not for the increase of the cell size. The growth rate depends on several factors and varies depending on the species of microalga.
Simultaneously with the growth, cell death also occurs, with its own kinetic. The observed growth is the result of the combination of these two rates.
In the curve, on the ordinate axis the biomass concentration, the number of cells or indirect concentration measurements such as optical density or turbidity can be found, while the rate value in a point is the slope of the tangent line at that point.

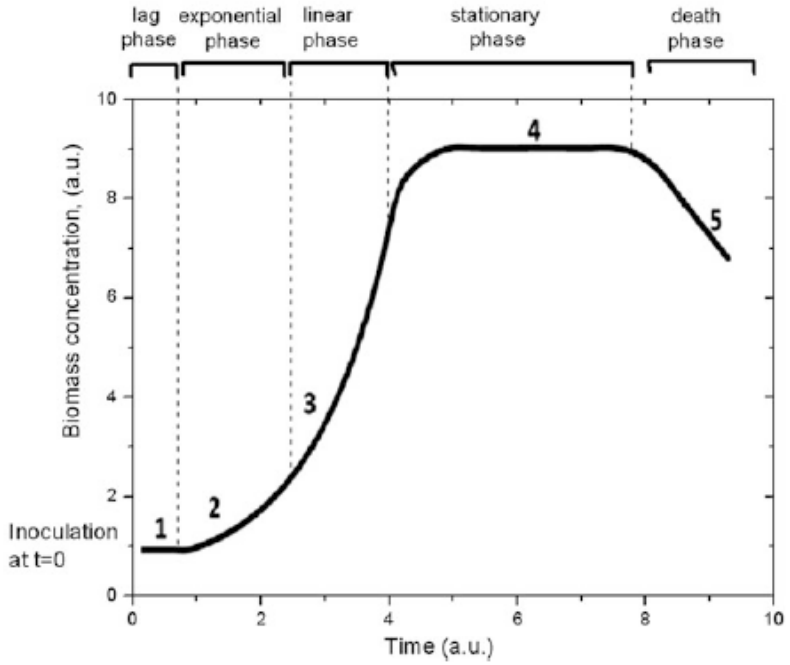

Figure 2.3 – Microalgal growth pattern.

The growth curve consists of 5 stages:

1. Lag phase
2. Exponential phase
3. Linear Phase
4. Stationary phase
5. Death Phase

In some texts, the growth curve is divided in 4 stages, because various authors represent the exponential phase and the linear phase together.

When a culture is inoculated into a photobioreactor containing fresh medium, the growth is not instantaneous, but occurs only after a certain period of time. The time interval at the beginning of the growth from the inoculation is the lag phase, or acclimation. During this phase, the algae do not proliferate, but they consume nutrients for synthesizing metabolites necessary to perform their vital functions, in particular the enzymes suitable to assimilate the nutrients. The adaptation duration depends on several parameters, in particular on the conditions of the inoculum and the culture medium (temperature, pH, concentration of nutrients), the stage of growth and on the time of inoculation. For example, if a culture is inoculated in the exponential phase, the acclimatization time will be lower than that of a culture inoculated in stationary phase, because the cells in the exponential phase already possess the right amount of enzymes and coenzymes necessary to assimilate the

nutrients. Once the cells have adapted, they begin the exponential phase. During this stage microalgae grow at maximum rate and replicate exponentially with time.
The culture remains at this stage as long as the conditions that influence growth may be maintained at optimum values. The growth continues with a linear trend for another period of time, which takes the name of linear phase.
During the early stages, the curve has a positive and high slope, because the cellular death rate is negligible compared to the speed of growth. Once the conditions are not the optimal ones, the growth rate slows down and the slope of the curve decreases. At this point, the culture enters the stationary phase, where the value of the cell growth rate is approximately equal to that of cell death. In this phase, the curve has a zero slope. During the stationary phase, even if there is no biomass generation, microalgae consume nutrients to synthesize secondary metabolites, necessary to their survival. Lipids are secondary metabolites that are produced during the stationary phase and act as reserve materials. The final phase of growth is the death phase, where the cell growth rate is less than the one of cell death. In this phase the growth curve has a negative slope.

The characteristics and composition of microalgae significantly depend on the growing conditions (Chojnacka and Marquez-Rocha, 2004). There are four major types of growing conditions for microalgae: photo-autotrophic, heterotrophic, mixotrophic and photo-heterotrophic These mechanisms are described in Table 2.4 (Chen et al., 2011).

Photo-autotrophic cultivation

Photo-autotrophic cultivation occurs when microalgae use a source of light, such as solar light, as energy source and inorganic carbon, for example CO_2, as carbon source in order to obtain chemical energy through photosynthesis. The absorption of light is necessary to reduce CO_2 and to oxidize substrates, in particular water, with the release of O_2. This is the most common cultivation method for the growth of microalgae.
The main advantage of this method is the consumption of CO_2 as a carbon source for cell growth and production of various compounds. In such case, it would be convenient to couple the microalgal cultures to factories or power plants that can provide large quantities of CO_2. Additionally, the contamination problem is much less severe in these conditions compared to other types of cultivation. Therefore, the scale-up of outdoor microalgae cultivation systems, such as ponds and channels, are usually carried out under conditions of photo-autotrophic cultivation (Mata et al., 2010).

Table 2.4 – Comparison characteristics of different cultivation of microalgae.

Growing conditions	Energy source	Carbon source	Cell density	Cultivation system	Cost	Issues
Photo-autotrophic	Light	Inorganic	Low	Open ponds or photobioreactor	Low	Low cell density High condensation cost
Heterotrophic	Organic	Organic	High	Conventional fermenter	Medium	Contamination High substrate cost
Mixotrophic	Light and organic	Inorganic and organic	Medium	Closed photobioreactor	High	Contamination High equipment cost High substrate cost
Photo-heterotrophic	Light	Organic	Medium	Closed photobioreactor	High	Contamination High equipment cost High substrate cost

Heterotrophic cultivation

Heterotrophy is the condition of animals or plants, which need organic carbon sources to support their growth. Some microalgae are able to assimilate and use organic carbon as a source of energy for growth in the dark. The heterotrophic growth solves technical and physiological problems related to the presence and distribution of light and CO_2 associated with the growth in autotrophy. Therefore, it offers the possibility of increasing the cell concentration and productivity as shown in the literature. For example, during the heterotrophic growth, an increase of lipid content of 40% in the strains of *Chlorella protothecoides* respect to photo-autotrophic growth was found (Xu et al., 2006).
Microalgae can assimilate a wide variety of organic carbon sources such as glucose, acetate, glycerol, fructose, sucrose, lactose, galactose and mannose for growth. So many studies have been focused on the research of economic organic carbon sources, such as powder of hydrolyzed cereal in place of sugar. The main drawback of these systems is linked to the fact that they suffer more frequently from problems of contamination (Xu et al., 2006).

Mixotrophic cultivation

The mixotrophic growth is defined as a growth regime during which the CO_2 and the organic carbon are assimilated simultaneously, operating both the photosynthetic metabolism that cellular respiration. The CO_2 released following cellular respiration is blocked and reused below photo-autotrophic growth conditions. Normally, the growth rate of cells in mixotrophic conditions is approximately the sum of the rate of growth of heterotrophic and autotrophic cultures. The advantages of heterotrophy, such as high concentration and productivity, are also applicable to mixotrophy. Furthermore, the ability of microalgae to grow using the two metabolic pathways is unique, and shows numerous advantages (Mata et al., 2010).

Photo-heterotrophic Cultivation

Photo-heterotrophy, also known as photo-assimilation or photo-metabolism, is a metabolism in which the presence of light is required to use organic compounds as a carbon source. The main difference between mixotrophic and photo-heterotrophic cultivation is that the latter requires light as an energy source, while the other may use organic compounds for this purpose (Chen et al., 2011).

Nutrition

For microalgae cultivation, essential elements are light, water, carbon (in the form of CO_2 or as organic carbon) and certain nutrients such as nitrogen (N), phosphorus

(P) and potassium (K). Also silica, iron and other trace elements are important because their deficiency can limit algal development. It is also necessary to reach the correct balance between the various parameters, such as oxygen, CO_2, pH, light intensity, removal of the products and by-products. In the presence of favorable climatic conditions and with a sufficient concentration of nutrients, microalgae usually double their biomass in 24 h (3.5 h in the exponential growth phase), considering that they have a very short collection cycle (1-10 days).

Table 2.5 – The main factors that influence the growth of algae.

Algal strain	Influences the type of product to be produced; for the production of biodiesel algae with high oil content and a faster growth rate are preferred.
Aeration and CO_2	Algae require aeration to fix CO2 and grow; it is possible to use a secondary source of CO2, such as the exhaust gases of power plants.
Nutrients	The composition of the growth medium and/or water affects the growth rate of algae; the use of waste water, with a high nitrogen concentration, stimulate the growth of algae.
Light	Usually sunlight is used for photosynthesis; however, artificial light sources, more expensive, could be employed for the growth in the dark.
pH	The optimal growth of algae requires a pH between 7 and 9. pH value can be influenced by the amount of CO2 and nutrients.
Mixing	Mixing is required in order to equally expose all algae cells to the light and to prevent sedimentation.
Temperature	Some species of algae require mild temperatures during growth (20-30 °C).

The algae growth is influenced by several factors resumed in Table 2.5 (Christi, 2007):

- abiotic factors (light, temperature, concentration of nutrients, oxygen, carbon dioxide, pH, salinity, presence of toxic chemicals);
- biotic factors (pathogens such as bacteria, fungi and viruses, competition with other algae);
- operational factor (depth, frequency of collection, presence of acid carbonates).

It is well known that the condition of limited nitrogen supply between the nutrients induces a higher production of lipids in microalgae. The biochemical reasons for this effect are being investigated, although oil production in nutritional stress can be explained as a defensive action taken by the algal cell. The limitation of nitrogen sources can therefore maximize the productivity of biooil, however, at the expense of the production of biomass (Bondioli et al., 2012).

Microalgal culture systems

The microalgae cultures are divided into laboratory and massive cultures, the first are used to preserve purity in different strains and ensure the injection volumes for massive ones, the second are employed to achieve adequate quantity and quality to the production requirements. The laboratory cultures allow performing fundamental research on microalgae.
In general, massive cultures are characterized by high concentrations, for which the conditions of cultivation must be strictly controlled to allow a good biomass development. The techniques vary depending on cultivation volumes and methods (closed or open systems) and on the final purpose.
Cultures begin in small volumes to get to higher volumes (20-30 L in real growth basins) through passages in increasing scales. This technique allows the reduction of time as the microalgae are always in the exponential growth phase, ensuring a more accurate control and a more programmable development.

Once achieved the required volumes, microalgae can be grown in semi-continuous, continuous or discontinuous mode. The semi-continuous way is utilized to maintain active culture for a long period of time, taking 20-30% of the biomass at predetermined intervals and bringing again to volume with enriched aqueous means. When sampling and filling are continuous, the growth is called continuous. However, these techniques expose microalgae to higher risks of contamination.
The discontinuous cultivation technique consists in bringing the culture to the maximum possible concentration (which varies with the cultivated species). Compared to the cultivation technique in continuous systems, cultures in batch

systems are easier, and ensure greater purity of the algal population. On the contrary, they require rigorous planning of cultivation (Mata et al., 2010).

The exploitation of microalgae necessitate of proper culture system. Although initially closed reactors were preferred, now open basins are suggested, as they are cheaper and easier to manage. Among these, "raceway" bath is the most widespread (Fig. 2.4). Currently 98% of microalgal world production (about 10,000 t in 2010) is cultivated in open ponds. The open basins, however, present serious limitations including the difficult control of the contaminants, the loss of large quantities of water by evaporation (100-200 m^3 per ha per day) and consequent variations in salinity and the strong contribution of the rainwater that jeopardize the stability of the system.
There are, however, many types of closed systems (photobioreactors), which can vary for orientation, inclination, stirring system (Fig. 2.5). These can be made of different materials (glass, rigid plastic plates or flexible plastic films).
Although it is of high cost and still not optimized, the algal biotechnology now seems to bet on closed systems that achieve higher areal productivity and allow the cultivation of those species which, as they don't grow on selective media, are difficult to maintain monoalgal cultivation in open basins (Menetrez, 2012).

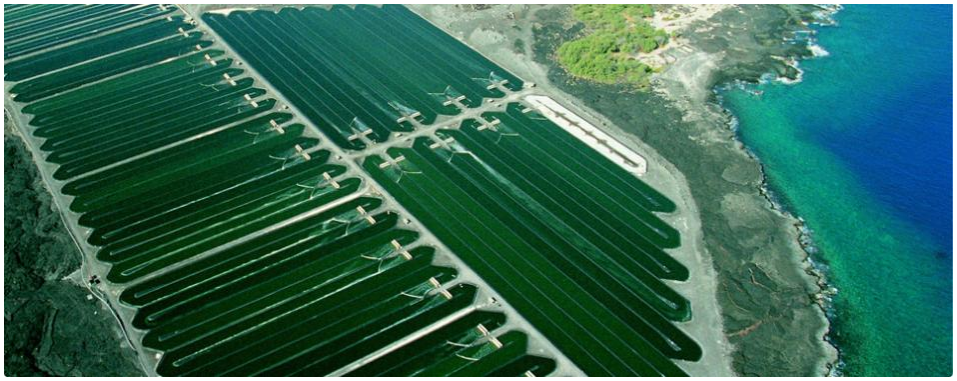

Figure 2.4 – Raceway basins.

Figure 2.5 – An example of photobioreactior (tubular shape).

The comparison between the two culture systems (Table 2.6) is not simple, as different parameters have to be considered. Typically the volumetric productivity (productivity per unit volume of the reactor), the areal productivity (productivity per unit of surface area occupied by the reactor) and the oil yield are evaluated. Closed systems are better than open ponds for the volumetric productivity (8-13 times higher). Biomass recovery with photobioreactors costs less as it provides a higher concentration of about 16-30 times, while total costs of production and management are lower for raceway systems (Chisti, 2007, Mata et al. , 2010 S. Amin 2009).

Table 2.6 – Comparison between raceway basins and photobioreactors.

	Raceway system	***Photobioreactor***
Biomass production (kg)	100.000	100.000
Volumetric productivity (kg/m³/g)	~ 0,12	> 1,5
Areal productivity (kg/m²/g)	0,035	0,048
Biomass concentration (kg/m³)	0,14	4
Necessary surface (ha)	> 0,75	> 0,55
Oil yield (L/ha)	99.400* / 42.600°	136.900* / 58.700°
Annual CO_2 consumption (kg)	183.333	183.333
System description	978 m² (12 m x 82 m x 0,30 m)	132 parallel tubes, each of 80 m length x 0.06 m in diameter
Unities	8	6
Area/volume ratio	Low	High
Biomass density	Low	High
Productivity	Low	High
Biomass concentration	Low	High
Contamination risk	High	Low
Contamination control	Hard	Easy
Process control	Hard	Easy
Temperature control	Hard	Easy
Light conversion efficiency	Low	High
Water loss	Very high	Low
CO_2 loss	High	Low
Cleaning	Not necessary	Necessary
Cost (million $/ha)	0.5-2.5	5-12 for polypropylene tubes 12-25 for polycarbonate tubes

* for biomass with oil content of 70%

° for biomass with oil content of 30%

Research has recently switched towards the use of cultivation of hybrid systems, which combine PBRs and open ponds in order to enhance the advantages of each. There are two types of hybrid systems: the first one uses both systems in two different steps, while the other attempts to blend the two concepts into one reactor step.

In hybrid two-step systems, PBRs are used to grow the initial culture under controlled conditions to minimize any contamination and maximize growth rates. Then, the culture is transferred to open ponds for less expensive operating conditions and easier exposure to nutrient stresses that facilitate lipid accumulation within the cells.

The second type of hybrid system consists in covered raceway ponds. The covering allows sunlight penetration, but separates the air directly above the pond from the atmosphere to minimize contamination risks. This system is currently used by Atacama Bio Natural Products Inc. in the first stage of microalgae growth for astaxanthin production, while the second stage of growth is transferred to a standard, uncovered pond (Dickinson et al., 2016).

2.3.2 Lipid synthesis

Lipids in microalgae are stored in lipid bodies in the cytoplasm (Fig. 2.6). Lipid bodies are spherical organelles that are also responsible for lipid transport, protein storage and degradation and other roles (Dickinson et al., 2016).

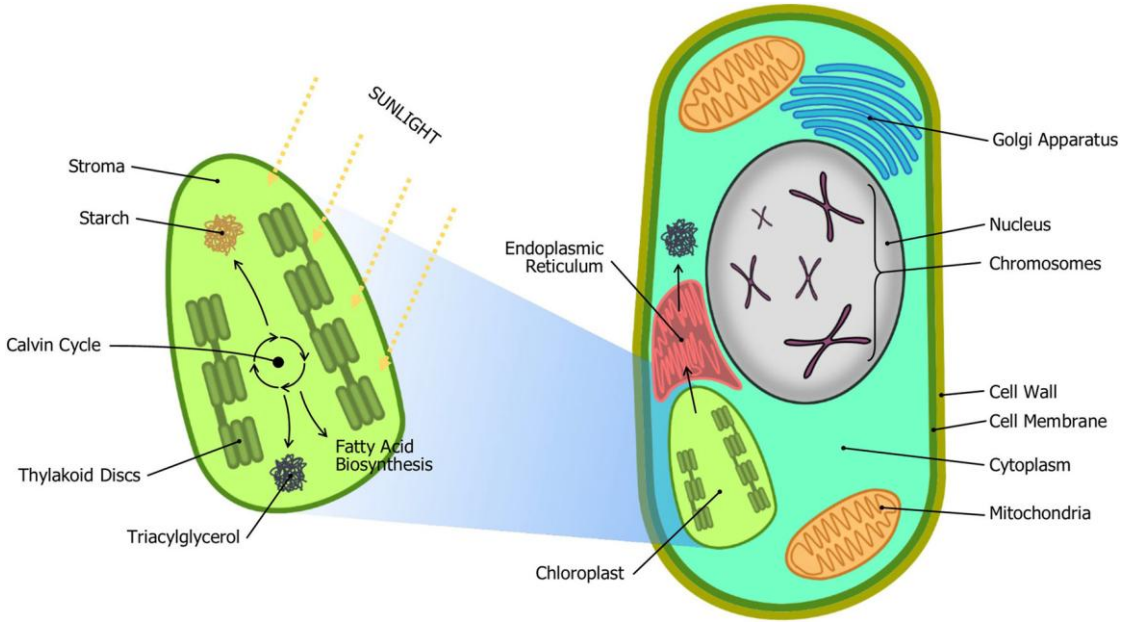

Figure 2.6 – Accumulation of energy reserves in microalgae.

Lipids are traditionally subdivided in two main classes: polar and neutral (nonpolar) lipids, based on their chemical characteristics. Neutral lipids include acylglycerols (tri-, di- and monoglycerides), free fatty acids, waxes and isoprenoid-type lipids (e.g. carotenoids). Polar lipids include phospholipids and glycolipids. The latters are esters of fatty acids and glycerol in which one of the hydroxyl groups of the glycerol is combined with an oligosaccharide. This distinction in the main lipid classes is important for the subsequent conversion of microalgal oils to biofuels, as the composition of the lipid feedstock affects the efficiency and yield of fuel conversion by catalytic routes.

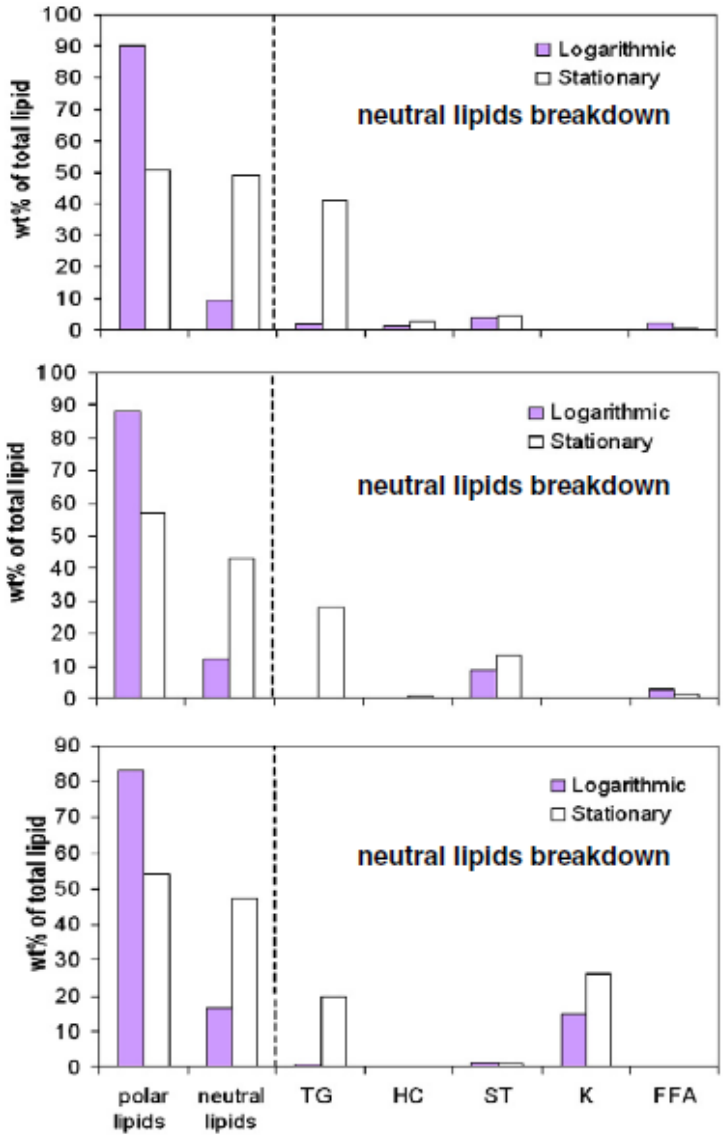

Figure 2.7 – Compositions of crude lipids extracted from three microalgal species during logarithmic phase and stationary phase. Top: *Nannochloropsis oculata*, middle: *Pavlova lutheri*, bottom: *Isochrysis* sp. For neutral lipids, TG: triacylglycerols, HC: hydrocarbons, ST: sterols, K: ketones, FFA: free fatty acids.

Existing technology is optimized for a lipid feedstock containing amounts greater than 95% in triglycerides (TAGs). Acylglycerols are desirable for commercial-scale biodiesel production for two main reasons:

- industrial-scale alkaline-catalyzed transesterification is designed to process acylglycerols and has limited efficacies on other lipid fractions, such as polar lipids and free fatty acids;
- since acylglycerols generally have a lower degree of unsaturation than other lipid fractions, they produce FAME with higher oxidation stability.

As shown by the lipid profiles of three microalgal species (*Nannochloropsis oculata*, *Pavlova lutheri*, *Isochrysis* sp.) in Fig. 2.7, microalgal lipids usually comprise high levels of polar lipids and non-acylglycerol neutral lipids (HC, ST, K, FFA). As such, they often need to be purified before transesterification. When comparing lipids obtained from logarithmic and stationary growth phase, the latters, despite having an abundance of polar lipids at 51–57 wt %, contain higher levels of TG (20–41 wt % of total lipid) and appear more attractive for biodiesel processing (Halim et al., 2012).
The relative composition of microalgal lipids depends greatly on the species used and the nutrient, environmental and developmental conditions in which the cells are cultured and harvested (Greenwell et al., 2010).

TAGs act as both electron sinks and energy reserves for microalgae metabolism. Fig. 2.5 shows light entering the cell and being absorbed by the chloroplast photosystem, which causes an oxidation–reduction reaction that generates high-energy electrons that are then shuttled by NADPH into the Calvin cycle. The products of this cycle are used to create a variety of precursors to molecules including TAGs. TAGs can be synthesized in the chloroplast and endoplasmic reticulum (Dickinson et al., 2016).

Lipid molecules buffer microalgal cells against light/nutrient irregularity and allow microalgae to maintain cellular processes such as DNA replication, nuclear division, cytokinesis, and cell survival in the face of chemical or physical environmental stimuli, either acting individually or in combination. The major chemical stimuli are nutrient starvation, salinity and growth-medium pH. The major physical stimuli are temperature and light intensity. In addition to chemical and physical factors, growth phase and/or aging of the culture also affects TAG content and fatty acid composition (Hu et al., 2008).

However, it seems that there is a trend of a decreasing growth rate with an increase in lipid content. This apparent inverse relationship could have important implications on the economics of algal biofuels. In *Nannochloropsis* sp., triglycerides accumulate during the day and are subsequently rapidly mobilized in the dark to supply the energy needed for cell division (Greenwell et al., 2010).

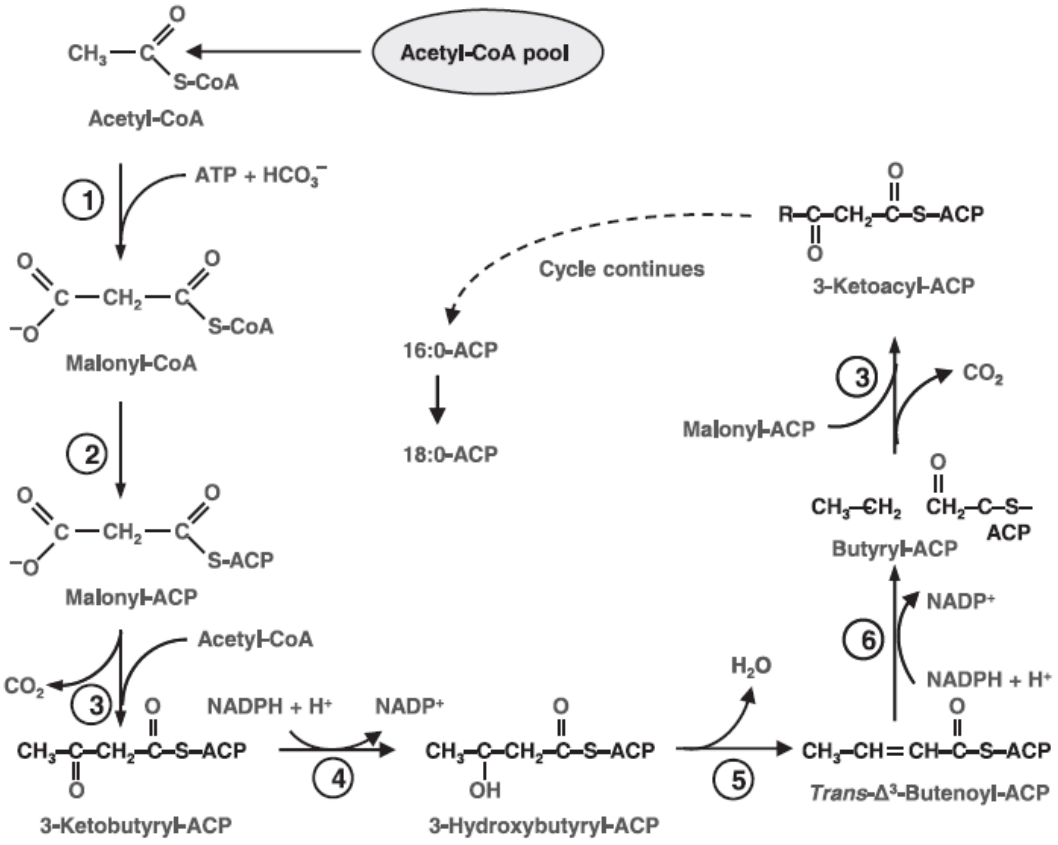

Figure 2.8 – The de novo TAG synthesis pathway.

On the contrary, the de novo TAG synthesis pathway (described in Fig. 2.8) serves as an electron sink under photo-oxidative stress. Under stress, excess electrons that accumulate in the photosynthetic electron transport chain may induce over-production of reactive oxygen species, which may in turn cause inhibition of photosynthesis and damage to membrane lipids, proteins and other macromolecules. The formation of a C18 fatty acid consumes approximately 24 NADPH derived from the electron transport chain, which is twice that required for synthesis of a carbohydrate or protein molecule of the same mass, and thus relaxes the overreduced electron transport chain under high light or other stress conditions. The TAG synthesis pathway is usually coordinated with secondary carotenoid synthesis in algae. The molecules (e.g. β-carotene, lutein or astaxanthin) produced in the carotenoid pathway are esterified with TAG and sequestered into cytosolic lipid bodies. The peripheral distribution of carotenoid rich lipid bodies serves as a 'sunscreen' to prevent or reduce excess light striking the chloroplast under stress (Hu et al., 2008).

2.4 Downstream processing

After microalgae have been cultivated, downstream processing must occur. Therefore, microalgae have to be harvested, pretreated to allow to extraction of lipids. There are several methods to select the order of unit operations involved in a production facility.
Choices in harvesting and pretreatment affect the efficiency of the lipid extraction process downstream. After the extraction step, neutral lipids are separated from the biomass and converted into biodiesel through a transesterification reaction. Extraction fluids vary in cost, selectivity, and efficacy and thus affect the end product cost, quantity, and purity. It is also during the extraction step that valuable co-products are removed for further processing.

2.4.1 Harvesting

The high water content (up to 90%), the size of microalgae (from 2 to 40 microns) and the low concentration of biomass in the cultivation broths of (0.05 to 5 kg/m^3) is one of the most stringent constraints for the conversion of algae into energy. It is therefore necessary to combine a series of techniques for recovering and drying trying to minimize the impact of these steps on cost and efficiency of the overall system. The result of this downstream processing step represents an operating constraint for the subsequent stages of conversion.
The harvesting must be optimized depending on the algal species used (density, size) and targets the cultivation process. It may be desirable, if not mandatory, the choice of species which have characteristics which allow facilitating this stage.
Harvesting and its subsequent unit operation, pretreatment, account for 20–30% of the total production costs.

Flocculation

Flocculation aggregates microalgae cells to form flocs, which cause them to settle more quickly. This is the least energy-intensive harvesting method because the addition of flocculants is all that is needed.
Flocculation could be performed chemically or physically and allows obtaining a biomass concentration of 3%.
Chemical flocculation methods use metal salts, polymers, or biopolymers to form flocs. The metal salts and polymers may cause harmful contamination to the microalgae for further processing, so biopolymers are a safer option. Two biopolymers with potential are chitosan and cationic starch. Cationic starch has proven to work better than chitosan for microalgae flocculation because it is pH independent (Dickinson et al., 2016). In fact, chitosan loses its ability at low ionic strengths, resulting entirely ineffective in the presence of salinity (over 5 kg/m^3). However, this biopolymer is not expensive (about 2 $/kg) and allows coagulating

suspended negatively charged particles by means of a physical mechanism known as bridging: varying the pH of the broth to bring it to 7, a very effective flocculation could be obtained with degrees of turbidity removal up to 90% (Molina Grima et al., 2003).
There are also physical flocculation methods that can be used, such as electrocoagulation-flocculation and the use of electrostatically positive magnetic nanoparticles. The latters have gained attention recently due to their high efficiency due to their capacity to interact with the negatively charged microalgae cells. Moreover, they could be separated from the stream magnetically and can be recovered and recycled on the large scale if cost-effective recycling processes are developed. The main concern regarding magnetic nanoparticles for flocculation is their potential effect on the downstream processes, if not properly removed (Dickinson et al., 2016).

Flotation

Flotation is a process in which air microbubbles carry microalgae to the surface of the culture where the biomass can be collected. This process depends on the size and surface characteristics of the microalgae being used and on the size of the bubbles. The bubbles with high surface-to-volume ratio are preferred for their higher stability. An ideal bubble has a diameter of 10–30 μm. The charge and hydrophobicity of the microalgal cell also play a major role in cell-bubble interaction. This phenomenon can affect the efficiency of the bubbles to carry the cells.
However, this method has a low efficiency and is not economically viable rather to other methods (Brennan and Owende, 2009). Advancements in microbubble production need to be made in order to let flotation to be feasible as a harvesting method for the production of biofuel from microalgae (Dickinson et al., 2016).

Sedimentation and centrifugation

The gravity settling is ideal for large volumes and at low biomass concentrations. However, it has low applicability, in particular because of the size of the microalgae. This method could be used in association to flocculation.
Centrifugation is a commonly used separation technique in bioprocessing. An advantage of this process is that there is no contamination of the microalgae.
The centrifugation is relatively expensive in terms of energy consumption, but it is a method with high efficiency. It requires about 1 kWh/m^3 with concentration factors of 120-150 and concentrations in the order of 10-15%. Efficiencies greater than 95% could be obtained at 13,000 g (Molina et al., 2003).

Although improvements are being made in order to reduce operation costs, centrifugation still is too energy intensive and expensive to make it a feasible option for the separation of the microalgal biomass from water (Dickinson et al., 2016).

Filtration

There are several filtration methods, which includes the use of membranes and gravity settling. For most microalgae strains, it has been shown that membranes with a pore size of 0.1–0.5 μm are preferable. The main disadvantage of membrane filtration is the fouling of the filter, which causes flux reduction and, consequently, an increase in processing costs. Cross-flow filtration has shown to be able to reduce fouling by using tangential flow (Dickinson et al., 2016).
As for the gravity settling, filtration is not suitable for small particle size (under 10 microns) dispersed in high volumes. As for sedimentation, filtration could be used if coupled with flocculation.
Micro and ultra-filtration, by the use of appropriate membranes and overpressure, can overcome this limitation, however, both the membrane replacement costs of the water processing, may make this a more expensive solution compared to the centrifugation (Brennan and Owende, 2009).

2.4.2 Drying and dehydration

The drying and extraction phases are linked to one another. The decisions made at this stage can condition the economic and energy costs in a very important way.
The slurry obtained by the step of harvesting (5-15% of biomass concentration) can be dried by exposure to the sun (drum-drying), spray-drying or freeze-drying. The choice of the drying method should consider the perishability of metabolites that have to be extracted, in particular for nutraceutical use. Freeze-drying is suited in these cases.
Drum-drying is the cheapest solution, but it is also the longest and requires elevated surfaces. The biomass could be exposed directly to the sun (it is convenient to apply a protective layer to protect the material from precipitations), or contained in special closed containers in which outside air is vented. The convection drying can be interesting when this is promoted by using the heat of the flue gas from installations for the production of electricity: it will be necessary, however, to assess the impact of high temperatures also on the biomass and the targeted products.
Spray drying is commonly used for extraction of high value products, but it is relatively expensive and can cause a significant deterioration of some algal pigments. Freeze drying is equally expensive, especially for large scale operations, but it eases extraction of oils. Intracellular elements such as oils are difficult to extract from wet biomass with solvents without cell disruption, but are extracted more easily from freeze-dried biomass (Brennan and Owende, 2009).

2.4.3 Cell disruption

To extract materials efficiently, some forms of cell disruption are generally required. In most cases, these disruption processes are carried out in concentrated cell preparations (50–200 kg/m^3 dry weight) because of the cost and energy involved. There are many ways to disrupt microalgal cells. The key criterion for the choice is the maximization of the value of the materials obtained from the processes, which means that rapid and precise disruption should be used (Greenwell et al., 2010).
In general, these techniques are divided into two main groups based on the working mechanism of microalgal cellular disintegration (Günerken et al., 2015):

- mechanical methods,
- non-mechanical methods (Fig. 2.9).

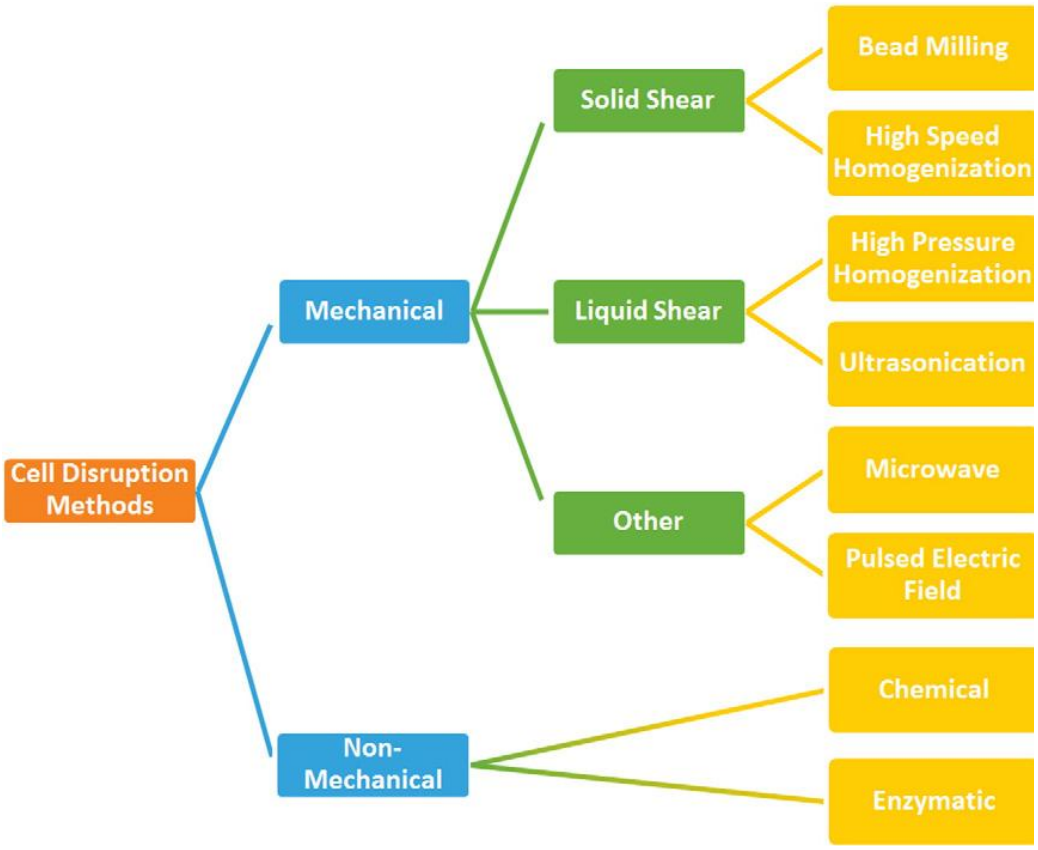

Fig. 2.9 – Classification of the cell disruption methods.

These methods may be applied individually or in various combinations. However, there are several additional parameters which collectively determine the suitability of a cell disruption process: the toughness of the cell walls, the economics of the process, the ease of scalability from laboratory to industrial-scale and the extent of contamination of the lipid product. For the production of low valued commodities, such as biodiesel, the energy requirements and cost of cell disruption will become a critical consideration. The demand for energy and the necessary economies of scale require the processing of microalgal culture in the order of thousands of tons per hour to be economically feasible (Lee et al., 2012).

Mechanical methods are usually preferred for their effectiveness and because they are less dependent on the microalgae species and less likely to lead to contamination of the lipid product. However, these methods usually have higher energy requirements than the chemical or enzymatic methods. In addition, heat is generated during mechanical disruptions and cooling is often necessary to heat sensitive products. The additional cooling energy and equipment costs have to be taken into account. A further disadvantage is that, during disruption, some lipids may be released into the surrounding medium to form a complex mixture with proteins, cell debris, etc, which may subsequently increase the difficulty of separation (Lee et al., 2012). In addition, ultrasounds, microwave and chemical treatments may damage the most easily degradable algal components, such as proteins and carotenoids, which could be co-extracted with lipids in a biorefinery perspective (Gerardo et al., 2015).

These methods are compared qualitatively based on their working mechanism, efficiency, product quality, process parameters, energy demand, and scalability. The main characteristics with a focus on industrial applicability are summarized in Table 2.7 (Günerken et al., 2015).

Bead milling and grinding

Bead mills disrupt cells by the impact of grinding beads against the cells. There are two types of bead mills: shaking vessels and agitated beads. Shaking vessels are usually made up of multiple containers or well-plates on a vibrating platform. However, this set-up is only suitable for laboratory scale. The second type consists in a rotating agitator in a fixed vessel filled with beads and cell culture; the vessels are equipped with cooling jackets to prevent the denaturing of proteins. The degree of cell disruption depends on the residence time, shear forces, the type of microorganisms and the cell concentration. In turn, the residence time is influenced by the feeding speed, the volume of the chamber, the design of the agitator and the volume of the beads. The optimal diameter of the beads is 0.5 mm, while the optimal volume fraction of bead loading is about 0.5.

Table 2.7 – Comparison of cell disruption methods in terms of key aspects.

Disruption method	Mildness	Selective product recovery	Optimum biomass concentration	Energy consumption	Practical scalability	Repeatability
Bead milling	Yes/no	No	Concentrated	High/medium	Yes	High
High pressure homogenization	Yes/no	No	Diluted/concentrated	High/medium	Yes	High
High speed homogenizer	No	No	Diluted	High/medium	Yes	High/medium
Ultrasound	Yes/no	No	Diluted	Medium /low	Yes/no	Medium
Microwave	Yes/no	No	Diluted	High/medium	Yes/no	Medium
Pulsed electric field	Yes/no	No	Diluted/very diluited	High/medium/ low	Yes	High
Chemical treatment	Yes/no	Yes	Diluted/concentrated	Medium /low	Yes/no	Medium
Enzymatic lysis	Yes	Yes	Diluted	Low	Yes	High

The disruption efficiency can be improved by using beads made of zirconia-silica, zirconium oxide or titanium carbide, because of their greater hardness and density. After treatment, the beads are separated by gravity. This type of bead mill can be scaled from laboratory scale-up to few m^3 and, therefore, it is more suitable for industrial scale applications (Lee et al., 2012).

Doucha and Livansky (2008) found that most of the algal cells can be destroyed by a single pass of the suspension through the homogenizer. Fig. 2.10 shows a suspension of *Chlorella vulgaris* before and after the destruction (degree of disintegration of 99%).

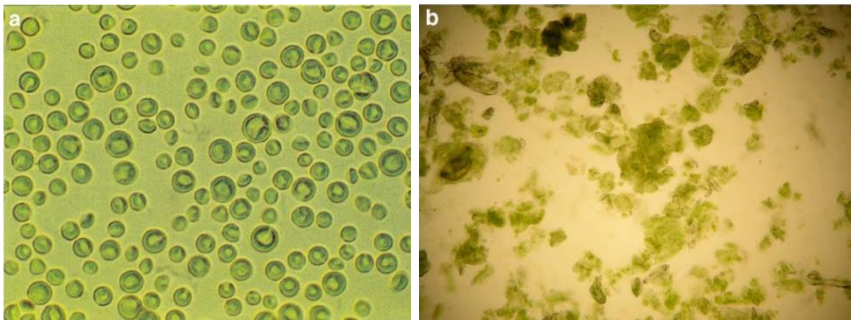

Figure 2.10 – Suspension of *Chlorella vulgaris* cells before (a) and after disintegration (b) (DynoMill KDL-Pilot A, biomass density 107 g/L, glass beads 0.42–0.58 mm, feed rate 5 kg/h, discs speed 14 m/s).

An alternative to the bead milling is represented by grinding in the presence of powders or liquid nitrogen. In the latter case, the cryo-impact freezes the cells, which require much lower breaking forces. Then, nitrogen evaporates not influencing the lipid extraction. Moreover, the low temperature reduces lipid oxidation phenomena by improving the quality of the product. Zheng et al. (2011) compared different cell disruption methods of *Chlorella vulgaris* for the release of lipids. They found that the highest yield (29%) was obtained by milling in liquid nitrogen, 9.7 times greater than the grinding of quartz dust, ultrasonic, microwave, bead milling and enzyme lysis.

High speed homogeneization

A high-speed homogenizer is a stirring device working at high rpm. These devices consist of a high speed rotating blade (rotor) enclosed within a static tube (stator). Both rotor and stator can have various configuration and they are preferably made of stainless steel. It can be used in batch, semi-batch or continuous mode.

The diameter of the rotor-stator probes varies from a few mm for sample volume under 1 mL to much larger units with batch capacities of up to 20 m^3. The speed of the rotor tip ranges from 10 to 50 m/s, with rotational speed varying from about 310 to about 6300 rad/s (Lee et al., 2012).
The effective cell disruption mechanisms are hydrodynamic cavitation, generated by stirring at high rpm, and shear forces at the solid–liquid interphase. When the impeller tip speed reaches a critical value (8500 rpm), hydrodynamic cavitation occurs due to a local pressure decreases nearly down to the vapor pressure of the liquid. Subsequently, as the liquid moves away from the impeller, the liquid pressure restores proportional to the decrease in velocity and the distance from impeller tip and causes the collapse of the cavities.
Factors that can affect the disruption efficiencies are the design and size of rotor-stator, the viscosity of the medium, flow rate and cell concentration.
High speed homogenization is the most simple, very effective, but aggressive cell disruption method. Advantages are short contact times and the potential to process suspensions with relatively high dry cell weight concentration (2–6% w/w) thus reducing the water footprint and downstream process costs. Unfortunately, the lowest energy consumption and protein denaturation due to shear induced local and bulk temperature increase make this method less favorable for mild microalgae biorefinery (Günerken et al., 2015).

High pressure homogenization

High pressure homogenization, also known as "French press", was invented by Charles Stacy French. This cell disruption process uses hydraulic shear forces generated when the suspension is shot under high pressure through a narrow tube. High pressure homogenizers (HPHs) are especially suitable for emulsification processes. The specific energy consumption of HPHs is highly dependent on biomass concentration, algae species and the growth conditions of biomass. It has many advantages, such as a little release of heat, reduced risk of thermal degradation, low-cost cooling, no dead volume in the reactor, and easy scale-up. The main drawback is the use of low dry cell weight concentrations (0.01–0.85% w/w), that increases the energy demand of downstream processing and water footprint due to isolation of products from dilute streams. Other problems of using HPHs are the non-selective intracellular compound release, difficulties to break hard cell walls and the generation of very fine cell debris (Günerken et al., 2015).

Several studies report the high efficiency of this method. Sheng et al. (2012) found that HPH was the best method of cell disruption for *Synechocystis*. Halim et al. (2012) compared bead milling, ultrasound, treatment with sulfuric acid and HPH for cellular destruction of wet biomass of *Chlorococcum* sp. through the cell count and the reduction of their diameter. The results showed that the HPH can destroy 70% of the total cells.

Ultrasonication

Ultrasonication works by generating sonic waves, with frequencies around 25 kHz. When the ultrasonic waves become strong enough, bubbles appear in the liquid. These bubbles, collapsing, lead to the phenomenon of cavitation. The collapse is due to sudden changes of temperature and pressure inside the bubbles. Temperatures could reach 5000 °C, with pressures up to 1000 bar. By means of the cavitation, the cell wall can be penetrated and/or swollen, increasing the extraction efficiency.
Ultrasonic cavitation is affected by the viscosity and the temperature of the liquid media. Low temperatures are favorable for effective sonolysis. Therefore, it is necessary to continuously cool the liquid media because the temperature increases rapidly due to heat dissipation. There are two basic types of sonicators: the horn and the bath. Both are used for batch operations but can be adapted for continuous operations by the addition of flow cells. However, due to the fact that sonication energy dissipates rapidly in regions away from the source, there will be a practical upper limit on the effective volume of these reactors. The major drawback of ultrasonication of microalgal biomass is the relatively low cell disruption efficiency for some species and the local and overall heat production. Temperature control during treatment can improve product quality, lowering however, the effectiveness of cell disruption significantly (Lee et al., 2012).

Araujo et al. (2013) studied the influence of ultrasound in the solvent extraction of lipids from *Chlorella vulgaris*. Sonication increased the efficiency of the extraction since it was partially responsible for cell disruption (Fig. 2.11). The Bligh and Dyer method assisted by ultrasound resulted in the highest extraction of oil from *C. vulgaris* (52.5% w/w). These results are similar to those by a parallel study conducted by Ranjan et al. (2010), which notes that the Bligh and Dyer method assisted with ultrasound is more efficient in the extraction of lipids from microalgae *Scenedesmus* sp. compared with the Soxhlet method.

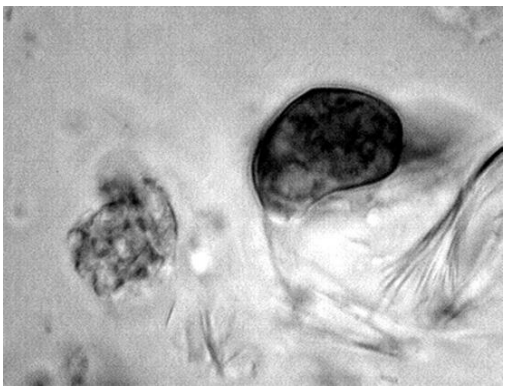

Figure 2.11 – Cells of *Chlorella vulgaris* after application of the Bligh and Dyer method, showing a normal cell in the right and a disrupted cell in the left.

Microwaves

Microwave is an electromagnetic wave with a frequency between 300 MHz and 300 GHz, but only small-range microwaves of approximately 2450 MHz are used in microwave ovens. This frequency is also used for cell disruption because it can rotate the dipole of OH bonds in water or alcohols, generating heat. Through this mechanism, microwaves can damage the cell envelopes and directly break the weak hydrogen bonds in the cell wall (Kim et al., 2013). Water exposed to microwaves reaches the boiling point rapidly, resulting in expansion within the cell and increase in the internal pressure. The local heat and pressure combined with the microwave induce damage to the cell membrane/wall, facilitating the recovery of intracellular metabolites.

This efficiency depends mainly on the energy of the microwaves, the treatment time and the temperature used. In general, an increase in temperature increases the rate of solute extraction, but it should be careful to the formation of undesirable compounds at too high temperature. However, the temperature increase is more homogeneous compared to conventional heating, thus heat related denaturation occurs less readily. Even though microwave assisted processes have the potential to increase the extraction yield and decrease the amount of solvent, there are also numerous problems. The technique is limited to polar solvents and not suitable for volatile target compounds.

In the literature there are many studies on the use of microwaves on microalgae. Biller et al. (2013) analyzed the effect of irradiation with microwave (HPM hydrothermal treatment with microwave) at different temperatures (80, 100, 120 and 140 °C) to recover lipid from three different strains of microalgae: *Nannochloropsis oculata*, *Chlorogloeopsis fritschii* and *Pseudochoricystis ellipsoidea*. Pretreatment with microwave increased lipid extraction yield of 3-7 times, proved to be a low energy intensive process for microalgae and allowed producing a good quality crude bio-oil.

Prabakaran and Ravindran (2011) compared the influence of some of the major cell disruption methods on lipid extraction efficiency. Their results are shown in Fig. 2.11. For *Chlorella* sp. and *Nostoc* sp. ultrasonic and microwave were the most effective methods, while for *Tolypothrix* sp. microwave was the most effective treatment. A similar study by Lee et al. (2010) with *Botryococcus* sp, *Chlorella vulgaris* and *Scenedesmus* sp., microwaves led the highest efficiency in extracting the lipid, 10 to 28.6% compared to 6.1-8.8% of the ultrasounds.

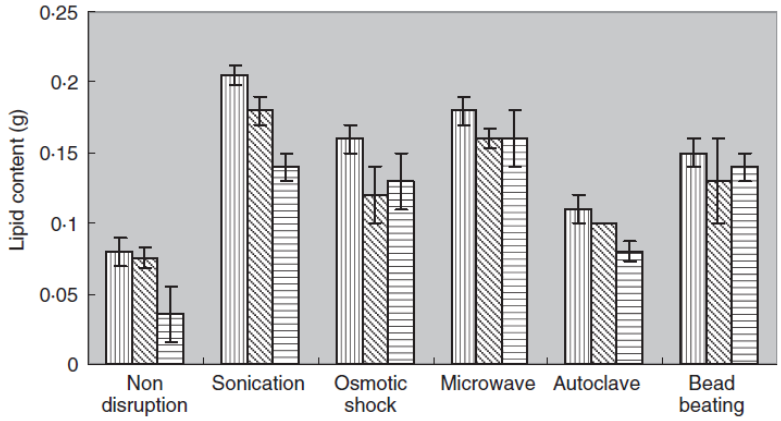

Figure 2.12 – Influence of some of different cell destruction methods on lipid extraction efficiency. In order: *Chlorella sp.; Nostoc sp; Tolypothrix sp.*

Koberg et al. (2011) compared the efficiency of microwave and ultrasound pre-treatments on the extraction of lipid from *Nannochloropsis*. Ultrasounds at 20 KHz were applied for 5 min, while microwave oven operating at 2.45 GHz was used for 5 min at 70% power. Lipid yield with microwaves was of 32.8% compared to 18.9% of the ultrasounds.

Pulsed electric field

Pulsed electric field (PEF) uses an external electric field to induce a critical electrical potential across the cell membrane/wall. Cell disruption by PEF is caused by electromechanical compression and electric field-induced tension inducing pore formation in the membrane/wall (electroporation). The size and number of the pores is directly related to the electric field strength and pulses. It is a technique already used in biotechnology for the transfer of DNA into cells. The electrolytic process is based on the superposition of waves that cause a resonance phenomenon. The resonance is usually obtained with the natural frequency of the water molecules that break the interatomic bonds. The fragments of H^+ and O^{2-} that are formed are very reactive and promote the formation of strongly oxidizing species (O_3, H_2O_2 and –OH) that may act on the destruction of the cell.
Pulsed electric field can be scaled-up easily, with a processing rate up to 2000 L/h, and can be combined with different biomass treatment methods. Energy requirements are also favorable compared to HPH and bead milling (Dickinson et al., 2016). The use of this method, however, leads to some problems. In fact, PEF also affects the molecules inside the cells. The increase in bulk temperature during treatment leads to the decomposition of fragile compounds. Moreover, the solution must be free of ions and electrically non-conductive, thus limiting the use of this cell disruption method in microalgae biorefineries. Additionally, the energy

consumption and cell disruption yield vary dramatically depending on medium composition (Günerken et al., 2015).

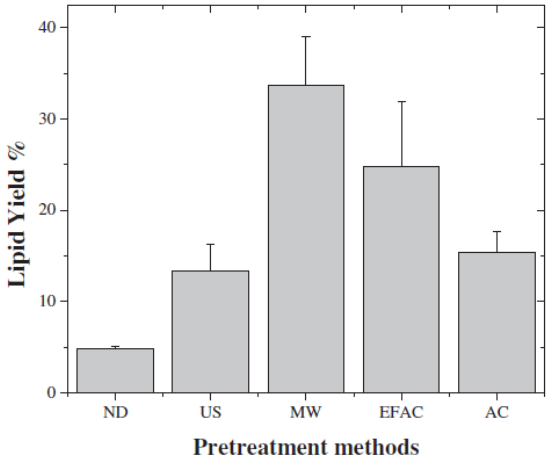

Figure 2.13 – Lipid yield obtained by the use of different pretreatment methods. ND – no disruption; US - ultrasonication; MW - microwave; EFAC - electroflotation by alternating current; AC - autoclave.

In the literature there are only few studies about the use of PEF in microalgal pretreatment. Florentino de Souza Silva et al. (2013) compared the extraction yield using electroflotation by alternating current (EFAC) with the most common pretreatments. The results were satisfactory as shown in Fig. 2.13. Microwave treatment showed the highest yield lipid with percentages of 33.7 ± 5.3% followed by EFAC with 24.8 ± 7.1%.
Sheng et al. (2011) applied a pulsed electric field (PEF) to a *Synechocystis* PCC 6803 suspension (0.3 g/L) and compared the cell disruption efficiency obtained when the same biomass was treated with heating. Almost every cell treated with PEF was ruptured, whereas a small number of cells were stained when the culture was treated by heating.

Chemical treatments

Microalgal cells can be disrupted by chemical means, such as treatments with acids, alkalis and surfactants, which can degrade chemical linkages on the cell envelope, or osmotic pressure, which induces the “pop-out” of the cells.
Cell disruption can be caused by increased permeability of cells by the use of a large variety of chemical compounds such as antibiotics, surfactants, chelating agents, chaotropes, cationic detergents, polycationic peptides, solvents, hypochlorites, acids and alkali. If the permeability exceeds a certain limit, the cells will rupture. Acids and alkalis induce hydrolysis of the cell envelope. The cell envelope can also be

weakened by heating, which can result during hydrolysis, as cell wall proteins can be denatured (Kim et al., 2013).

Selectivity, suitability and efficiency of these compounds depend on the cell wall composition of the microorganism. As all chemical substances disrupt the cells differently, there are several mechanisms of chemical cell disruption.
The main advantage of chemical treatment is its lower energy consumption compared to mechanical methods because it does not require a large amount of heat or electricity (Günerken et al., 2015). Despite the good results obtained, chemical treatments have some important drawbacks: reagents are continuously consumed, acids and alkalis can corrode the reactor surfaces, neutralization requires an additional cost, and reagents may react with the key products and/or denature them.
Miranda et al. (2012) found that treatment with 2N sulfuric acid of dried *Scenedesmus obliquus* increases the fermentation yield of ethanol of 95.6% compared to that obtained from a control sample.
Sathish and Sims (2012) used a type of extraction using acids and alkalis for the destruction of wet biomass composed primarily by *Chlorella* and *Scenedesmus* sp. The cell envelopes were hydrolyzed by 1M sulfuric acid and 5M sodium hydroxide at 90° C for 30 min; 0.5 M sulfuric acid was subsequently added to dissolve the precipitated chlorophyll and free fatty acids. The precipitate, extracted with hexane, contained 60% of total lipids.
Chemical treatments have been also used to facilitate the extraction of astaxanthin, an antioxidant with high value added, by *Haematococcus pluvialis* (Sarada et al. 2006). Among the various reagents such as acetone, methanol and organic acids, HCl 4N was found to be the most effective, allowing a recover of 94% of total astaxanthin.

Osmotic shock disrupts cells through a sudden increase or decrease in the salt concentration of the liquid media, which disturbs the balance of osmotic pressure between the interior and the exterior of the cells. There are two types of osmotic stresses: hyper-osmotic stress and hypo-osmotic stress. The first one is when the salt concentration is higher in the exterior. As a result, the cells shrink as fluids inside the cells diffuse outwards, and damage is caused to the cell envelopes. In contrast, hypo-osmotic stress occurs when the salt concentration is lower in the exterior and the water flows into the cells to balance the osmotic pressure. Thus, the cells swell or burst if the stress is too high. In the literature there are only more studies that utilize hyper-osmotic shock than hypo-osmotic shock, because the latter requires a large amount of water for the dilution of the liquid media, which makes the process unrealistic at the industrial scale (Kim et al., 2013).
Yoo et al. (2012) showed that the use of sorbitol and sodium chloride increased the extraction yield from wild type and cell wall-less mutant strains of *Chlamydomonas reinhardtii* in comparison to control experiments.

Biological methods

Biological methods are based on the degradation of the cell envelope using enzymes, virus or autolysis, but most of the studies utilize enzymes because of their easier availability.
As described in Chapter 1, the high content of various polysaccharides in the cell walls of microalgae limits the accessibility to the compounds of interest. Generally the main polysaccharides are made up of cellulose and hemicelluloses. Furthermore, the microalgal cell wall is much more complex both structurally and chemically, and very heterogeneous with respect to that of terrestrial plants. They are also composed of mixtures of sulfated polysaccharides and intertwined that are associated with proteins and various ions such as sodium and potassium.
The advantages of enzymatic methods are mild reaction conditions and high selectivity. In fact, an enzyme can selectively degrade these specific chemical linkages, whereas mechanical methods destroy almost every particle existing in the solution, and chemical methods sometimes induce side-reactions of the target products (Kim et al., 2013).
At present, the main limitations of using enzymes in biorefineries are their high cost and the fact that not many enzymes are suitable for algae disruption. Enzyme immobilization could lower the needed amount of enzymes and additionally reduce the downstream process costs since separation of the enzymes from the products would be avoided (Günerken et al., 2015).

A deepening of the state of the art of the enzymatic pretreatment of microalgae will be given in Chapter 3.

2.4.4 Fractionation and lipid extraction

Fractionation and extraction of lipids can be carried out once the microalgal cells have been disrupted.
Generally, the principles of separation of materials from disrupted cells are well established. Anyway, it is necessary to develop microalgae-specific optimized protocols. The main need is for fractionation schemes that recover all fractions of the microalgae at the maximum value, such as carbohydrates and silica from cell debris and other organics such as pigments and other metabolites (Greenwell et al., 2010).

During lipid extraction, the microalgal biomass is exposed to an eluting extraction solvent which extracts the lipids out of the cellular matrices. Ideally, a lipid extraction technology for microalgal biodiesel production needs to display a high level of specificity towards acylglycerols in order to minimize the co-extraction of non-lipid contaminants, such as protein and carbohydrates and therefore to reduce downstream fractionation/purification. In fact, other lipid fractions (polar lipids and non-acylglycerol neutral lipids, such as free fatty acids, hydrocarbons, sterols,

ketones, carotenes, and chlorophylls) are not readily convertible to biodiesel. Additionally, the selected technology should be efficient (both in terms of time and energy), non-reactive with the lipids, relatively cheap (both in terms of capital cost and operating cost) and safe.

Depending on its pre-treatment pathway, microalgal biomass to be submitted to lipid extraction can assume one of the following physical states:

- concentrate,
- disrupted concentrate,
- dried powder.

Since dewatering the microalgal biomass beyond a paste consistency is energy intensive, a cost reduction can be achieved if the selected lipid extraction technology is directly applied to wet feedstock, i.e. concentrate or with concentrations between 10 and 200 g dried microalgal biomass/L culture (Halim et al., 2012).
Two main techniques of extraction could be utilized at industrial scale: extraction with supercritical fluids or with organic solvents.

Supercritical fluid extraction (SFE)

The supercritical fluid extraction (SFE) is a relatively recent technique based on improved dissolver power of fluids when brought to their critical point.
Supercritical fluid appears suitable to be used as an extraction solvent for lipid recovery from microalgal biomass due to the following reasons:

- Tunable solvent power;
- Favorable mass transfer;
- Production of solvent-free crude lipids.

Most of the applications use CO_2, due to the moderate critical conditions (31.1 °C and 72.9 atm), low flammability and lack of reactivity.

During the lipid extraction process, the microalgal biomass is packed tightly inside a cylindrical extraction vessel. Supercritical carbon dioxide ($SCCO_2$) travels on the surface of the packed mixture and lipids are desorbed from the microalgal biomass. Immediately upon dissolution, $SCCO_2$ encloses the lipids to form a complex with lipids, which diffuses across the static $SCCO_2$ film and enters the $SCCO_2$ flow. The mixture then leaves the extraction vessel to enter the collection vessel, where a valve is used to rapidly depressurize the incoming fluid. After complete depressurization, $SCCO_2$ returns to gaseous state and the extracted crude lipids precipitate in the collection vessel. SFE-derived crude lipids are free from any extraction solvent and do not need to undergo an extraction solvent removal step.

$SCCO_2$ extraction can be operated either in batch or in continuous, but the latter process has higher yields. $SCCO_2$ solvent power during lipid extraction is a direct function of the extraction pressure and the extraction temperature. Higher extraction pressure leads to a higher fluid density and, thus, to an increase in solvent power, but also increases operating cost, lowers selectivity, and often results in the co-extraction of unwanted cellular components. Temperature increase leads to two competing phenomena: the decrease in fluid density lowers $SCCO_2$ solvent power and simultaneous increase in lipid volatility, enhancing the lipid mass transfer into the bulk $SCCO_2$ flow (Halim et al., 2012).
Despite the range these high extraction yield and selectivity, the process is strongly limited both by high energy costs both from the considerable difficulty of scale-up.

Organic solvent extraction

The solvent extraction is a process in which the target compound (lipids) is transferred from the source phase (dried or wet microalgal biomass) in a second immiscible phase (the solvent or a mixture of solvents).
The solubility of the objective compound in the solvent is governed by the Gibbs energy of the dissolution process, which is linked directly to the equilibrium constant K, which determines the distribution of the compound in both phases:

$$K = \frac{[\text{Target compound}]^{\text{solvent phase}} \cdot [\text{Solvent}]^{\text{solvent phase}}}{[\text{Target compound}]^{\text{source phase}} \cdot [\text{Solvent}]^{\text{source phase}}}$$

$$\Delta G = -RT \ln K = \Delta H - T\Delta S$$

For a value of K greater than unity, Gibbs free energy is negative and the operation proceeds spontaneously.
The solubility of the target compound in various solvents is determined by two independent parameters: the mixing enthalpy and entropy. The solubility of the compound in the solvent is therefore favored for negative values for enthalpy and positive values of entropy; being independent, the positive change in one might (or might not) counterbalance an unfavorable change in the other. The total sum of these two terms is defined by the total relative contribution of all intermolecular forces that occur between molecules of the target compound and the solvent: electrostatic and London forces, hydrogen and hydrophobic bonds. Consequently, the most appropriate solvent are those that lead to a set of possible chemical interactions more favorable than those due to solvent self-association and between lipids and microalgal biomass.
In general, the strongly associated molecules dissolve better in strongly associated solvents and vice versa. In other words polar solutes will be better dissolved in polar solvents, while non-polar solutes will be dissolved better in similar non-polar solvents.

There are different lipid extraction procedures (for lab scale), which obviously lead to different yields. Essentially they vary for the type, the report and the order of the solvents used. The most known and used methods are the following:

- Bligh and Dyer, 1959 (chloroform:methanol:water, 1:2:0.8 v/v/v);
- Folch et al. 1957 (chloroform:methanol:water, 8:4:3 v/v/v);
- Chen et al. 1981 (dichloromethan:methanol:water, 8:4:3 v/v/v);
- Hara and Radin, 1978 (Isopropanol:hexane, 2:3 v/v);
- Soxhlet, 1879 (acetone in a Soxhlet extractor).

These methods often use a non polar solvent with a more polar one, which destroys the cell membrane, making them sufficiently porous, allowing the less polar co-solvent extracting lipids. Pressure and temperature facilitate these methods.
Most of microalgal lipids are neutral lipids, found in the cytoplasm complexated with polar lipids. This complex is strongly linked via hydrogen bonds to proteins in the cell membrane. The Van der Waals interactions formed between non-polar organic solvent and neutral lipids in the complex are inadequate to disrupt these membrane-based lipid–protein associations. On the other hand, polar organic solvent are able to disrupt the lipid–protein associations by forming hydrogen bonds with the polar lipids in the complex. The mechanism in which the non-polar/polar organic solvent mixture extracts membrane-associated lipid complexes can be divided into 5 steps.

1) The organic solvent (both non-polar and polar) penetrates through the cell membrane into the cytoplasm.
2) The organic solvent interacts with the lipid complex. During this interaction, the non-polar organic solvent surrounds the lipid complex and forms van der Waals associations with the neutral lipids in the complex, while the polar organic solvent also surrounds the lipid complex and forms hydrogen bonds with the polar lipids in the complex. The hydrogen bonds are strong enough to displace the lipid–protein associations binding the lipid complex to the cell membrane.
3) An organic solvent–lipids complex is formed and dissociates away from the cell membrane.
4) The organic solvent–lipids complex diffuses across the cell membrane.
5) The organic solvent–lipids complex diffuses across the static organic solvent film surrounding the cell into the bulk organic solvent.

As such, the addition of a polar organic solvent to a non-polar organic solvent facilitates the extraction of membrane-associated neutral lipid complexes. However, the process also inevitably leads to the co-extraction of polar lipids and other unsaponifiable compounds (Halim et al., 2012).

Two important concepts must be taken into consideration when choosing the appropriate system of solvents to extract the lipids:

1) the ability of the polar solvent to destroy the hydrogen bonds or electrostatic forces between the lipid and membrane proteins and the cell wall to create so a sufficient porosity;
2) the capacity of the non polar solvent of better solubilize the target lipids.

The mixture of chloroform and methanol is the most performing solvent. These compounds, however, have problems of toxicity. Consequently, less volatile and less toxic alcohols (ethanol, isopropanol) are usually selected in place of methanol, in combination with hexane, which replaces chloroform.

CHAPTER 3

Enzymatic degradation of microalgae cell wall

In this chapter the classification of enzymes and a review of the main studies on enzymatic treatments of microalgae are described. A particular focus will be made on *Nannochloropsis* sp., the microalga utilized in this work, and on the composition of its cell wall was analyzed. The aim is to identify one or more particular classes of enzymes that are effective in the degradation of microalgal cell wall allowing a better efficiency of extraction of the metabolites of interest contained in them.

3.1 Enzymes

3.1.1 Enzyme classification

Enzymes are macromolecular biological catalysts which accelerate chemical reactions. Enzymes names often derived from its substrate or the chemical reaction it catalyzes, with the word ending in *-ase*. However, since several enzymes have common names that do not refer to their function or what kind of reaction they catalyze, an enzyme classification system was established. The International Union of Biochemistry and Molecular Biology developed a nomenclature for enzymes, EC numbers, according to which each enzyme is described by a sequence of four numbers preceded by "EC". The first number classifies the enzyme on the basis of its mechanism. The second number refers to the subclass, the third to sub-subclass and the fourth is specific for each enzyme. There are six classes of enzymes according to

the type of reaction catalysed: oxidoreductases, transferases, hydrolases, lyases, isomerases and ligases.

1) Oxidoreductases catalyze oxidation-reduction reactions in which hydrogen, oxygen atoms or electrons are transferred between molecules. This extensive class includes dehydrogenases (hydride transfer), oxidases (electron transfer to molecular oxygen), oxygenases (oxygen transfer from molecular oxygen) and peroxidases (electron transfer to peroxide).

2) Transferases catalyze the transfer of an atom or group of atoms. The transfer occurs from one molecule that will be the donor to another molecule that will be the acceptor. Generally, the donor is a cofactor that is charged with the group about to be transferred.

3) Hydrolases catalyze reactions that involve hydrolytic reactions and their reversal. These usually involve the transfer of functional groups to water. These enzymes could also be classified under transferaes since hydrolysis can be viewed as a transfer of a functional group to water as an acceptor. This is the most commonly encountered class of enzymes within the field of enzyme technology and includes esterases, glycosidases, lipases and proteases.

4) Lyases catalyze reactions where functional groups are added to break double bonds in molecules or the reverse, where double bonds are formed by the removal of functional groups. This includes aldolases, decarboxylases, dehydratases and some pectinases.

5) Isomerases catalyze reactions that transfer functional groups within a molecule so that isomeric forms are produced. These enzymes allow for structural or geometric changes within a compound. This class includes the epimerases, racemases and intramolecular transferases.

6) Ligases, also known as synthetases, form a relatively small group of enzymes which involve the formation of a covalent bond joining two molecules, due to condensation. These reactions are coupled to ATP cleavage.

It is difficult to determine in absolute terms (e.g. grams) the amount of enzyme used for a chemical reaction or in a process, because the purity is often low and a part could be inactive. Activities of enzyme preparation and of any contaminating enzymes are the most relevant parameters. These activities are usually measured in terms of the activity unit (U) which is defined as the amount of enzyme that catalyzes the transformation of 1 micromole of substrate per minute under standard conditions.

3.1.2 Cell wall degrading enzymes

As seen in Chapter 1, carbohydrates are the main constituents of the cell wall. The enzymes that break down cell wall sugars belong to the class of hydrolases, subclass carbohydrases, sub-subclass glycosidases (EC 3.2.1). The main glycoside-hydrolytic enzymes are described below.

Cellulases

Cellulases (EC 3.2.1.4) are a class of enzymes capable of hydrolyzing β-1-4 glycosidic bond of the cellulose fibers. Industrially, they are widely used in the textile sector and for the production of pulp in paper mills. They are typically obtained from fungi and mold species *Pleorotus*, *Aspergillus* and *Trichoderma*.
Cellulases are divided into three main classes:

- Endocellulases (12-50 kDa), which can attack cellulose structure in "central" positions of polysaccharide chains, significantly decreasing their average molecular weight;
- Exocellulases (42-60 kDa), enzymes that attack polysaccharide chains in terminal position, freeing sequentially low molecular weight oligomers of glucose (cellobiose);
- Cellobiases or β-glucosidases (35-218 kDa), capable of hydrolyzing the cellobiose in its glucose monomers.

The action of β-glucosidase is extremely important when employed in industrial applications, because cellulases, as all carbohydrases, suffer from product competitive inhibition. The presence of β-glucosidase, which removes cellobiose, can improve performances of hydrolytic-based cellulase treatments. β-glucosidase has also a good specificity for β-D-galactosidic, α-L-arabinosidic, β-D-xylosidic and β-D-fucosidic residues. Many cellulases have amino acid composition, solubility and pH similar to the optimal one. Thermal stability and substrate specificity can vary. In addition, cellulase preparations often contain other enzyme activities that could affect the properties of preparations. These enzymes are effective at pH values comprised between 3 and 7, with optimum values between 4 and 5. The optimal temperature is between 40 and 50 °C. Cellulase is inhibited by Hg, while ions of Mn, Ag, Cu and Zn are only weak inhibitors. The activity of cellulase preparations collapses completely after 10-15 minutes of treatment at 80 °C.

Hemicellulases

Hemicellulases are generally defined as a class of enzymes that hydrolyze the glucosidic linkages of the various polysaccharide structures that form hemicellulose.

As cellulases, generally, these enzymes are produced by fungi and molds (e.g. *Trichoderma* sp.). They are extremely important in several industrial applications as cellulase adjuvant in the previously described applications or other important processes such as the production of beer. Given the great complexity and diversity of hemicelluloses present in nature, the same complexity and differentiation is also found in naturally selected biocatalysts for the hydrolysis of such structures. These enzymes are capable of hydrolyzing polysaccharides of various branched structure, consisting of a main chain of hexose sugars (glucose, mannose and galactose) and pentoses (xylose and arabinose) polycondensates by β-1,4 bonds. In nature, among the most prevalent sugars in plant cell walls, there are the xylans, mannans, arabans and galactans respectively hydrolyzed by xylanase (EC: 3.2.1.8), mannanase (EC: 3.2.1.78), arabinase (EC: 3.2.1.99) and galacturonase (EC: 3.2.1.15).
Xylanase (EC 3.2.1.8) are a class of enzymes that degrade the linear polysaccharide β–1,4-xylan into xylose. There are different forms of these enzymes, which show various aspects, mechanisms of action, substrate specificity, hydrolytic activities and physico-chemical properties.
B-mannanase (EC 3.2.1.78) catalyzes the hydrolysis of β–1,4 linkages between mannoses which constitute the main chain of mannan, galactomannan and glucomannan, the key polymers of hemicellulose. It is widely used in food processing, paper, pharmaceutical and biofuel industry, and particularly in the production of animal feed. The optimum operating conditions are 40-60 °C and a pH of 4-7.

Other hydrolytic enzymes

Endo-1,3(4)-β-glucanase (3.2.1.6) are a class of enzymes that act on glycosidic bonds β-1,3 and β-1,4-glucan, the major components of the soluble fiber fraction of food. Enzyme preparations containing β-glucanase are used extensively in oenology to facilitate the filtration of musts and wines produced from botrytis grapes and to induce the elimination of mannoproteins and oligosaccharides from the cell walls of yeast. The main compounds that inhibit the activity in the wine industry are ethanol and phenols contained in red wine. They are more active between 36 and 45 °C and at a pH between 4.5 and 5.0.

Xyloglucanase (EC 3.2.1.151) is an enzyme that catalyzes the reaction between a water molecule and xyloglucans, to give oligosaccharides of xyloglucan. The enzyme, obtained from *Aspergillus aculeatus*, is highly specific for the xyloglucan. It is stable at a pH of 3.4 and a temperature below 30 °C.

Galactosidases (3.2.1.23): are a group of enzymes responsible for hydrolysis of galactosides into monosaccharides. Depending on whether the glycosidic bond lies "above" or "below" the plane of the galactose molecule, the galactosides are classified in α- or β-galactosidases.

B-galactosidase is a hydrolytic enzyme that catalyzes the hydrolysis of terminal residues of β-D-galactose, breaking β-glycosidic bonds terminals. Some β-galactosidases are also able to hydrolyse α-L-arabinosides, β-D-fucosides and β-D-glucosides.

Lysozyme (EC 3.2.1.17) is an enzyme present in animal tissues with bactericidal activity. It hydrolyzes the cell wall of certain bacteria (Gram +) catalyzing the hydrolysis of beta–1,4 bond between N-acetylmuramic acid (NAM) and N-acetylglucosamine (NAG) which are the main component of peptidoglycan (breaks the glycoside bond uniting the C1 of NAM to NAG C4).
It is abundantly present in numerous human and animal secretions such as tears (except those of cattle) and saliva. It has also been found in high concentrations in egg white. It consists of 129 amino acids and has a structure consisting of two domains: a domain is essentially composed of α-helices; the other is composed of a β-sheet and by two antiparallel α-helices. The three-dimensional configuration of the molecule is maintained by the presence of few polar residues and three disulfide bridges in its interior portion, two located in the α-helical domain and one in the one on the β-sheet. Catalysis rate is maximal at pH 5.

Pectinases include many enzymes, which are capable of attacking the diverse and complicated polygalacturonic structures. These biocatalysts are among the most widely used for industrial applications, especially in food production, especially of juices. It is estimated that these preparations constitute 25% of enzymes global market. The most common source from which they are extracted is *Aspergillus niger*. Pectinases are classified according to the type of bond that hydrolyzes the pectic structure:

- polymethylgalacturonase and polygalacturonase (EC 3.2.1.15) hydrolyze the α-1,4 bonds between galacturonic acid units;
- pectinesterase (EC 3.1.1.11) removes the methyl group of the pectin hydrolyzing the ester bond of the galacturon and of the carboxyl;
- pectin lyase (EC 4.2.2.10) hydrolyze the α-1,4 bonds between galacturonic acid units via an elimination of the carbohydrases that produces galacturonates or unsaturated methylgalacturonates.

3.2 Enzymatic hydrolysis of microalgae: state of the art

The purpose of enzymatic pretreatment of microalgae is the disruption of the cell wall in order to improve the availability of their biomolecular constituents. Cell wall can be degraded by purified enzymes, enzymatic cocktails (either a mixture of purified enzymes or extracts produced by hydrolytic microorganisms) and by cultures of microorganisms with hydrolytic activities. Such enzymatic pretreatments

are not energy intensive and have a good selective product recovery, thus having a positive impact on steps in the downstream process.

The major disadvantages are high cost of enzyme production, handling, high enzyme-to substrate specificity and enormous diversity in algal cell envelope composition and structure. In fact, microalgae are composed mainly of carbohydrates (4–64%), proteins (6–61%) and lipids (2–55%), but their composition can vary significantly according to environmental and growth conditions, affecting the production of different macromolecules. However, a common component is cellulose, as in higher plants; they also typically contain other polysaccharides, such as pectin and hemicellulose.
One of the most exceptional characteristics of microalgal composition is the presence of a complex, dynamic and polysaccharide-rich cell wall. This extracellular matrix ensures the cell physical and microbial protection and helps, in some cases, with cell-cell adhesion. Moreover, the presence of some biopolymers such as sporopollenin and algaenans, give supplementary resistance to the algal cells. Sporopollenin composition is not well understood because of its unusual chemical stability and resistance to degradation by chemicals under very harsh conditions. Analyses revealed that it is a mixture of biopolymers, mainly containing long chains of fatty acids, phenylpropanoids, phenolic compounds and trace carotenoids (Carrillo-Reyes et al., 2016).

The diversity in composition and polymer arrangement of microalgae cell wall ensures its mechanical strength, shape and rigidity as necessary characteristics for cell protection against infection or predators. Consequently, an effective microalgae cell wall disruption method must be optimized for the targeted cell wall to lyse (Demuez et al., 2015).
The most exploited enzymes for these purposes are those with cellulase, hemicellulase, pectinase, protease and amylase activities, due to the ease of their extraction and purification from fungi (Carrillo-Reyes et al., 2016).

A number of studies have reported the efficiency of enzymatic cell wall disruption by adding externally single or cocktails of cell wall-degrading enzymes (Demuez et al.:, 2015). Due to cell wall characteristics, single enzymatic treatment (Table 3.1) is often performed with carbohydrases, in order to couple both cell wall disruption and polysaccharides hydrolysis. It can be considered as a saccharification step as it hydrolyzes both cell wall and storage carbohydrates. This saccharification involves the use of cellulases, hemicellulases, amylases, and amyloglucosidases to convert polymeric carbohydrates into simple sugars. Recently, the use of enzymes with protease activity has also been tested, because of the presence of glycoproteins with structural role in the cell wall.
Moreover, several studies have attempted to hydrolyze the different biopolymers constituting the cell walls using enzymatic cocktails to produce a synergistic effect (Table 3.2).

Table 3.1 – Content, classification and lipid recovery of different microalgal species.

Microalga	Product	Enzyme	Conditions	Outcome	Ref.
Chlamydomonas reinhardtii	CH_4	Alcalase 2.5 L	0.2 mL/g_{DCW} at pH 8 for 2 h, 50 °C,. Volume not given	289 mL CH_4/g COD; 10% increase the methane production	Mahdi et al., 2014
Chlorella pyrenoidosa	Carbohydrates, lipids	Cellulase	140 mg/m^2 24 h, pH 4.6, 50 °C; 2%$_{DCW}$. 15 mL	62% cellulose hydrolysis; 75% increase the in lipid extraction	Fu et al., 2010
Chlorella vulgaris	CH_4	Alcalase 2.5 L	0.2 mL/g_{DCW} at pH 8 for 2 h, 50 °C. Volume not given	287 mL CH_4/g COD; 51% increase the methane production	Mahdi et al., 2014a
Chlorella vulgaris	Proteins solubilization	Alcalase 2.5 L	0.585 AU/g_{DW}, 130 rpm, 3 h, 50 °C, pH 8. Volume not given	49% hydrolysis efficiency; 256 mL CH_4/g COD, increasing methane production 1.59 fold	Mahdi et al., 2014b
Chlorella vulgaris	Lipids	Cellulase	5 mg/L, 10 h, pH 4.8, 55 °C. 500 mL	8.1 fold more than untreated cell	Zheng et al., 2011
Chlorella vulgaris	Lipids	Lysozyme	5 mg/L, 10 h, 55 °C. 500 mL	7.6 fold more than untreated cell	Zheng et al., 2011
Chlorella vulgaris	Glucose	Pectinase (Pectinex SP-L)	240 U/mg, pH 4.8, 200 rpm, 72 h. Volume not given	79% saccharification yield	Kim et al., 2014
Chloroccum sp.	Glucose	Cellulase from *T. reesei*	40 °C, pH 4.8, 72 h. 100 mL	Glucose yield of 64% 0.02 g enzyme/g substrate	Harun et al., 2011
Laminaria digitata	Reducing sugars	Cellulase (Sigma C9748)	1.25 mL/g_{DCW}, pH 5, 37 °C 24 h, 300 rpm. 5 mL	18 mg/mL reducing sugars	Vanegas et al., 2012

Table 3.2 – Content, classification and lipid recovery of different microalgal species.

Microalga	Product	Enzyme	Conditions	Outcome	Ref.
Botrycoccus braunii	Methane	Enzymatic extract of *A. discolor*.	1000 U/L of MnP activity, 24 h, 200 rpm, 30 °C. 50 mL	521 mL CH_4/g; 62% increase compared to the microalgae without treatment	Ciudad et al., 2014
Chlamydomonas reinhardtii	Dextrin, glucose	Thermoestable α-amylase Glucoamilase	0.005% (v/w), 90 °C, 30 min. 0.2%, 55 °C, pH 4.5, 30 min. Volume not given	2.5 g Dextrin/L, 98% carbohydrates hydrolysis	Choi et al., 2010
Chlamydomonas reinhardtii	Methane	Viscozyme L Alcalase 2.5 L	0.3 mL g/g $_{DCW}$ at pH 5.5 for 3 h 0.2 mL/g $_{DCW}$ at pH 8 for 2 h, 50 °C. Volume not given	311 mL CH4/g COD; increasing methane production 1.17 fold	Mahdi et al., 2014a
Chlorella vulgaris	Hydrogen	Crude enzyme solution	35 °C, 150 rpm, pH 7.4, 52 h. 100 mL	43 mL H2/g DCW; 1.42 fold more than untreated cell	Yun et al., 2014
Chlorella vulgaris	Lipids	Snailase	5 mg/L, 2 h, 37 °C. 500 mL	2.36 fold more than untreated cell	Zheng et al., 2011
Chloroccum sp.	Glucose	Cellulase from *T. reesei*	40 °C, pH 4.8, 72 h. 100 mL	The highest glucose yield of 64% was found at 0.02 g enzyme/g substrate	Harun et al., 2011
Chroococcus sp.	Total sugar	Crude enzyme 20% (v/v) of A. *lentulus*.	Biomass concentration 2 g/L, 30 °C, pH 5, 48 h, 150 rpm. 20 mL	44% hydrolysis efficiency	Prajapati et al., 2013
Haematococcus pluvialis	Astaxanthin	0.1% Protease K and 0.5% driselase	1 h, pH 5.8, 30 min. Volume not given	1.65 fold more extraction than untreated cell	Mendes Pinto et al., 2001

The combined use of various carbohydrases and/or endopeptidases or proteases in enzymatic pretreatment for biofuels production has gained particular interest as it strongly improves cell lysis and biomass degradation. The combined action of glucanase and protease at optimum dosage and hydrolysis conditions intensifies the extraction efficiency.

Below, some studies on the use of enzymatic pre-treatments are discussed as examples.

Cho et al. (2013) studied the lipid extraction of *Chlorella vulgaris* cells and the subsequent conversion into FAME (fatty acid methyl ester). The enzymatic hydrolysis was effective in weakening the cell wall, allowing a better solvent extraction. A buffer solution 0.1 M of citric acid and 0.1 M of sodium citrate mixed with 2% (v/v) of Celluclast 1.5 L (rich in cellulase) and 1% (v/v) of Novozyme 188 (rich in β-glucosidases) was added to the lyophilized biomass and maintained in enzymatic hydrolysis for 72 hours. Results are shown in Fig.3.1.

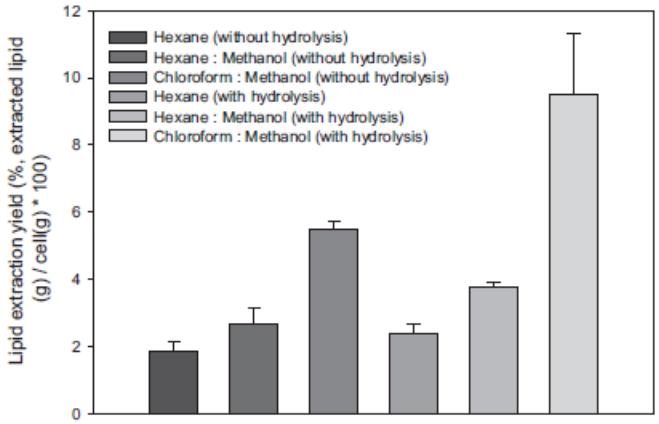

Figure 3.1 – Extraction lipid yield from *Chlorella vulgaris* with and without enzymatic treatment.

The extraction was carried out with 3 different mixtures of solvents: hexane/methanol 7:3 (v/v), chloroform/methanol 2:1 (v/v) and hexane alone. The agitation was conducted at 1000 rpm for 6 hours at room temperature. The lower yield obtained with hexane can be explained by the fact that it is a non-polar solvent which extracts mainly the hydrophobic lipids, while the other solvents, being more polar, can extract also hydrophilic lipids. An evident improvement of the extraction with enzymatic hydrolysis is evident, from 29 to 73% approximately depending on the organic solvent used.
In this study the effect of temperature, pH and cell concentration on the yield of extraction were also tested. Temperature acts on the enzymatic deactivation: the optimum was found to be between 45 and 50 °C. The optimum pH was 4.8. The hydrolytic yield decreased with the algal concentration. This is due to the increase of

resistance to the mass transfer at high substrate concentrations and to the product inhibition.
Best yields were obtained by extracting dried biomass directly with solvent, but drying is an expensive process. Therefore, the enzymatic hydrolysis may be an excellent choice to improve the yield of lipid extraction from wet biomass.

Zheng et al. (2011) compared and evaluated a number of different physical, chemical and biological treatments on the disruption of marine *Chlorella vulgaris* cells for the recovery of lipids. Before physical and chemical treatments, biomass was exposed to sunlight for 10 minutes, to destroy chlorophyll, which would alter the quality of extracted lipids. Cell suspension was extracted with a mixture of chloroform:methanol (1:1 v/v) in proportion 1:2 with the samples using a modified Bligh and Dyer method. The organic phase was then separated and evaporated with a rotary evaporator at 30 °C. The lipids were measured with an electronic balance and their concentration defined as the ratio between the lipid extracts and the biomass. The results are shown in Fig. 3.2.

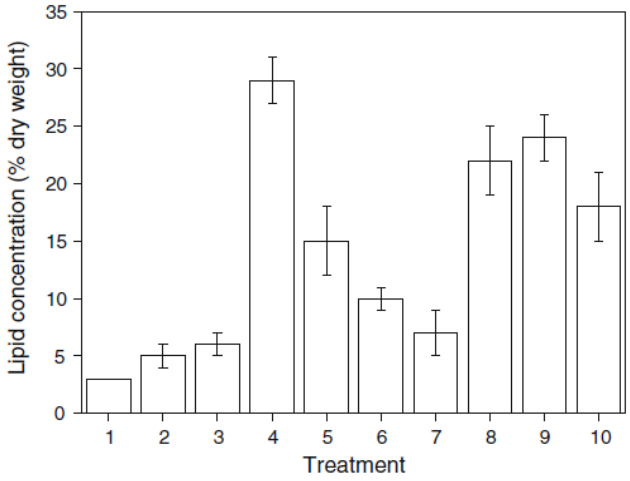

Figure 3.2 – Effect of different cell disruption methods on *Chlorella vulgaris*. 1 control, 2 wet grinding with quartz powder, 3 dry grinding with quartz powder, 4 grinding in liquid nitrogen, 5 ultrasound, 6 bead milling, 7 snailase, 8 lysozyme, 9 cellulase, 10 microwave.

The most effective technique was grinding in liquid nitrogen with a yield of 29%, 9.7 times higher than that of the control sample. Enzymatic lysis reached the second best yields of 24% and 22%, respectively with cellulase with lysozyme (55 °C for 10 hours). The enzymatic lysis with snailase showed a lower yield (7%).

In order to reuse the enzymes employed during cell lysis and minimize costs, enzyme dosages need to be optimized to reach a maximum of cell degradation with the minimum amount of enzymes. In this context, Fu et al. (2010) attempted to

reduce the global cost of the process by immobilizing cellulases. They studied the hydrolysis of the cell wall of *Chlorella pyrenoidosa* (consisting for 45% of cellulose) to produce reducing sugars. The treatment was carried out inside a membrane reactor containing inner supports coated with immobilized cellulase. Lipid extraction was performed with n-hexane at 28 °C for 1, 3 and 6 hours. Lipid content before and after the hydrolysis remained constant, indicating that there was no leakage of lipids after 72 h of reaction. Hydrolytic yield increased with lipid content, due to lower cellulose content per unit weight of microalgae. The optimum temperature was 50 °C, because at higher temperatures the enzyme degraded. The immobilized cellulose appeared to be stable and had a good activity at a pH of 4.6. The hydrolytic yield decreased with the concentration of microalgae, probably due to an increase of resistance to mass transfer and inhibition of products. The lipid extraction was 56, 62 and 84% after 1, 3 and 6 hours, showing a yield higher than that obtained from hydrolytic microalgae not hydrolysed (32%).

Gerken et al. (2013) analyzed the degree of degradation of *Chlorella vulgaris* cell walls after enzymatic treatment, with the intent to find a specific enzyme cocktail that allows efficient degradation of the wall. TEM analysis showed that the cell wall was constituted by a double layer; the inner one had a lower electron density than the outer one. The latter also presented a number of flagella on the outer surface, as observable in Fig. 3.3 c.
Lysozyme was found to have the most drastic effect, reducing cell wall density, thereby improving the permeability and allowing the entry of other specific enzymes that do not normally degrade the wall. In addition it was able to digest the external flagella, as observed in Fig. 3.3 b.

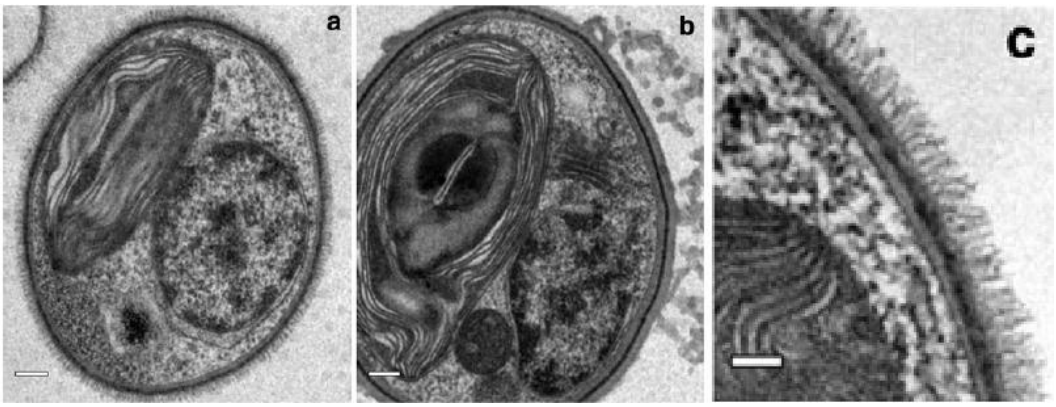

Figure 3.3 – TEM Images of *Chlorella vulgaris*. a) no enzyme, b) lysozyme, c) particular of the cell wall.

The best synergistic effects on the permeability of the cell wall (Fig. 3.4) were obtained using lysozyme with sulfatase (96.8%) and with glusulase (β-glucoronidase and sulfatase, 76.1%).

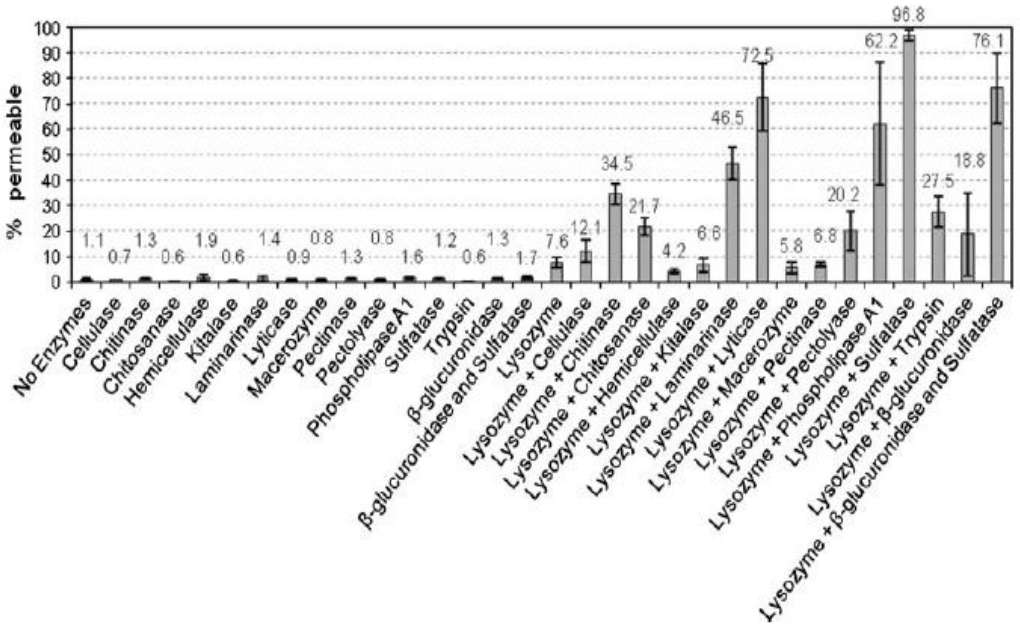

Figure 3.4 – Permeability of the cell wall of *Chlorella vulgaris* after different enzyme treatments.

Nannochloropsis sp. and *S. capricornutum* strains were also tested. For the first one, most of the cells were permeabilized by the combination of lysozyme with sulfatase, but also lysozyme with trypsin or liticase. The second, however, did not respond to changes in permeability using the individual enzymes, but it has been observed that about 1/3 and 2/3 of the cells were permeabilized respectively from sulfatase and lysozyme, and lysozyme and liticase.

The enzymatic treatment could be associated to other pretreatments to increase cell wall disruption and, therefore, metabolites recovery, such as acid hydrolysis (Hernandez et al., 2015), ultrasound (Liang et al., 2012), mechanical disruption (Wang et al., 2005) or polymer treatment (Zheng et al., 2016).

Hernandez et al. (2015) evaluated the effect of amylase and cellulase on the extraction of sugars from three microalgae: *Chlorella sorokiniana*, *Nannochloropsis gaditana* and *Scenedesmus almeriensis*. Before enzymatic hydrolysis with cellulase or amylase, biomass was suspended in sulfuric acid (0%, 4%, 7% and 10%) and then placed in an autoclave at 121 °C for 30 min. Results are shown in Fig. 3.5.

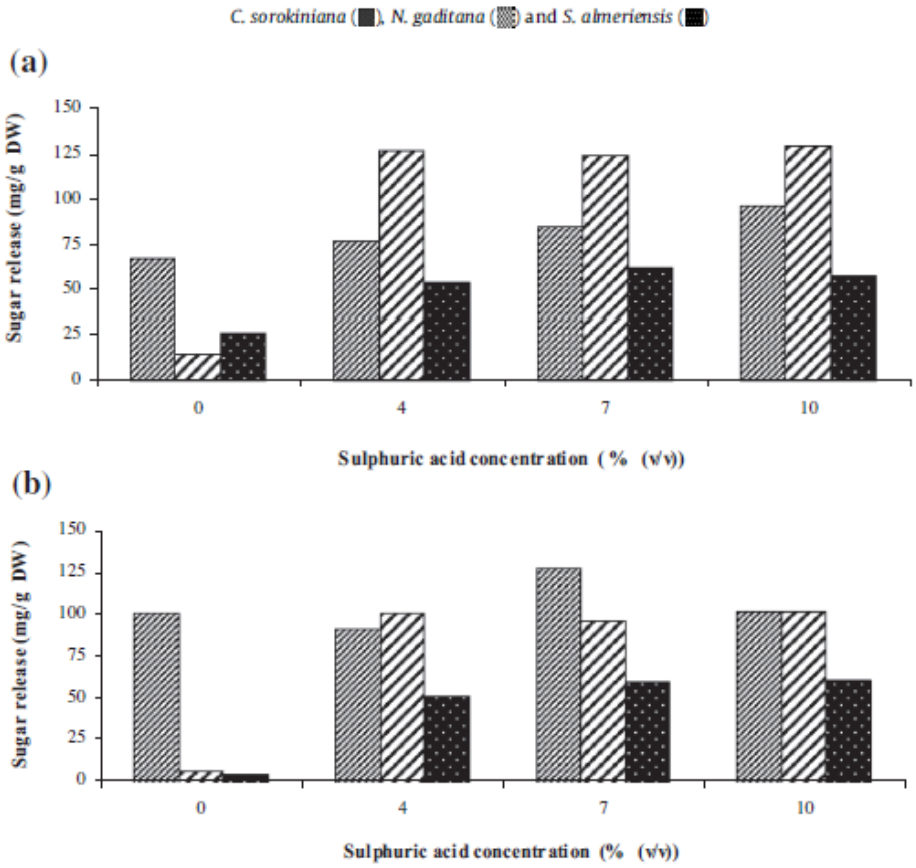

Figura 3.5 – Treatment with cellulase (a) and amilase (b) of *Chlorella sorokiniana*, *Nannochloropsis gaditana* and *Scenedesmus almeriensis*, with and without acid hydrolysis.

The study showed the efficiency of combined pre-treatments to disrupt microalgal cell wall and hydrolyze carbohydrate chains into monosaccharides. Acid hydrolysis has proven to be efficient to disrupt the cell wall, allowing enzymes to access carbohydrates and, therefore, increasing enzymes efficiency. Thus, the combined pre-treatment of H_2SO_4 with enzymatic hydrolysis gave the highest sugar release in *Chlorella sorokiniana* (128 mg/g_{dw}) and *Nannochloropsis gaditana* (129 mg/g_{dw}). In the case of *Scenedesmus almeriensis*, the highest sugar release was obtained after acid hydrolysis with H_2SO_4 for 60 min (88 mg/g_{dw}). The enzymatic hydrolysis with amylases of *Chlorella sorokiniana* released a remarkable monosaccharide concentration (101 mg/g_{dw}). The most difficult microalga to hydrolyze was *Scenedesmus almeriensis* due to its cell wall structure and composition.

Liang et al. (2012) developed an aqueous extraction process assisted by enzymes (EAEP: enzyme-assisted aqueous extraction processing) from *Chlorella vulgaris*, *Scenedesmus dimorphus*, and *Nannochloropsis* sp. Microalgae were in the form of concentrated paste (18% of solid). Samples were pre-treated with ultrasound at 600 W, supplied in regular intervals of 2 seconds for 15 minutes, in the presence of water

ice to prevent overheating. Subsequently, the enzyme was added and temperature and pH were set as shown in Table 3.3. After the treatment, the enzyme reaction was stopped by deactivating the enzyme at 95 °C for 10 minutes. Subsequently the hydrolysates were centrifuged and separated into three distinct phases: oil phase, intermediate phase and aqueous phase. The oily phase was recovered by the addition of hexane and the lipids were measured after the solvent evaporation.
The enzymes used and the results are reported in the Table 3.3.

Table 3.3 – Enzymes used and results obtained by Liang et al. (2012).

Enzyme	Activity (U/mg)	Optimal temperature (°C)	Optimal pH	Lipid recovery (%)
Cellulase	2.9	55	4.8	17
Snailase	-	37	5.8	12
Neutral protease	200	50	7.0	9
Alcalin protease	200	55	8.5	35
Trypsin	40	37	8.0	35

Snailase is a complex of over 30 enzymesm, such as pectinase and β-glucuronidase that degrade efficiently the constituents of the cell wall, while the proteolytic enzymes can hydrolyse the membrane proteins and the cytoplasm and change the emulsifying capacity of some proteins. Trypsin attacks the basic residues (arginine, lysine), and is very efficient in the hydrolysis of the protein.

Different times (Fig. 3.6) and different enzyme concentration (Fig. 3.7) were tested.

The recovery of lipids increased with enzyme dosages up to 4%; after this percentage, there were no further benefits on the yield. The yield also increased with the time of extraction till 12 h and then remained constant. The yield was also strongly dependent on the pH; it was possible to achieve yields of 50% by adjusting the pH to 4 due to the destabilizing effect of pH on the emulsion.

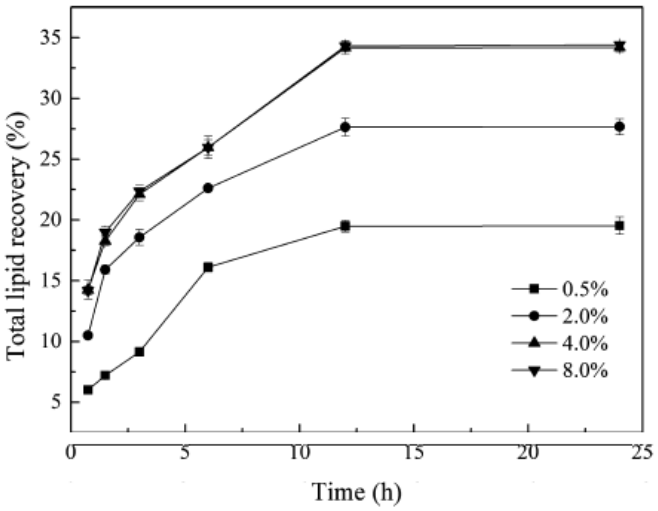

Figure 3.6 – Effect of time on lipid recovery.

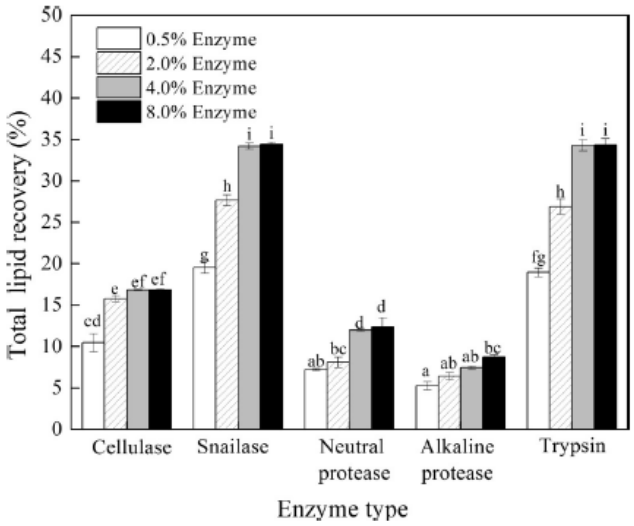

Figure 3.7 – Effect of enzyme dosage (%) on lipid recovery.

One of the main advantages of this method is the use of water as solvent, although the chloroform/methanol solvent system was found to be the best from other studies (Sheng et al., 2011) for lipid extraction, but its toxicity is something to consider especially for large industrial consumption. In this method (EAEP) milder operating conditions (ambient T and P) were used and the use of ultrasound enhanced the breakage of the cells.

Efficacy was confirmed with investigations by SEM (Figure 3.8).

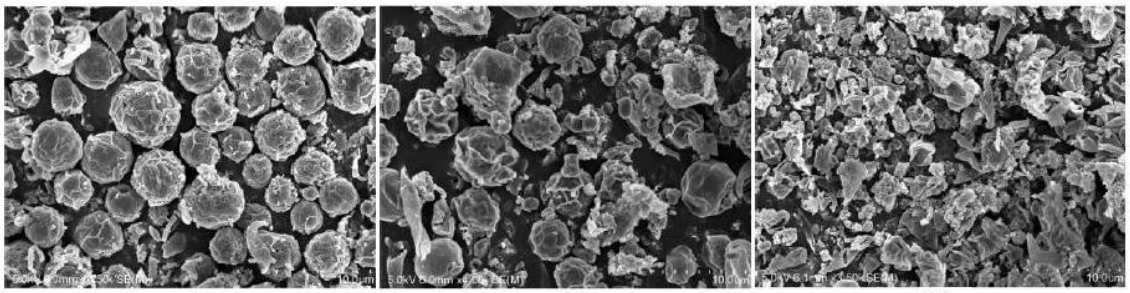

Figure 3.8 – *Chlorella vulgaris*: untreated (A), ultrasound treated (B), treated with ultrasound and snailase (C).

The optimized EAEP treatment was subsequently verified on two other microalgal species (*Scenedesmus dimorphus* and *Nannochloropsis* sp.). Results are reported in Table 3.4, with the detail of the lipid classes.

Differences in the extraction yield depended on the different lipid composition of the three species, in particular in terms of neutral lipids. Neutral lipids are formed by a hydrophobic core surrounded by a monolayer of phospholipids and are more easily removed with the EAEP process. On the other hand, glycolipids and phospholipids are polar and hydrophilic molecules that disperse more easily in the aqueous phase, moving with more difficulty in the organic phase. The process was found to have a low yield for *Nannochloropsis* sp., due to the low quantity of neutral lipid content in the microalgae used for this study.

Table 3.4 – Content, classification and lipid recovery of different microalgal species.

Species	Lipid content (% dw)	Lipid classes (% total lipids)			Lipid yield (%)	Lipid classes by EAEP (% extracted lipids)		
		Neutral	Glycolipids	Phospholipids		Neutral	Glycolipids	Phospholipids
Chlorella vulgaris	15.11	66.88	26.30	6.82	49.82	72.29	25.28	2.43
Scenedesmus dimorphus	10.62	65.09	31.75	3.16	46.81	71.51	27.47	1.02
Nannochloropsis sp.	15.98	52.95	44.20	2.85	11.73	60.57	38.51	0.92

Wang e al. (2015) studied the effect of various pre-treatment on the extraction of lipids from microalga *Neochloris oleoabundans*. They employed ultrasonication, high-pressure homogenization, enzymatic hydrolysis and the combination of enzymatic hydrolysis with high-pressure homogenization and ultrasonication. Cell morphology before and after disruption was assessed by transmission electron microscopy (TEM) (Fig. 3.9).

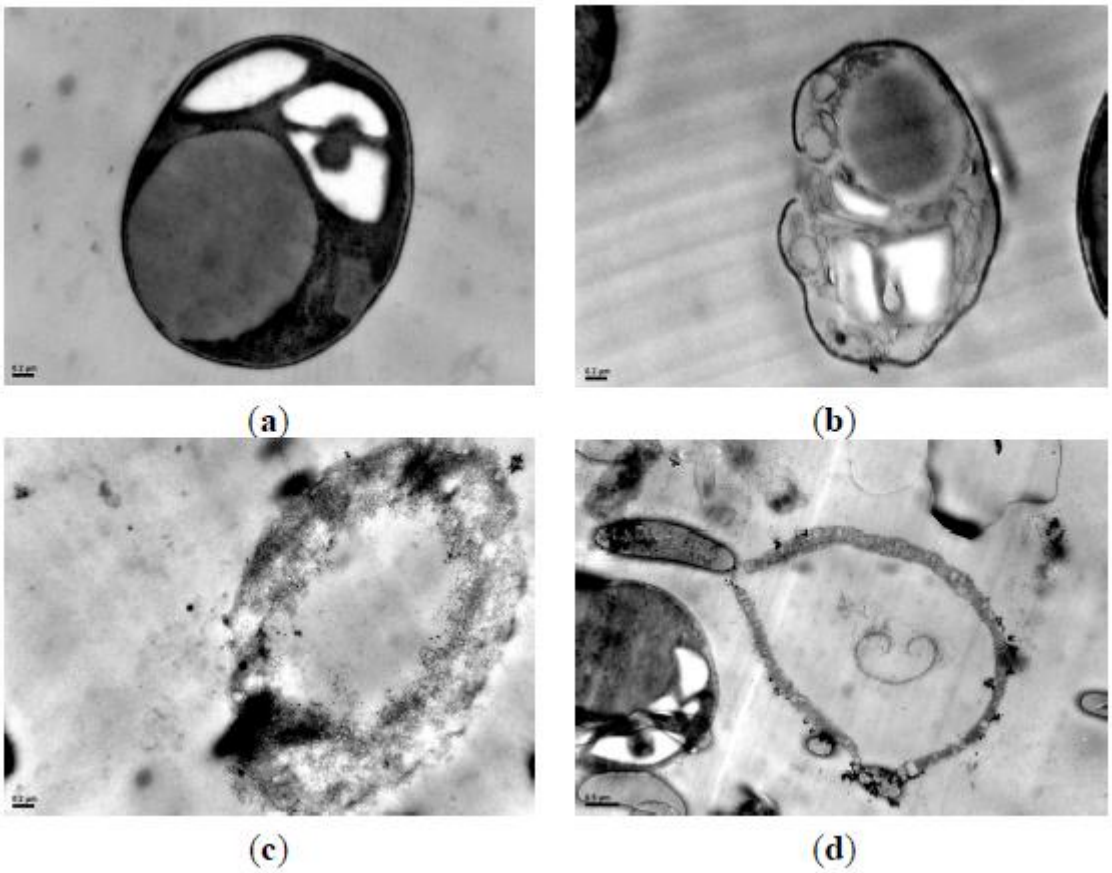

Figure 3.9 – Transmission electron microscopy (TEM) images of algae cell before and after disruption. (a) TEM image of an intact cell of *Neochloris oleoabundans* (40,000×); (b) TEM image of an algal cell disrupted with ultrasonic wave (40,000×); (c) TEM image of an algal cell disrupted with high pressure homogenization (40,000×); and (d) TEM image of an algal cell disrupted with enzymatic hydrolysis (25,000×).

The highest disruption degree was achieved by the combination of enzymatic hydrolysis and high-pressure homogenization, with a lipid recovery of 92.6%. Among enzymatic disruption process, combined use of cellulase and protease provided higher disruption efficiency than either of the two enzymes solely.
The combination of enzymatic treatment and mechanical technique gave higher disruption efficiency than any sole process.

Zheng et al. (2016) described a novel and highly efficient approach to enhance enzymatic disruption of *Chlorella protothecoides* cell walls to recover the lipid contents and cell wall compositional sugars, using thermoresponsive polymers, such as poly-(N-isopropylacrylimide-co-allylamine). Cell disruption was increased from 22% with only cellulase treatment to 68% (Fig. 3.10), with equivalent increases in lipid recovery (59%, Fig. 3.11), using 10 % (mol) amine copolymers with a loading of 0.05 g/g algal biomass dry weight. During this process, about 50% of dry algal cell wall was converted to reducing sugars.

Results indicated that polymers were also able to disrupt microalgal cell walls for lipid extraction without enzymes, but unable to hydrolyze cell walls. With the presence of pNcAA-10, 68% and 33% cell disruption can be achieved with and without enzyme, respectively, resulting in lipid and reducing sugar yields of 59% and 50% (g/g, reducing sugar/dry algal cell wall, Fig.3.12).

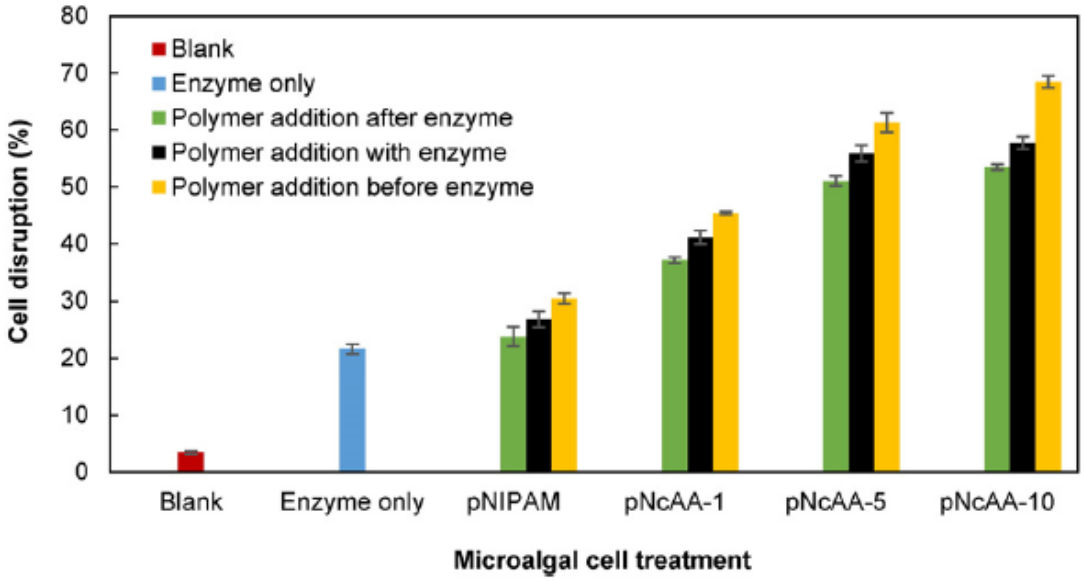

Figure 3.10 – Effect of polymer composition (amine mol-%) and addition sequence on enzymatic microalgal cell wall disruption. Algae concentration = 10 mg/mL, enzyme loading = 6% (g enzyme/g total working weight, equivalent to 0.1 g EP/g $_{BDW}$), polymer loading = 0.2 g/g $_{BDW}$, pH= 4.8, mixing speed= 120 rpm, and mixing time = 6 h at 30 °C.

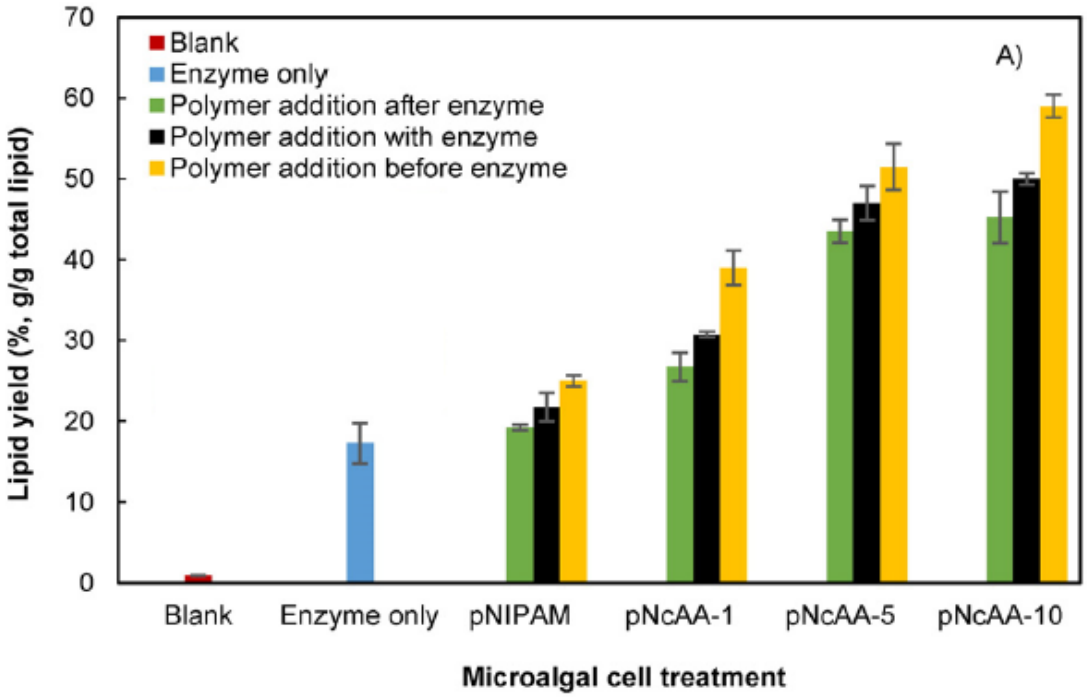

Figure 3.11 – Lipid yield from different treatments. In each treatment, algae concentration = 10mg/mL, enzyme loading = 6%, polymer loading = 0.2 g/g $_{BDW}$, pH = 4.8, mixing speed = 120 rpm, and mixing time = 6 h at 30 °C.

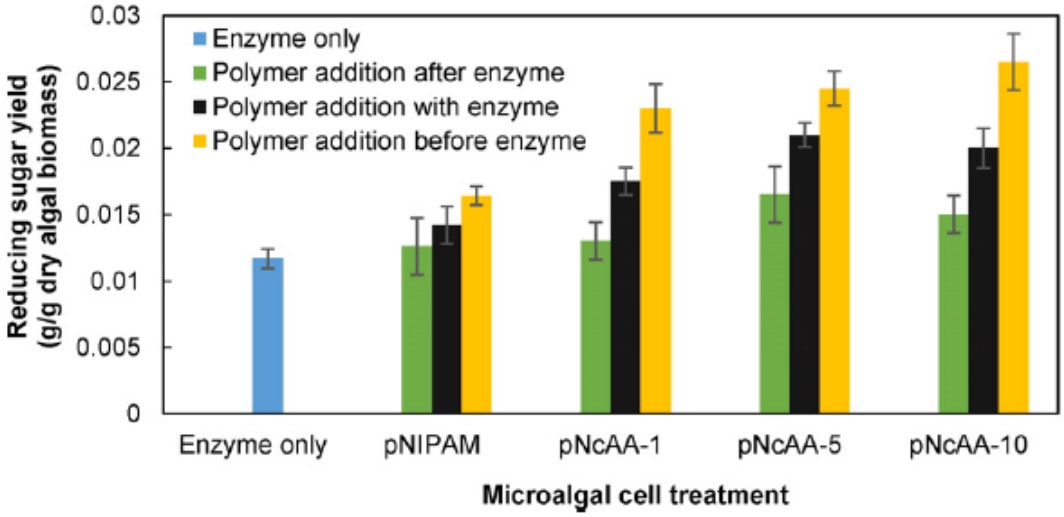

Figure 3.12 – Reducing sugar generation during enzymatic disruption of microalgal cells with and without polymers. In each treatment, algae concentration = 10mg/mL, enzyme loading = 6% (g enzyme/g total working weight, equivalent to 0.1 g EP/g $_{BDW}$), polymer loading = 0.2 g/g $_{BDW}$, pH = 4.8, mixing speed = 120 rpm, and mixing time = 6 h at 30 °C.

The use of polymers in addition to enzymes resulted in faster cell disruption with higher breakdown efficiency for improved lipid yield (Fig.3.13).

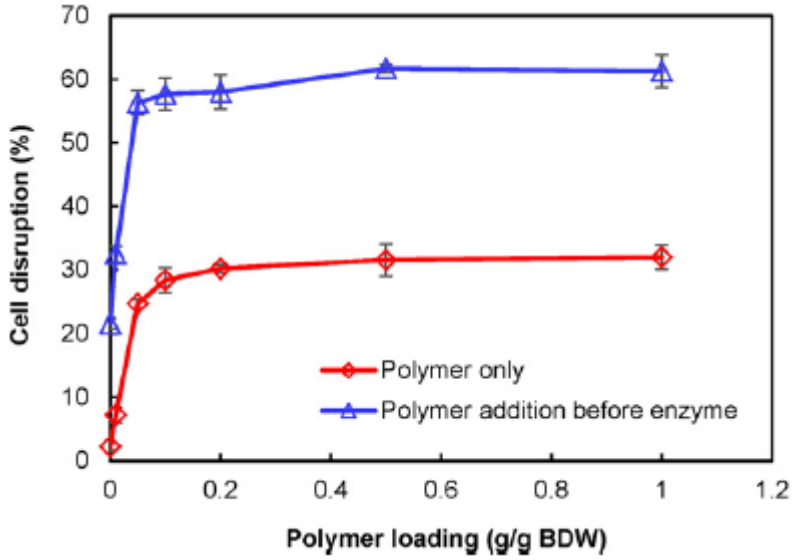

Figure 3.13 – Effect of polymer loading on microalgae cell disruption. The polymer was added into cell suspension 1 h before enzyme. Enzyme loading = 6% (g enzyme/g total working weight, equivalent to 0.1 g EP/g $_{BDW}$). Algae concentration = 10 mg/mL, pH = 4.8, mixing speed = 120 rpm, and mixing time = 6 h at 30 °C.

The polymer was shown to act by:

- stressing and disrupting the cell wall to improve the susceptibility to enzyme cleavage;
- protecting the enzyme from denaturation.

This bibliographic analysis is the evidence that better hydrolysis efficiency is obtained using combined pretreatments or an enzyme mixture instead of using a single enzyme. Additionally, it is more technically and economically feasible to obtain an enzymatic extract of one or more hydrolytic microorganisms than purified enzymes. This is due to the fact that the presence of side activities could enhance cell disruption.

3.3 *Nannochloropsis* sp.

3.3.1 Features and applications

Nannochloropsis is a genus of alga of the phylum *Heterokonta* (class *Eustigmatophyceae*), comprising 6 known species:

- *Nannochloropsis gaditana*
- *Nannochloropsis granulata*
- *Nannochloropsis limnetica*
- *Nannochloropsis oceanica*
- *Nannochloropsis oculata*
- *Nannochloropsis salina*.

These species have mostly been known to live in marine environment but some of them can live in fresh and brackish water. All species are small, nonmotile spheres which do not express any distinct morphological feature (Fig. 3.14). They have a diameter about 2 to 3 micrometers and a very simple ultrastructure with reduced structural elements compared to neighbouring taxa.

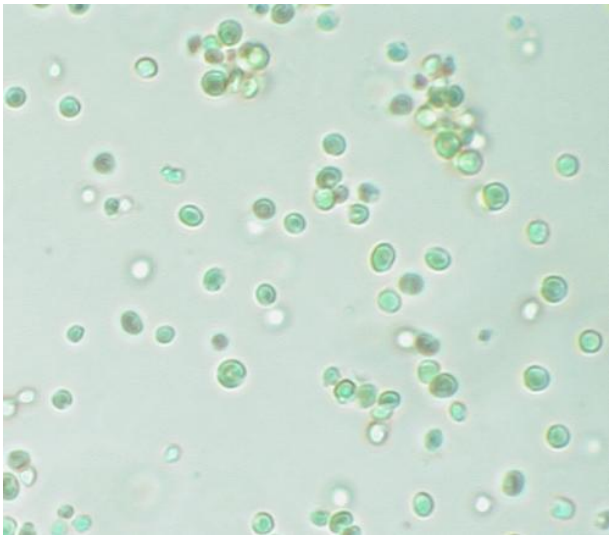

Figure 3.14 – *Nannochloropsis* viewed under a light microscope.

The algae of the genus *Nannochloropsis* differ from other related microalgae in the fact that they have chlorophyll “a” and completely lack chlorophyll “b” and “c”. In addition, they are able to accumulate high concentrations of a range of pigments such as astaxanthin, zeaxanthin and canthaxanthin.

At the moment, it is mainly used as an energy-rich food source for fish larvae and rotifers. Nevertheless, *Nannochloropsis* is considered a promising alga for industrial applications because of its ability to accumulate high levels of polyunsaturated fatty acids. In fact, it has been shown that marine *Nannochloropsis* species are suitable for algal biofuel production because of their ease of growth and high oil content (28.7% of dry weight), mainly constituted of unsaturated fatty acids, with a significant percentage of palmitic acid (Fig. 3.15). It also contains enough unsaturated fatty acid linolenic acid and polyunsaturated acid (>4 double bonds) for a quality biodiesel. Moreover, it shows promising features that can allow genetic manipulation aimed to improve the features of oleaginous strains currently used (Corteggiani Carpinelli et al., 2014).

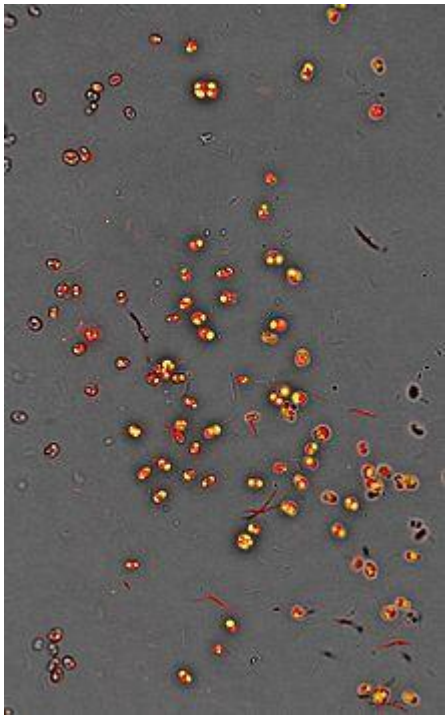

Figure 3.15 – Oil accumulation in *Nannochloropsis* cultures. In red the chlorophyll, in yellow the oil.

Laboratory productivity numbers have been extrapolated to calculate potential lipid yields in comparison with other algae and to other biofuel production platforms (Fig. 3.16).

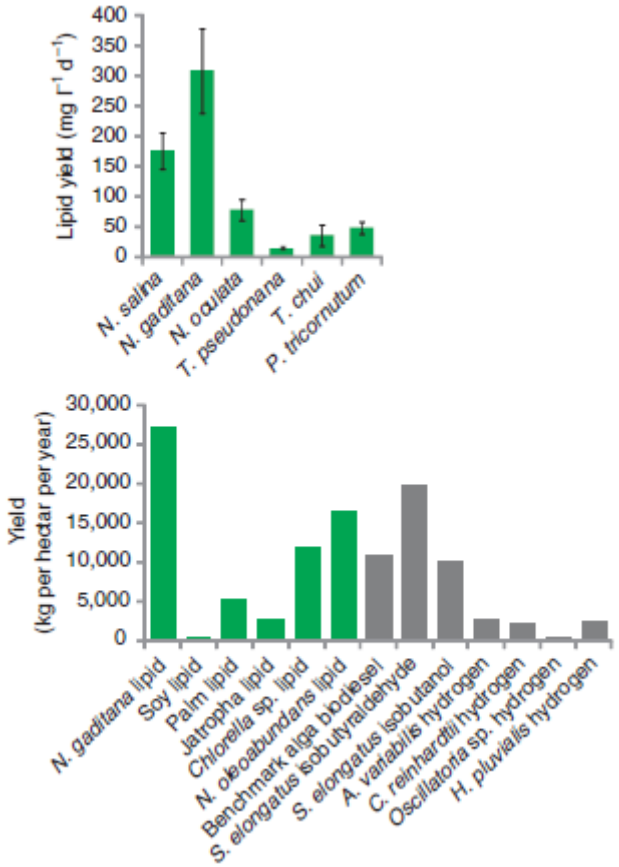

Figure 3.16 – Up: Comparison of *N. gaditana* lipid production rates with other algae examined in this work. Values are from at least three separate experiments and error bars show the standard deviation. Bottom: Comparison of *N. gaditana* large-scale production rates with other biofuel production platforms.

N. gaditana lipid production yields have been derived from small scale cultures with 12 h light/12 h dark cycles and therefore provide a more realistic estimation. Robust lipid yields were obtained from *Nannochloropsis* from 25 mL scale cultures to 8 L cultures, under laboratory conditions, and from 10-hectare outdoor ponds, where this microalga is grown on a commercial scale by Hairong Electric Company and Seambiotic (Radakovitset al., 2012).

3.3.2 Biochemical composition

Nannochloropsis is rapidly emerging as a model organism for the study of biofuel production in microalgae, but, being a relatively new model organism, it is still very poorly characterized (Corteggiani Carpinelli et al., 2014).
Biomass composition and productivity of *N. Gaditana* is shown in Fig. 3.17 (Radakovitset al., 2012).

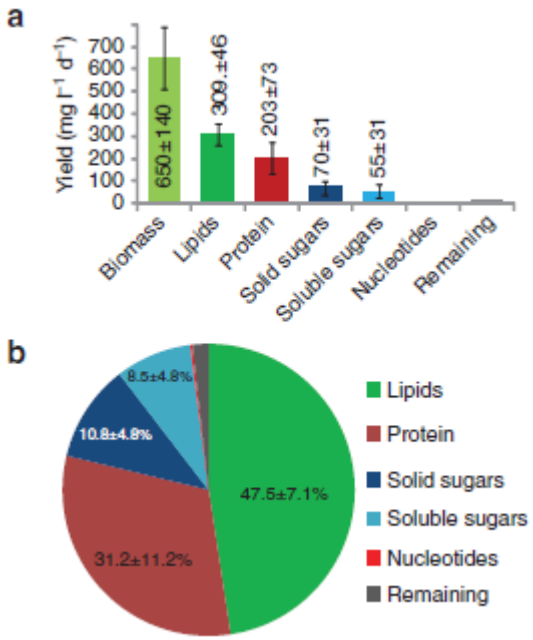

Figure 3.17 – Biomass production by *N. gaditana*. (a) *N. gaditana* production of biomass, lipids, protein and sugars quantified during continuous growth over a period of 3 months in 50 % salinity seawater medium supplemented with nitrate, phosphate and CO_2 with continuous 1,000 µE light. (b) Chart illustrating collected biomass compositions, the majority of which consists of lipids. Inset values show percentage of total biomass.

Nannochloropsis cells are embedded in a thick cell wall. Characterization of this external layer is of primary importance for biotechnological applications, but its composition is yet to be determined.

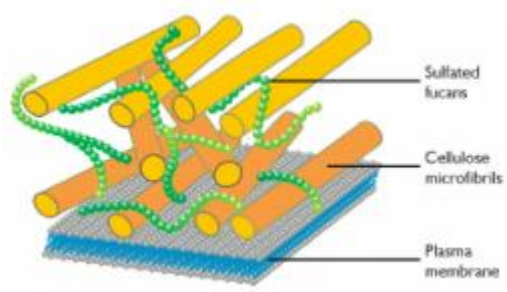

Figure 3.18 – Cell wall structure of *N. gaditana*.

Corteggiani Carpinelli et al. (2014) sequenciated *Nannochloropsis gaditana* genome. They found two cellulose synthases indicating that the wall may contain a certain amount of cellulose. Cellulases and xyloglucan-specific endo-β-1,4-glucanase were also found likely to be involved in remodeling and expansion of cell wall during growth. Moreover, there is evidence of the presence of sulfated fucans in the cell wall of *Heterokonts* (Fig. 3.18).

Brown (1991) determined the biochemical compositions of 16 species of microalgae commonly used in mariculture, one of which was *Nannochloropsis oculata*. However, sugar composition of microalgal polysaccharides showed major differences among species and classes. Glucose was the principal sugar (68%), along with about 4 to 8% each rhamnose, mannose, ribose, xylose, fucose and galactose.

Volkman et al. (1993) assessed the biochemical composition of four strains of *Nannochloropsis* (*N. salina* CS-190 from Scotland, two strains of *N. oculata* CS-179 and CS-216 from Japan and an unnamed eustigmatophyte CS-246 isolated from Queensland waters that appears to be closely related to *N. oculata*) to establish main features for chemotaxonomic studies. Gross compositional features were similar: total carbohydrate ranged from 5.2% (*N. oculata* CS-179) to 8.9% (*N. salina*) of cell dry weight. Glucose was the principal polysaccharide sugar (45.2–66.2% of total sugars). Other sugars included fucose, galactose, mannose, rhamnose, ribose and xylose (2.0–14.0%). Arabinose was a minor constituent in all species (0.6–1.7%). Protein varied from 17.8% (*N. salina*) to 22.1% (*N. oculata* CS-216) of the cell dry weight. The major amino acids were arginine, glutamate, and asparatate (7.2–10.4% of total amino acids), with methionine, cystine, histidine, tryptophan, hydroxy-proline, ornithine and γ-aminobutyric acid much less abundant (0.03–2.6%). Chlorophyll “a” ranged from 0.6% (*N. oculata* CS-216) to 1.7% (*N. oculata* CS-179 and *N. salina*) of cell dry weight. Chlorophylls “b” and “c” were not detected. All strains contained a characteristic pattern of carotenoid pigments, which included violaxanthin, β-carotene, zeaxanthin and a pigment tentatively identified as vaucheriaxanthin-ester.

Vieler et al. (2012) characterized neutral carbohydrates in the alcohol-insoluble residue (AIR) of *Nannochloropsis oceanica* (strain CCMP 1779) cell extracts. This residue, enriched in cell wall material, was hydrolyzed with trifluoroacetic acid (TFA) followed by Saeman hydrolysis. Authors observed that nearly 9% of the AIR was constituted by carbohydrates, 90% of which was glucose, 3.5% mannose, and the rest traces of rhamnose, fucose, arabinose, xylose, and galactose.
These results show that *Nannochloropsis* lacks the polysaccharide diversity associated with land plants or other heterokonts. Glucose can be a component of several types of polysaccharides, including storage polysaccharides, such as starch and laminarin (a β-1,3-glucan), and structural polysaccharides, such as hemicelluloses and cellulose. In two other heterokonts, oomycetes and brown

algae, cellulose and laminarin are the main structural and storage polysaccharides, respectively.
The subsequent treatment of the residue with endoglucanase II, a hydrolyzing enzyme specific for β-1,4-linked glucans, liberated 85% of glucose, while laminarinase, an enzyme that hydrolyzes β-1,3- glucans, liberated 20% of glucose.

Dong et al. (2016) determined the carbohydrate composition of *Nannochloropsis granulata*. Biomass underwent to acid hydrolysis (sulfuric acid, 72%wt) and then it was autoclaved for 1 h at 121 °C. After cooling, the sample was neutralized to pH 6–8 using calcium carbonate and filtered through a 0.2-μm nylon membrane filter for HPLC analysis. The carbohydrate composition was tested with a calibration range of 0.05 g/L to 6 g/L for cellobiose, glucose, xylose, galactose, arabinose, fructose, and mannose. The results of the process indicated the release of monomeric sugars for fermentation, primarily glucose and mannose ($9\%_{DW}$).

Nannochloropsis cell wall also contains an outer layer composed by algaenans, which likely encompass several lipid-related species. Algaenans are highly resistant to alkali/acid hydrolysis and aqueous/organic solubilization. Literature studies indicate that *Nannochloropsis* algaenan comprises long-chain aliphatic hydrocarbons that are subjected to ether cross-linking reactions.

Scholz et al. (2014) used quick-freeze, deep-etch electron microscopy, Fourier transform infrared spectroscopy, and carbohydrate analyses to characterize the architecture of the *Nannochloropsis gaditana* (strain CCMP 526) cell wall, whose recalcitrance presents a significant barrier to extraction of target compounds. The data indicate a bilayer structure consisting of a cellulosic inner wall (nearly 75% of the mass balance) protected by an outer hydrophobic algaenan layer (Fig. 3.19).

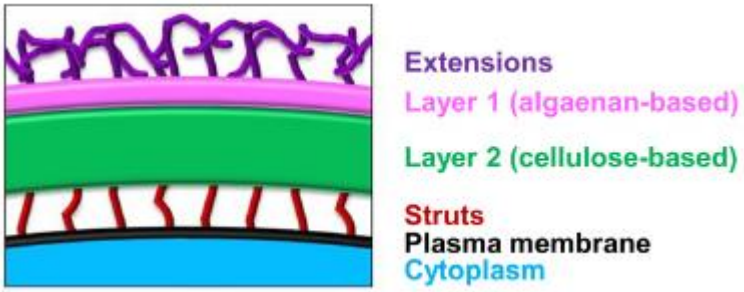

Figure 3.19 – Model of the *Nannochloropsis gaditana* wall proposed by Scholz et al. (2014).

Since cellulose and hemicelluloses (in particular, mannans) are the main constituents of the cell wall of *Nannochloropsis*, it would be possible to

hypothesize, according to the composition of monosaccharides, the type of hemicellulose and, therefore, the more appropriate enzyme.

3.4 Enzymatic degradation of *Nannochloropsis* sp.

Scholz et al. (2015) performed enzymatic degradation of *Nannochloropsis gaditana* to characterize the composition of the cell wall. Several pure enzymes (from Sigma Aldrich or Serva) were tested for their ability to deconstruct pressed walls from cultures grown in f/2 medium (Table 3.5).

Table 3.5 – Monosaccharide composition of *N. gaditana* cell walls determined after enzymatic digestion.

Enzyme	% of solubilized cell wall	% of carbohydrated	% of glucose	Other carbohydrates detected
Cellulase 1	76.0 ± 2.5	81.4 ± 8.3	98.9	Fuc, Man, Rha, GalA
Cellulase 2	71.5 ± 2.0	70.1 ± 2.0	97.2	Fuc, Gal, GalA
Chitinase	69.6 ± 6.3	64.3 ± 1.7	98.9	Fuc, GlcN, Rha, GalA
Chitosanase	11.3 ± 1.3	11.6 ± 0.5	100.0	None
Lyticase	68.9 ± 3.5	65.4 ± 4.1	99.2	Fuc, Rha, GalA
Protease	9.9 ± 6.2	1.1 ± 0.2	28.5	Fuc, GlcN, Man, Rha, GalA
Zymolyase	71.0 ± 2.2	71.7 ± 3.5	99.9	Fuc, GlcN

Two cellulase formulations, cellulase 1 (Sigma) and cellulase 2 (Serva), were the most effective, hydrolyzing up to 76% of the cell wall mass. Cocktails containing additional enzymes (chitinase and lyticase) in combination with these cellulases failed to liberate additional biomass. With the exception of the protease treatment, 98 to 99% of the sugar released by each of these enzymes was glucose; however, lyticase and zymolase liberated the majority of the glucose in polymeric form, indicating that these enzymes were acting on cross-links and not directly on the cellulose polymer. Small amounts of rhamnose, fucose, galactose, galacturonic acid, mannose, and glucosamine were also detected after hydrolysis with 72% sulfuric acid.

The vast majority of the residues were common to cellulose, namely, 1,4–linked glucopyranosyl (78%) and terminal glucopyranosyl (8%), the latter included both reducing and non reducing terminal residues. Small amounts of 1,6–linked (3%),

1,3–linked (1.2%), 1,4,6–linked (0.6%), and 1,3,4–linked (0.5%) glucopyranosyl residues were also found; glucose accounted for 91.4% of the total residues detected. Traces of fucopyranosyl, rhamnopyranosyl, mannopyranosyl, galactopyranosyl, xylopyranosyl, and N–acetylglucopyranosyl carbohydrates were also detected.

Cell walls sequentially exposed to a cellulase and then a protease and then to HCl acid hydrolysis were analyzed by attenuated total reflectance Fourier transform infrared (ATR–FTIR) spectroscopy (Fig. 3.20).

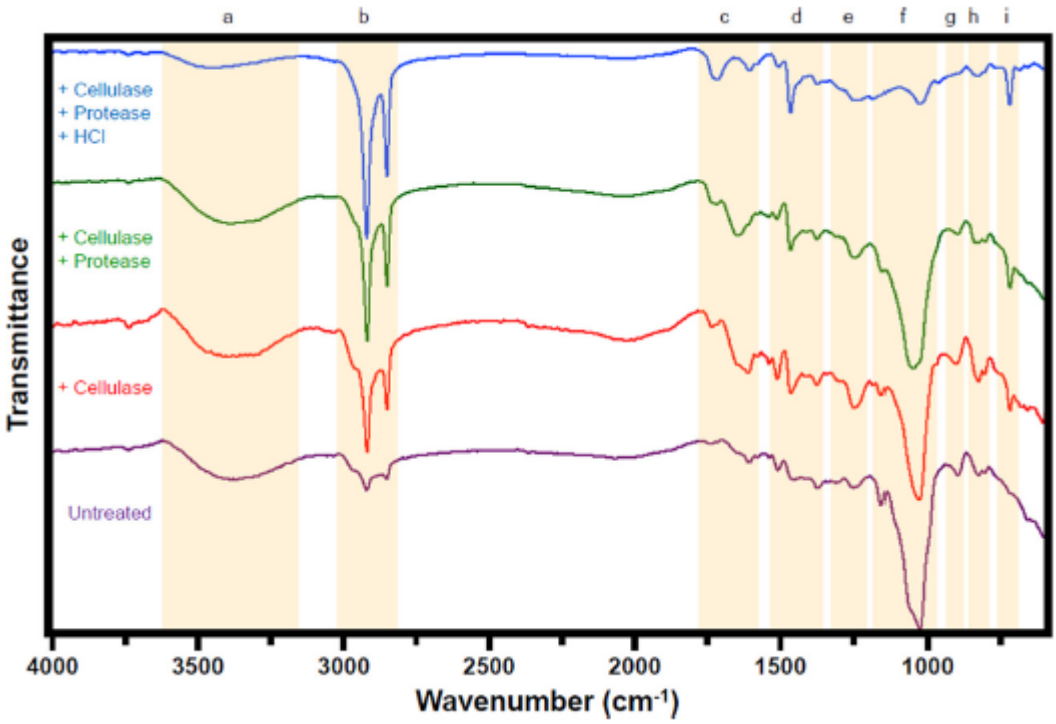

Figure 3.20 – FTIR spectra of pressed walls and following stepwise cellulase, protease and HCl digestion. Nine notable wavenumber regions (a to i) have been highlighted.

Spectra of undigested walls are dominated by chemical groups associated with carbohydrates, such as the broad band centered around 3,380 cm^{-1} (hydroxyl, H–bonded, O–H stretch), the intense band maximizing at 1,029 cm^{-1} (hydroxyl/ether, C–O stretch) and the narrow band at 1,157 cm^{-1} (glycosidic ether, C–O–C stretch). Treatment with cellulase greatly diminishes these bands, although it does not eliminate them entirely, and allows vibrational frequencies associated with the long aliphatic chains of algaenans becoming more apparent, such as intense bands at 2,920 cm^{-1} (methylene, C–H symmetric stretch) and 2,852 cm^{-1} (methyl/ methylene, C–H asymmetric stretch), plus narrow bands at 1,465 cm^{-1}

(methylene, C–H scissoring), 1,376 cm^{-1} (methyl, C–H rock) and 720 cm^{-1} [methylene, – $(CH_2)_n$, C–H rock].

Horst et al. (2012) studied an enzymatic approach for the degradation of the cell wall of *Nannochloropsis oculata*. Various classes of enzymes were examined and operating parameters were optimized. Table 3.6 shows the enzymatic effects on the integrity of the wall.

Table 3.6 – List of enzymes tested by Horst et al. (2012). (+) Samples showed a significant increase in the lipid content in the supernatant; (-) Differences between the samples tested and control were not significant.

Enzyme	*pH*	*Effect*
Viscozyme	5.0	+
Driselase	5.0	-
Papain	7.4	-
Lipase	8.0	-
Proteinase K	8.0	+

Vismozyme is a mixture of many enzymes containing a wide range of carbohydrases, which also act on the branched pectin-like substances. Driselase contains polysaccharases such as cellulase, pectinase, xylanase and β-mannanase. Papain is derived from papaya and contains many enzymes including cysteine endopeptidase, chymopapain, glycyl endopeptidase, chitinase, lysozyme, a series of proteases and cysteine, lipases and glycosidases. Lipase catalyzes the hydrolysis of the triglyceride molecules. Proteinase K has specificity for proteins.
All treatments were performed on the cell suspension in buffer solution containing the enzymes of interest at 37 °C and for 2 hours. 30 mL of culture were collected by centrifugation at 2000 xg for 10 min. The extraction was performed with heptane, hexane:IPA 3: 2 (v/v) and chloroform: methanol 2:1 (v/v). The results are shown in Fig. 3.21.

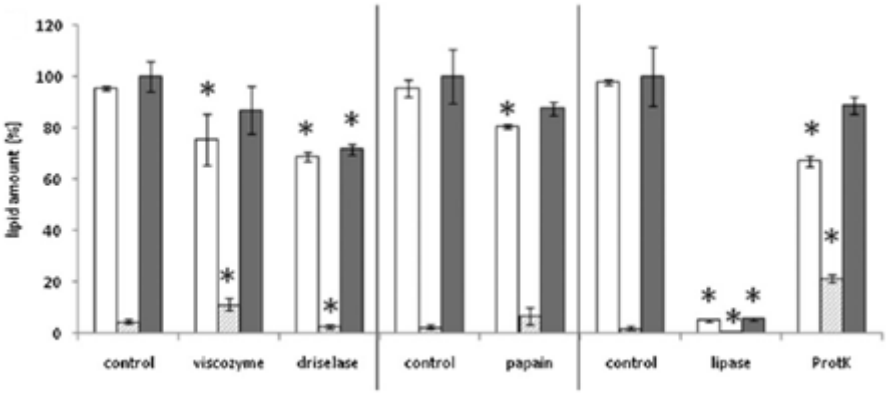

Figure 3.21 – Release of lipids using different enzymes on *N. oculata*. In dark gray the amount of lipids in the supernatant and cell pellets is reported; the asterisks indicate a significant change in lipid content.

All enzymes involved a lipid reduction on *N. oculata* pellets. Viscozyme and Proteinase K increased the lipid content in the supernatant, while lipase and driselase reduce such content. Total lipid content decreased by treating cells with driselase and lipase.

Wang and Wang (2012) used enzyme-assisted aqueous means to extract algal oil from *Nannochloropsis*. The objective of their study was to fully quantify the distribution of lipid and non-lipid biomass during aqueous enzyme-assisted processing (AEP). The four enzymes used in AEP were obtained from Genencor; their optimum conditions are given in Table 3.7. All enzymes were used under their optimum conditions.

Table 3.7 – Enzymes used in aqueous enzyme-assisted processing (AEP).

Enzyme	Commercial name	Optimum pH	Optimum Temperaure (°C)
Cellulase/Hemicellulase	Optimase CX 15L	4.6–5.0	50–60
Protease	Protease 6L	8.0–9.0	40–50
Phospholipase A2	Multifect LI 10L	8.5	40–50
Lyso-phospholipase	G-zyme G999	4.5	50

Hydrolysis reaction with cellulase/hemicellulase and lyso-phospholipase at 5% was performed for 24 h at 50 °C and pH 4.5. After the reaction, hydrolysates were

centrifuged and the supernatant was transferred to a separatory funnel for lipid extraction. Quantified lipid was designated as Lipid 1. The solid phase was dispersed into a second aqueous system at pH 8.5 and phospholipase A2 (5%) was added. The reaction performed for 4 h, followed by addition of 5% protease 6L. After 24 h, the pH of the hydrolysates was adjusted to 3.5 to precipitate the proteins followed by another centrifugation. The liquid phase was transferred to a separatory funnel for lipid extraction. The lipid in this liquid phase was extracted in the same manner as for Lipid 1 and was designated as Lipid 2. The solid phase was collected and oven-dried (105 °C for 2 h) for further lipid extraction and biomass quantification. The residual oil in the dried cake was firstly extracted twice with a 10-fold quantity of hexanes and the lipid obtained was designated as Lipid 3. The cake was then further extracted twice with a 10-fold quantity of chloroform:methanol 2:1 and the lipid obtained was designated as Lipid 4. Any residual lipid in the final cake after Lipid 3 and Lipid 4 removal was extracted by acid hydrolysis.

The same procedure was performed after that the sample was treated for 5 min with ultrasounds. Samples were then subjected to the enzymatic treatments described above.

No treatment effect (enzyme alone vs. sonication plus enzyme) was observed for the enzyme concentration and sonication conditions used, as shown in Table 3.8.

Table 3.8 – Lipid (% of total) distribution through AEP processing.

Fraction/Treatment	Enzyme	Sonication/Enzyme
Lipid 1	17.5 ± 10.9	15.2 ± 13.2
Lipid 2	8.7 ± 4.2	11.4± 4.8
Lipid 3	3.4 ± 2.7	9.3 ± 2.8
Lipid 4	19.5 ± 6.4	22.6 ± 2.1
Cake oil	35.4 ± 6.2	24.6 ± 2.6
Total lipid recovery	84.4 ± 9.2	83.1 ± 10.5

Lipid recovery in the AEP aqueous phases (sum of Lipid 1 and 2) was only 26.2% for enzyme treatment and 26.6% for sonication-enzyme treatment. More than 70% of total lipid was left in the cake, retained by other cellular components or in the intact cells. Subsequent hexanes and chloroform:methanol extraction of the residue yielded 3.4 and 19.5% of total lipid, respectively, for the enzyme treatment alone and 9.3 and 22.6% of total lipid, respectively, for sonication-enzyme treatment. Further lipid extraction from the cake by use of the acid hydrolysis procedure gave 35.4 and 24.6% of total lipid with the two treatments. These “cake” lipids were tightly bound to the solids or in the unbroken cells of *Nannochloropsis*.

Muñoz et al. (2014) designed and evaluated a microalgal pretreatment method using cellulolytic bacteria that naturally degrades microalgae in their native habitat. They selected nine bacterial strains that had endoglucanase activity: five strains from *Mytilus chilensism* and four strains from *Mesodesma donacium*. The cellulase-producing capacities of these strains were characterized and the degradation of cell walls in *Nannochloropsis gaditana* was tested with "whole-cell" cellulolytic experiments, measuring the methane production (Fig. 3.22).

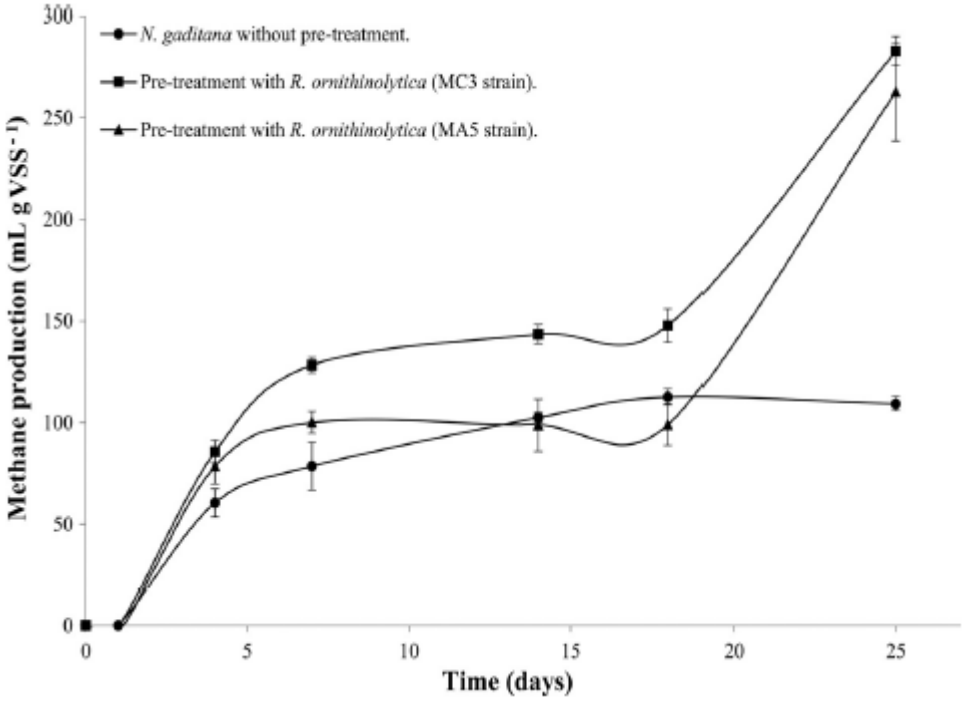

Figure 3.22 – Degradation of *N. gaditana* by a "whole-cell" enzymatic pretreatment. IC, initial cells at 0 h; FC, final cells after 72 h of pretreatment; –: negative control.

Two strains (MC3 and MA5) were used in the pretreatment assay because they degraded *N. gaditana* most effectively. After 25 days of incubation, the rate of methane production from the untreated microalgae was 109.37 ml g VSS^{-1}, whereas production from biomass pretreated with *R. ornithinolytica* strain MC3 or MA5 was 262.84 ml g VSS^{-1} or 282.92 ml g VSS^{-1}, respectively. Therefore, it was shown that a "whole-cell" cellulolytic pretreatment can increase the performance and efficiency of biogas production.

Surendhiran and Vijay (2014) carried out various pretreatment processes for nitrogen replete and depleted algal cultures of *Nannochloropsis oculata* to check the most feasible and effective technique to disrupt cells for procuring lipids. The disruption methods utilized were enzyme treatment, acid hydrolysis, ultrasonication, microwaves, autoclave and osmotic shock. Enzyme disruption was performed with cellulase from Hi Media. Cellulase enzyme solution was prepared with 0.1 M sodium citrate buffer and the enzymatic hydrolysis was carried out at 37 °C for 8 h, 10 h and 12 h. The concentration of cellulase enzyme was 5 mg L^{-1}.
The pH was adjusted to 5.5 with diluted HCl before disruption. Cellulase was inactivated by heating at 100 °C for 10 min. The amount of extracted oil was considered as an indication of the efficiency of different cell disruption methods used. A significant difference was found between the studied techniques and this study proved that all pretreatment methods were able to disrupt *N. oculata* to release intracellular lipids (Table 3.9).

Table 3.9 – Lipid content at various pretreatment processes of *N. oculata* under nitrogen rich and nitrogen starved conditions.

Pretreatment	Time	Normal growth	Nitrogen depleted growth
Control	–	26.43	40.52
Acid	1 h	31.23	48.38
	2 h	33.18	54.26
	3 h	33.18	54.26
Enzyme	8 h	29.38	45.28
	10 h	30.62	48.52
	12 h	32.74	51.68
Ultrasounds	5 min	28.14	44.16
	10 min	29.32	45.24
	15 min	30.12	45.77
Autoclave	10 min	27.68	42.39
	20 min	28.06	43.38
	30 min	28.81	43.90
Microwave	5 min	26.51	41.28
	10 min	22.88	35.36
	15 min	16.79	23.21
Osmotic shock	24 h	26.45	40.54
	48 h	26.49	40.56
	72 h	26.49	40.56

Among several methods for pretreating *N. oculata* for oil extraction, the enzymatic method gave maximum efficiency for normal culture and nitrogen depleted culture and also revealed that this method was the best for microalgal cell wall lysis. A maximum efficiency by enzymatic pretreatment was found to be at 12 h as 32.74% from nitrogen rich cultures and 51.68% under nitrogen starvation condition. Acid pretreatment gave second maximum yield. Poor efficiency was shown by ultrasonication, autoclaving, microwave oven and osmotic shock pretreatment.

Wu et al. (2017) employed different combinations of commercially available enzymes (including cellulase, protease, lysozyme and pectinase) to develop an effective method to degrade the cell wall of *Nannochloropsis* sp. for lipid extraction in association with an acid or alkaline pretreatment. They also investigated the effects of the reaction conditions including pretreatment pH, temperature, enzyme dosage and residence time. Cellulase (2000 IU/g), protease (200000 IU/g) and pectinase (20000 IU/g) were from Beijing Hongrun Baoshun Technology, while lysozyme (20000 IU/g) was from Sinopharm Chemical Reagent.

The lipid yield of enzymatic degradation, acid treatment, and alkaline treatment was 23.59%, 10.73% and 20.73%, respectively, indicating that both acid and alkaline treatment would help degrade the cell wall of *Nannochloropsis* sp. However, the lipid yield of algae under alkaline treatment was higher than under acid treatment. On the other hand, the yield increased remarkably to 54.23% by combining the alkaline pretreatment and enzymatic treatment together. They also coupled different types of enzymes in different combination. Results are shown in Table 3.10.

Table 3.10 – Effect of enzymes combinations on lipid yield. +: the enzyme was added; –: the enzyme was not added. Reaction Condition: Pretreatment pH: 9; Time: 8 h; Temperature: 100 °C; Cellulose dosage: 200 IU/g; pH: 5; Time: 10 h; Temperature: 50 °C.

Enzymes				Lipid yield
Cellulase	Protease	Lysozyme	Pectinase	(%)
+	–	–	–	54.23
+	–	–	+	55.00
+	–	+	–	56.18
+	–	+	+	61.29
+	+	–	–	66.05
+	+	–	+	68.45
+	+	+	–	69.85
+	+	+	+	73.11

The highest lipid yield was obtained when cellulase, protease, lysozyme and pectinase were added into the algae suspension simultaneously, resulting in a lipid yield of 73.11%.
Finally, they investigated the enzymatic reaction conditions, including reaction pH, time, temperature and enzyme dosage. Results are reported in Table 3.11.

Table 3.11 – Influence of enzymatic treatment conditions on lipid yield. Conditions in assays for determining the influence of pH: dosage 200 IU/g of each enzyme, 50 °C, 10 h. Conditions in assays for determining the influence of treatment time: dosage 200 IU/g of each enzyme, 50 °C, pH 4.0. Conditions in assays for determining the influence of temperature: dosage 200 IU/g of each enzyme, pH 4.0, 30 min. Conditions in assays for determining the influence of enzyme dosage: 50 °C, pH 4.0, 30 min treatment time. Before enzymatic hydrolysis, all the algae suspensions were pretreated by alkaline hydrolysis under the following conditions: 110 °C, pH 10.5, 4 h treatment time.

Influence of pH		Influence of time		Influence of temperature		Influence of dosage	
pH	Lipid yield (%)	Time (h)	Lipid yield (%)	Temperature (°C)	Lipid yield (%)	Dosage (IU/g)	Lipid yield (%)
3.5	81.03	0	47.22	35	68.31	100	85.74
4.0	87.37	0.5	87.69	40	82.66	200	90.00
4.5	82.89	1	88.00	45	89.09	300	90.13
5.0	81.94	2	87.51	50	89.63	400	89.90
5.5	80.67	4	88.55	55	82.30	500	90.36
6.0	76.87	6	88.23	60	81.89		

The highest lipid yield was obtained when the pH of the suspension was 4.0 (87.37%). The lipid yield decreased gradually to 76.87% by increasing pH to 6.0 and to 81.03% by decreasing pH to 3.5. Lipid yield increased dramatically from 47.22% to 87.69% after 30 min of enzymatic treatment, however, after 30 min of treatment; the lipid yield was essentially maintained at nearly 88%, despite even prolonging the treatment time to 6 h. The short enzymatic treatment time also confirmed that alkaline pretreatment could make it easier for enzymes to disrupt algal cell wall. The increase of enzymatic treatment temperature enhanced the lipid yield when the reaction temperature was lower than 50 °C, while it decreased at higher temperatures. The increase in enzyme dosage led to an enhancement in lipid yield, however, the lipid yield did not change substantially when the enzymes dosage was more than 200 IU/g. The optimal conditions for enzymatic hydrolysis of *Nannochloropsis* sp. cell walls were 50 °C, pH of 4.0, 30 min reaction and 200 IU/g of enzymes dosage, with a lipid yield of 90.0%.

Al-Zuhair et al. (2016) studied extraction of chlorophyll and carotenoids from lysozyme treated and untreated biomasses of *Nannochloropsis* sp. (Table 3.12). Lysozyme from chicken egg white (activity > 40,000 U mg-1) was purchased from Sigma-Aldrich. During the assay, biomass was suspended in enzymatic solution and added to phosphate buffer solution (pH 7.0). The mixture was then incubated in a water bath shaker at 37 °C for 12 hours.

Table 3.12 – Comparison between the amounts of extracted pigments from lysozyme treated and untreated biomass of *Nannochloropsis* sp.

Pigment	Untreated	Lysozyme treated
Chlorophyll "a" (mg/g)	0.11 ± 0.01	14.38 ± 0.10
Chlorophyll "b" (mg/g)	0.37 ± 0.01	3.54± 0.51
Total carotenoids (mg/g)	0.16 ± 0.00	3.8 ± 0.12

It was found that lysozyme pre-treatment significantly increased the amount of extracted pigments. This justifies the need for effective cell disruption, using lysozyme, which significantly enhanced the extraction.

Chen et al. (2016) proposed an improved aqueous extraction method combing thermal and enzymatic lysis in algal slurry of *Nannochloropsis oceanica* (96.0% moisture).
The tested enzymes were cellulose from *Aspergillus niger*, lipase (Solarbio) and protease (Novozyme).
Thermal lysis of microalgae was carried out in a laboratory autoclave at 121 °C for 20 min. For enzymatic hydrolysis, a concentrated enzyme solution was added to algal slurry at a certain concentration at a moderate temperature (25-50 °C) and pH (4-10) for variable time. Moreover, several surfactants were added singly or jointly to promote oil extraction and the optimized surfactant composition was used for aqueous extraction.
The lipid extraction efficiency obtained from aqueous extraction combined with thermal lysis (24.5%) was 3-fold the value of control experiment. However, no evident breaking of cell wall was observed, because no glucose was determined during thermal lysis process and most cells of *N. oceanica* remained intact after thermal lysis.

For enzymatic lysis, the effect of cellulose on the cell-wall disruption was better than those of protease and lipase. Thereafter, the parameters involved in enzymatic hydrolysis, including incubation time, temperature, pH, as well as enzyme dosage

and liquid/solid ratio were investigated. The optimal incubation temperature and pH in this study was 37 °C and pH 5.0.

Although a higher cell wall degradation degree was achieved at a bigger cellulase dosage (Fig. 3.23 A), 1.3% of enzyme dosage was still chosen because of efficiency and cost. With this dosage, the effect of liquid/solid ratio on cell wall degradation was also investigated (Fig. 3.23 C). A higher concentration of glucose could be detected with decrease of liquid/solid ratio, while the highest glucose yield was achieved when liquid/solid ratio was 15 mL/g. The glucose concentration increased also increasing the incubation time (Fig. 3.23 B). As a result, the optimal conditions for enzymatic lysis of microalgae *N. oceanica* were determined as a cellulase dosage of 1.3%, an incubation time of 5 h and an incubation temperature of 37 °C. Under this condition, lipid extraction efficiency increased up to 28.8%, 4-fold higher of the value of control experiment.

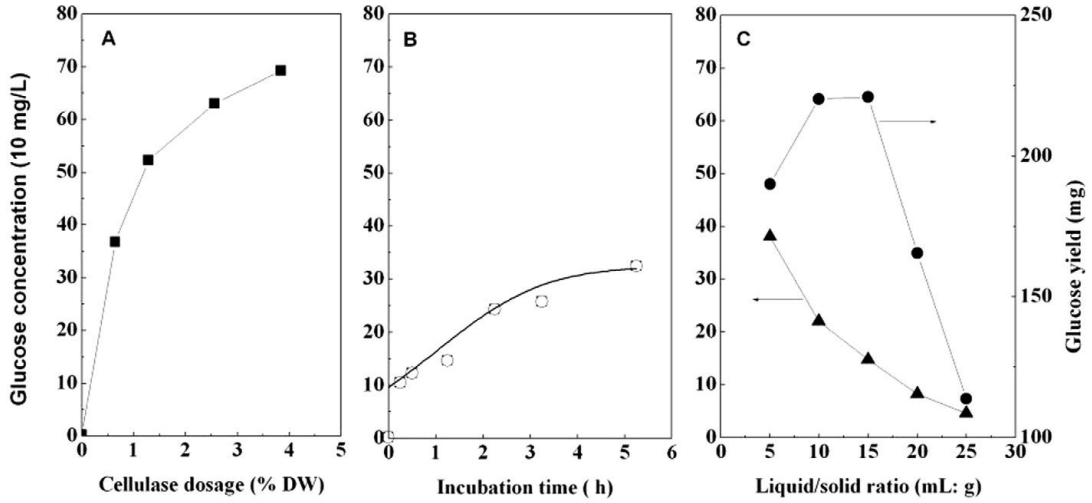

Figure 3.23 – Parameters optimization for enzymatic lysis of *Nannochlropsis oceanica*, including dosage of cellulase (A), incubation time (B) and liquid to solid (dry weight) ratio (C). The experiments were operated at pH 5.0 and 37 °C. Data are expressed as means ± SD of three replicates.

Even though the cell disruption by single thermal or enzymatic lysis showed an improvement in lipid extraction yield, the efficiency was still unsatisfying. Based on single-factor experiments, a complete factorial experiment was employed to analyze the efficiency of aqueous surfactants combining with thermal and enzymatic lysis on cell-wall disruption, lipid extraction and protein extraction from wet microalgal biomass. The experimental arrangement and the results obtained are shown in Table 3.13.

Table 3.13 – Effect of cell disruption processes on lipid and protein extraction efficiency. 1 indicates positive treatment, –1 indicates negative treatment.

Run	Thermal lysis	Enzymatic lysis	Aqueous extraction	Extraction efficiency (%)	
				Proteins	Lipids
1	–1	–1	–1	6.9 ±0.1	2.2 ±0.6
2	1	–1	–1	28.5 ±0.6	13.9 ±2.1
3	1	1	–1	53.3 ±4.2	54.6 ±5.2
4	1	1	1	62.4 ±1.9	88.3 ±0.8
5	–1	1	–1	26.1 ±0.1	18.7 ±5.3
6	–1	1	1	29.9 ±0.0	28.8 ±0.0
7	–1	–1	1	12.6 ±2.3	7.2 ±2.4
8	1	–1	1	31.8 ±0.6	24.5 ±1.5

Lipid extraction efficiency for combined cell lysis prior to aqueous surfactant extraction (88.3%) was significantly higher than that for either single thermal lysis process (24.5%) or single enzymatic lysis process (28.8%). Remarkably, a similar situation occurred in the case of using water rather than surfactant as extraction medium. These results confirmed that the two cell lysis processes have a synergistic effect on cell-wall disruption.
This method possesses many advantages over other methods, for example, direct acting on algal slurry containing 96.0% of moisture, non-toxic characteristic compared to organic solvents, co-extraction of both lipids and protein in a single extraction process, lowing extraction cost and enhancing economic success.

With the increasing interest in using algae for producing biofuels, new cost-effective cell disruption procedures have to be developed in order to overcome problems associated with traditional expensive pretreatment methods, such as enzymatic disruption.

Cellulases are the most studied and applied to microalgae and, specifically, to *Nannochloropsis* sp. Despite this, reports suggest that the combined use of enzymes with other activities, such as hemicellulases, proteases and chitinases, are of equal priority, mainly for those microalgae that are highly abundant in recalcitrant materials.

CHAPTER 4

Enzyme-assisted lipid extraction from *Nannochloropsis* sp.

In this chapter, experimental results obtained for lipid extraction after an enzymatic pre-treatment of *Nannochloropsis* sp. microalgae are shown.
In the first part, a "screening" of commercial enzyme preparations has been carried out in order to identify the preparations most active in the disintegration of the cell wall. All assays were performed under the same experimental conditions. The screening was conducted only on commercial low cost enzyme preparations, specifically formulated for food applications, such as the brewing, food, animal feed industry, etc.
On the basis of screening results, three mixtures of commercial enzyme preparations were chosen. Performances of these enzyme cocktails were studied through the use of the method of *mixture design*, with the aim of obtaining an optimal composition of the pretreatment solution to be used for further experiments. Subsequently, the influence of the most important process parameters on the yield of lipid extraction was analyzed. These experiments were carried out using the pretreatment mixture

with optimized composition. Four parameters (pretreatment time, enzymes to biomass ratio, pH and temperature of pre-treatment) were taken into account and a *factorial design* has been identified with the purpose to analyze their effect on the yield of lipid extraction. In a second phase, the influence of the dosage of the two chosen enzyme preparations was evaluated individually and times of pretreatment and extraction have been modified.
By using the *Design Expert* software, regression models were built from the values obtained in the experimental design through the methodology of response surfaces. This statistical analysis technique is useful to visualize the influence of the various parameters taken into account.
Finally, the optimal pretreatment conditions were identified by means of numerical optimization of the model obtained, in terms of extraction yield and cost of the pretreatment. These points have been experimentally verified and used, together with other points inside and outside the experimental region, to validate the regression model. The recovery of the enzyme pre-treatment solution for the re-use in subsequent cycles was also evaluated to lower the operating cost.

4.1 Materials and methods

4.1.1 Microalgae

Nannochloropsis sp. was provided in lyophilized form by the Department of Agri-Food Production and Environmental Sciences of the University of Florence (Italy).
Nannochloropsis sp. F&M-M24 was cultivated outdoors under nitrogen deprivation during summer in a 590-L, 10 m-long, 1 m-high, Green Wall Panel (GWP), placed facing South. The cultivation was carried out for seven days in a semi-continuous mode adopting a 44% daily dilution rate, with the exception of the first and the last two days of the experiment, in which the culture was not diluted (Bondioli et al. 2012).
The fatty acid composition of the different lipid fractions of the starved *Nannochloropsis* F&M-M24 biomass together with the corresponding iodine value is shown Table 4.1 (Bondioli et al. 2012).

In all fractions, 16-carbon fatty acids were predominant, being as high as 75% of the total fatty acids in neutral lipids, 51% in polar lipids and 31% in phospholipids. Unsaturated fatty acids largely prevail in polar lipids (63%) and, particularly, in phospholipids (73.5%). Neutral lipids contain a similar amount of unsaturated and saturated fatty acids. Eicosapentaenoic acid (EPA, 20:5 n3), which represents 19-22% of the fatty acids in both phospholipids and polar lipids, is 3.3% in neutral lipid fraction.

Table 4.1 – Fatty acid composition (%) of three different lipid classes (neutral-, polar- and phospho-lipids) of nitrogen starved *Nannochloropsis* sp. biomass (Bondioli et al. 2012).

Fatty acid	Lipid class		
	Neutral	Polar	Phospholipids
C14:0	4.39	5.36	2.51
C16:0	44.49	30.10	22.20
C16:1 n-7	30.54	21.36	9.28
C18:0	1.37	1.56	1.80
C18:1 n-7 + n-9	12.83	13.73	23.62
C18:2 n-6	1.10	4.05	6.68
C18:3 n-3	0.23	0.00	1.26
C18:3 n-6	0.00	0.78	0.32
C20:2	0.02	0.00	0.00
C20:3 n-6	0.32	0.00	0.78
C20:4 n-6	1.39	1.40	12.29
C20:5 n-3	3.32	21.65	19.26
Total saturated	50.25	37.02	26.51
Total monounsaturated	43.37	35.09	32.90
Total polyunsaturated	6.38	27.88	40.59
Iodine Value ($gI_2/100g$)	61.5	129.2	164

It is to mention that the iodine value of 61.5, calculated for the neutral lipid fraction of starved *Nannochloropsis* biomass, is significantly lower than the limit established by the EN 14214. However, the polyunsaturated fatty acid (PUFA) content exceeds the established limit of 1% (EN 14214 Standard), but this problem can be easily solved separating the biodiesel fractions by means of fractional distillation (Bondioli et al. 2012).

4.1.2 Chemicals and enzymes

Methanol (CAS No. 67-56-1), isopropanol (CAS No. 67-63-0), chloroform (CAS No. 67-66-3), hexane (CAS No. 110-54-3), sodium chloride (CAS No. 7647-14-5), hydrochloric acid (37 wt%, CAS No. 7647-01-0) and sodium hydroxide (CAS No. 1310-73-2), all of analytical grade, were purchased from Carlo Erba (Milano, Italy).

Lysozyme was obtained from EPS SPA (Rovigo, Italy). All other enzyme preparations used were obtained from Lyven SA (Colombelles, France) and were stored in the dark at a temperature of 4 °C. For the preparation of the enzymatic aqueous solutions, demineralized water (Carlo Erba) was used.

These enzyme preparations were selected on the basis of the characteristics of the cell wall of *Nannochloropsis* and the bibliographic study, reported in Chapter 3. Their main enzyme components and activities indicated by the manufacturer are listed in Table 4.2.

Enzymes of Cellulyve family are used in pharmaceutical, cosmetic and food applications for the extraction of active substances with a high value (antioxidants, food dyes, oligosaccharides, lipids, glycoproteins, and vitamins), thanks to the degradation of the cell wall by means of cellulases, hemicellulases, pectinase and protease.

Enzymes of Feedlyve family are used to hydrolyze the polysaccharides into simple sugars, releasing cell wall nutrients (proteins, amino acids, minerals) and reducing the intestinal viscosity for animal feed application.
In particular Feedlyve AXC and Feedlyve AGL improve the efficiency, reduce intestinal viscosity and increase the performance of poultry feed. Instead, Feedlyve GMA and Feedlyve α-Gal are enzymes specific for the digestion of polysaccharides containing no starch, such as soy flour, rich in galactomannans and α-galactosides, thereby improving the energy content and the availability of amino acids from soy flour used for chickens and pigs.

They are used for the production of beer. Filterlyve AXC 1500L and Filterlyve PEM are proteolytic enzymes used in the treatment of malt and barley for brewing. The Superlyve SH is particularly suitable for increasing the filterability of the beer.
For enzyme preparations of Filterlyve family, the optimal temperature and pH ranges are not provided by the manufacturer.

4.1.3 Determination of total lipid content

Total lipid content of *Nannochloropsis* was determined by the method of Ma et al. (2013) with slight modifications. Specifically, 0.2 g of biomass were mixed with 18 mL of chloroform/methanol (2:1, v/v) and stirred at 37 °C for 1 h (Kika Werke 10 power). Then, the mixture was centrifuged at 10,000 ×g for 10 min (Centrifuge MPW 380, Med. Instruments, Poland), the supernatant collected and the residual biomass re-extracted two more times under the same conditions. The three supernatants were combined and a 1% sodium chloride solution (20% of the total volume) was added. After 10 min stirring at 37 °C, the mixture was centrifuged (10,000 ×g, 10 min), the organic phase recovered and evaporated under vacuum at 40 °C (Rotavapor R-215, BUCHI Labortechnik AG, Switzerland). The lipid content was calculated from the weight of the residue and expressed as grams of lipids per 100 g of dry biomass.

Table 4.2 – Properties indicated by the manufacturer of the enzyme preparations used.

Commercial name	Biological source	Main enzymatic activity	EC number	Activity	Optimal temperature range	Optimal pH range
Cellulyve 50LC	*Trichoderma resei*	Cellulase (active on native cellulose)	3.2.1.4	≥ 240 U/g	45-60 °C	4-6
Cellulyve AN 1500L	*Aspergillus niger*	β-glucanase, cellulase, β-mannanase	–	–	40-50 °C	3.5-5.5
Peclyve EXG	*Aspergillus niger*	Pectinase, xylo-glucanase	–	–	40-55 °C	4-6
Feedlyve AXC	*Aspergillus niger*	Xylanase	3.2.1.8	≥ 1500 U/g	50-58 °C	4.7-5.8
Feedlyve AGL	*Aspergillus niger*	β-glucanase	3.2.1.6	≥ 1500 U/g	45-55 °C	4.6-5.2
Feedlyve GMA	*Aspergillus niger*	Galacto-mannanase	3.2.1.78	≥ 10000 U/g	40-60 °C	4-7
Feedlyve α-Gal	*Aspergillus niger*	Endo-1,4-β-galactanase α-galactosidase	3.2.1.89 3.2.1.22	≥ 1700 U/g ≥ 45 U/g	40-45 °C	4.5-5.5
Filterlyve AXC 1500L	*Trichoderma longibrachiatum*	Xylanasi, β-glucanase	–	–	–	–
Filterlyve PEM	*Aspergillus niger*	Thermostable β-glucanase	–	–	–	–
Superlyve SH	*Aspergillus niger*	Cellulase and hemicellulase with β-glucanase side activity	–	–	–	–
Lysozyme	Hen egg white	Lysozyme (>99%)	3.2.1.17	47500 FU/mg	–	–

4.1.4 Enzyme-assisted lipid extraction

The enzyme-assisted extraction of lipids from *Nannochloropsis* was investigated in batch mode according to the following procedure. Briefly, 0.2 g of microalgae and 20 mL of the aqueous enzyme solution were loaded into 20-mL screw-capped flasks. The flasks were placed in a thermostated water bath and magnetically stirred for the appropriate time. Then, the algal suspension was centrifuged (10,000 ×g, 10 min) and the supernatant removed. The resulting biomass was contacted with 10 mL hexane/isopropanol (3:2, v/v) and stirred at room temperature. After this time, the suspension was centrifuged (10,000 ×g, 5 min) and the amount of extracted lipids determined gravimetrically after solvent evaporation.
Results were expressed as the amount of lipids extracted per dry weight of biomass (Y_{lip}, g/100 g).

4.2 Screening of enzyme preparations

Screening tests were performed at 50 °C, pH 5, for 60 minutes, with a nominal enzyme dosage of 10 mg/g. Solvent extraction was carried out at room temperature for 60 minutes.
Each test has been carried out in duplicate and repeated in the case of sensitive variations of yields.

Table 4.3 – Yields, standard deviation and percentage errors obtained after pretreatment with the enzyme preparations tested.

Enzyme preparation	Mean Y (%)	St. Dev. Y (%)	Error (%)
Untreated	16.7	0.82	4.91
Control	22.10	1.34	6.54
Cellulyve50LC	23.41	0.43	1.23
Feedlyve GMA	37.78	0.34	0.94
Feedlyve alpha-Gal	37.22	0.22	0.59
Peclyve EXG	31.31	0.20	0.55
Feedlyve AXC	21.98	0.67	1.96
Feedlyve AGL	31.33	1.10	3.02
Superlyve SH	21.52	1.10	3.22
Filterlyve PEM	21.63	0.46	1.46
Lysozyme	21.13	1.36	4.91
Cellulyve AN	31.58	0.17	6.54

Extraction yields obtained after the pretreatment with the tested enzyme preparations are reported in Table 4.3. The respective standard deviation values and percentage change were found to be quite low, confirming the reliability of obtained data and the reproducibility of the tests.
Results of this screening are also shown in Fig. 4.1. It is possible to distinguish three different groups. The first one includes two particular enzyme preparations (Feedlyve GMA and Feedlyve Alpha Gal), both based on galactosidase, an enzyme capable of hydrolyzing the residues of galactose terminals and the fucosides, of which the specie *Nannochloropsis* is particularly rich. The pretreatment with these enzymes allowed a lipid yield of around 37%. In the second intermediate zone, there are preparations that reached a yield of around 31%. These are Cellulyve AN, rich in cellulase, beta-glucanase and beta-mannanase, Peclyve EXG, rich in pectinase and xyloglucanase, and Feedlyve AGL, rich in beta-glucanase. In the third group there are preparations that led to yields similar to the control (about 21-22%).

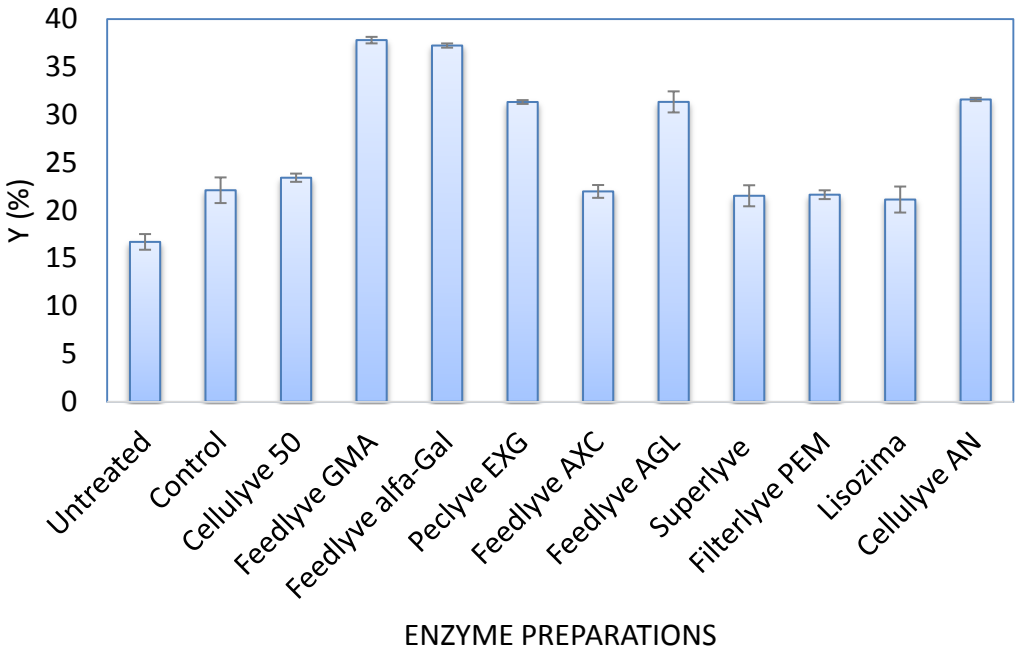

Figure 4.1 – Extraction yields as a function of the commercial enzyme preparation employed for the pretreatment.

The direct extraction with solvent mixture showed a yield of only 16%, highlighting that there is a sensitive enzymatic effect for some of the chosen enzyme preparations.

4.3 Enzyme preparations mixtures

4.3.1 Mixture design

DOE (Design of Experiments) statistical methods were used to identify the effective composition of the enzyme mixture to be employed in pre-treatment phase. The DOE technique provides an efficient way to optimize processes and can lead to interesting results when applied to formulations, as in this study. Generally, designs with factor models at two levels are used, involving the choice of all combinations of each factor to its high and low levels. When many factors are involved, DOE allows performing only a fraction of the tests to assess the main effects and interactions between the studied parameters. However, when the dependent variable measured depends on the proportions of the ingredients, as in the chemical or food formulations, the factor models may not make sense. In these cases, the use of Mixture Design can be used to optimize the formulation.
In this work, a standard mixture design, called simplex lattice design, was used. The design of the model structure is as follows: the order is defined by {q, m}, where q is the number of components and m represents the degree of the polynomial used to correlate the experimental data. The components are divided into m+1 multiples values of 1/m.
The validity of the model can be tested by the addition of q + 1 additional points (test points), which can be incorporated into the design using the same model or a more complex one to improve its accuracy. These test points are selected to be as far as possible from the experimental points of the basic model. The first of these points is represented by the centroid of the domain (1/q, 1/q, 1/q). The remaining q points are intermediate points between the centroid and each vertex of the domain. The first is given by (q+1)/2q and the remaining by 1/2q.

In this study:

q = 3 (enzyme preparations);
m = 2 (correlation polynomial degree);
test points = 4;

from which 6 axial points are generated (3 vertices representing the individual pure preparations, and 3 binary mixtures at 50% in composition) and 4 points inside the domain: the centroid with coordinates (1/3, 1/3, 1/3) and 3 points for each median of the triangle with coordinates (2/3, 1/6, 1/6), (1/6, 2/3, 1/6) and (1/6, 1/6, 2/3), as represented in Fig. 4.2.
Moreover, the three experimental points representing the pure components and the centroid were repeated in duplicate in order to estimate the pure error (i.e. the experimental error, not due to the inadequacy of the model), to study the analysis of variance (ANOVA) and evaluate the lack-of-fit. Therefore, the number of experiments for each enzyme preparations mixture is equal to 14.

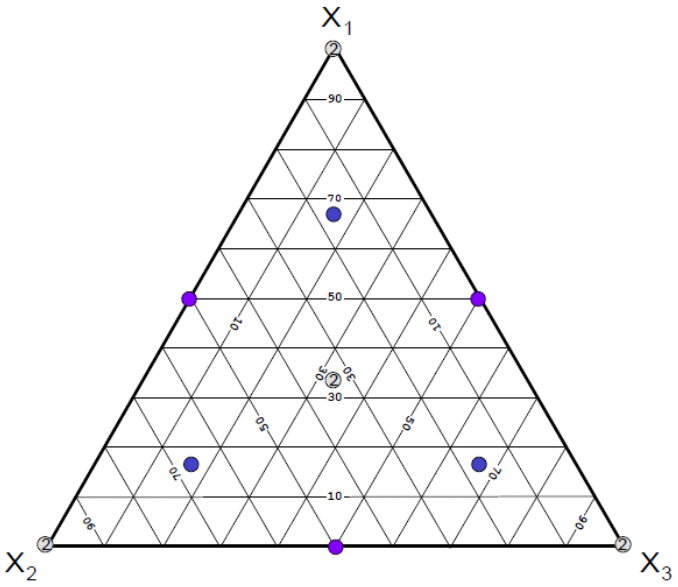

Figure 4.2 – Scheme of the simplex lattice design used.

Table 4.4 shows the 14 experimental tests carried out for each mixture of enzyme preparations.

Table 4.4 – Experimental design performed for each mixture of enzyme preparations.

Run	Weight fraction of component A	Weight fraction of component B	Weight fraction of component C
1	1	0	0
2	0	1	0
3	0	0	1
4	0.5	0.5	0
5	0.5	0	0.5
6	0	0.5	0.5
7	0.667	0.167	0.167
8	0.167	0.667	0.167
9	0.167	0.167	0.667
10	0.333	0.333	0.333
11	1	0	0
12	0	1	0
13	0	0	1
14	0.333	0.333	0.333

Ternary mixtures triangles were built with pure enzyme preparations on the vertices to better highlight the effectiveness of each class of enzyme activity and their synergistic effect. Enzyme preparations were chosen taking into account the results of the screening tests and from the composition of the cell wall of *Nannochloropsis*.
An enzyme preparation rich in cellulase (Cellulyve 50LC, third band) and one at the base of β-glucanase (Feedlyve AGL, intermediate level) were used to construct two cocktails of enzyme preparations. Cellulyve 50LC (instead of Cellulyve AN 1500L, more effective, but containing different enzyme activities) and Feedlyve AGL were chosen for the presence of individual enzyme activities of cellulase and β-glucanase. The two preparations with the highest yield were added as third components.
Moreover, a third mixture of enzyme preparations was designed, containing both more efficient preparations (Feedlyve GMA and Feedlyve alphaGAL), in order to study their possible synergistic effect, and Lysozyme was added as third component. Lysozyme was selected because, as seen in Chapter 3, evidence has been provided that this enzyme can cause growth inhibition and affect cell wall permeability of certain types of microalgae (Gerken et al., 2013). In fact, it seems able to open the cell wall by increasing its thickness, reducing its density and improving the permeability, allowing the entry of other specific enzymes. In Table 4.5 the three mixtures of enzyme preparations used are listed.

Table 4.5 – Mixtures of enzyme preparations used.

Enzyme preparation mixture	ID	Enzyme preparation	Main enzymatic activity
I	*A*	*Cellulyve 50LC*	Cellulase
	B	*Feedlyve AGL*	β-glucanase
	C	*Feedlyve GMA*	Galacto-mannanase
II	*A*	*Cellulyve 50LC*	Cellulase
	B	*Feedlyve AGL*	β-glucanase
	C	*Feedlyve alphaGal*	α-galactosidase
III	*A*	*Lisozima*	Lysozyme
	B	*Feedlyve GMA*	Galacto-mannanase
	C	*Feedlyve alphaGal*	α-galactosidase

4.3.2 Results

The experimental conditions were the same used for the screening tests, with the exception of the enzyme dosage, which, for these assays, has been set equal to 5 mg/g. This value has been halved compared to the previous tests to limit the leveling effect on the extraction yield due to excessive enzyme concentration or to a possible synergy effect. In Table 4.6 results of systematic tests are shown.

Table 4.6 – Lipid extraction yields obtained in mixture design experiments.

Enzyme preparation mixture	ID	Enzyme preparation
I	1	23.53
	2	29.95
	3	36.43
	4	28.73
	5	34.89
	6	35.37
	7	30.53
	8	31.90
	9	36.29
	10	32.72
	11	22.50
	12	30.03
	13	38.51
	14	33.33
II	1	20.86
	2	29.95
	3	34.20
	4	27.43
	5	31.29
	6	32.46
	7	29.77
	8	31.33
	9	33.45
	10	31.34
	11	22.50
	12	29.26
	13	33.47
	14	31.79
III	1	20.27
	2	36.43
	3	34.20
	4	31.02
	5	30.70
	6	32.62
	7	28.81
	8	33.00
	9	31.69
	10	31.18
	11	19.18
	12	35.01
	13	33.47
	14	29.66

The composite designs comprising 14 run tests for each mixture of enzyme preparations were then subjected to statistical analysis using the Design Expert software (version 7.0.0). A prediction model has been determined and, by the use of the response surface and the analysis of variance (ANOVA), optimal points for each mixture of enzyme preparations have been identified and tested.
The models traditionally used in the formulation of mixtures experiments are Scheffé polynomials in canonical form (Cornell, 2002).

The quadratic model used is the following:

$$P\ (\beta, x) = \sum_{i=1}^{q} \beta_i x_i + \sum \sum_{i<j}^{q} \beta_{ij} x_i x_j$$

Expliciting the model with q = 3, the following expression is obtained:

$$y = \beta_1 \cdot x_1 + \beta_2 \cdot x_2 + \beta_3 \cdot x_3 + \beta_{12} \cdot x_1 x_2 + \beta_{13} \cdot x_1 x_3 + \beta_{23} \cdot x_2 x_3$$

where β_i are the coefficients of the model (referring respectively to preparations A, B and C and their linear combinations) and x_i are the fractions in weight of the different preparations. Y is the response, i.e. the yield of lipid extraction expressed as a percentage.

In Table 4.7 the analysis of variance for all three mixtures of enzyme preparations is reported.
In the first column the source (model, linear terms, quadratic, etc.) is indicated, while DF represents the degrees of freedom of each source. They are given by the sum of the degrees of freedom of each term and the ones of error. SS values are the sums of sequential squares that include the various terms of the model (linear, quadratic or residual error) in sequence. MS is the average of the squares for each term given by the ratio between SS and the relative degrees of freedom. The residual error is given by the sum of errors due to the lack of fit of the model and the pure error that takes into account the variability of the tests (repetition of the central point and the vertices of the triangle).
The last two values are the ones that have greater interest because they are used to give an assessment of the significance of the various terms. The parameter F is used to check whether the effect of a term in the model is significant. It is calculated by dividing the MS value of the source by the residual error. This parameter is compared with tabulated values of critical F. It is also possible and much easier to control the value of p. A test to verify the hypothesis is performed, initially, setting a level of significance, generally indicated with α, which determines the rejection region for the null hypothesis. If this p-value is less than α, the test rejects the null hypothesis at the level of significance set. In this study, a value of α = 0.05 was

chosen. Finally the Lack of fit test is a tool that allows checking the goodness of the model. It is used when repeated assays are expected in the experimental design.

Table 4.7 – Analysis of variance.

Enzyme preparation mixture	Source	SS	DF	MS	F	p
I	Model	279.95	5	55.99	96.90	< 0.0001
	Linear terms	248.46	2	124.23	215.01	< 0.0001
	AB	4.16	1	4.16	7.21	0.0277
	AC	20.12	1	20.12	34.82	0.0004
	BC	1.34	1	1.34	2.33	0.1656
	Residual error	4.62	8	0.58		
	Lack of fit	1.74	4	0.43	0.60	0.6818
	Pure error	2.88	4	0.72		
	Total	284.57	13			
II	Model	197.17	5	39.43	54.09	< 0.0001
	Linear terms	166.55	2	83.28	114.21	< 0.0001
	AB	6.31	1	6.31	8.65	0.0187
	AC	17.41	1	17.41	23.87	0.0012
	BC	0.98	1	0.98	1.34	0.2805
	Residual error	5.83	8	0.73		
	Lack of fit	3.88	4	0.97	1.99	0.2607
	Pure error	1.95	4	0.49		
	Total	203.01	13			
III	Model	318.99	5	63.80	62.70	< 0.0001
	Linear terms	290.06	2	145.03	142.53	< 0.0001
	AB	8.76	1	8.76	8.61	0.0189
	AC	12.07	1	12.07	11.86	0.0088
	BC	9.90	1	9.90	9.73	0.0143
	Residual error	8.14	8	1.02		
	Lack of fit	5.11	4	1.28	1.69	0.3126
	Pure error	3.03	4	0.76		
	Total	327.13	13			

From the analysis of data obtained, it can be observed as all three models developed are significant ($p < 0.05$), and the lack of fit is not significant ($p > 0.1$), an indication that the proposed model fits well the experimental data. The term BC of the mixture I and II was not significant ($p > 0.05$), but it was not excluded because the number of experimental points is low. Moreover, some normalized residuals of the reduced model would have been outside the range ± 2.
In Table 4.8 values for the coefficients estimated by the models for all three mixtures of enzyme preparations are reported.

Table 4.8 – Coefficients values estimated for the predictive model.

Enzyme preparation mixture	Term	Estimated coefficient value	Standard error	Lower limit	Upper limit
I	A	23.19	0.53	21.97	24.40
	B	30.00	0.53	28.79	31.22
	C	37.46	0.53	36.25	38.68
	AB	7.97	2.97	1.12	14.81
	AC	17.51	2.97	10.67	24.36
	BC	4.53	2.97	–2.32	11.37
II	A	21.86	0.59	20.50	23.23
	B	29.58	0.59	28.21	30.94
	C	33.73	0.59	32.36	35.09
	AB	9.81	3.33	2.12	17.49
	AC	16.29	3.33	8.60	23.98
	BC	3.86	3.33	–3.83	11.55
III	A	20.02	0.70	18.41	21.63
	B	35.75	0.70	34.14	37.36
	C	33.79	0.70	32.18	35.40
	AB	11.56	3.94	2.47	20.64
	AC	13.57	3.94	4.48	22.65
	BC	–12.28	3.94	–21.37	–3.20

It can be observed that the linear term of C prevails for the first two mixtures of enzyme preparations. It is therefore predominant the effect of the two individual preparations GMA and GAL on the extraction yield. A positive effect of the coefficients terms of binary interaction for the pair AC, even if milder, can be also noticed. Therefore, there is a modest synergistic effect between GMA and 50LC for the first mixture and between 50LC and GAL for the second mixture. However, for both cocktails of enzyme preparations, the term BC (combination of AGL and GMA for the first mixture and AGL + GAL for the second) is not within the set significance

threshold. This is also observable by the fact that the extremes of the limit interval (the range for which the probability that the value falls in it is 95%) change sign.
For the third mixture of enzyme preparations containing lysozyme (A) and the two best enzyme preparations (B and C), a substantial effect on the yield of the values of the linear coefficients (particularly B and C) can be highlighted. The quadratic terms have an opposite effect on the yield, positive for BC and AB, negative for BC, with a significance level higher than 95%.

A)

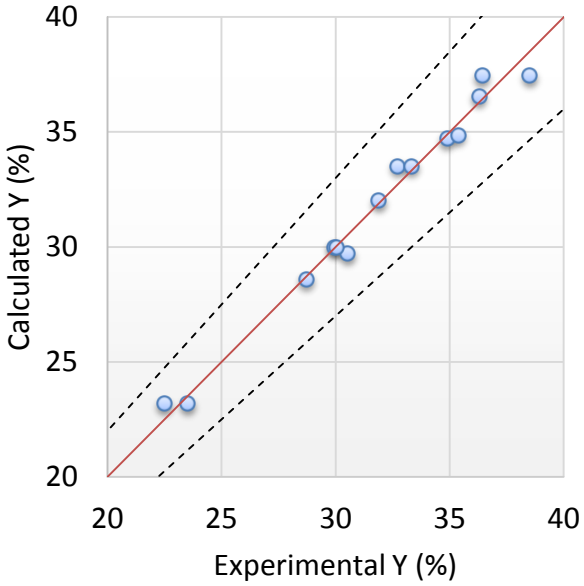

B)

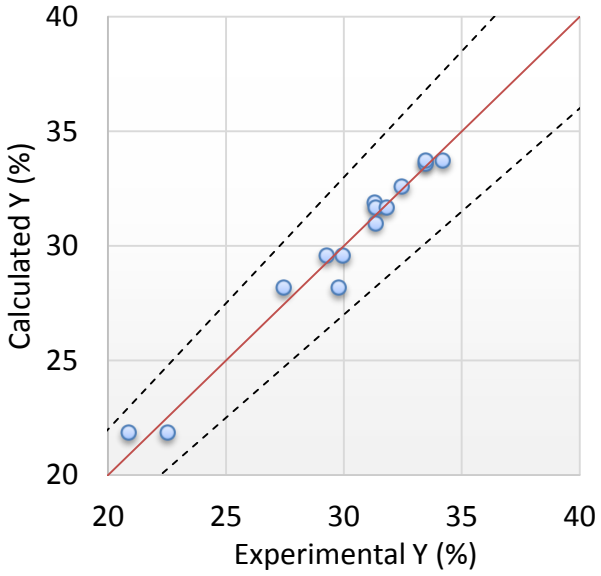

C)

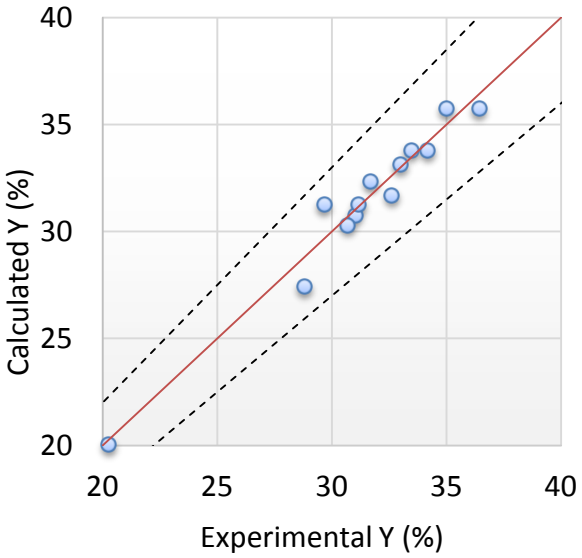

Figure 4.3 – Experimental vs. calculated values for the first (A), second (B) and third (C) mixture of enzyme preparations.

In Fig. 4.3 graphs reporting experimental values of the three mixtures of enzyme preparations against those predicted by the model are shown. As it can be observed, in all cases points are arranged all around the bisecting line indicating that the model approximates well all the experimental data.
Another method to determine the reliability of the generated model is the analysis of residuals, defined as:

$$R_j = Y_j^{Exp} - Y_j^{Calc}$$

i.e. the difference between the experimental values and the responses of the model. These give a qualitative indication of how far predicted values are. If the prediction of the model is correct, the residuals should approximate the random error that determines the relationship between the independent variables and the response. Furthermore, in a good model residuals should be disposed in random manner and should not present a systematic trend. In this case the normalized residuals, ensuring that any data has the same statistical weight, were analyzed.

A)

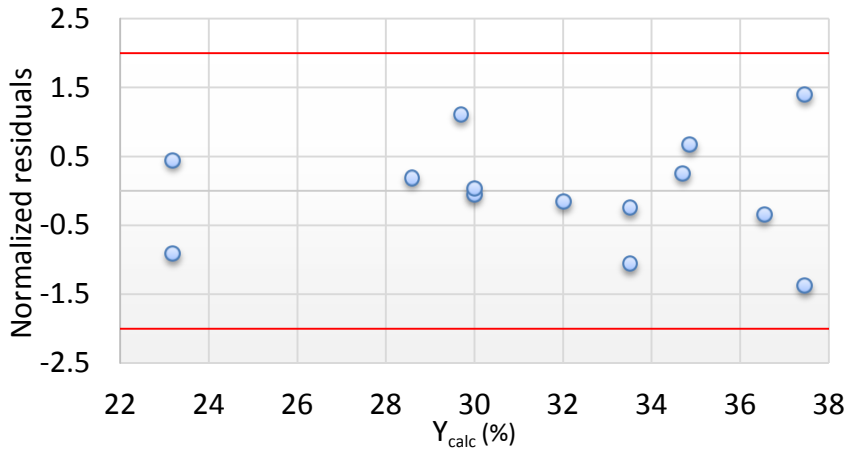

B)

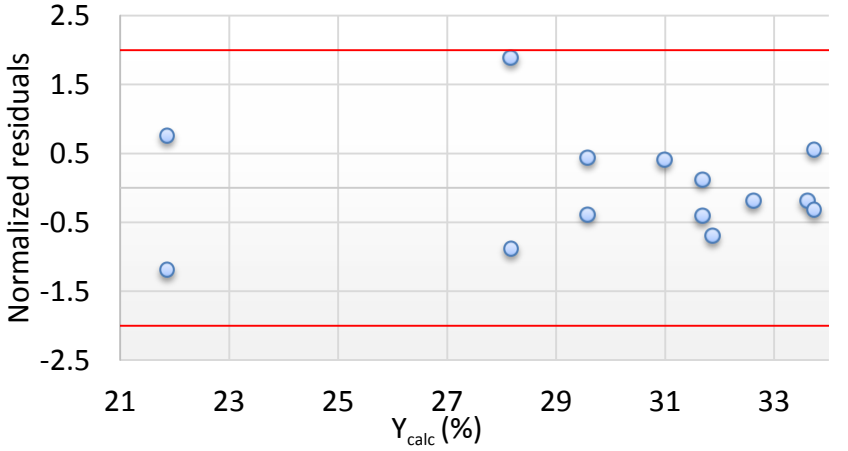

C)

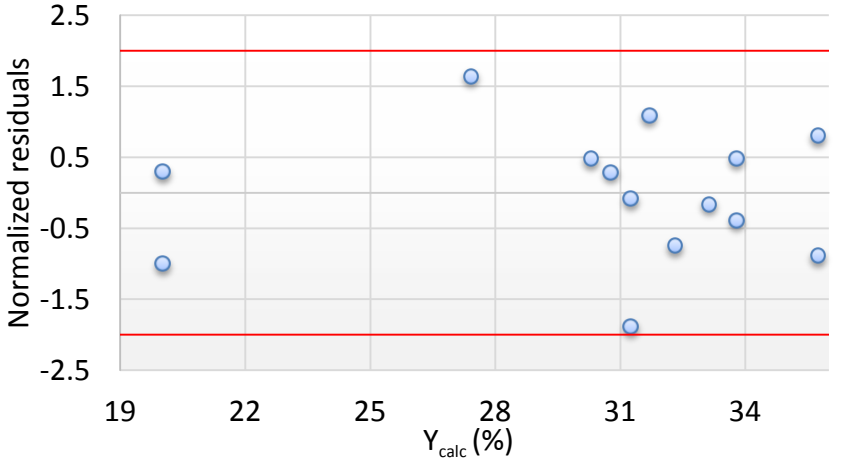

Figure 4.4 – Normalized residuals vs predicted yield value for the first (A), second (B) and third (C) mixture of enzyme preparations. The horizontal lines of the residuals (± 2) determine the area with 95% confidence.

They are defined as:

$$R_j * = \frac{R_j}{[(\frac{1}{N-P}) \sum_{j=1}^{n} R_j^2 \ ]^{0.5}}$$

where N is the number of experimental data (N = 14) and P the number of model parameters (P = 6). 95% of the normalized residual should be within the range ± 2. The residual plots as a function of the response are shown in Fig. 4.4. These residuals are arranged random between –2 and 2.
In Fig. 4.5 Normal Probability Plots are reported. They are useful to verify the plausibility of the hypothesis of normality, which is to ascertain whether a set of data can come from a normal distribution. If graph points are located approximately on a straight line inclined positively, it is possible to say that the observed data are distributed approximately according to the normal law. This can be done by calculating residuals normalized with respect to the corresponding standard cumulative frequency observed, defined as:

$$\Phi_j = R^{-1}\left(\frac{j-0.5}{N}\right)$$

where Φ is the standard normal cumulative distribution function. The values in the chart, as it can be appreciated from the value of R^2, follow a quite linear trend.

A)

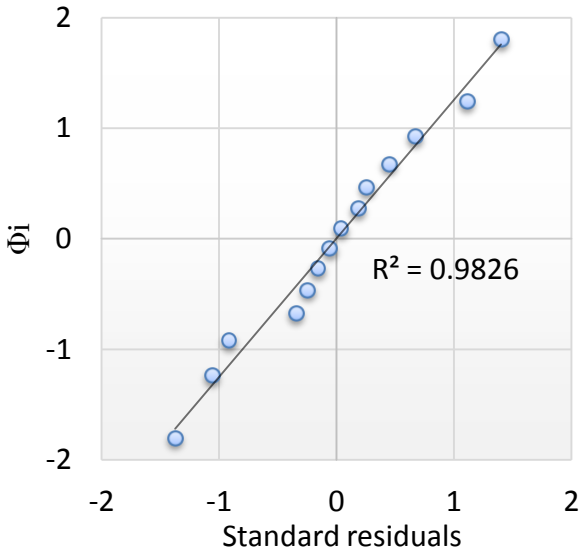

B)

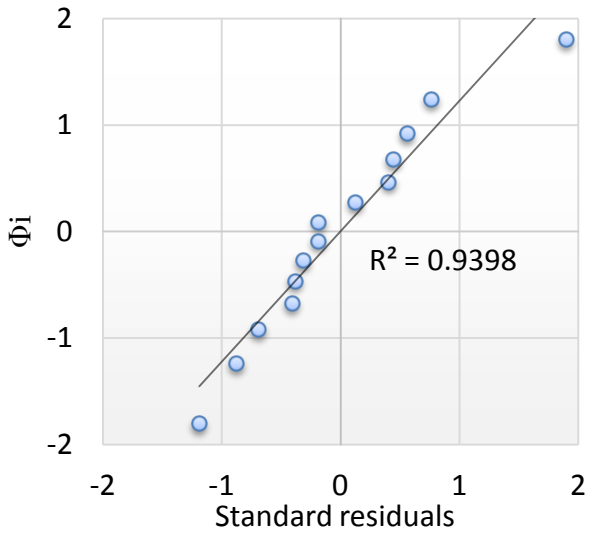

C)

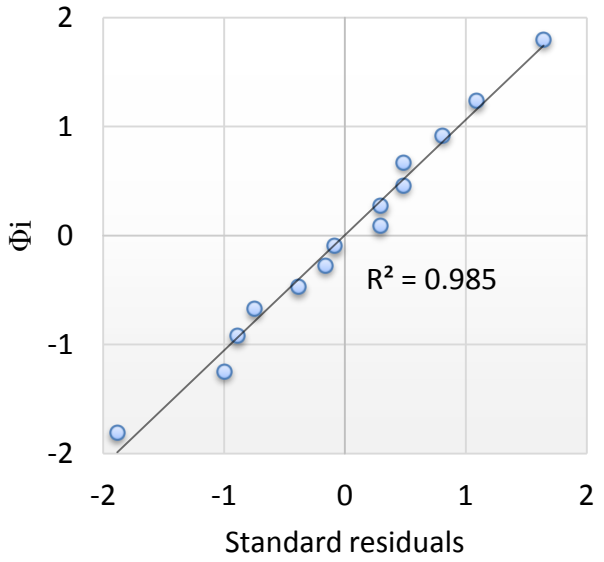

Figure 4.5 – Normal Probability Plots: standard normal cumulative distribution function vs. normalized residuals for the first (A), second (B) and third (C) mixture of enzyme preparations.

Response surfaces with the relative contour plots were then generated utilizing these models (Figures 4.6-4.8). These surfaces are useful to understand how the different enzyme preparations interact with each other on the lipid yield.

It is possible to observe that the response surfaces of the first two mixtures of enzyme preparations are similar, with the higher yields moved toward the enzyme preparations that have given the best yields in screening tests. In fact, for such mixtures, the coefficient C was found to have the greatest contribution.

For the first two mixtures, it can also be observed that the best synergistic effect was obtained for AC couple (highest value between the quadratic terms). This allows highlighting a possible favorable combined effect between Cellulyve 50LC, that catalyzes the hydrolysis of 1,4-bonds β-D-glycosidic linkages in cellulose (a major constituent of the *Nannochloropsis*) and Feedlyve GMA (mixture I), rich in galactomannanase, and Feedlyve alphaGal (mixture II), rich in alpha-galactosidase, respectively. Both Feedlyve GMA and Feedlyve alphaGal contain galactosidase activity that, as seen from literature, has effects on the hydrolysis of fucosides, particularly present in *Nannochloropsis* species. In particular, the highest yields were obtained with the first mixture of enzyme preparations (~ 37% vs. ~ 34%), highlighting a better effect of GMA, with respect to GAL, perhaps due to a presence of mannanase, an enzyme active on straight chain of mannans of hemicellulose. Mannose residues were found in *Nannochloropsis* cell wall after acid hydrolysis (Chapter 3). A more modest synergistic effect was observed for the pair AB, for both mixtures of enzyme preparations between Cellulyve 50LC and Feedlyve AGL, based on β-glucanase. In that case, the highest yields are moved towards AGL which acts both on the β-1,3 and β-1,4 glucans linkages destabilizing, at the same time, the cellulosic matrix essentially characterized by β-1,4 glycosidic bonds. The pair BC was the least significant for both mixtures of enzyme preparations. In fact, a linear trend is observable from response surfaces.

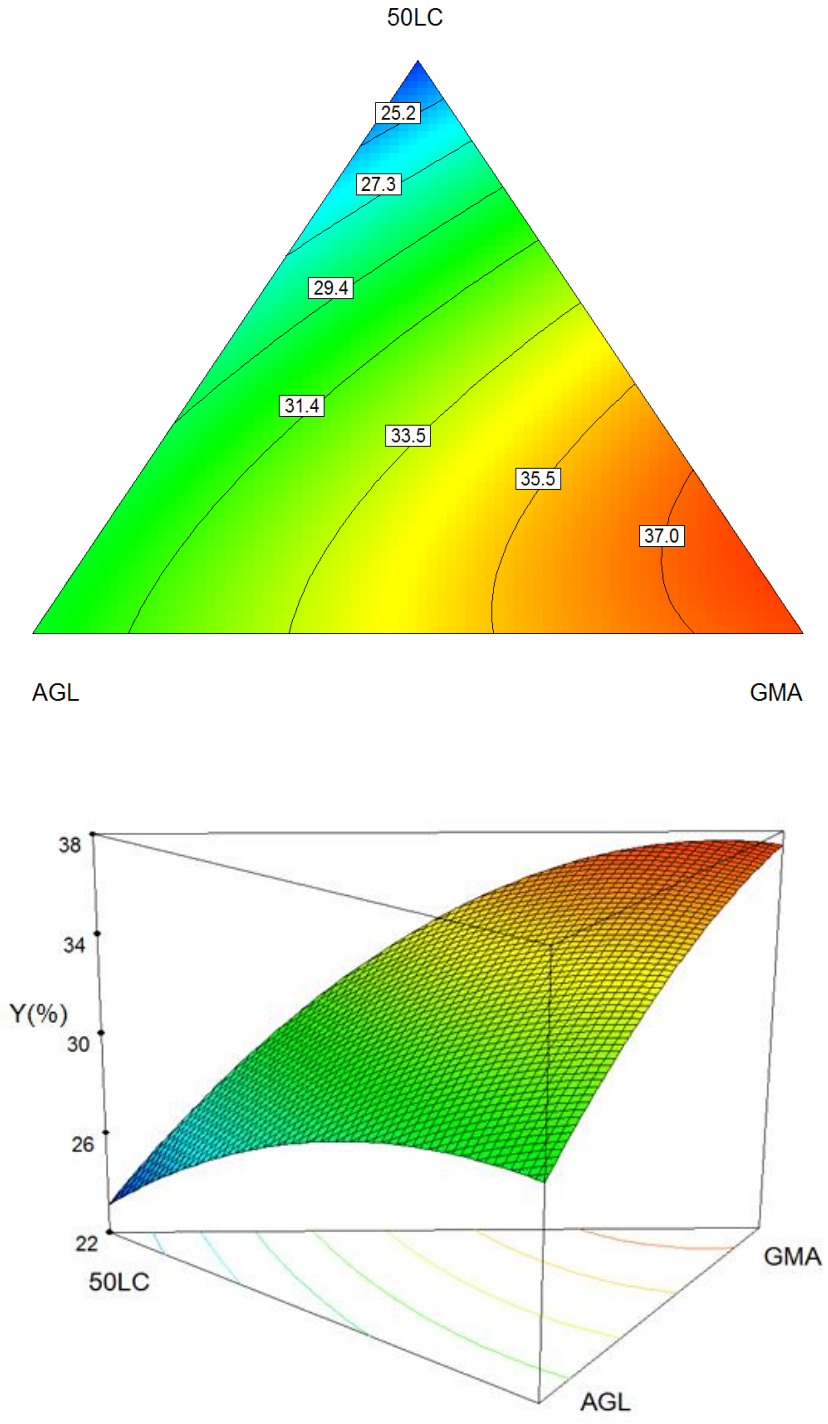

Figure 4.6 – Contour plot and response surface for mixture I.

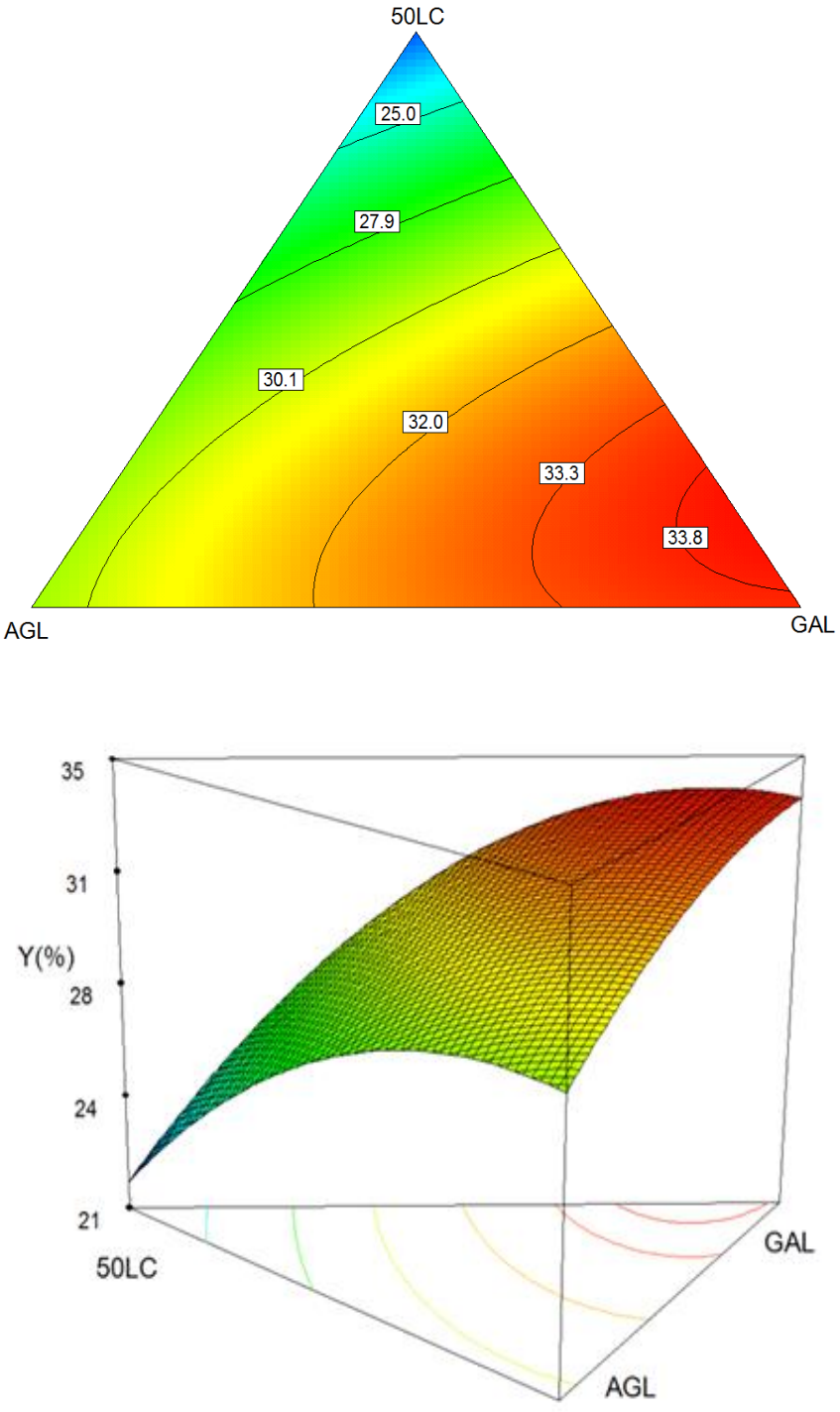

Figure 4.7 – Contour plot and response surface for mixture II.

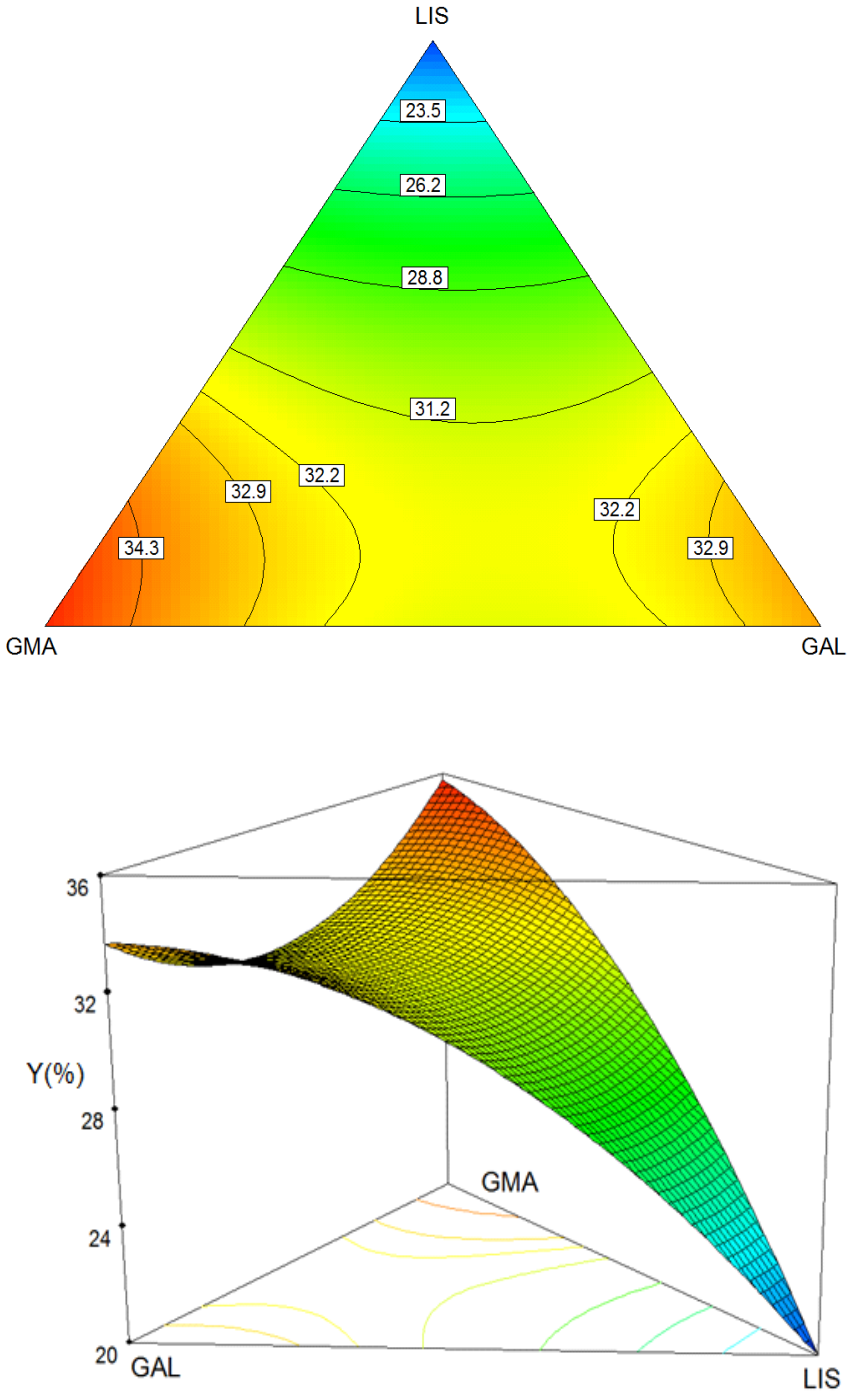

Figure 4.8 – Contour plot and response surface for mixture III.

4.3.3 Optimization and validation

Through numerical optimization, it is possible to determine the best composition of the enzyme mixtures, taking advantage of any synergistic effects analyzed before. Optimal points have been identified for each mixture of enzyme preparations, as reported in Table 4.9.

Table 4.9 – Optimal points and respective theoretical yield percentages for each mixture of enzyme preparations.

Enzyme preparation mixture	Enzyme preparation	Weight fraction (%)	Y_{exp} (%)	Y_{calc} (%)	Deviation (%)
I	*Cellulyve 50LC*	9.3	37.1	37.6	1.41
	Feedlyve AGL	0			
	Feedlyve GMA	90.7			
II	*Cellulyve 50LC*	13.6	34.4	34	-1.04
	Feedlyve AGL	0			
	Feedlyve alphaGal	86.4			
III	*Lisozima*	0	35.4	35.8	0.89
	Feedlyve GMA	100			
	Feedlyve alphaGal	0			

Optimual points for the first two mixtures of enzyme preparations have been found in correspondence of the AC binary mixtures, i.e. in correspondence of the couple that presented a greater synergistic effect. On the contrary, for the third mixture of enzyme preparation the maximum was found at the vertex B, i.e. pure GMA, since there were no significant synergistic effects which have led to higher yields.
Subsequently, the optimal points obtained were validated experimentally. The tests were performed in duplicate and results are shown in Table 4.9. The average of the experimental values obtained for the optimum points and the relative percentage difference between the experimental value and the value predicted by the model are reported.
The optimized enzyme cocktails gave results in accordance with those expected from the models, with very low deviations between experimental and predicted values.
Based on these results, the best pre-treatment was obtained utilizing the first mixture of enzyme preparations with a composition of 90% of Feedlyve GMA and 10% of Cellulyve 50LC.

4.4 Effect of treatment conditions on lipid yield

4.4.1 Experimental design

This part of the work has as objective the study of the more important process parameters that affect the pretreatment and, thus, the extraction yields.
A central composite design (CCD) of 4 factors on 2 levels was used (Zuorro et al., 2015). CCD has three types of experimental points:

- factorial points on 2 levels, corresponding to all possible combinations of the levels –1 and +1 of the factors;
- axial points, also called star points (–α, + α), have all setup factors at level 0 (center) but one that takes the value ± α; to ensure the rotatability of the design space, the value of α was taken as $(16)^{1/4} = 2$ (Montgomery, 2012);
- central points with all levels of the various factors set at central value.

An example scheme of a 2 factors CCD is shown in Fig. 4.9.

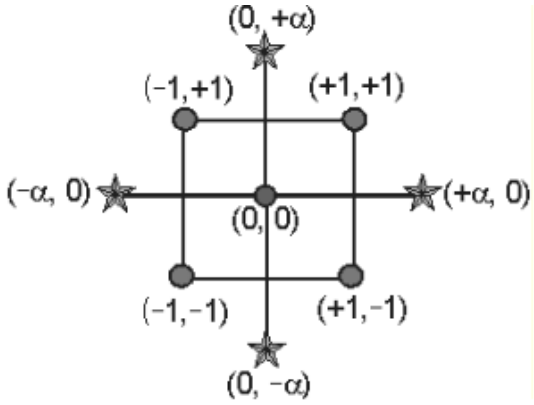

Figure 4.9 – Scheme of a 2 factors Central Composite Design.

With 4 factors, 16 factorial, 8 axial and 6 central points are then obtained. The central points are usually repeated 4 to 6 times to obtain a good estimate of the experimental error (pure error).
The four factors considered are:

P = pre-treatment time
D = ratio enzyme / micro-algae
pH
T = temperature.

Factor levels were chosen to cover a range of values of practical interest and are reported in Table 4.10 in coded and actual variables.

Table 4.10 – Factors and levels of experimental design.

Factor	Unit	Levels				
		–2	**–1**	**0**	**1**	**2**
P-time	min	30	60	90	120	150
D-Dosage	mg/g	0.0	0.5	1	1.5	2.0
pH		2	4	6	8	10
T-Temperature	°C	15	30	45	60	75

Coded values were obtained from the following equations:

$$x_1 = \frac{P - 90}{30}$$

$$x_2 = \frac{D - 1}{0.5}$$

$$x_2 = \frac{pH - 6}{2}$$

$$x_4 = \frac{T - 45}{15}$$

Table 4.11 shows the experimental design in coded units. In the second column the execution order of test is indicated. Tests were randomized to avoid the effects of uncontrolled factors.

For all tests the enzyme solution optimized previously was used (90% wt of Feedlyve GMA and 10% wt of Cellulyve 50LC.

The Design-Expert® software (version 7.0, Stat-Ease Inc., Minneapolis, MN, USA) was used for the design and analysis of experiments.

Table 4.11 – Coded experimental design.

ID	Run	Time	Dosage	pH	Temperature
1	28	–1	–1	–1	–1
2	29	1	–1	–1	–1
3	1	–1	1	–1	–1
4	30	1	1	–1	–1
5	2	–1	–1	1	–1
6	3	1	–1	1	–1
7	4	–1	1	1	–1
8	5	1	1	1	–1
9	7	–1	–1	–1	1
10	8	1	–1	–1	1
11	9	–1	1	–1	1
12	10	1	1	–1	1
13	11	–1	–1	1	1
14	12	1	–1	1	1
15	13	–1	1	1	1
16	14	1	1	1	1
17	18	–2	0	0	0
18	19	2	0	0	0
19	25	0	–2	0	0
20	23	0	2	0	0
21	27	0	0	–2	0
22	6	0	0	2	0
23	17	0	0	0	–2
24	16	0	0	0	2
25	15	0	0	0	0
26	20	0	0	0	0
27	21	0	0	0	0
28	22	0	0	0	0
29	24	0	0	0	0
30	26	0	0	0	0

4.4.2 Results

Results of the experimental design are reported in Table 4.12.

Table 4.12 – Results of the experimental design.

ID	Time (min)	Dosage (mg/g)	pH	Temperature (°C)	Y (%)
1	60	0.5	4	30	34.81
2	120	0.5	4	30	35.25
3	60	1.5	4	30	35.00
4	120	1.5	4	30	36.21
5	60	0.5	8	30	29.91
6	120	0.5	8	30	27.13
7	60	1.5	8	30	32.06
8	120	1.5	8	30	30.83
9	60	0.5	4	60	32.34
10	120	0.5	4	60	32.24
11	60	1.5	4	60	35.18
12	120	1.5	4	60	36.34
13	60	0.5	8	60	22.28
14	120	0.5	8	60	23.24
15	60	1.5	8	60	23.03
16	120	1.5	8	60	25.84
17	30	1.0	6	45	35.92
18	150	1.0	6	45	35.55
19	90	0	6	45	22.98
20	90	2.0	6	45	34.46
21	90	1.0	2	45	30.00
22	90	1.0	10	45	20.82
23	90	1.0	6	15	34.85
24	90	1.0	6	75	25.76
25	90	1.0	6	45	35.24
26	90	1.0	6	45	35.87
27	90	1.0	6	45	33.24
28	90	1.0	6	45	34.12
29	90	1.0	6	45	36.51
30	90	1.0	6	45	35.15

Tests on central point (ID 25–30) provided an average yield of 35.02 ± 1.18% with a deviation of 3.37 %, indicating a good reproducibility of the data obtained.

Different empirical models (linear, two-factor interaction, quadratic and cubic) were considered and tested for their statistical significance in order to correlate

experimental data. The best results were obtained by the following second-order polynomial equation:

$$Y = \beta_0 + \sum_{i=1}^{4} \beta_i x_i + \sum_{i=1}^{4} \beta_{ii} x_i^2 + \sum_{i=1}^{3} \sum_{j=i+1}^{4} \beta_{ij} x_i x_j$$

where Y is the response variable, x_i are the independent variables, β_o is the intercept and β_i, β_{ii} and β_{ij} are the linear, quadratic and interaction regression coefficients.
The estimated model coefficients, together with their standard errors, F -values and p -values are reported in Table 4.13. Coefficient of determination (R^2), adjusted-R^2 and prediction-R^2 are shown in Table 4.14.

Table 4.13 – Estimated model coefficients and analysis of variance of the complete model.

Source	Estimated coefficient	SS	DF	MS	F	p
Model	–	685.15	14	48.94	14.45	< 0.0001
Intercept	35.02	–	1	–	–	< 0.0001
P-Time	+0.072	0.12	1	0.12	0.037	0.8504
D-Dosage	+1.68	67.50	1	67.50	19.93	0.0005
pH	–3.39	276.29	1	276.29	81.58	< 0.0001
T-Temperature	–2.04	99.59	1	99.59	29.41	< 0.0001
P×D	+0.34	1.84	1	1.84	0.54	0.4721
P×pH	–0.18	0.54	1	0.54	0.16	0.6943
P×T	+0.45	3.23	1	3.23	0.95	0.3442
D×pH	+0.069	0.077	1	0.077	0.023	0.8822
D×T	+0.21	0.68	1	0.68	0.20	0.6613
pH×T	–1.27	25.93	1	25.93	7.66	0.0144
P×P	+0.29	2.35	1	2.35	0.69	0.4177
D×D	–1.46	58.54	1	58.54	17.29	0.0008
pH×pH	–2.29	143.49	1	143.49	42.37	< 0.0001
T×T	–1.06	31.09	1	31.09	9.18	0.0084
Residual error		50.80	15	3.39		
Lack of Fit		43.81	10	4.38	3.14	0.1095
Pure error		6.99	5	1.40		
Total		735.95	29			

Table 4.14 – Coefficient of determination of the complete model.

Mean values (%)	**31.41**
Standard deviation (%)	1.84
R^2	0.93
adjusted-R^2	0.87
prediction-R^2	0.64
adjusted-R^2 – prediction-R^2	0.22

The model is significant at 99%, while the lack of fit is not significant. Furthermore, the value of R^2, which gives a measure of the variation around the average of the values of the model, is high, confirming the validity of the model. However, analysis of coefficients shows that the influence of the time factor is negligible in comparison to that of other factors.
It is also evident that all terms that contain time and mixed terms are not significant. That is the reason why the difference between the values of adjusted and predicted R^2 is so high. The first one gives a measure of the variation around the average of the values of the model corrected for the number of parameters. The second gives a measure of the goodness of the model prediction. The difference between these two values should not exceed 0.2 to be in reasonable agreement; otherwise there may be a problem with either data or model.
Therefore, a stepwise regression method was used to identify the statistically significant terms in eq. (5). This procedure consists in the iterative addition and removal of terms from the model equation so as to meet a specified significance level (in our case, $p < 0.05$). Elimination of the non-significant terms led to the following reduced model:

$$Y = \beta_0 + \beta_2 \cdot x_2 + \beta_3 \cdot x_3 + \beta_4 \cdot x_4 + \beta_{22} x_2^2 + \beta_{33} x_3^2 + \beta_{44} x_4^2 + \beta_{34} \cdot x_3 x_4$$

The analysis of variance of the new reduced model is reported in Table 4.15 and 4.16.

The reduced model is still significant at 99% and the lack of fit is not significant. The R^2 value is just reduced, while the deviation between predicted and adjusted R^2 is reduced up to make this difference acceptable (less than 0.2).

Table 4.15 – Estimated model coefficients and analysis of variance of the reduced model.

Source	Estimated coefficient	SS	DF	MS	F	p
Model	–	676.30	7	96.61	35.63	< 0.0001
β_0	35.36	–	1	–	–	< 0.0001
D-Dosage	+1.68	67.50	1	67.50	24.90	< 0.0001
pH	–3.39	276.29	1	276.29	101.90	< 0.0001
T-Temperature	–2.04	99.59	1	99.59	36.73	< 0.0001
pH×T	–1.27	25.93	1	25.93	9.57	0.0053
D×D	–1.50	63.23	1	63.23	23.32	< 0.0001
pH×pH	–2.33	151.88	1	151.88	56.02	< 0.0001
T×T	–1.11	34.28	1	34.28	12.64	0.0018
Residual error		59.65	22	2.71		
Lack of Fit		52.66	17	3.10	2.22	0.1933
Pure error		6.99	5	1.40		
Total		735.95	29			

Table 4.16 – Coefficient of determination of the reduced model.

Mean values (%)	**31.41**
Standard deviation (%)	1.72
R^2	0.92
adjusted-R^2	0.88
prediction-R^2	0.72
adjusted-R^2 – prediction-R^2	0.16

From coefficient values in Table 4.15, it is possible to highlight that:

- three of the four main factors, namely, enzyme dosage (D), pH and temperature (T), were statistically significant, their effect on lipid recovery increasing in the order: D < T < pH;
- they all affected the response variable through both linear and quadratic terms;
- there was a statistically significant interaction between pH and T, indicating that the effect of pH on lipid recovery was dependent on the temperature level considered (Zuorro et al., 2015).

Considering only the linear terms a dominant effect of pH (negative) is evident, followed by temperature (negative) and dosage (positive).

Fig. 4.10 shows the experimental values against those predicted by the model.

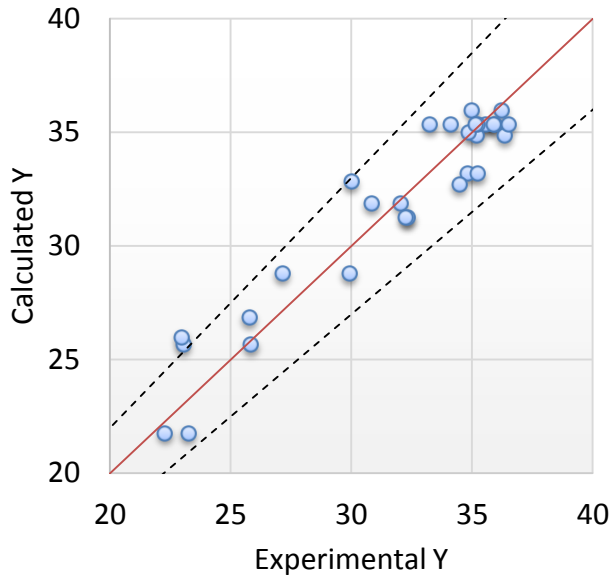

Figure 4.10 – Experimental vs. calculated values.

As it can be seen, the points are distributed fairly around the bisector line, indicating that the model approximates well the experimental points.

In Figure 4.11 it is reported the plot with normalized residuals in function of the response of the model.

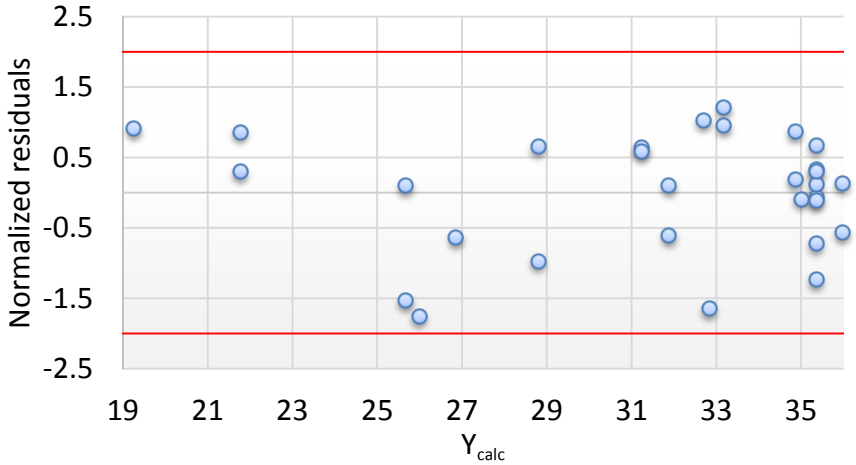

Figure 4.11 – Normalized residuals vs predicted yield value.

All points are arranged randomly within ± 2, with 95% of probability that points of the factorial region are well predicted by the model.
Fig. 4.12 shows the Normal Probability Plot useful to check if the points are arranged in a normal distribution.
The points are located approximately along a straight line, with deviations limited to the upper and lower ends. Therefore, it can be said that they are distributed according to the normal law.

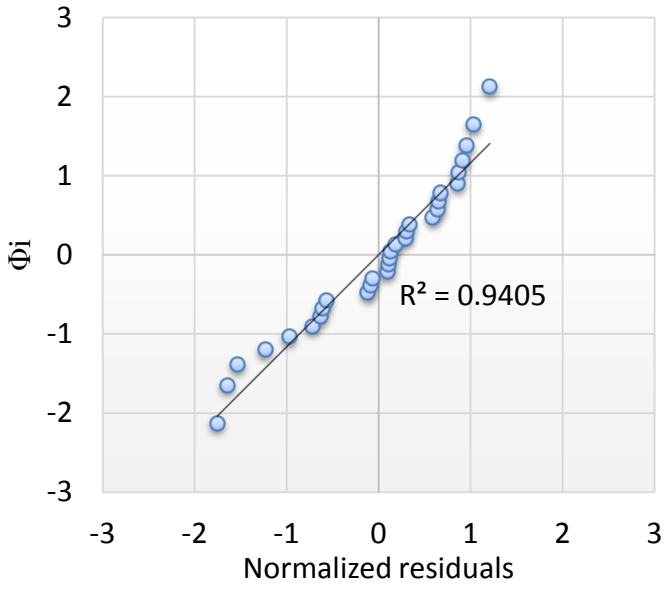

Figure 4.12 – Normal Probability Plots: standard normal cumulative distribution function vs. normalized residuals.

Response surfaces and contour plots have been obtained from the calculated model (Figures 4.13–15). The surfaces display two factors at a time, while the other factors are set to their central value (1 mg/g for the dose, 6 for the pH and 45 °C for temperature, time is not significant).

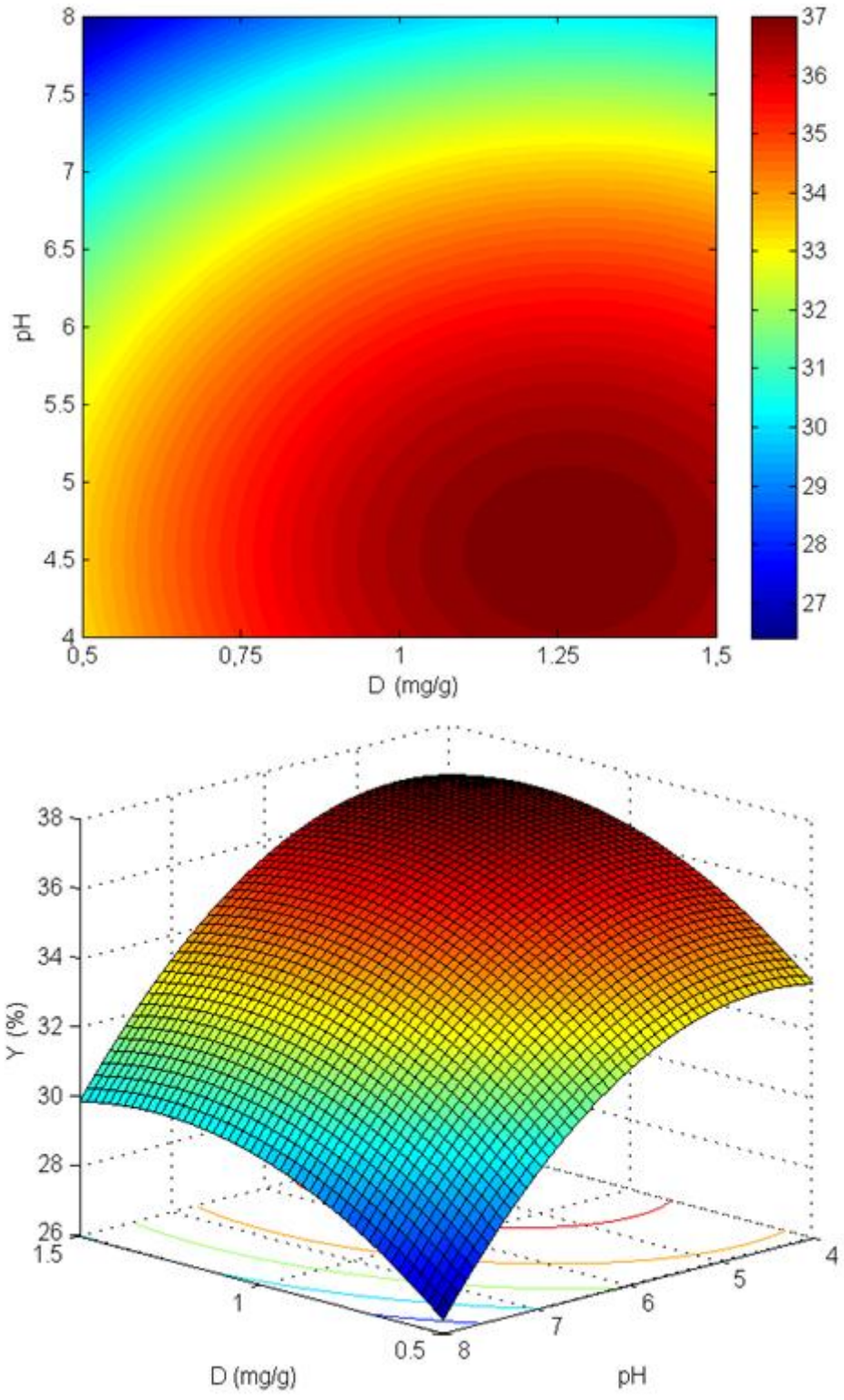

Figure 4.13 – Contour plots and response surfaces for the parameters Dosage-pH.

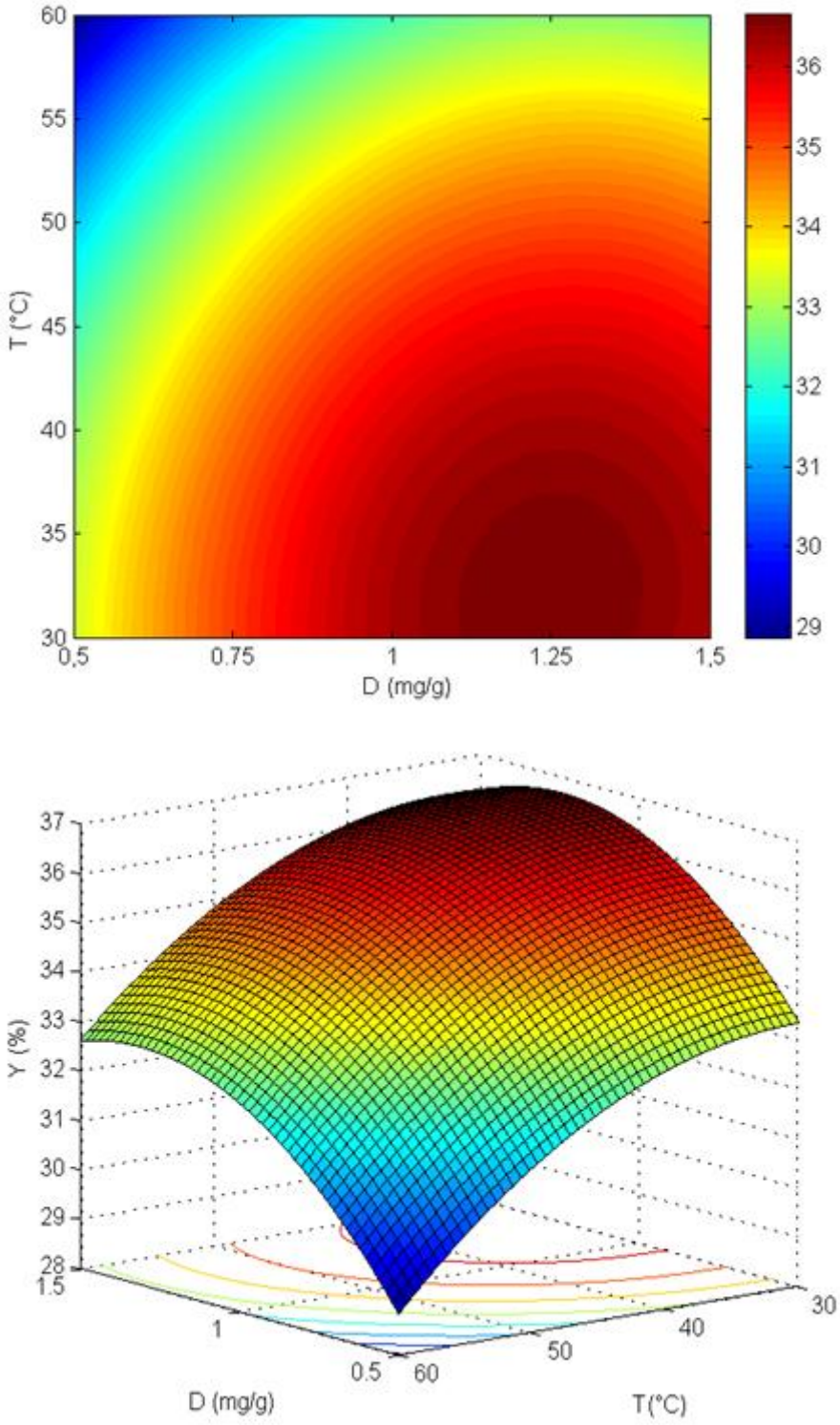

Figure 4.14 – Contour plots and response surfaces for the parameters Dosage-Temperature.

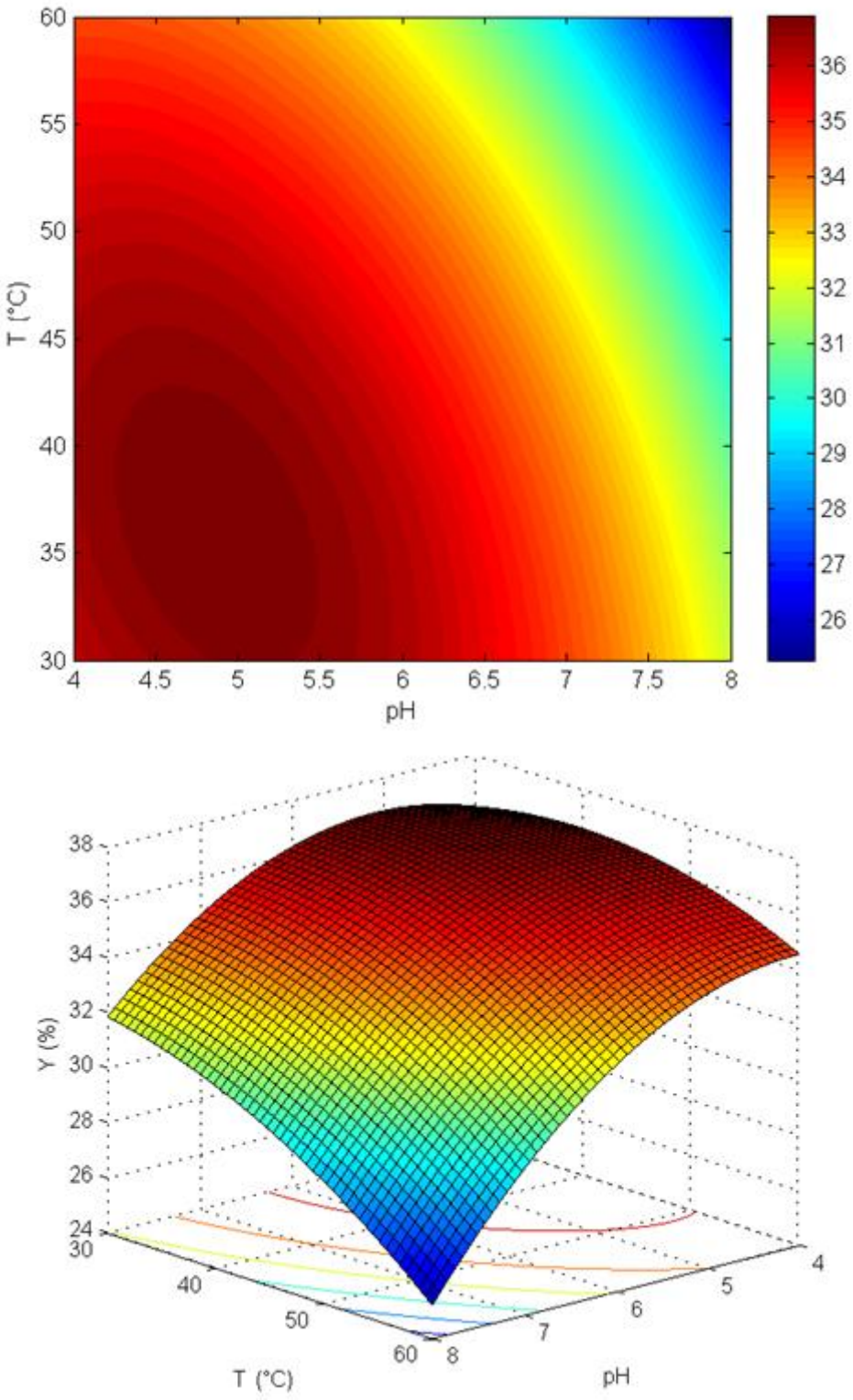

Figure 4.15 – Contour plots and response surfaces for the parameters pH-Temperature.

As it can be seen from surfaces, an increase in enzyme dosage increased lipid recovery, while an increase in pH caused a decrease in lipid recovery. The ladder effect can be attributed to a progressive departure from the optimal pH values of the enzymes present in the mixed preparation, which were all close to 5. Too high pretreatment temperatures had a negative effect on lipid.

Analyzing the response surface relative to the pair dosage-pH, it is possible to observe how pH has a significant linear effect, approximately double compared to the effect of the dosage, in agreement with the values of the coefficients. The quadratic effect is much more pronounced for the pH compared to the dosage, while the interaction between these two factors is not appreciable.

Looking at the surface relative to the factors Dosage and Temperature, the trend is similar, although the effect of temperature is less relevant than pH, being comparable to that of dosage. The effect of interaction is not appreciable as witnessed by the low interaction coefficient value equal to 0.21.
It is clear that the dosage is independent from the other factors and, in any case, its increase leads to an increase in the yield. Its positive influence leads to a greater degradation of the biomass matrix facilitating the penetration of the solvent for the subsequent extraction phase.

Finally, analyzing the last surface relative to the pair pH-Temperature, it is remarkable negative interaction (coefficient of term equal to –1.27) between the two parameters. In fact, it can be observed how, at fixed pH, the yield decreases with increasing temperature and this decrease is much more pronounced with increasing values of pH. In addition, when pH decreases the surface tends to flatten.

4.4.3 Optimization of the pretreatment conditions

The enzymatic treatment of *Nannochloropsis* was optimized by maximization of the response variable (eq. 6) using the reduced model.
The search domain was restricted to the factorial part of the design and the pretreatment time was set to its central level (P = 90 min), as it was not significant.
We obtained: pH = 5, D = 1.3 mg g^{-1}, T = 36 °C and y_{max} = 37.3 wt%,
These points were also performed experimentally to validate the model.

Table 4.17 shows tests in the optimum condition and the relative mean, standard deviation and percentage error.

Table 4.17 – Validation experiments.

Y (%)	Mean (%)	St. Dev. (%)	Error (%)
36.63	35.66	0.88	2.46
34.93			
35.41			

Validation experiments under the above conditions gave y = 35.7 ± 2.5 wt%, thus confirming the good descriptive and predictive capabilities of the developed model.

It is possible to conclude that, with the same amount of recovered lipids, operating in optimum conditions can lead to a great reduction of enzyme concentration of about 4 times (5 to 1.3 mg/g). It can easily be assumed that such new conditions will result in a significant benefit on the operating costs.

4.5 Improved enzyme-assisted lipid extraction

To better understand the effect of the pretreatment time and that of individual enzyme preparations, the experimental design has been modified, by separating the dosage of the two enzymes and increasing the search domain of the parameter 'pretreatment time'. The extraction time with solvents has been also reduced from 60 to 30 minutes to reduce the effect related to the action of the extraction solvent mixture (Zuorro et al., 2016).

4.5.1 Experimental design

The new central composite design was used to investigate the effect of temperature (T, °C), pH, pretreatment time (P, min), Cellulyve 50LC dosage (D1, mg/g) and Feedlyve GMA dosage (D2, mg/g) on the yield of lipids extracted (y). Factorial points were identified as the points from the one-half fraction of the 2^5 factorial design. Factor levels were chosen on the basis of the results obtained in preliminary experiments.

As before, extra-points were added according to a central composite design: one at the centre of the design, that was replicated six times, and 10 points along the five coordinate axes at distance $\alpha = 2$ from the central point. Design-Expert® software (version 7.0, Stat-Ease Inc., Minneapolis, MN, USA) was used for the design and analysis of experiments.

Chosen levels are reported in Table 4.18.

Table 4.18 – Factors and levels of experimental design.

Factor	Unit	Levels				
		–2	**–1**	**0**	**1**	**2**
T-Temperature	°C	15	30	45	60	75
pH		2	3.5	5	6.5	8
P-time	min	30	90	150	210	270
D1-Dosage CEL	mg/g	0.0	5	10	15	20
D2-Dosage GMA	mg/g	0.0	0.5	1.0	1.5	2.0

Coded variables were obtained from the following equations:

$$x_1 = \frac{T - 45}{15}$$

$$x_2 = \frac{pH - 5}{1.5}$$

$$x_3 = \frac{P - 150}{60}$$

$$x_4 = \frac{D1 - 10}{5}$$

$$x_5 = \frac{D2 - 1}{0.5}$$

Replicates at the centre were used to estimate the experimental error. Overall, the experimental design consisted of a total of 16 + 10 + 6 = 32 runs (Table 4.19).
Experiments were performed in a randomized order to minimize the effects of variability in the observed responses due to extraneous factors.

Table 4.19 – Experimental design layout. SO is the standard order and RO the randomized order of runs.

SO	RO	Temperature	pH	Time	Dosage CEL	Dosage GMA
1	13	–1	–1	–1	–1	1
2	28	1	–1	–1	–1	–1
3	17	–1	1	–1	–1	–1
4	29	1	1	–1	–1	1
5	24	–1	–1	1	–1	–1
6	9	1	–1	1	–1	1
7	18	–1	1	1	–1	1
8	31	1	1	1	–1	–1
9	21	–1	–1	–1	1	–1
10	22	1	–1	–1	1	1
11	14	–1	1	–1	1	–1
12	15	1	1	–1	1	–1
13	19	–1	–1	1	1	1
14	26	1	–1	1	1	–1
15	1	–1	1	1	1	–1
16	30	1	1	1	1	1
17	2	–2	0	0	0	0
18	23	2	0	0	0	0
19	11	0	–2	0	0	0
20	10	0	2	0	0	0
21	8	0	0	–2	0	0
22	27	0	0	2	0	0
23	20	0	0	0	–2	0
24	16	0	0	0	2	0
25	4	0	0	0	0	–2
26	3	0	0	0	0	2
27	5	0	0	0	0	0
28	12	0	0	0	0	0
29	32	0	0	0	0	0
30	6	0	0	0	0	0
31	25	0	0	0	0	0
32	7	0	0	0	0	0

4.5.2 Results

Results obtained are shown in Table 4.20.

Table 4.20 – Observed (Y_{exp}) and predicted (Y_{pred}) lipids extraction yields under different experimental conditions together with their 95%-confidence intervals (CI).

SO	Y_{exp} (%)	Y_{pred} (%)	Deviation (%)	Low CI	High CI
1	28.67	28.9	–0.78	27.08	30.72
2	27.00	26.6	1.35	24.81	28.45
3	21.35	21.1	1.26	19.26	22.90
4	27.88	28.6	–2.65	26.80	30.44
5	27.93	27.9	0.27	26.04	29.68
6	33.68	33.5	0.64	31.65	35.29
7	25.08	25.2	–0.40	23.36	27.00
8	24.39	24.9	–1.90	23.03	26.67
9	28.50	28.2	1.01	26.40	30.03
10	32.78	33.8	–3.27	32.03	35.66
11	25.48	25.5	–0.04	23.67	27.31
12	24.99	25.2	–0.65	23.34	26.98
13	31.28	32.4	–3.57	30.59	34.21
14	29.86	30.0	–0.48	28.19	31.83
15	23.12	24.6	–6.25	22.76	26.38
16	32.43	32.0	1.35	30.17	33.81
17	24.36	23.8	2.26	21.85	25.77
18	29.40	29.1	1.06	27.13	31.05
19	28.53	28.3	0.86	26.32	30.24
20	20.34	19.7	3.03	17.76	21.68
21	30.88	30.7	0.48	28.77	32.69
22	34.52	33.8	2.07	31.84	35.76
23	28.83	29.0	–0.45	26.99	30.91
24	33.62	32.6	2.95	30.67	34.59
25	27.82	27.7	0.33	25.77	29.69
26	36.38	35.6	2.12	33.65	37.57
27	33.69	33.2	1.42	31.55	34.88
28	32.36	33.2	–2.65	31.55	34.88
29	32.31	33.2	–2.80	31.55	34.88
30	33.79	33.2	1.71	31.55	34.88
31	32.85	33.2	–1.11	31.55	34.88
32	33.42	33.2	0.63	31.55	34.88

The yield of lipids extraction from untreated biomass was 21.7 ± 0.2%, while the values determined for the enzyme-treated material were between 21.3% and 36.4% (mean value: 29.3%), depending on the treatment conditions used. The maximum recovery was achieved at T = 45 °C, pH = 5, t = 150 min, D1 = 10 mg g^{-1}, and D2 = 1 mg g^{-1}.

As before, to correlate the experimental data, among different empirical models (linear, two-factor interaction, quadratic and cubic) the best results were obtained by the following second-order polynomial equation:

$$Y = \beta_0 + \sum_{i=1}^{5} \beta_i x_i + \sum_{i=1}^{5} \beta_{ii} x_i^2 + \sum_{i=1}^{4} \sum_{j=i+1}^{5} \beta_{ij} x_i x_j$$

where Y is the response variable, xi are the independent variables, β_o is the intercept and β_i, β_{ii} and β_{ij} are the linear, quadratic and interaction regression coefficients.

The non-significant coefficients were eliminated and a new reduced model was developed by using the stepwise regression method, with model terms entered and eliminated at a confidence level of 90%. The new coefficients were re-estimated from the experimental data, leading to the following final regression equation:

$$Y = \beta_0 + \beta_1 \cdot x_1 + \beta_2 \cdot x_2 + \beta_3 \cdot x_3 + \beta_4 \cdot x_4 + \beta_5 \cdot x_5 + \beta_{11} x_1^2 + \beta_{22} \cdot x_2^2 + \beta_{33} \cdot x_3^2 + \beta_{44} \cdot x_4^2 + \beta_{55} \cdot x_5^2 + \beta_{12} \cdot x_1 x_2 + \beta_{15} \cdot x_1 x_5$$

This equation provided a very good fit to the data, with coefficient of determination (R^2), adjusted-R^2 and prediction-R^2 equal, respectively, to 0.980, 0.968 and 0.933. No violations of basic ANOVA assumptions were present and the lack of fit was not significant (Table 4.21), thus confirming the adequacy of the reduced model to describe experimental data.

Table 4.21 – Analysis of variance.

Source	SS	DF	MS	F	p
Model	515.25	12	42.94	78.30	< 0.0001
Residual error	10.42	19	0.55	–	–
Lack of Fit	8.25	14	0.59	1.36	0.3911
Pure error	2.17	5	0.43	–	–
Total	525.67	31	–	–	–

As shown in Table 4.21, the Model F-value of 78.30 implies the model is significant, with a confidence level of 99%. Furthermore, the mean sum of squares for pure error (MSPE = 1.53 with 5 degrees of freedom) was compared to the mean sum of squares for lack of fit (MSLoF = 2.08 with 14 degrees of freedom) of the above polynomial. Their ratio (MSLoF/MSPE = 1.36) was less than the percentage point of the F distribution (2.96) at the 95% confidence level. This indicates that lack of fit was not significant and that the simplified polynomial was a reasonable approximation of the mean structure in the region of experimentation. Therefore, the overall error variance of this composite design was estimated by combining the mean sum of squares for lack of fit and pure error, giving a value or 1.93 with 19 degrees of freedom.

The estimated model coefficients, together with their standard errors, F-values and p-values, are reported in Table 4.22.

Table 4.22 – Estimates of the regression coefficients of model equation with their corresponding standard errors, F-values and p-values.

Coefficient	Term	Estimated coefficient	SS	F	p
β_0	Intercept	33.214	–	–	< 0.0001
β_1	T	1.320	41.77	76.18	< 0.0001
β_2	pH	−2.141	109.93	200.48	< 0.0001
β_3	P	0.767	14.13	25.77	< 0.0001
β_4	D1	0.919	20.28	36.98	< 0.0001
β_5	D2	1.969	93.00	169.60	< 0.0001
β_{11}	T × T	−1.691	83.83	152.88	< 0.0001
β_{22}	pH × pH	−2.303	155.59	283.74	< 0.0001
β_{33}	P × P	−0.237	1.64	3.00	0.0995
β_{44}	D1 × D1	−0.605	10.76	19.62	0.0003
β_{55}	D2 × D2	−0.386	4.38	7.98	0.0108
β_{12}	T × pH	0.483	3.74	6.81	0.0172
β_{15}	T × D2	0.681	7.43	13.55	0.0016

It is possible to individuate the significance of the individual regression coefficients by analyzing p-values reported in the last column in Table 4.21, as follows:

- all linear coefficients and the quadratic coefficients β_{11} and β_{22} were significant at the 99% confidence level;
- the quadratic coefficients β_{44} and β_{55} and the interaction coefficients β_{12} and β_{15} were significant at the 95% confidence level;
- the quadratic coefficient β_{33} was statistically significant at the 90% confidence level.

The following considerations can be made:

- the five main factors (temperature, pH, pretreatment time, CEL dosage and GMA dosage) were all statistically significant and affected the response through both linear and quadratic terms;
- temperature, pH and CEL dosage exerted the largest effect on lipid extraction;
- temperature was involved in two statistically significant and positive interactions, one with pH and the other with GMA dosage, indicating that it has a greater effect on lipid extraction at higher pH or GMA dosage (Zuorro et al., 2016).

Considering only linear terms, there is clearly a dominant effect of the dosage of GMA on the extraction of lipids. The influence of temperature, time and dosage of CEL is also positive. By contrast, lower pH values seem to favor higher extraction yields. In addition to these terms, however, it is to emphasize the significance of the quadratic terms for all the five factors, all with negative sign, indicating that the dependence of the yield on the parameters considered does not exhibit a linear trend, but a negative curvature.

Fig. 4.16 shows a comparison between experimental and calculated results.

It can be noticed that all the points are uniformly distributed around the bisecting line, indicating that the model approximated well the experimental data. Moreover, center point results (replicated six times) gave a mean of 33.1 ± 0.7 %, with an error of 2.0 %, revealing that experimental data are reproducible.

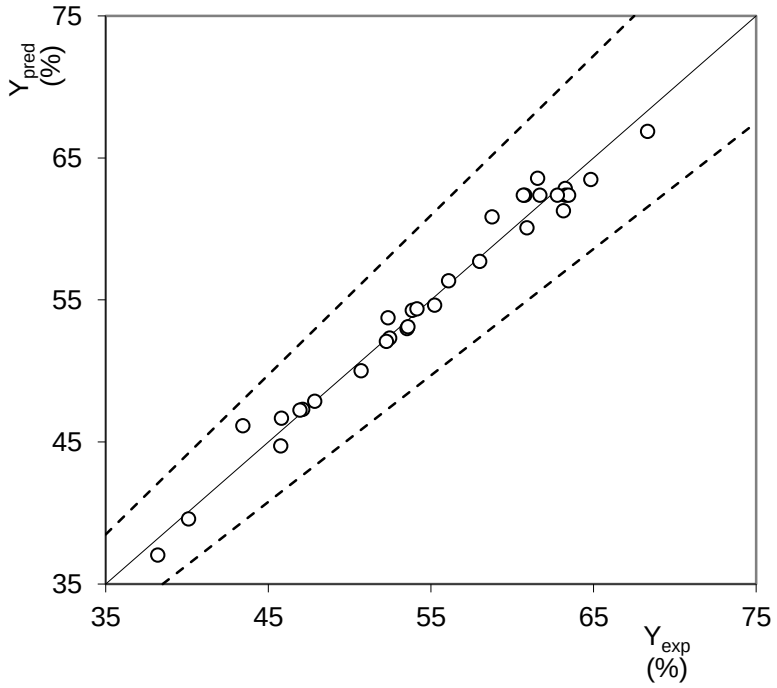

Figure 4.16 – Comparison between experimental (Y_{exp}) and calculated (Y_{calc}) lipid extraction yields for CCD experiments. The dashed lines delimit the ±10% deviation band.

In Figure 4.17 the plot of normalized residuals as a function of the response of the model is reported.

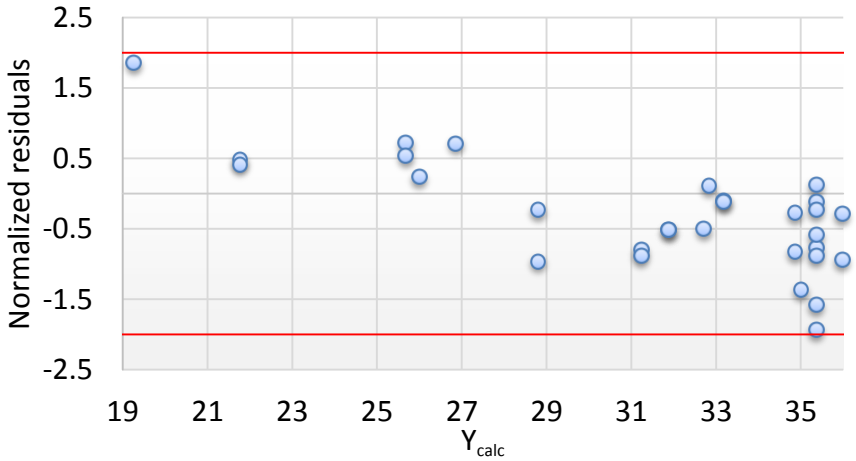

Figure 4.17 – Normalized residuals vs predicted yield value.

All points are arranged randomly within ± 2, with 95% of probability that points of the factorial region are well predicted by the model.
Fig. 4.19 shows the Normal Probability Plot.

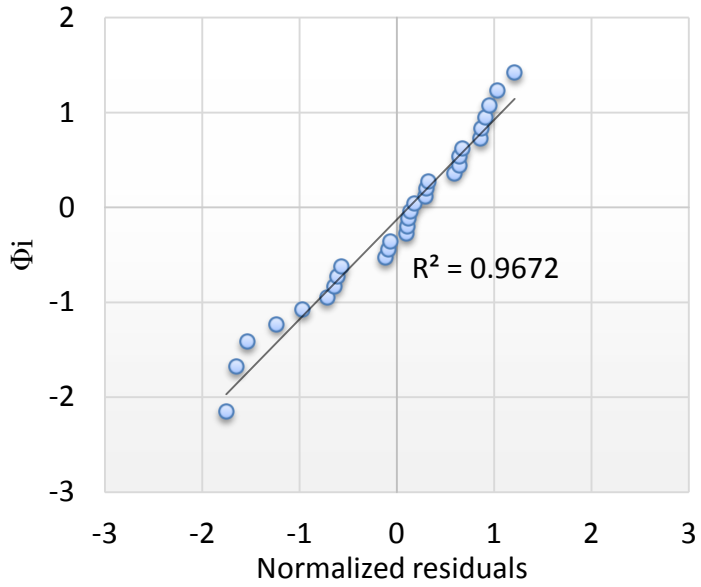

Figure 4.18 – Normal Probability Plots: standard normal cumulative distribution function vs. normalized residuals.

Points are located approximately along a straight line. Therefore it can be said that they are distributed according to the normal law.

The effect of the five main factors (T, pH, P, D1, D2) on the response variable is shown in Fig. 4.20, while the most significant response surfaces and contour plots generated from the model are displayed, respectively, in Figs. 4.21 and 4.22. Examination of Fig. 4.21 a and b reveals that the pretreatment temperature and pH had a strong effect on the curvature of the response surface, in agreement with the large negative values of their associated quadratic coefficients: β_{11} =–1.691, β_{22} =–2.303. This led to a maximum at approximately T = 50 °C and pH = 4.5 (Fig. 4.22 a). Pretreatment time affected positively the extraction yield, but with limited effect on response surface curvature (Fig. 4.20 b and c), in agreement with the small value of the corresponding quadratic coefficient: β_{33} =–0.237. Finally, Fig. 4.21 d shows that lipid recovery increased with the amount of added enzymes, over the whole dosage range for GMA (0-2 mg/g) and between 0-15 mg/g for CEL.

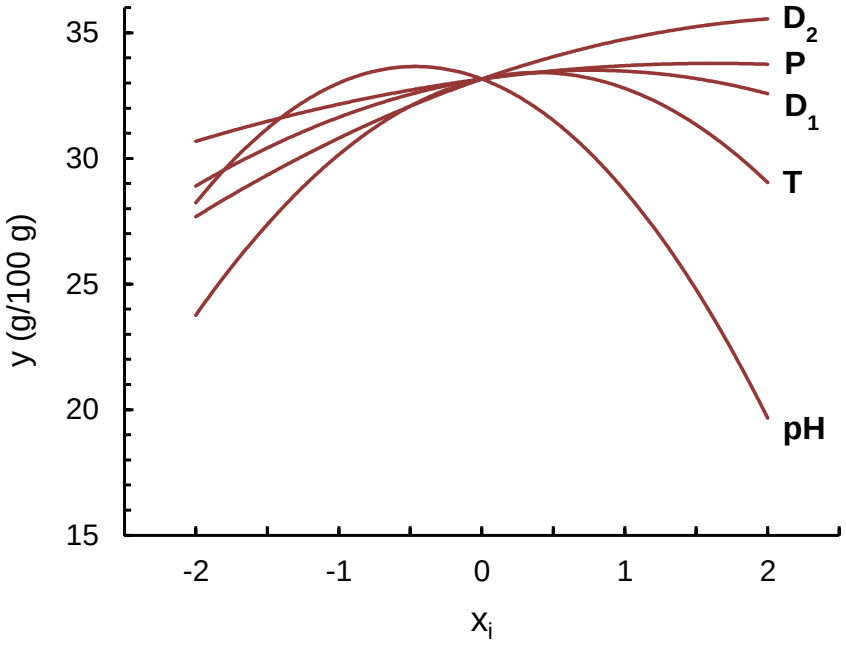

Fig. 4.19 – Effect of individual main factors on the lipid extraction yield (y). Each curve is plotted by keeping the remaining factors at their central values (T = 45 °C, pH = 5, P = 150 min, D_1 = 10 mg g^{-1}, D_2 = 1 mg g^{-1}).

a)

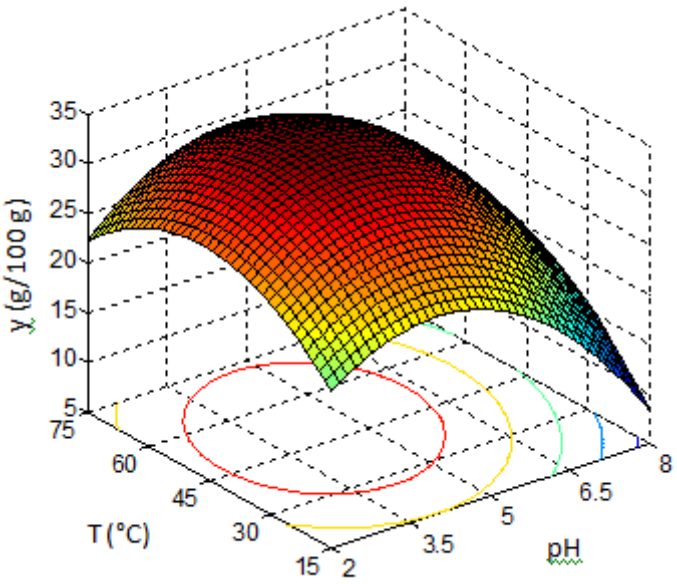

b)

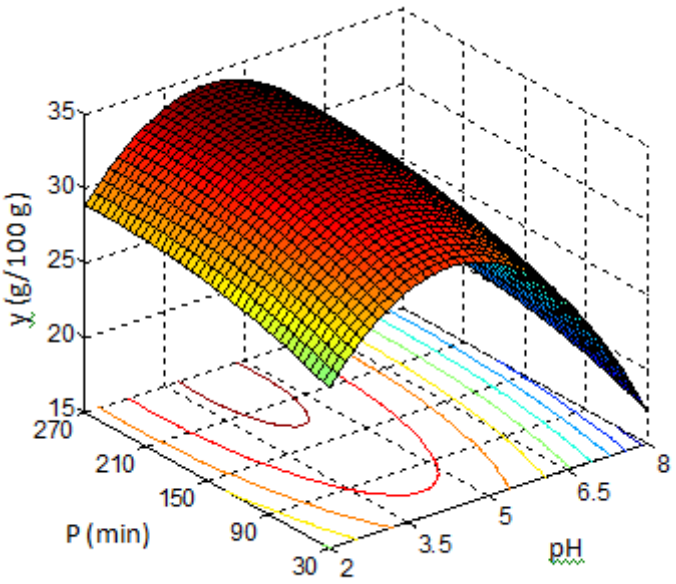
35
30
25
20
15
y (g/100 g)
270
210
150
90
30
P (min)
2
3.5
5
6.5
8
pH

c)

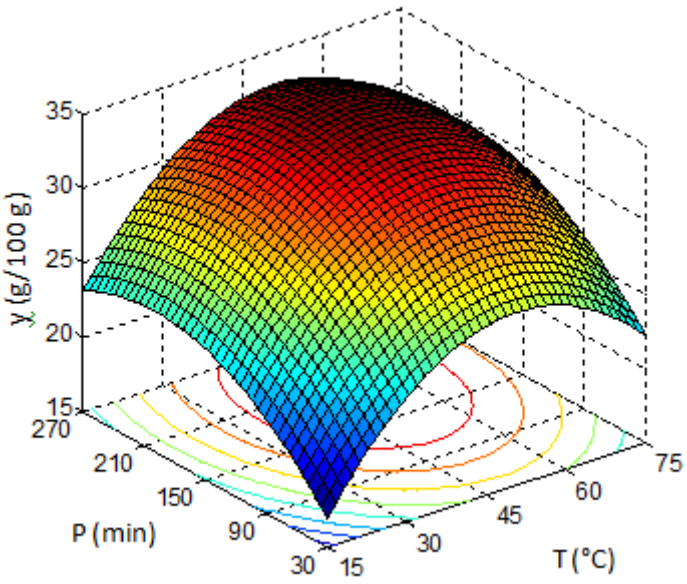
35
30
25
20
15
y (g/100 g)
270
210
150
90
30
P (min)
15
30
45
60
75
T (°C)

d)

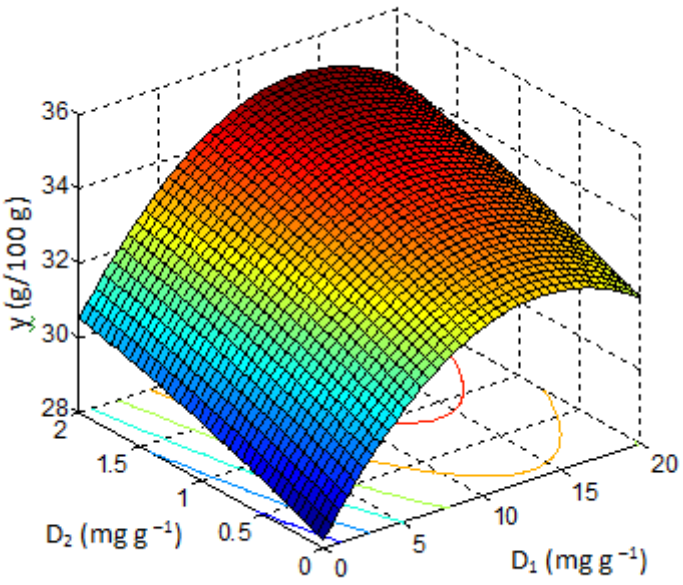

Figure 4.20 – Response surface plots showing the effect of: (a) temperature (T) and pH; (b) pretreatment time (P) and pH; (c) pretreatment time (P) and temperature (T) and (d) CEL dosage (D_1) and GMA dosage (D_2) on the lipid extraction yield (y). For each plot, the levels of the other factors are held at their central values (T = 45 °C, pH = 5, P = 150 min, D_1 = 10 mg g^{-1}, D_2 = 1 mg g^{-1}).

a)

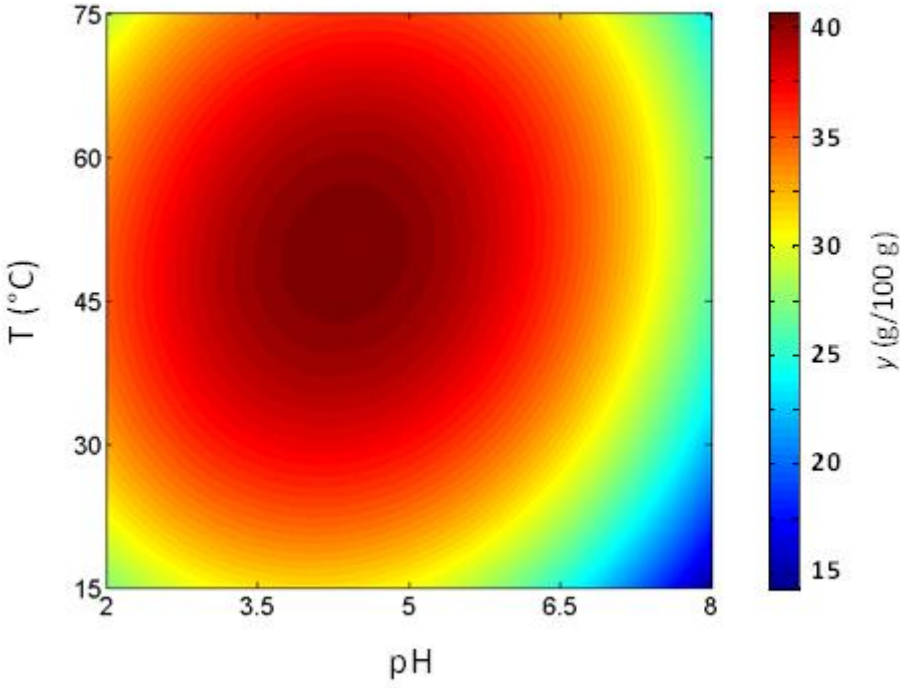

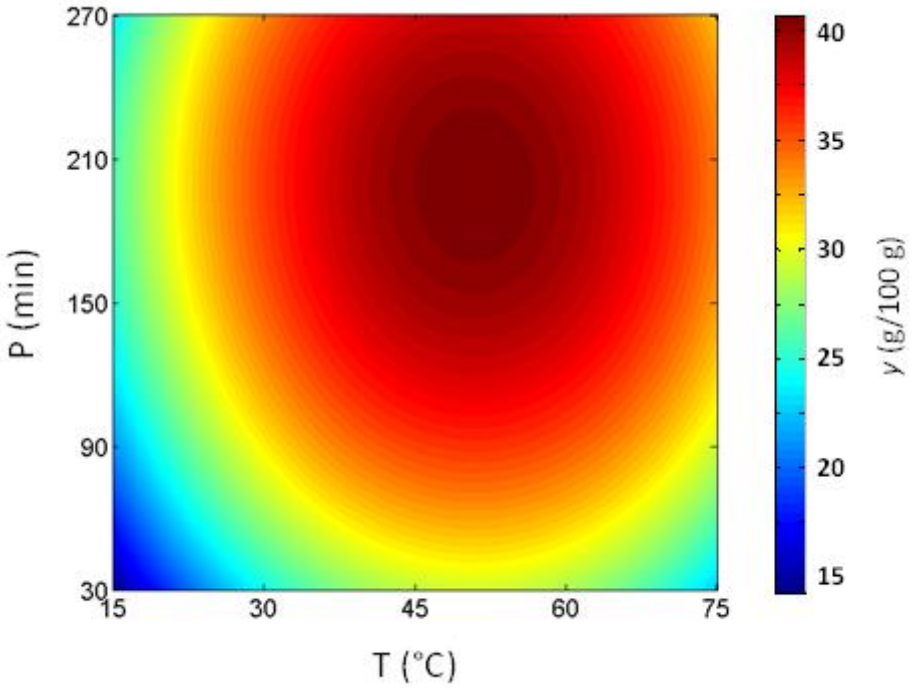

Figure 4.21 – Contour plots showing the effect of temperature (T) and pH (a) and temperature (T) and pretreatment time (P) (b) on the lipid extraction yield (y). For each plot, the levels of the other factors are held at their central values (T = 45 °C, pH = 5, P = 150 min, D_1 = 10 mg g^{-1}, D_2 = 1 mg g^{-1}).

4.5.3 Optimization and model validation

Maximization of the response variable calculated from the model was performed numerically, within the factorial region ($-1 \leq x_i \leq +1$), by the gradient descent method. The following results were obtained: T = 53 °C, pH = 4.4, P = 210 min, D1 = 13.8 mg/g, D2 =1.5 mg/g, with a maximum extraction yield of 36.6 g/100 g.

The results of optimization experiments performed under the reported conditions are summarized in Table 4.23.

Table 4.23 – Observed (Y_{exp}) and predicted (Y_{pred}) lipids extraction yields under optimal conditions together with their 95%-confidence intervals (CI).

SO	Y_{exp} (%)	Mean %	Dev.st %	Error %	Y_{pred} (%)	Deviation (%)	Low CI	High CI
Opt1	38.1				36.7	2.1	34.9	38.3
Opt2	37.5	37.8	0.5	0.7	36.7	1.1	34.9	38.3

The resulting percentage deviations were around 3% and a mean extraction yield of 37.8 % was reached. This value is effectively higher of each result obtained in the experimental design.

As it can be noticed, the values of temperature, pH and CEL dosage fall within the range of analysis taken into consideration. For the pre-treatment time and the GMA dosage, instead, this value corresponds with the +1 level. Therefore, it was decided to verify whether a further increase of these parameters (keeping fixed the others to the optimal values) could improve the extraction yields. Results are presented in Fig. 4.22.

a)

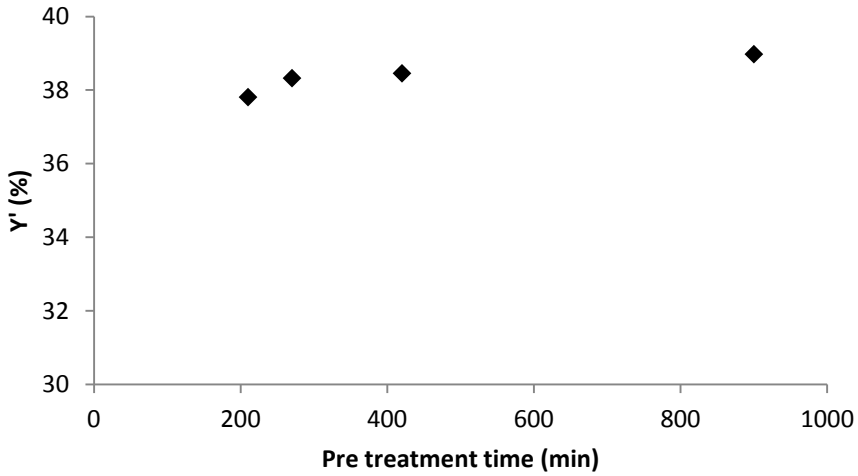

b)

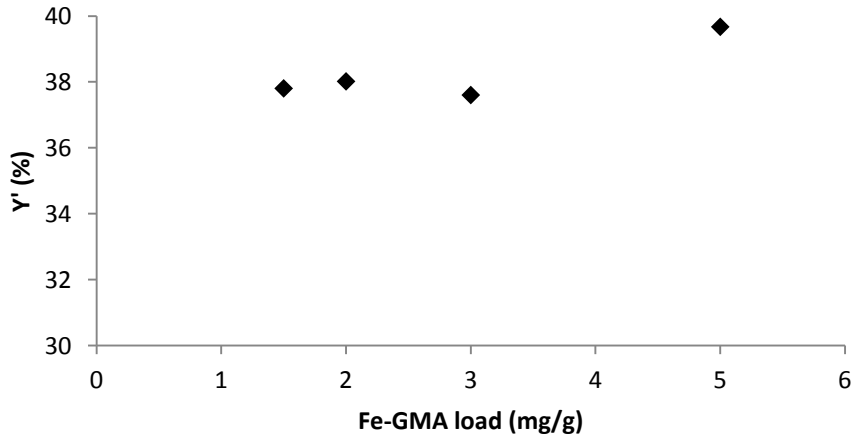

Fig. 4.22 – Effect of pre-treatment time and Fe-GMA load (D2) on lipid extraction yield. For each assay, the other factors are held at their optimal values.

From these trends, it can be highlighted that both parameters show small and not significant effects on the extraction yield, confirming the choice of the intervals taken into consideration in the experimental design. This could indicate that at 210 min the cell wall degradation operated by enzyme preparations is already occurred and/or that the permanence for prolonged times at a temperature higher than 50 °C causes the deactivation of the enzyme. Instead, the slight improvement of the extraction yield after an increase of GMA dosage does not justify an increase in its value and, consequently, of the cost of the process.

Other experiments were carried out and used together with optimal points to validate the model. The experiments were performed under the conditions reported in Table 4.24. Predicted lipid yield were calculated through the model under the experimental conditions adopted for the validation experiments as well as their 95%-prediction interval (Table 4.25).

Table 4.24 – Process conditions for validation points.

SO	Temperature (°C)	pH	Time (min)	Dosage CEL (mg/g)	Dosage GMA (mg/g)
V1	53	4.3	90	12.5	0.75
V2	40	6.5	60	7.5	1.25
V3	40	7	180	5	0.5

Table 4.25 – Observed (Y_{exp}) and predicted (Y_{pred}) lipids extraction yields for validation points together with their 95%-confidence intervals (CI).

SO	Y_{exp} (%)	Y_{pred} (%)	Deviation (%)	Low CI	High CI
V1	60.3	59.8	0.9	56.7	63.0
V2	52.3	49.7	5.0	47.8	54.1
V3	40.7	41.5	–2.0	38.2	44.8

As shown in Fig. 4.23, the extraction yields predicted by the model fall within a 10% deviation band and were in good agreement with the observed responses, with a mean difference of 2.8%. Furthermore, all the predicted responses were included into the 95%-prediction intervals, confirming that the developed models had good descriptive and predictive capabilities.

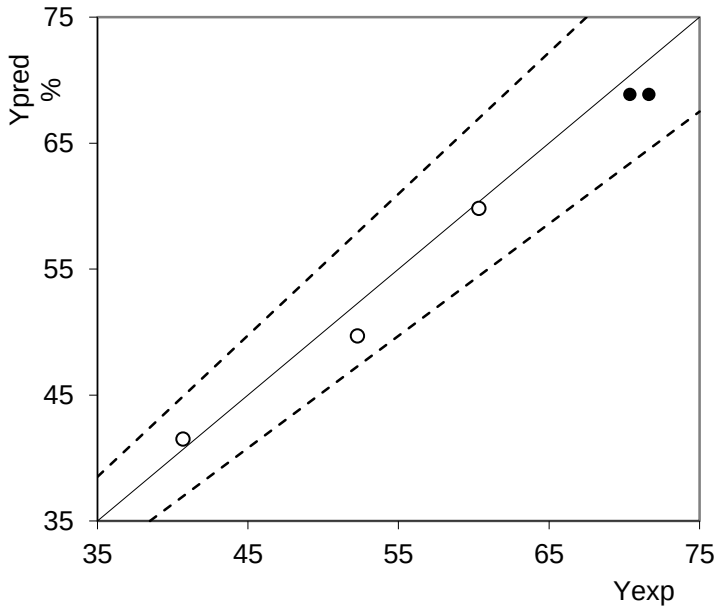

Figure 4.23 – Comparison between experimental (Y_{exp}) and calculated (Y_{calc}) lipid extraction yields for validation (open symbols) and optimal (solid symbols) points. The dashed lines delimit the ±10% deviation band.

4.5.4 Effect of extraction time

Additional experiments were carried out under the optimum treatment conditions determined from the model, by increasing the extraction time up to 6 h (compared to the value of 0.5 h used in central composite design experiments).
Results are shown in Fig. 4.24.
In optimal conditions, a sharp increase with time can be noticed, reaching a value of about 47 g/100 g after approximately 4 h, against the value of nearly 28 g/100 g in the absence of enzymes. Assuming that the total lipid content is 53.25 g/100 g, as determined by the method of Ma et al. (2012), the above value leads to a percentage yield close to 90%.
A mean difference of 35% of yield between optimal and blank assays has been found.

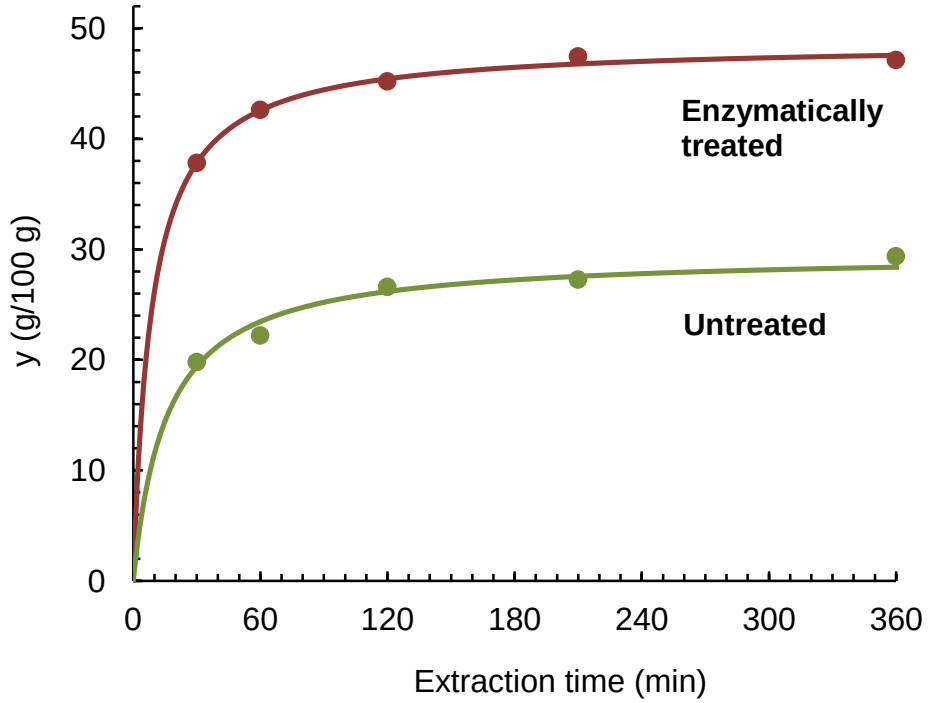

Figure 4.24 – Effect of extraction time on the yield of lipid extraction (y) from *Nannochloropsis* subjected to enzymatic treatment under optimal conditions (T = 53 °C, pH = 4.4, P = 210 min, D_1 = 13.8 mg g^{-1}, D_2 = 1.5 mg g^{-1}) or kept in pure water (untreated) under the same conditions.

4.6 Economic considerations

The costs of the enzyme preparations utilized in this study are 6.26 €/kg for Cellulyve 50 LC and 238.8 €/kg for Feedlyve GMA. These costs are modest compared to those of pure enzymes. The use of commercial enzyme preparations currently employed in other sectors of industry allows having not purified preparations, which, therefore, may contain side activities capable of improving the performances of the enzymatic pretreatment.

The cost of the pretreatment for all experimental points was calculated from the dosage of the two enzyme preparations and was used as second response variable of the experimental design.

A multi-objective optimization (Pareto optimization) was performed numerically by the gradient descent method, maximizing the extraction yield within the factorial region ($-1 \leq x_i \leq +1$) whilst minimizing the pretreatment cost. The following results were obtained: T = 47 °C, pH = 4.3, P = 210 min, D1 = 10 mg/g, D2 =0.5 mg/g, with a maximum extraction yield of 31.9 g/100 g.

These optimum conditions (Opt–2) were tested experimentally and results obtained were compared to those of the previous optimization (Opt–1), as reported in Table 4.26.

Table 4.26 – Observed (Y_{exp}) and predicted (Y_{pred}) lipids extraction yields under optimal conditions together with their 95%-confidence intervals (CI).

SO	Cost €/ton	Y_{exp} (%)	Y_{pred} (%)	Deviation (%)	Low CI	High CI
Opt–1	446	38.1	36.7	1.6	34.9	38.3
Opt–2	182	32.2	31.9	0.9	30.2	33.6

The cost of the Opt–2 mixture turns out to be 2.5 times lower than Opt–1 against a not too significant reduction in the extraction yield (lower than 5%). Further reduction of pre-treatment cost can be represented by the reuse of the multienzymatic mixture for more pre-treatment cycles. This solution was tested experimentally.

Fig. 4.25 shows the extraction yields obtained after subsequent pretreatments using the enzyme solution recovered by centrifugation after each cycle. All tests were carried out at the optimum point selected previously (Opt–1).

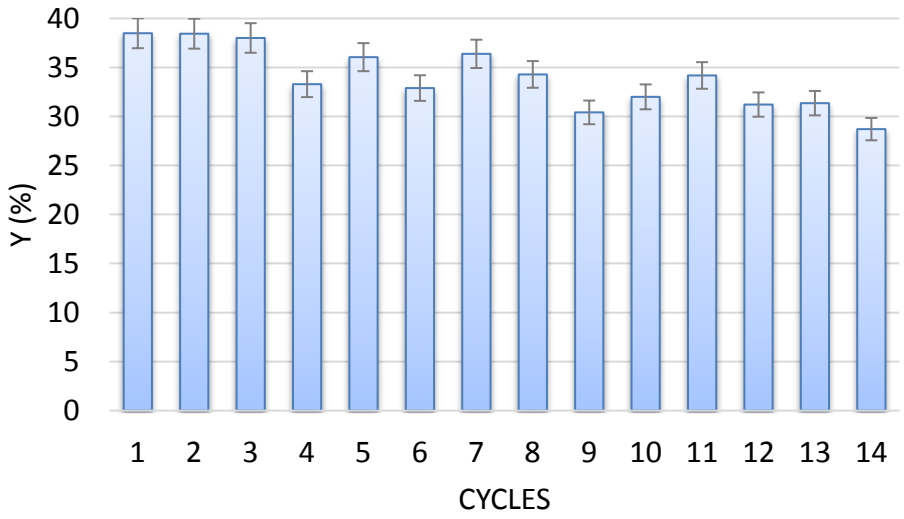

Figure 4.25 – Extraction yields of lipid as a function of the number of reuse cycles of the pretreatment solution.

As it can be seen from the figure, the extraction yield remains high enough for a good number of cycles and decreases more or less linearly losing about 8 percentage points only after 11 reuse cycles. These results highlight the convenience of recovering the pre-treatment enzyme solution. This could significantly reduce the cost if the solution is used in a continuous cycle for several times.

4.7 Discussion of results

Total lipid content of the microalga was found to be 53.25 ± 1.25 mg/100 mg. This is a very high value if compared to other microalgal species (Griffiths and Harrison, 2009), confirming the ability of *Nannochloropsis* sp. to accumulate high amounts of lipids when grown under appropriate conditions (Perin et al., 2014).
The pretreatment with some enzymes allowed a lipid yield of around 37%, while control experiments led to a yield of around 21% and the direct extraction with solvent mixture showed a yield of only 16% extraction, highlighting that there is a sensitive enzymatic effect for some of the chosen enzyme preparations.
The beneficial effect of enzymes on lipid recovery can be explained by considering that the cell wall of microalgae acts as a significant barrier to the extraction solvent (Lee et al., 2012). As a result, it can be expected that weakening or destroying this barrier favors the penetration of solvent molecules into the cell.
Weakening or destroying this barrier can favor the penetration of solvent molecules into the cell.
Moreover, as it can be seen from the mixture of design experiments, the use of a mixture of enzyme preparations brings an increase in the extraction yield compared to pre-treatment with individual enzymes.
The observed enhancement in lipids extractability can be explained by the fact that the microalgal cell wall is composed in cellulose and hemicelluloses (Safi et al., 2014). Cellulose and hemicellulose are the structural cell wall components that are specifically degraded by the enzymes used. As known, cellulose is composed of linear polymeric chains of β-(1,4)-D-glucopyranose units that form microfibrils consisting of well-packed hydrogen bonded stretches of crystalline cellulose and less ordered amorphous regions (Nishiyama, 2009). The amorphous matrix consists of two major groups of polysaccharides, hemicelluloses and pectins, plus a small amount of structural proteins. The ratio of amorphous to crystalline cellulose greatly affects the susceptibility of the cell wall to chemical or enzymatic attack. In fact, while amorphous domains are easily hydrolyzable, crystalline regions are highly resistant to hydrolytic degradation (Zhao et al., 2012). During enzymatic hydrolysis, the amorphous cellulose is attacked first, followed by the hydrolysis of the more recalcitrant crystalline composition. Cellulose microfibrils are extensively cross-linked by hemicelluloses such as xylans, xyloglucans, glucomannans and mixed linkage glucans (Scheller and Ulvskov, 2010). The positive synergistic effects observed when cellulase and hemicellulase were used in combination can be explained by considering that the tight packing of crystalline cellulose chains limits the accessibility of cellulase to the substrate and that the presence of hemicelluloses molecules around the cellulose microfibrils can reduce the number of surface sites available for enzymatic attack. Once hemicelluloses components in the cell wall of *Nannochloropsis* are degraded, the exposure of cellulose to cellulase increases, thus allowing more effective degradation of cellulose microfibrils. The synergistic effects of cellulolytic and hemicellulolytic enzymes in the treatment of lignocellulosic materials is well documented, such as for the recovery of oil from pumpkin seeds

(Jiao et al., 2014) and of lycopene from tomato peels (Lavecchia and Zuorro, 2008; Zuorro, 2009). Thus, it can be inferred that for this type of applications mixing hydrolytic enzyme preparations are more appropriate than those that utilize individual enzymes. Although plant and algal cells display great diversity, which is likely the result of the different expression of a vast array of genes, their cell walls exhibit some similarities, such as the richness in polysaccharides and the fact that cellulose microfibrils form a network crosslinked by hemicellulose polymers (Popper et al., 2014). Accordingly, it seems plausible to hypothesize that synergistic effects in the presence of multiple enzymes can also occur with microalgae. In agreement to this, a study on the enzyme-assisted oil recovery from *Scenedesmus* sp. using cellulase, hemicellulase and pectinase showed that the recovery was maximum when the biomass was treated with cellulase-hemicellulase-pectinase mixtures in the ratio of 1:1:1 or 1:2:1 w/w (Huo et al., 2015). In another study, Gerken et al. (2013) found that most of the individual enzymes tested had little or no effect on the enzymatic cell wall degradation of *Chlorella vulgaris*, while their binary mixtures increased, although to different extents, cell wall permeability. An indirect indication of the efficiency of multi-enzyme systems is also provided by the high capacity of cellulase-containing microbial extracts from bacteria (Muñoz et al., 2014) or fungi (Ciudad et al., 2014) to degrade algal cell walls.

An analysis of the results of the experimental design reveals that response surfaces determined through the model have a concavity downwards (also confirmed by the quadratic coefficients with a negative sign). In particular, when the levels of time and GMA dosage are kept constant, the response surface plots for each couple of the other variables show a maximum-like behavior. However, time and GMA dosage have a quadratic dependence too (less pronounced than the effect linear). In fact, analyzing the trend of response surfaces, it can be assumed that a further increase of the values of these parameters does not lead to a significant improvement of the extraction yields.

Moreover, the presence of a positive interaction between the temperature and the parameters pH and GMA load can be noted from response surfaces and contour plots. This is probably due to the fact that the activity of the enzyme preparation rich in galactomannanase is influenced by the temperature (Chang et al., 2006). In addition, temperature and pH have a maximum, likely due to the optimal conditions in which enzyme preparations used operate. The effect of temperature and pH on enzymatic activity has been widely studied in literature (Yin et al., 2011).

Higher pretreatment times allow an increase of the effect of degradation of the cell wall operated by the enzyme preparations, even if contact period between enzyme and substrate influences the extent of the reaction as long as the enzyme is still active. Time of hydrolysis could vary from 10 minutes up till 24 hours, due to variations in other processing parameters, such as temperature and pH, which directly influence time of hydrolysis (Hammed et al., 2013).

The simultaneous use of the two enzyme preparations led to an increased lipid extraction. As said cellulase (EC 3.2.1.4) hydrolyzes the β-1,4 linkages of cellulose,

while mannanase (EC 3.2.1.78) cleaves the internal β-1,4 linkages of mannans, galactomannans and glucomannans. It is also known that, in both plant and algal walls, cellulose microfibrils are extensively cross-linked by mannans and other hemicelluloses. When these hemicellulose bridges are enzymatically degraded, the accessibility of cellulase to the surface sites of cellulose could increase, resulting in an enhancement of cellulase activity. Mannan-rich hemicelluloses (polymers of ß-mannose) were found in some algae cell wall. Structurally, these polysaccharides contain ß-1,4-linked residues of mannose or a combination of glucose and mannose. These may be substituted with α-1,6-linked galactose short side chains. Several types of mannans have been found: pure mannans, galacto-mannans, gluco-mannans and galacto-gluco-mannans (Del Carmen Rodriguez-Gacio et al., 2012). Galactomannans, in particular, were isolated from different species of green microalgae, such as *Kirchneriella lunaris* (Abo Shady et al., 1993), *Capsosiphon fulvescens* (Na et al., 2010) and *Haematococcus lacustris* (Park et al., 2011). An analysis of alcohol insoluble residues of *Nannochloropsis oceanica* polysaccharides (Chapter 3) showed that the alga contains 90% of glucose residues, 3% of mannose and the rest traces of galactose, rhamnose, fucose, arabinose and xylose (Vieler et al., 2012).

The positive effect of enzyme dosage can be ascribed to the enhanced degradation of cell wall components at higher enzyme concentrations. The decrease in extraction yields at CEL dosages approximately higher than 14 mg/g could result from a kinetic effect known as “competitive non-productive enzyme adsorption” (Norsker et al., 1999). This phenomenon occurs in multi-enzyme systems when enzyme molecules adsorb temporarily on sites that they cannot attack (Zuorro et al., 2016). When the number of sites occupied in this way becomes high, the adsorbed species may cause steric hindrance to the enzymes that are specific for those active sites, leading to a reduction of the hydrolysis rate. While these effects have not been specifically investigated in microalgae, they are well documented in plant materials such as, for example, black currant pomace (Kapasakalidis et al., 2009) and cauliflower leaves (Huynh et al., 2014).

The lipid yield increased with extraction time. The positive effect of solvent extraction time was also reported by Prommuak et al. (2012), for the recovery of lipids from *Chlorella vulgaris*, using maceration ultrasound-assisted and microwave-assisted extractions.

A percentage yield close to 90% of total lipids was reached in optimal conditions after approximately 4 h of extraction with solvent mixture.

These yields are much higher than those reported for the enzyme-assisted recovery of lipids from other microalgal species. In Table 4.27, some literature data on enzyme-assisted lipid extraction from various microalgae are shown.

Table 4.27 – Results of studies on enzyme-assisted lipid extraction from different microalgae.

Microalgae species	Treatment	Enzymes and conditions	Lipid content (g/100 g)	Lipid extraction yield (%)	Reference
Nannochloropsis sp.	Enzyme-assisted aqueous extraction on sonicated microalgae	Snailase, Trypsin 12 h, 37°C, pH 5.8/8	15.98	11.7	Liang et al. (2013)
Scenedesmus dimorphus	Enzyme-assisted aqueous extraction on sonicated microalgae	Snailase, Trypsin 12 h, 37°C, pH 5.8/8	10.62	46.8	Liang et al. (2013)
Chlorella vulgaris	Enzyme-assisted aqueous extraction on sonicated microalgae	Snailase, Trypsin 12 h, 37°C, pH 5.8/8	15.11	49.8	Liang et al. (2013)
Scenedesmus sp. G4	Enzymatic hydrolysis followed by solvent extraction	Cellulase + Pectinase + Hemicellulase (1:1:1 or 1:2:1 w/w/w) 72 h, 30/50 °C, pH 3.5/4.5	48.8	86.1	Huo et al. (2015)
Scenedesmus sp.	Enzymatic hydrolysis followed by solvent extraction	Lysozyme 0.5 h, 37 °C, pH 7.48	21.1	78.7	Taher et al. (2014)
Scenedesmus sp.	Enzymatic hydrolysis followed by solvent extraction	Cellulase 0.5 h, 37 °C, pH 7.48	21.1	72.0	Taher et al. (2014)

We note that extraction yields vary over a wide range of values, depending on the algal species and the treatment conditions. It is also interesting to point out that a 12-h treatment of *Nannochloropsis* sp. with snailase and trypsin gave a lipid recovery of only 11.7% (Liang et al., 2013), which confirms that the structural features of the cell wall of this microalga make it highly resistant to enzymatic, mechanical and thermal treatments (Scholz et al., 2015).

CHAPTER 5

Characterization of untreated and enzymatically treated microalgae

In this chapter, the characterization of untreated and enzymatically treated *Nannochloropsis* microalgae biomass is described in details. Several techniques have been utilized in order to understand the effect of enzymatic hydrolysis, such as TOC, proximate, ultimate and compositional analysis, FTIR, XRD, TGA/DTG, SEM and TEM.

The only use of extraction yield as a sign of the pretreatment effectiveness cannot be considered as indicative as it is also affected by the contribute of the solvent utilized for the recovery, in particular when the extraction time is not negligible. Moreover, the influence of partially ruptured cells on the increase in solvent accessibility during lipid recovery is relatively less significant; these cells could be considered as unruptured (Yap et al., 2014). The ability to carry out reliable biomass

characterization, targeting specific recalcitrance-related properties of the cell wall after the pretreatment is essential (Foston and Ragauskas, 2012), in order to understand the action of each enzyme. This can help to properly design the process and to facilitate its optimization.
Dissolved Organic Carbon (DOC) calculated by TOC released in the pretreating solution is useful to estimate the degree of hydrolysis of the cell wall of plants or yeasts after enzymatic treatments (He et al., 2006). Therefore, in this work the feasibility of using DOC values as a means to assess the effectiveness of an enzyme-assisted pretreatment of microalgae was investigated.
The use of instrumental methods, such as Fourier transform infrared spectroscopy (FTIR), X-ray diffraction spectrometry (XRD), thermogravimetry (TGA/DTG) and scanning and transmission electron microscopy (SEM and TEM) enables comprehensive and accurate characterization (Pereira et al., 2016), allowing the development of effective screening tools that can be useful to determine the best pretreatment specifically for the microalga of interest.
In particular, FTIR can be used to assess the microalgal cell chemical composition and to provide detailed structural elucidation of the effects of enzymatic treatments. TGA is widely utilized to study decomposition reactions of the different biomasses including microalgae and can be used to qualitatively compare their biochemical composition. XRD can estimate the crystallinity index of cellulose before and after an enzymatic treatment, while TEM and SEM provide information on the morphology of the untreated and digested cell walls.
The two commercial enzyme preparations selected in the previous Chapter were used for treating *Nannochloropsis* under the optimal conditions determined. One is rich in cellulase and the other one is rich in galactomannanase. Results lead to a better understanding of the effects of the enzymes used alone and in combination. This can allow relating these biological treatments to changes in structure.

5.1 Materials and methods

5.1.1 Chemicals, enzymes and microalgae

Methanol, 2-propanol, chloroform, hexane, potassium hydrogen phthalate, sodium chloride and hydrochloric acid (37 wt%) were purchased from Carlo Erba (Milano, Italy). Glutaraldehyde (CAS No. 111-30-8), uranyl acetate (CAS No. 541-09-3), lead citrate (CAS No. 512-26-5) and epoxy resin Embed-812 were from SIC (Roma, Italy); osmium tetroxide (CAS No. 20816-12-0) from Agar Scientific (Stansted, UK) and propylene oxide (CAS No. 75-56-9) from BDH Italia (Milano, Italy).
Cellulyve 50LC® (CEL) and Feedlyve GMA® (GMA) products were obtained from Lyven SA (Colombelles, France). These enzyme preparations were selected on the basis of the results obtained in Chapter 4. CEL from *Trichoderma reseei* is rich in cellulase (EC 3.2.1.4, activity ≥ 240 U/g), while GMA from *Aspergillus niger* is rich in Endo-β-1, 4-mannanase (EC 3.2.1.78, activity ≥ 10,000 U/g).

Nannochloropsis sp. biomass was provided in lyophilized form by the Department of Agri-Food Production and Environmental Sciences of the University of Florence (Italy). The growth conditions and the reactor configuration used are reported Bondioli et al. (2012).

5.1.2 Determination of total lipid content

Total lipid content of *Nannochloropsis* was determined by the method of Ma et al. (2013) with slight modifications. Specifically, 0.2 g of biomass were mixed with 18 mL of chloroform/methanol (2:1, v/v) and stirred at 37 °C for 1 h (Kika Werke 10 power). Then, the mixture was centrifuged at 10,000 ×g for 10 min (Centrifuge MPW 380, Med. Instruments, Poland), the supernatant collected and the residual biomass re-extracted two more times under the same conditions. The three supernatants were combined and 1% sodium chloride solution (20% of the total volume) was added. After 10 min stirring at 37 °C, the mixture was centrifuged (10,000 ×g, 10 min), the organic phase recovered and evaporated under vacuum at 40 °C (Rotavapor R-215, BUCHI Labortechnik AG, Switzerland). The lipid content was calculated from the weight of the residue and expressed as grams of lipids per 100 g of dry biomass.

5.1.3 Enzyme-assisted lipid extraction

The enzyme-assisted extraction of lipids from *Nannochloropsis* was investigated in batch mode according to the following procedure. Briefly, 0.2 g of microalgae and 20 mL of the aqueous enzyme solution were loaded into 20-mL screw-capped flasks according to the experimental design whose details will be described later. The flasks were placed in a thermostated water bath and magnetically stirred for the appropriate time. Then, the algal suspension was centrifuged (10,000 ×g, 10 min) and the supernatant was separated and collected for TOC analysis. For all other characterization, enzymatic pretreatments were performed using CEL (dosage 13.8 mg/g), GMA (dosage 1.5 mg/g) and a mixture of these two commercial preparations (OPT). In these experiments, 0.2 g of microalgae and the enzyme solution were loaded and magnetically stirred for 24 h at 53°C and pH 4.3. Temperature, pH and enzyme dosage values were determined on the basis of optimization performed previously. The initial pH of the microalgal suspension was adjusted with small amounts of HCl 0.1 N and then monitored during the assay.
The resulting biomass was contacted with 10 mL hexane/isopropanol (3:2, v/v) and stirred at room temperature. After this time, the suspension was centrifuged (10,000 ×g, 5 min) and the amount of extracted lipids determined gravimetrically after solvent evaporation.
Results were expressed as the amount of lipids extracted per dry weight of biomass (Y_{lip}, g/100 g).

5.1.4 DOC measurement and weight loss

The supernatant collected after enzymatic pre-treatment was characterized by TOC analysis. A TOC-L analyzer (Shimadzu, Japan) was used for Dissolved Organic Carbon (DOC) measurements. Before analysis, liquid samples were passed through a 0.45 μm nylon filter and diluted with double-distilled water. The DOC content was determined in terms of total carbon using a calibration curve obtained with standard solutions of potassium hydrogen phthalate. The contribution of the enzymes to the DOC was subtracted from the value obtained for whole liquid sample. Weight loss was determined gravimetrically after water separation.

5.1.5 Proximate, ultimate and compositional analysis

Proximate analysis of algal biomass samples (treated and untreated) was performed by TG analysis (ASTM 5142/02a). The elemental composition (ultimate analysis) was carried out using a CHN (Eurovector EA3000) elemental analyzer. The analyzer was calibrated using Acetanilide (C-71.09%, H-6.71%, N-10.36%) as standard. The amount of oxygen was calculated by difference from 100%. Protein content was estimated by multiplying the elemental N content by a factor of 4.87 (Lourenço et al., 2004). The carbohydrate content was determined by subtracting the ash content, lipid content, weight loss and protein content from 100%.

5.1.6 Thermal Characterization (TGA/DTG)

Thermogravimetric analysis (TGA) and derivative thermogravimetric (DTG) analysis were performed with a thermogravimetric analyzer SDT Q600 (TA Instruments). TG experiments were made on algal biomass, untreated and treated, cellulose and hemicelluloses (xylan) purchased from Sigma-Aldrich. Small amounts of sample, approximately 10 mg, were heated in nitrogen atmosphere, with a flux of 100 mL min^{-1}, at 10°C min^{-1} up to a temperature of 1000°C. The MagicPlot Pro® software (version 2.5.1, Magicplot Systems LLC, Saint Petersburg, Russia) was used to carry out the deconvolution computation of the DTG curves.

5.1.7 Fourier transform Infrared spectroscopy (FTIR)

Fourier-transform infrared (FTIR) studies were carried out on dry untreated and enzymatically treated biomass samples and on their residue after lipid extraction. The samples were grounded and quartered as described by Diniz *et al.* (2014) in order to obtain a representative portion of material from the total amount of biomass. Measurements were performed on a Bruker Vertex 70 spectrometer (Bruker Optics, Billerica, MA, USA) equipped with a Platinum ATR sampling

module. FTIR spectra were collected in quadruplicate in the mid infrared region (4000-400 cm^{-1}) with 128 scan at a resolution of 3 cm^{-1}.

5.1.8 Powder X-Ray Diffraction

The crystallinity of treated and untreated algal samples was determined by powder X-Ray diffraction (Philips PW 1830 Diffractometer). The diffraction patterns were collected on samples placed on a glass holder in the range 2θ = 5°-35° with a step length of 0.005° using Cu Kα radiation (wavelength of 1.5406 Å) at 40 kV and 30 mA. The crystallization index (*CrI*, %) has been calculated by the following equation:

$$CrI = \frac{(I_{main} - I_{am)}}{I_{main}} \cdot 100$$

where I_{main} and I_{am} are the diffraction intensity of the main peak (2θ = 20.1°) and the baseline (2θ = 17.4°), respectively. Crystalline and amorphous peaks were obtained by a curve-fitting process, assuming Gaussian functions, from the diffraction intensity profiles. The deconvolution was performed using the MagicPlot Pro® software (version 2.5.1, Magicplot Systems LLC, Saint Petersburg, Russia).

5.1.9 Electron microscopy

Scanning electron microscopy (SEM) and transmission electron microscopy (TEM) were used to investigate the morphological changes of microalgal cells due to the enzymatic treatment.
SEM images were taken for analyzing cell wall changes on the different pretreated microalgal cells. A small amount of sample was taken from the suspension, placed on silicon substrate, dried, chromium-coated and observed with a High Resolution-Field Emission Scanning Electron Microscope (HR-FESEM_AURIGA Zeiss) at 6kV.
Microalgal samples for TEM were smeared on poly-L-lysine coated slides, fixed in 2.5% glutaraldehyde and post-fixed in 4% osmium tetroxide followed by sequential dehydration with increasing concentrations of ethanol. Samples were then immersed in propylene oxide for solvent substitution and embedded in Embed-812 epoxy resin. A Leica EM UC6 ultramicrotome was used to obtain ultrathin cell sections (70–80 nm), which were stained with 2% uranyl acetate and Reynolds lead citrate and examined with a Zeiss EM10 electron microscope operated at 60 kV.

5.2 Determination of dissolved organic carbon (DOC)

5.2.1 Experimental design

A central composite design (CCD) was used to investigate the effects of temperature (T), pH, pretreatment time (P), CEL dosage (D1, mg/g) and GMA dosage (D2, mg/g) on the enzymatic treatment (Lavecchia et al., 2016). The DOC of the liquid at the end of the treatment (y) was used as the response variable. The CCD consisted of a half fraction of the full 2^5 factorial design augmented by six central points and two axial points at $\pm\alpha$ for each factor, for a total of 32 runs. To ensure the rotability of the design space, α was taken as $(2^{5-1})^{1/4} = 2$ (Montgomery, 2012). Furthermore, the run order was randomized to minimize the effects of uncontrolled factors.
The levels of each factor were chosen to cover a range of values of practical interest. They are reported in Table 5.1 in both actual (X_i) and coded (x_i) values. The latter values were obtained using the following equations:

$$x_1 = \frac{T - 45}{15}$$

$$x_2 = \frac{pH - 5}{1.5}$$

$$x_3 = \frac{P - 150}{60}$$

$$x_4 = \frac{D1 - 10}{5}$$

$$x_5 = \frac{D2 - 1}{0.5}$$

The design and analysis of experiments were performed by using the Design-Expert® software (version 7.0, Stat-Ease Inc., Minneapolis, MN, USA).

Table 5.1 – Factors and levels of experimental design.

Factor	Unit	Levels				
		–2	**–1**	**0**	**1**	**2**
T-Temperature	°C	15	30	45	60	75
pH		2	3.5	5	6.5	8
P-time	min	30	90	150	210	270
D1-Dosage CEL	mg/g	0.0	5	10	15	20
D2-Dosage GMA	mg/g	0.0	0.5	1	1.5	2.0

Table 5.2 – Experimental design layout. SO is the standard order and RO the randomized order of runs

SO	RO	Temperature	pH	Time	Dosage CEL	Dosage GMA
1	13	-1	-1	-1	-1	1
2	28	1	-1	-1	-1	-1
3	17	-1	1	-1	-1	-1
4	29	1	1	-1	-1	1
5	24	-1	-1	1	-1	-1
6	9	1	-1	1	-1	1
7	18	-1	1	1	-1	1
8	31	1	1	1	-1	-1
9	21	-1	-1	-1	1	-1
10	22	1	-1	-1	1	1
11	14	-1	1	-1	1	-1
12	15	1	1	-1	1	-1
13	19	-1	-1	1	1	1
14	26	1	-1	1	1	-1
15	1	-1	1	1	1	-1
16	30	1	1	1	1	1
17	2	-2	0	0	0	0
18	23	2	0	0	0	0
19	11	0	-2	0	0	0
20	10	0	2	0	0	0
21	8	0	0	-2	0	0
22	27	0	0	2	0	0
23	20	0	0	0	-2	0
24	16	0	0	0	2	0
25	4	0	0	0	0	-2
26	3	0	0	0	0	2
27	5	0	0	0	0	0
28	12	0	0	0	0	0
29	32	0	0	0	0	0
30	6	0	0	0	0	0
31	25	0	0	0	0	0
32	7	0	0	0	0	0

5.2.2 Results

Results obtained are shown in Table 5.3.

Table 5.3 – Observed (Y_{exp}) and predicted (Y_{pred}) DOC values.

SO	y_{exp} (mg L^{-1})	y_{calc} (mg L^{-1})	Deviation (%)
1	587.0	605.3	-0.78
2	712.7	764.1	1.35
3	639.9	650.2	1.26
4	809.4	809.1	-2.65
5	711.8	653.9	0.27
6	788.9	812.8	0.64
7	638.0	698.8	-0.40
8	823.2	857.7	-1.90
9	662.1	663.2	1.01
10	794.1	822.1	-3.27
11	754.0	708.2	-0.04
12	937.3	867.0	-0.65
13	675.4	711.9	-3.57
14	817.6	870.7	-0.48
15	668.9	747.2	-6.25
16	917.0	915.7	1.35
17	626.0	629.6	2.26
18	947.7	947.3	1.06
19	680.1	631.7	0.86
20	730.7	721.6	3.03
21	680.1	739.8	0.48
22	899.7	837.0	2.07
23	762.2	730.5	-0.45
24	852.1	846.4	2.95
25	744.3	788.4	0.33
26	840.3	788.4	2.12
27	817.0	788.4	1.42
28	792.6	788.4	-2.65
29	776.9	788.4	-2.80
30	781.5	788.4	1.71
31	845.6	788.4	-1.11
32	844.9	788.4	0.63

A preliminary control experiment was carried out without enzymes by setting the treatment conditions at their centre-point values (T = 45 °C, pH = 5, P = 5 min). The

resulting DOC was 419.0 ± 50.3 mg L^{-1}. In the presence of enzymes, DOC values ranging from 587.0 to 947.7 mg L^{-1} (mean value: 773.4 mg L^{-1}) were observed (Table 2). In the factorial space, the maximum DOC value (937.3 mg L^{-1}) was achieved at T = 60 °C, pH = 6.5, P = 90 min, D1 = 15 mg g^{-1} and D2 = 0.5 mg g^{-1}. These results clearly attest the effectiveness of the enzymatic treatment and the possibility of using DOC as a measure of the effects of enzymes on cell wall degradation. A similar conclusion was reached by He et al. (2006), who found a significant increase in the DOC of the liquid after the enzymatic hydrolysis of potato samples rich in carbohydrates and proteins.
The results of CCD experiments have been analyzed by different empirical models (linear, two-factor interaction, quadratic and cubic). The best result was obtained using the second-order polynomial equation:

$$Y = \beta_0 + \sum_{i=1}^{5} \beta_i x_i + \sum_{i=1}^{5} \beta_{ii} x_i^2 + \sum_{i=1}^{4} \sum_{j=i+1}^{5} \beta_{ij} x_i x_j$$

where Y is the response variable, x_i are the independent variables, β_o is the intercept and β_i, β_{ii} and β_{ij} are the linear, quadratic and interaction regression coefficients.

The non-significant coefficients were therefore eliminated and new reduced model was developed by using the stepwise regression method, with model terms entered and eliminated at a confidence level of 90%. The new coefficients were re-estimated from the experimental data, leading to the following final regression equation:

$$Y = \beta_0 + \beta_1 \cdot x_1 + \beta_2 \cdot x_2 + \beta_3 \cdot x_3 + \beta_4 \cdot x_4 + \beta_{22} \cdot x_2^2$$

The six model coefficients together with their standard errors, 95% confidence intervals and p-values, are listed in Table 5.4. The above equation provided a fairly good fit to the data, with coefficient of determination (R^2) and adjusted-R^2 of 0.802 and 0.764, respectively. An analysis of residuals showed no apparent violations of basic ANOVA assumptions, that is, normally distributed errors with constant variance and independent of one another.

Table 5.4 – Estimates of the regression coefficients of model equation with their corresponding standard errors (SE), 95 % confidence intervals (CI) and p-values

Coefficient	Term	Estimated coefficient	SE	Low CI	High CI	p–value
β_0	Intercept	788.42	10.25	767.34	809.49	< 0.0001
β_1	T	79.43	9.36	60.19	98.67	< 0.0001
β_2	pH	22.46	9.36	3.22	41.70	0.0239
β_3	P	24.31	9.36	5.07	43.55	0.0153
β_4	D1	28.98	9.36	9.74	48.22	0.0047
β_{22}	pH × pH	−27.95	8.37	−45.16	10.74	0.0026

Four out of the five factors, namely, T, pH, P and D1, were statistically significant, their effects on the response variable being all positive and increasing in the order: pH < P < D1 < T. pH affected the response through both a linear and a quadratic term. Finally, there were no statistically significant interactions between factors, implying that each factor exerted its effect independently of the others (Zuorro et al., 2016). The fact that GMA dosage did not affect in a statistically significant manner the process response, could be due to the fact that hemicelluloses, although essential in maintaining the architectural integrity of algal cell walls, are present in very low amounts (Razeghifard, 2013). Accordingly, their degradation can be expected to increase the DOC value of the liquid at the end of the treatment only to a limited extent.

To better appreciate the contributions of T, pH, P and D1 to lipid recovery, 3D response surfaces were generated from the model equation. Some representative plots are shown in Fig. 5.1, from which the positive effects of temperature, pretreatment time and CEL dosage on the release of organic compounds into the treatment solution are evident. We also note that pH had a non-monotonic effect on the response variable, with a maximum located at about pH 5, a value close to the optimal pH of the enzyme preparations used (Zuorro et al., 2016).

Lipid extraction yield from the untreated biomass was 40.73 ± 0.26 %, while those from the enzymatically treated material ranged from 43.43 % to 68.32 %, depending on the operating conditions. Plotting the observed lipid extraction yields (y_{LIP}) against the corresponding DOC values gave the results displayed in Fig. 5.2.

a)

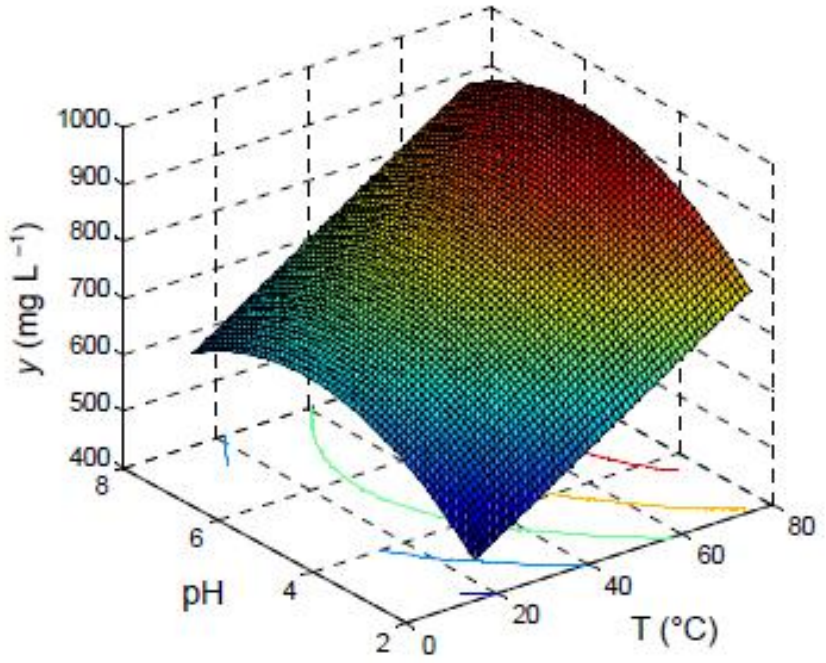

b)

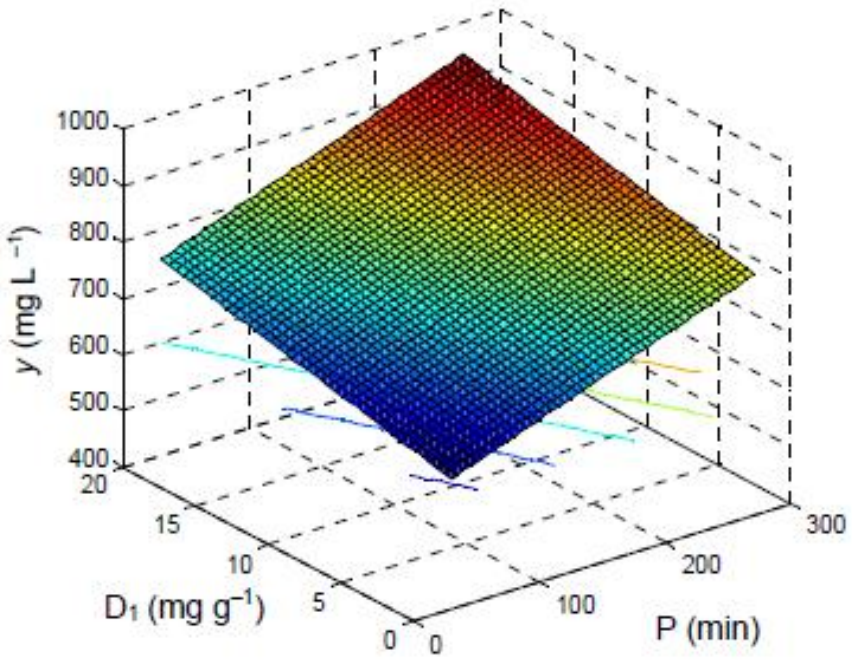

Figure 5.1 – Response surface plots showing the influence of temperature (T), pH, pretreatment time (P) and CEL dosage (D1) on DOC. For each plot, the of the other factors were set at their central values

A least-square regression analysis of the data provided the following relationship:

$$y_{LIP} = 0.095\ DOC - 17.035$$

The equation above was also validated by performing an additional experiment under conditions different from those of the CCD (T = 53 °C, pH = 4.2, t = 210 min, D1 = 14 mg g^{-1}, D2 = 1.5 mg g^{-1}). The percentage error of prediction was 8.9 %. The good correlation between the two variables (R^2 = 0.813) suggests that the enhanced recovery of lipids is a consequence of the enzyme-induced cell wall degradation, which in turn results in an increase in the DOC values of the liquid phase.

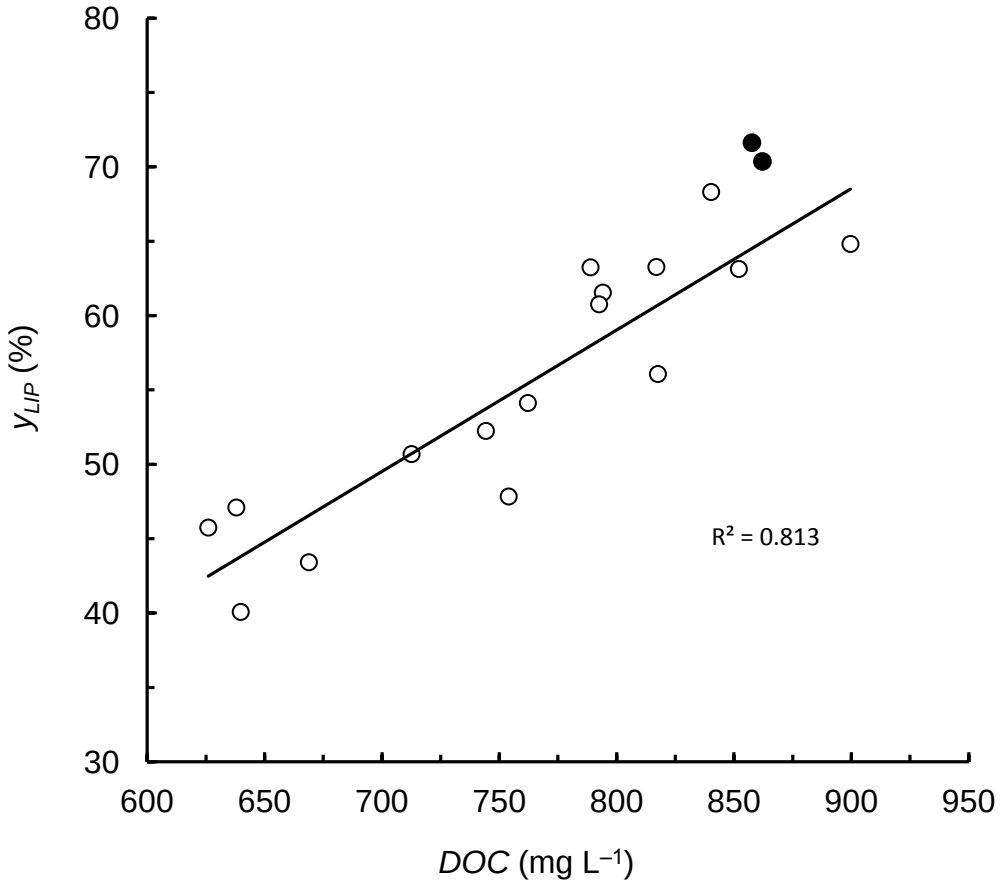

Figure 5.2 – Observed dependence of lipid extraction yields (y_{LIP}) from DOC values (solid symbol: validation point)

These results demonstrate that DOC measurements can give useful information on the enzyme induced degradation of algal cell walls. The determination of DOC by TOC analyzer is very rapid and easy to perform and, combined with other methods

for the characterization of the cell wall that will be presented in next paragraphs, could contribute to provide a more complete picture of the effects of enzymatic treatments on microalgae (Zuorro et al., 2016).

5.3 Proximate, ultimate and compositional analyses

The proximate, ultimate and compositional analyses of untreated and treated samples are shown in Tables 5.5, 5.6 and 5.7.

Table 5.5 – Proximate analysis of untreated and treated samples

Proximate analysis (wt % dry)	Untreated	Cellulase	Mannanase	Optimum
Moisture	3.3	1.5	2.2	1.3
Volatile Matter (VM)	81.0	88.8	86.1	83.9
Fixed Carbon (FC)	15.6	9.0	12.3	14.1
Ash (A)	3.4	2.2	1.6	2.0

Table 5.6 – Ultimate analysis of untreated and treated samples

Ultimate analysis (wt % dry)	Untreated	Cellulase	Mannanase	Optimum
C	53.39	61.62	61.74	63.42
H	7.95	9.09	9.08	9.57
N	4.02	4.05	4.05	3.83
O	31.24	23.04	23.53	21.18

Table 5.7 – Compositional analysis of untreated and treated samples

Ultimate analysis (wt % dry)	Untreated	Cellulase	Mannanase	Optimum
Lipids		53.25		
Proteins	19.22	19.36	19.36	18.31
Carbohydrates	24.13	15.96	18.02	16.41
Weight loss	6.52	9.23	7.77	10.03

Ash content and fixed carbon decreased after cellulase treatment and, consequently, the amount of volatile matter increased. Slighter changes were highlighted for

mannanase and optimum treatments. These changes could be due to the relative higher amount of lipids in treated samples. Algal oil, in fact, has lower FC and ash content than the entire algal biomass.
Weight loss increased after treatment. Consequently, the amount of carbohydrates lowered significantly. In particular, sugar content decreased from 24.13% to 15.96% when the biomass was hydrolyzed with cellulase. Less accentuated variations were obtained after mannanase treatment. This is in accordance with results obtained previously for DOC release.
As reported in Chapter 4, total lipid content of *Nannochloropsis* sp. was 53.25 ± 1.25 mg/100 mg.
The hydrolyzed biomass shows an increase in C and H, compared to unhydrolyzed biomass, in particular when the two enzymes were used simultaneously. In fact, after enzymatic treatment, carbohydrates content decreased, causing a relative increase of lipids in the hydrolyzed biomass. These lipids are richer in carbon and hydrogen. On the contrary, N content did not change remarkably after single enzyme treatment, while a slight decrease was observed after optimum treatment: a loss of proteins in this sample could have been happened following a more pronounced hydrolysis of the cell wall.

5.4 Thermal characterization

Thermogravimetric tests in inert atmosphere (N_2) were performed to evaluate the pyrolytic behavior of the biomass. The TGA curve of raw *Nannochloropsis* sp. biomass is reported in Fig. 5.3.
Three stages were found in the pyrolysis process. The first stage (I), from the starting temperature to the temperature of initial devolatilization, was due to the elimination of water (dehydration); in the second stage (II) there was a major weight loss in the range 300-350°C, which corresponded to the main pyrolysis process (devolatilization) that started at 130°C; the third stage (III) was from the second stage to the final temperature (800°C). Above 370°C, an abrupt change in the slope of the TGA occurred, leading to a slower weight loss in the temperature range 370-500°C. The evaluation of the weight loss of the samples between 130°C, end of moisture evaporation, and 600°C, indicates that more than 80 wt% of the volatile matter was released in this interval. During stage III, there was a slow continued loss of weight due to the decomposition of the solid residue resulting from the previous step and the solid residue reached an asymptotic value.

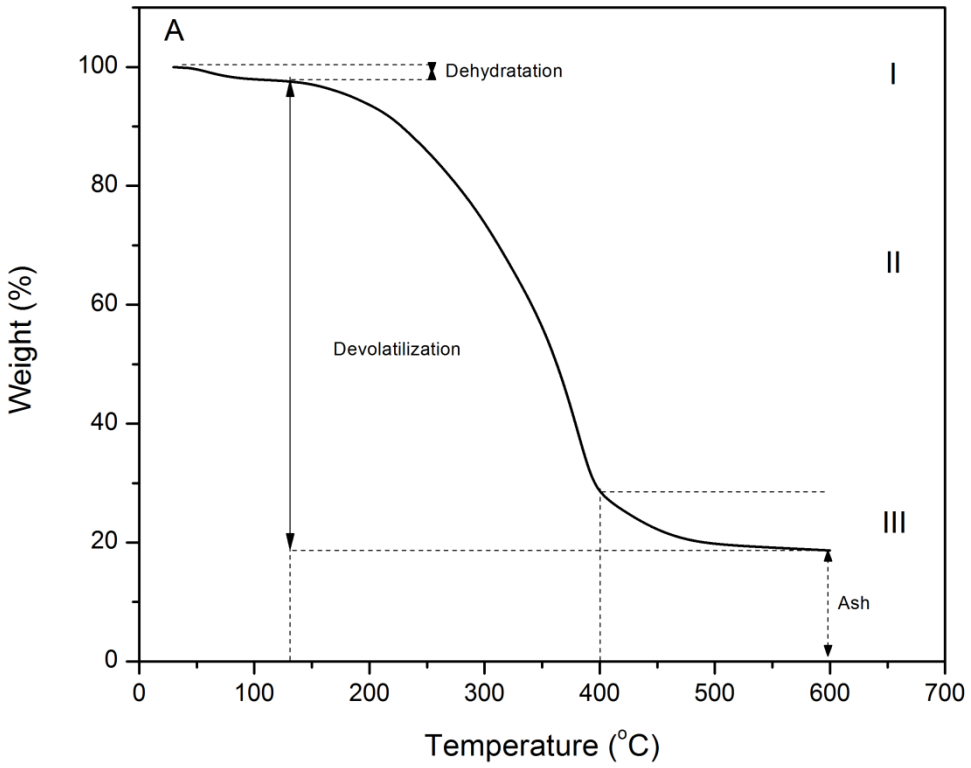

Figure 5.3 –Thermogravimetric curve of untreated *Nannochloropsis* sp. biomass

Fig. 5.4 shows the relative differential thermogravimetric (DTG) curve together with the curves of its standard macrocomponents: cellulose and hemicellulose. The MagicPlot Pro software (version 2.5.1, Magicplot Systems LLC, Saint Petersburg, Russia) was used to carry out the deconvolution computation of the DTG curve in order to have the hemicelluloses, cellulose and lipid peaks.

The main decomposition step, which occurred in the 120-400 °C range, is a very complex process, involving at least three overlapped steps which occur in the following ranges: 120-312°C, with around 19.7% weight loss, 300-353 °C, accounting for around 31% of weight loss, and 353-400°C, with around 21.9% of weight loss. According to Raveendran et al. (1996), across this temperature range predominately hemicellulose and cellulose decompose. Maddi et al. (2011) stated that hemicellulose is more thermally labile than cellulose and decomposes at 200 °C to 315 °C in an oxygen-free atmosphere, followed by cellulose at 270 °C to 370 °C. After the decomposition of hemicellulose and cellulose a further step at ~ 400 °C is related to the decomposition and volatilization of lipid present in the samples (Wang et al., 2007; Yang et al., 2007).
As it can be seen from the curves of standard components and from deconvolution, hemicellulose is more thermally labile than cellulose and decomposes at 200 °C to 315 °C in an oxygen-free atmosphere, followed by cellulose at 270 °C to 370 °C. After

the decomposition of hemicellulose and cellulose a further step at ~ 400 °C is related to the decomposition and volatilization of lipid present in the samples.

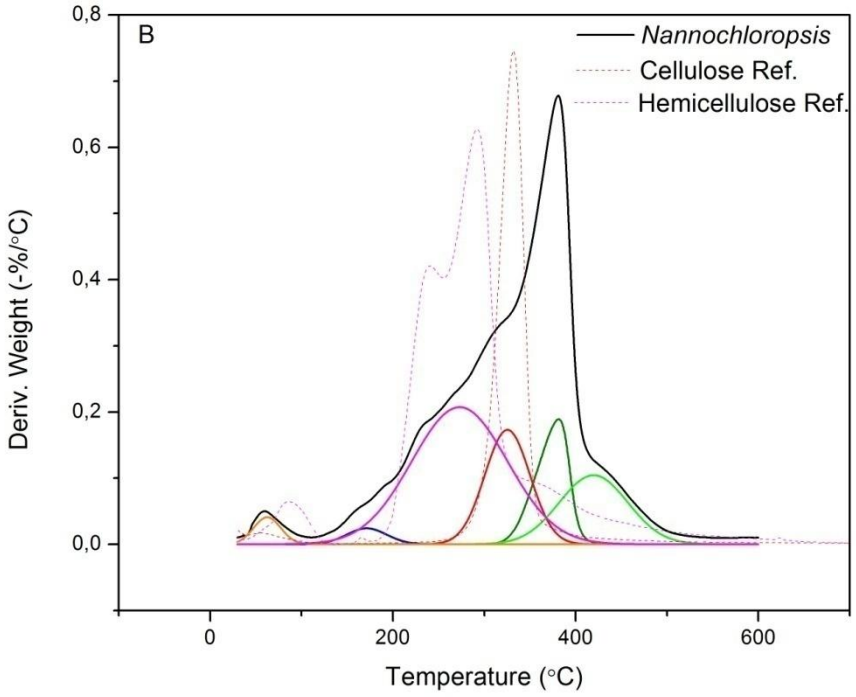

Figure 5.4 – Differential thermogravimetric curve of untreated *Nannochloropsis* sp. biomass (solid lines) and its standard macrocomponents: cellulose and hemicelluloses (dashed lines)

The DTG curve of the enzyme-treated samples (Fig. 5.5) changed considerably, with two main peaks with maxima around 267 and 390 °C. These single peaks encompassed hemicelluloses and both cellulose and lipids content, respectively.
However, the presence of the peak at 267 °C was not obvious in untreated *Nannochloropsis* suggesting that the pretreatments used in this study led to the loosening of the biomass polymer structure and thus weaker bonding interactions between the components in the pretreated samples that caused the formation of the separate peaks. Furthermore, the cellulose peak at around 350 °C shifted to higher temperature (nearly 360 °C) likely due to an increased crystallinity of the biomass. Moreover, the thermal degradation of biomass was found to reach its maximum in second stage observed to be within 290-420 °C temperature range. The peak in this region corresponds to the decomposition of cellulose and lipidic substances. All the pretreated samples showed a major mass loss between 360 and 420 °C, which indicates that lipids dominates biomass composition. The thermal degradation of the samples after enzyme hydrolysis, on the other hand, showed peak shifts in this

region. In particular, the pyrolytic degradation temperature assigned for hemicelluloses shifted from 120-312 °C to 220-290 °C.

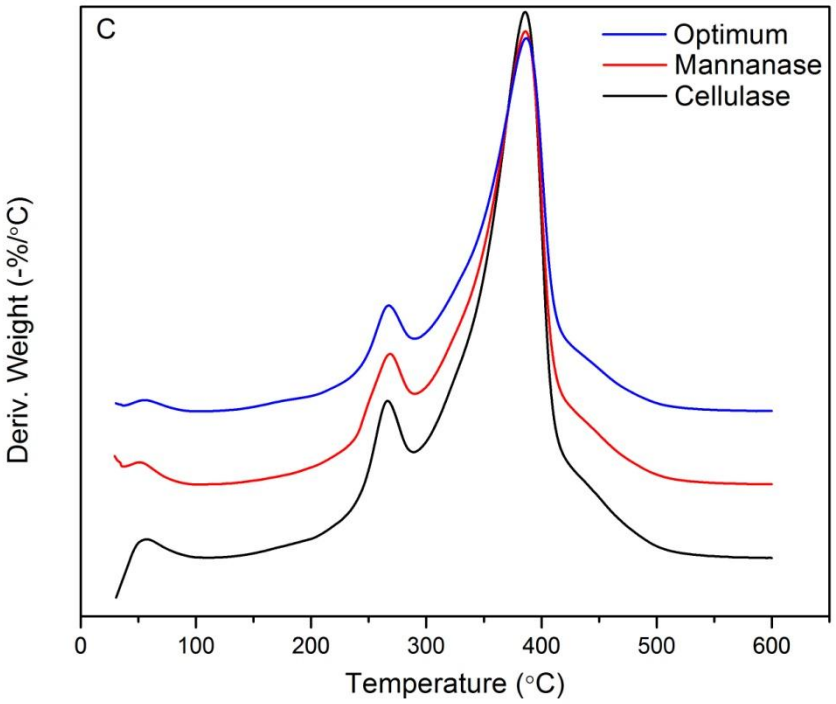

Figure 5.5 – Differential thermogravimetric (DTG) curves obtained from enzymatically treated biomass samples

DTG curves of residues after lipid extraction are reported in Fig. 5.6. It can be noted a gradual decrease of the peak related to the lipid, as a confirmation that lipid extraction had actually taken place. As a consequence, there was a relative increase of the peaks assigned to hemicelluloses and cellulose.
Moreover, as happened in the curves of enzymatically treated biomass samples, there was a shift of pyrolytic degradation peak assigned for hemicelluloses towards lower temperatures.
Instead, on the contrary to unextracted samples, even the cellulose shoulder moved to lower temperatures.

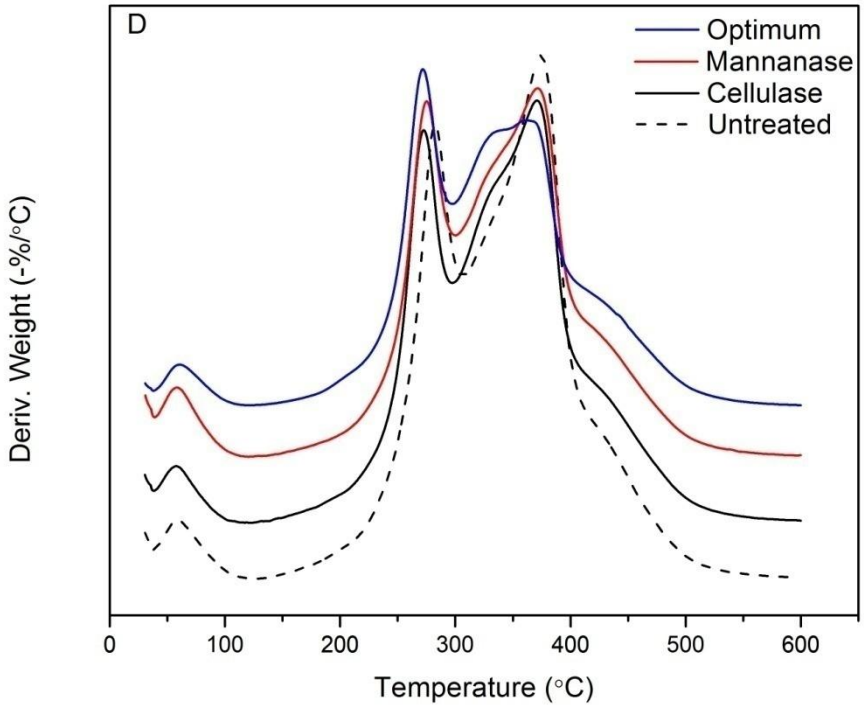

Figure 5.6 – Differential thermogravimetric (DTG) curves obtained from residue after lipid extraction

5.5 FTIR analysis

5.5.1 FTIR spectra

The FTIR spectrum of *Nannochloropsis* sp. biomass is shown in Fig. 5.7.
FTIR spectrum obtained from the *Nannochloropsis* sp. biomass is similar to those reported in literature for this microalgal specie (Mayers et al., 2013, Sukarni et al., 2014, Marcilla et al., 2009).
For the biomass, it could be observed nineteen distinct transmission bands over the wave number range of 4,000-400 cm^{-1}. These bands were assigned to specific molecular groups and were tentatively identified on the basis of biochemical reference standards and published FTIR spectra, as quoted in Table 5.8.

Cell wall macromolecules (proteins, lipids, and carbohydrates) could be identified by their distinct absorbance in different frequency regions. Notably, bands typically indicative of protein are at 1,649 cm^{-1} (amide I, C=O stretch), 1,546 cm^{-1} (amide II, N-H/C-N stretch), and 1,308 cm^{-1} (amide III, C-N stretch/N-H bend).

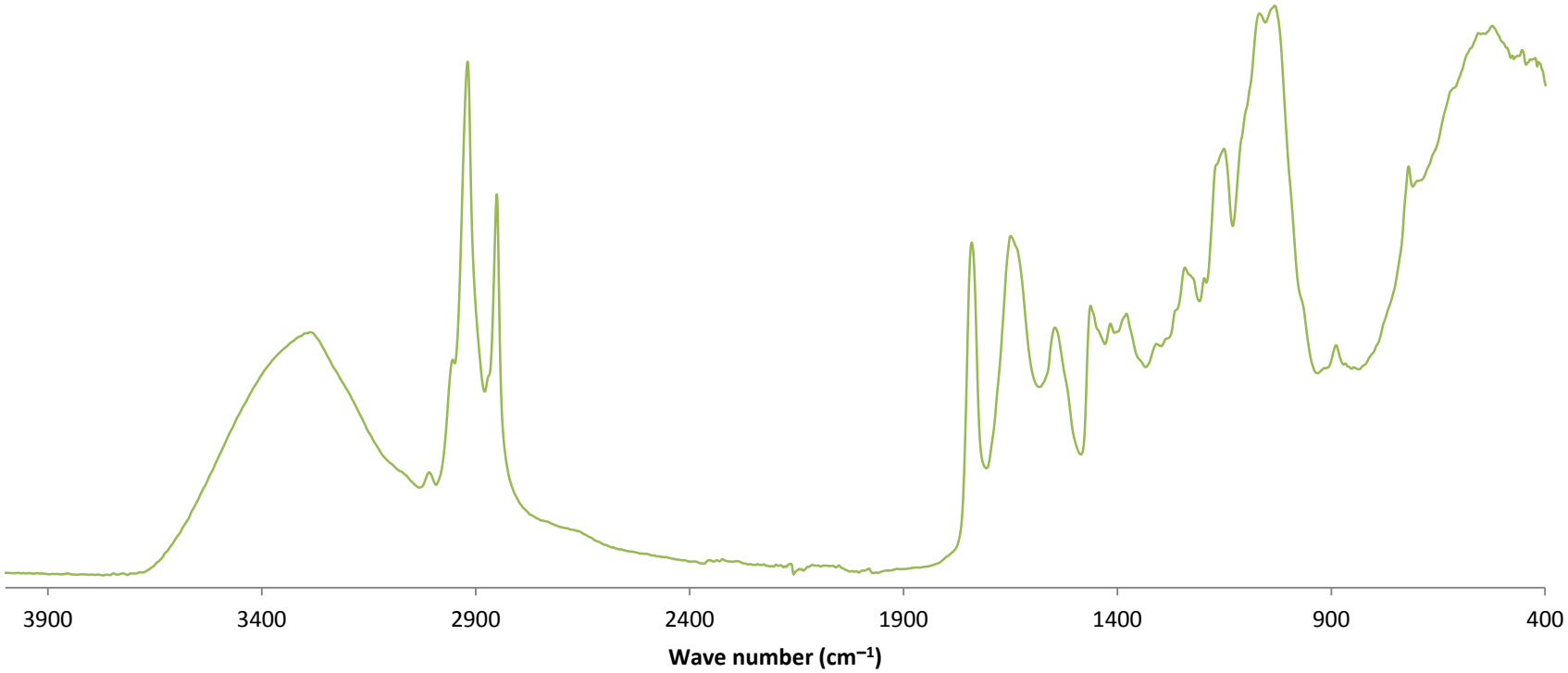

Figure 5.7 – FTIR spectrum of *Nannochloropsis* sp. biomass

Table 5.8 – Main absorption bands of *Nannochloropsis sp*. biomass in the IR

Main peak (cm^{-1})	Typical band assignment	Functional groups	References
3286	ν O-H / ν N-H	H_2O, proteins	Blokker et al. (1998), Salmon et al. (2009), Cao and Tan (2004), Scholz et al. (2014), Sukarni et al. (2014), Duygu et al. (2012), Mayers et al. (2013)
3009	vasCH_3	Unsaturated fatty acids	Salmon et al. (2009), Mereghetti et al. (2014)
2954	vasCH_3	Lipids, algaenans	Mayers et al. (2013), Mereghetti et al. (2014), Marcilla et al. (2009)
2919	vasCH_2	Lipids, algaenans	Blokker et al. (1998), Salmon et al. (2009), Scholz et al. (2014), Sukarni et al. (2014), Duygu et al. (2012), Mayers et al. (2013), Mereghetti et al. (2014), Marcilla et al. (2009)
2873; 2852	ν CH_2, CH_3	Lipids, algaenans	Blokker et al. (1998), Salmon et al. (2009), Scholz et al. (2014), Sukarni et al. (2014), Mayers et al. (2013), Mereghetti et al. (2014), Marcilla et al. (2009)
1741	ν C=O	Lipids, algaenans	Salmon et al. (2009), Scholz et al. (2014), Duygu et al. (2012), Mayers et al. (2013), Mereghetti et al. (2014), Marcilla et al. (2009)
1649-1630	ν C=O	Proteins (Amide I) α-helix, β-sheets	Scholz et al. (2014), Sukarni et al. (2014), Duygu et al. (2012), Mayers et al. (2013), Mereghetti et al. (2014)
1546-1538	δ N-H, ν C-N	Proteins (Amide II)	Scholz et al. (2014), Duygu et al. (2012), Mayers et al. (2013), Mereghetti et al. (2014)
1463	ν C-O	Lipids, algaenans	Blokker et al. (1998), Salmon et al. (2009), Scholz et al. (2014), Duygu et al. (2012), Mayers et al. (2013), Mereghetti et al. (2014)
1416	ν C-O	Cellulose, hemicellulose	Sukarni et al. (2014)

Main peak (cm^{-1})	Typical band assignment	Functional groups	References
1378	δ CH_3, δ CH_2,δ C-O	Lipids, algaenans	Salmon et al. (2009), Scholz et al. (2014), Duygu et al. (2012), Mereghetti et al. (2014)
1308	ν C-N, δ N-H	Proteins (Amide III)	Scholz et al. (2014)
1240	ν P=O, ν C-O-C	Nucleic acids, polysaccharides	Scholz et al. (2014), Sukarni et al. (2014), Mayers et al. (2013)
1197	ν C-O-H	Non cellulosic polysaccharides	Carballo-Meilan et al. (2014)
1158	asν C-O-C	Cellulose, hemicellulose	Cao and Tan (2004), Scholz et al. (2014), Duygu et al. (2012), Mayers et al. (2013), Marcilla et al. (2009), Spiridon et al. (2011), Kacurakova et al. (2000)
1068-1058	ν P=O, ν C-O	Nucleic acids, lipids, algaenans	Salmon et al. (2009), Mereghetti et al. (2014)
1032	ν C-O	Cellulose, hemicellulose	Cao and Tan (2004), Scholz et al. (2014), Duygu et al. (2012)
889-894	ω CH, ν C-O-C	β-linkages Cellulose, hemicellulose	Cao and Tan (2004), Sukarni et al. (2014), Spiridon et al. (2011), Kacurakova et al. (2000)
719	ρ $(CH_2)_{n>3}$, ω CH	Lipids, algaenans	Blokker et al. (1998), Salmon et al. (2009), Scholz et al. (2014)

Carbohydrate bands are characterized by peaks in the region 1,250-800 cm^{-1} due to C–O and C–O–C stretching. In particular, typical bands related to cellulose and hemicelluloses of the cell wall are present around 3,300 cm^{-1} (hydroxyl, H-bonded, O-H stretch), at 1,032 cm^{-1} (hydroxyl/ether, C-O stretch), and at 1,158 cm^{-1} (glycosidic ether, C-O-C stretch).
The bands associated to lipids were characterized by two strong peaks at around 2,940-2,835 cm^{-1} related to CH_2 stretching of methylene and a strong peak at 1,741 cm^{-1} as a result of C=O stretching of esters. These bands are associated to algaenans, long-chain aliphatic hydrocarbons present in the outer layer of the cell wall, that are subject to ether cross-linking reactions (Gelin et al., 1997, Blokker et al., 1998, Salmon et al., 2009).

FTIR spectra of *Nannochloropsis* biomass and its residue after enzymatic hydrolysis in the wave number range 1800-800 cm^{-1} were shown in Fig. 5.8.
It is possible to remark that there are significant differences between the spectrum of the untreated biomass and the treated ones. In particular, six particular changes are individuated:

- shift of the peak at 1,242 cm^{-1} to 1,234 cm^{-1};
- disappearance of the small peak at 1,197 cm^{-1}
- significant changes in the region 1,157-1,032 cm^{-1};
- shift and shape modification of the peak at 889 cm^{-1};
- bands associated to amines, lipids and algaenans become more evident;
- appearance of a more evident peak at 1,630 cm^{-1}.

Changes in the region 1,250-800 cm^{-1} are imputable to a different structure of polysaccharides of the cell wall due to the action of the enzyme preparations.

Because of the complexity of the absorption of various cellular polysaccharides, specific assignments are rather difficult and discrepancies between the spectra of treated samples with the enzyme preparations are better analyzable in second derivative (Fig. 5.9). More specifically, the peak at 1,242 cm^{-1} related to the stretching of C-O-C of cellulose and hemicelluloses, present in the untreated biomass spectrum, disappears and shifts to 1,234 cm^{-1}, characteristic of the stretching of P=O of nucleic acids and phospholipids. Moreover, it is possible to remark a difference in the interval 1,214-1,179 cm^{-1}, typical of non cellulosic polysaccharides. In fact, in the untreated biomass spectrum there is a peak at 1,197 cm^{-1}, that is not visible in the treated ones and, looking at the spectra in second derivative, it is possible to remark different peak shapes between CEL and GMA treated samples. Therefore, it is possible to assume that the enzyme preparations utilized act differently on the cell wall. Analogue considerations can be done for the peak at 889 cm^{-1}, characteristic of β-glycosidic bonds between sugar units of hemicelluloses and cellulose, which shifts to 894 cm^{-1} and presents different shapes depending on the pre-treatment.

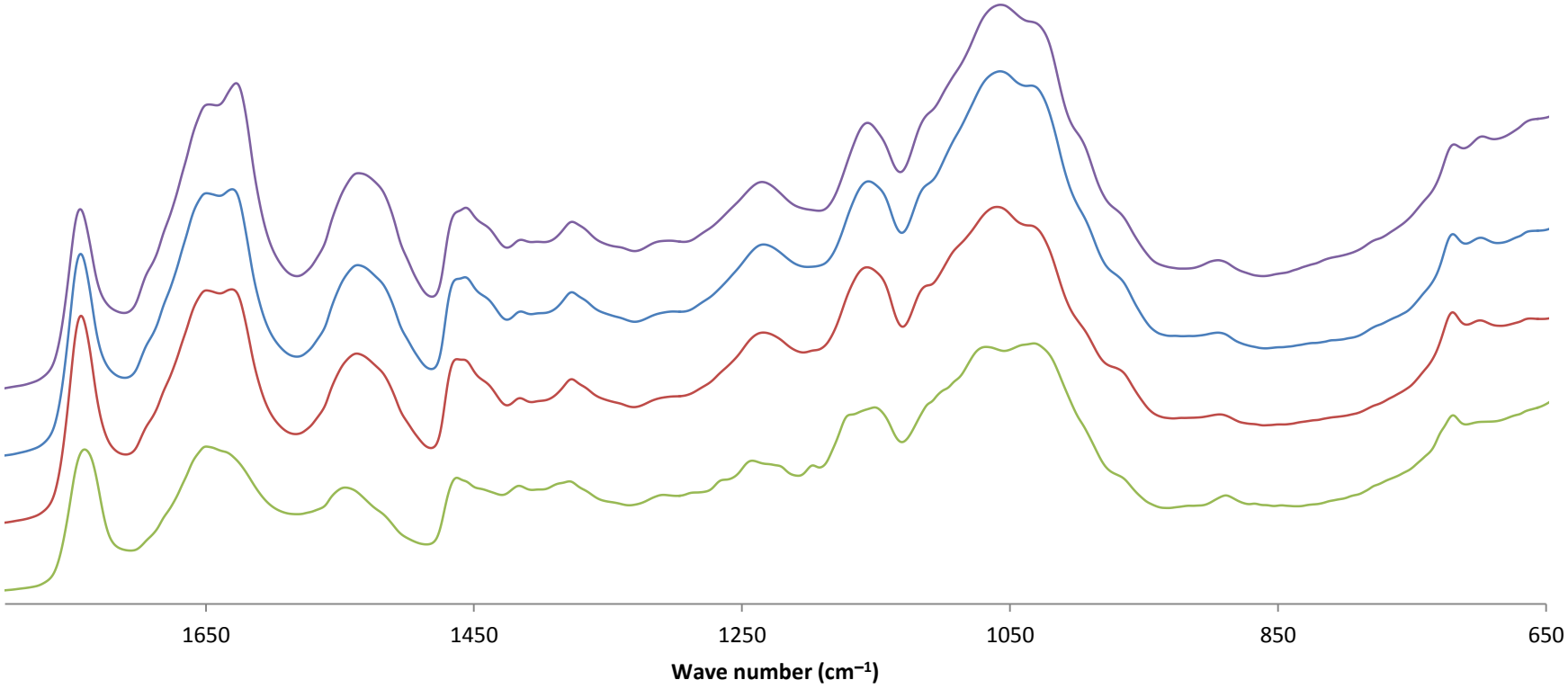

Figure 5.8 – FTIR spectrum of untreated (green line), CEL treated (red line), GMA treated (blue line) and OPT treated (violet line) *Nannochloropsis* sp. biomass

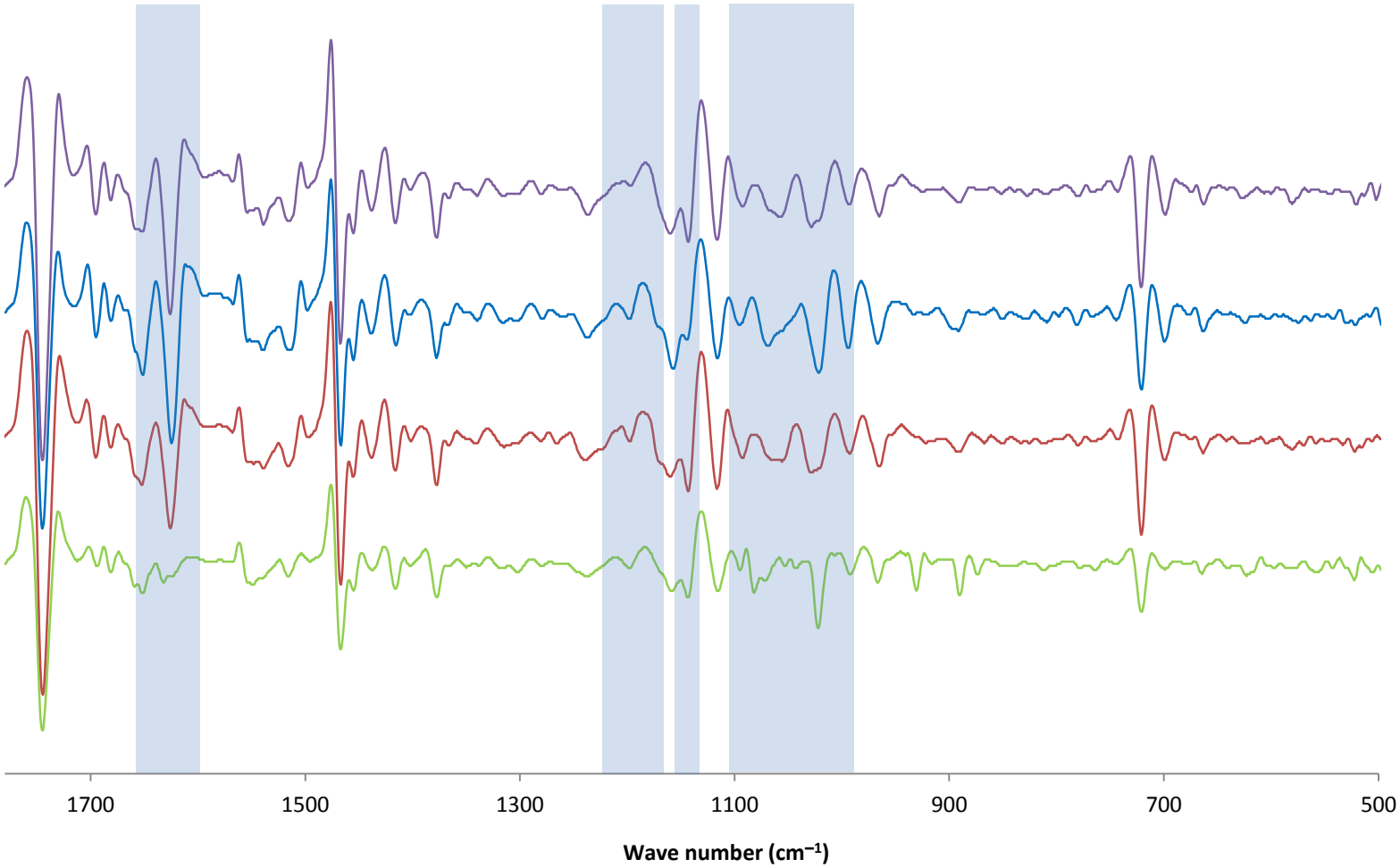

Figure 5.9 – Second derivative FTIR spectrum of untreated (green line), CEL treated (red line), GMA treated (blue line) and OPT treated (violet line) *Nannochloropsis* sp. biomass

Furthermore, significant changes have been found in the region between the two peaks at 1,158 and 1,032 cm^{-1}, pretty well remarkable in second derivative. In particular, the trends of the spectra of CEL treated and OPT treated biomass appear to be very similar, while GMA treated sample spectrum presents a higher number f peaks with a different shape. A significant example is the peak at 1032 cm^{-1}, associated with hydroxyl/ether C-O stretch of carbohydrates (mainly cellulose), that completely disappears in the spectra of CEL treated and optimum treated biomass, indicating that CEL has a great effect on the cellulosic matrix of the cell wall.
Finally, in the spectra of treated biomass, peaks related to cell wall carbohydrates are weaker, allowing vibrational frequencies associated to the long aliphatic chains of proteins, lipids and algaenans becoming more apparent. Examples are the intense bands at 2,919 cm^{-1} (methylene, C-H symmetric stretch) and 2,851 cm^{-1} (methyl/methylene, C-H asymmetric stretch), narrow bands at, 1540 cm^{-1} (amide II, C-N stretching), 1,465 cm^{-1} (methylene, C-H scissoring), 1,378 cm^{-1} (methyl, C-H rock) and 719 cm^{-1} (methylene, $(CH_2)_n$ when n>3, C-H rock). In addition to this, a strong difference in the shape of the amide I band is clearly visible. In fact, this provides information concerning the protein secondary structure. After the enzymatic treatment, in particular for GMA and OPT, the peak at 1630 cm^{-1}, assigned to intramolecular β-sheets, becomes significant, while the one at 1649 cm^{-1}, mainly due to α-helix structures (Barth, 2007), is less intense.

5.5.2 Lipids and carbohydrates correlations

Lipids have characteristic absorption bands around 1740 cm^{-1} which represents stretching of the bonds C = O groups of the esters primarily of lipids and fatty acids, in addition to those ad 3000-2800 cm^{-1} which represents the stretching of CH bonds of fatty acids. In general, one of the two bands of lipids is considered to determine the variability of lipid content, in relation to the bandwidth of the amide I or amides II (Liu et al., 2013).
Dean et al. (2010) used FTIR spectroscopy for a rapid determination of the accumulation of lipids in a culture of microalgae (*Chlamydomonas reinhardtii* and *Scenedesmus subspicatus*) in response to a deprivation of nitrogen. They used the ratio of the lipid band at 1740 cm^{-1} and that of the amide I.
As a reference this method was used and so for lipids was chosen the band at 1741 cm^{-1} because the other band, relative to the vibration of the CH bonds, could be distorted by the presence of the methyl groups of eventual residual hexane used as extraction solvent. Moreover, the band of amide I was chosen, because it is more intense than that the one of amide II and, therefore, less subject to variations due to the proximity of other peaks (Fig. 5.10).

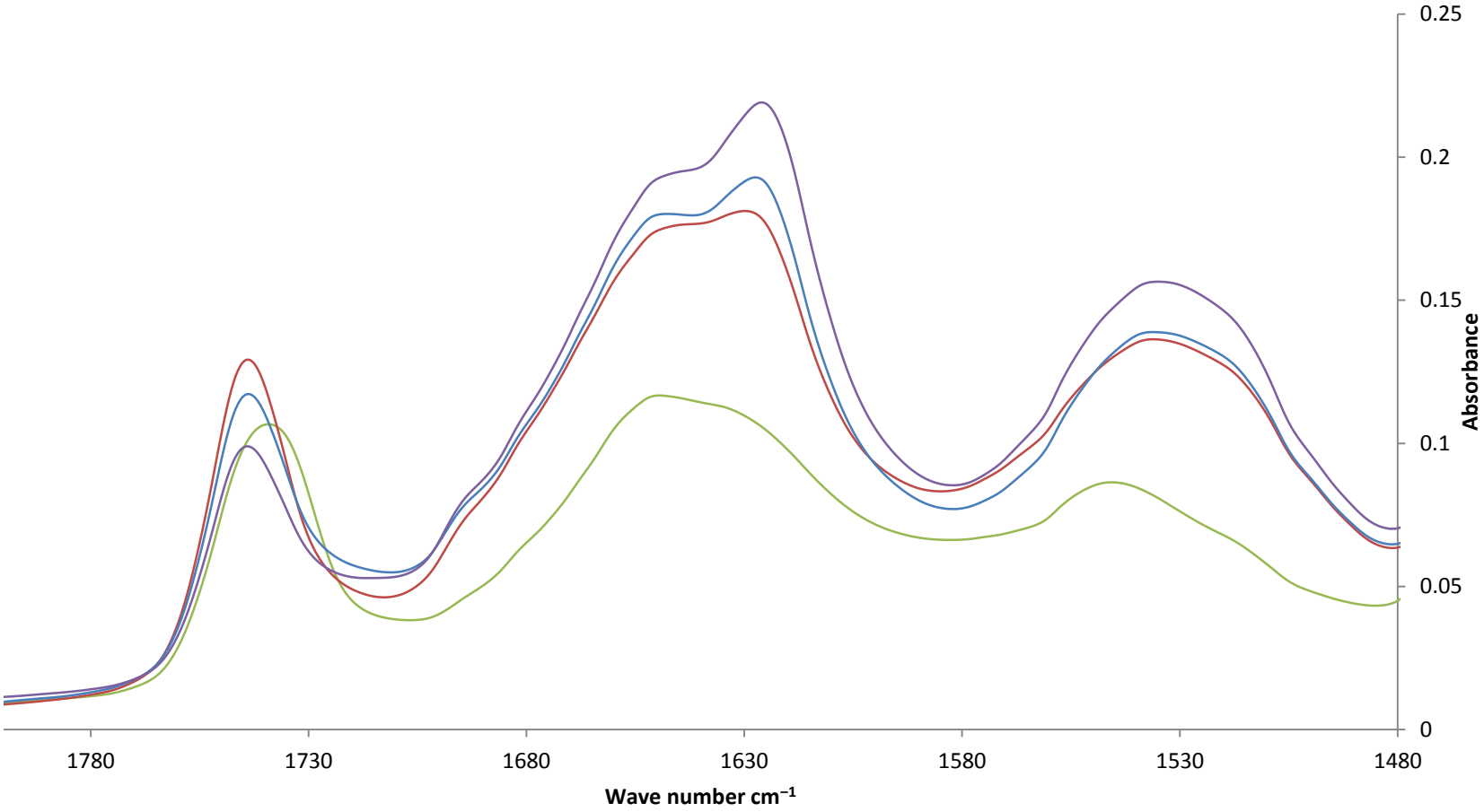

Figure 5.10 – FTIR spectrum of untreated (green line), CEL treated (red line), GMA treated (blue line) and OPT treated (violet line) *Nannochloropsis* sp. biomass

The values of the yields obtained experimentally and those calculated from the ratio between the cited bands are shown in Fig. 5.11. The lipid content measured by traditional gravimetric method showed that the samples treated with optimum mix yield to the highest lipid extraction of 73.25% followed by those treated with mannanase 56.97% and cellulase 54.39%. The lowest lipid extraction of 40.81% was observed for untreated samples.

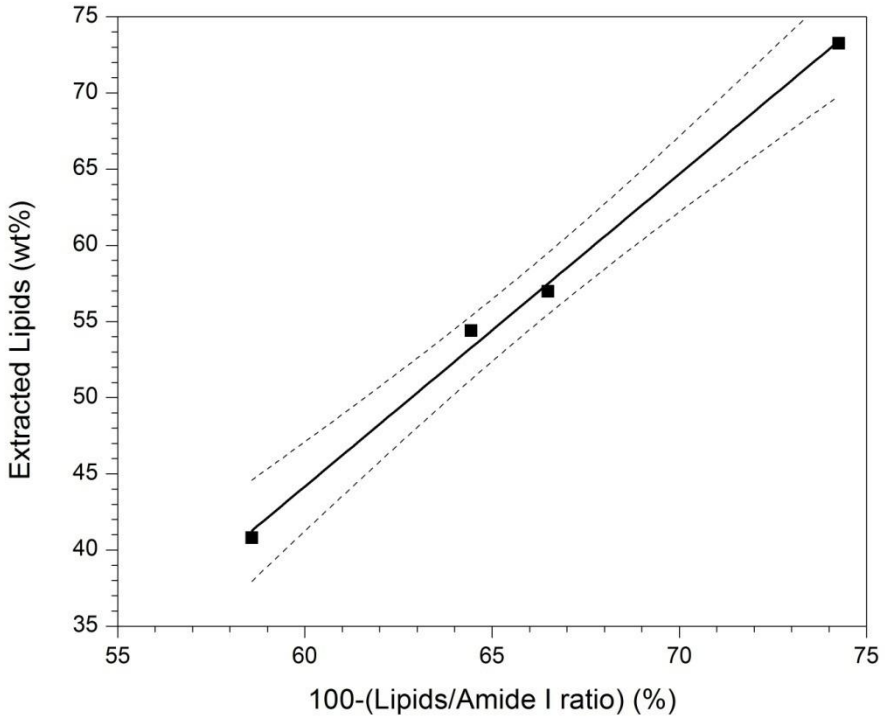

Figure 5.11 – Correlation between the lipid/amide I ratio from FTIR spectroscopy and the corresponding contents from gravimetrical method

These results are in accordance with those obtained from FTIR, indicating that the ratio of lipid/amide I band can correctly evaluate the efficiency of lipid extraction on enzymatically treated microalgal samples (Meng et al., 2014).

Relative carbohydrate content was determined on enzymatically treated samples by calculating the ratio of the carbohydrate (1200-950 cm^{-1}) bands to the amide I band. The values of the carbohydrates from compositional analysis and those calculated from the ratio between the cited bands are reported in Fig. 5.12.
Also in this case, results are in good accordance with those obtained from the FTIR method.

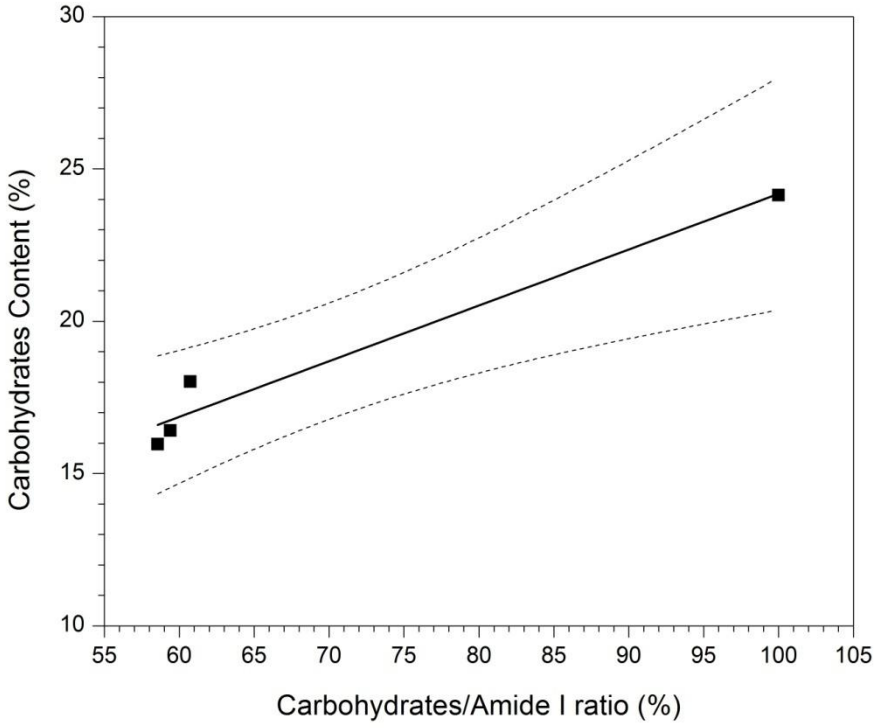

Figure 5.12 – Correlation between the carbohydrate/amide I ratio from FTIR spectroscopy and the corresponding contents from compositional analysis

5.6 X-ray diffraction analysis

As shown in Fig. 5.13, the characteristic peaks at diffraction angles 20.3° and 23.5°, attributed to the diffraction planes of $\bar{1}01$ and 002 in cellulose I, are present. The peak at 16.8°, typical of the diffraction plane 101, is slightly visible only in CEL treated sample.

The crystallization index of *Nannochloropsis* sp. microalgae increased after enzymatic hydrolysis, even if the changes in the XRD patterns after enzymatic hydrolysis were not very significant. The main difference is due to the increasing of the peak at 23.5°, due to the diffraction plane 002 of cellulose I.

Crystalline and amorphous peaks were obtained by a curve-fitting process, assuming Gaussian functions, from the diffraction intensity profiles. The deconvolution was performed using the MagicPlot Pro® software.

The Crystallinity index of untreated biomass was 25%, while for CEL, GMA and OPT were 48%, 40% and 41% respectively. Crystallinity indices increased after enzymatic pretreatment, because the crystallites surface corresponding to amorphous region diminished.

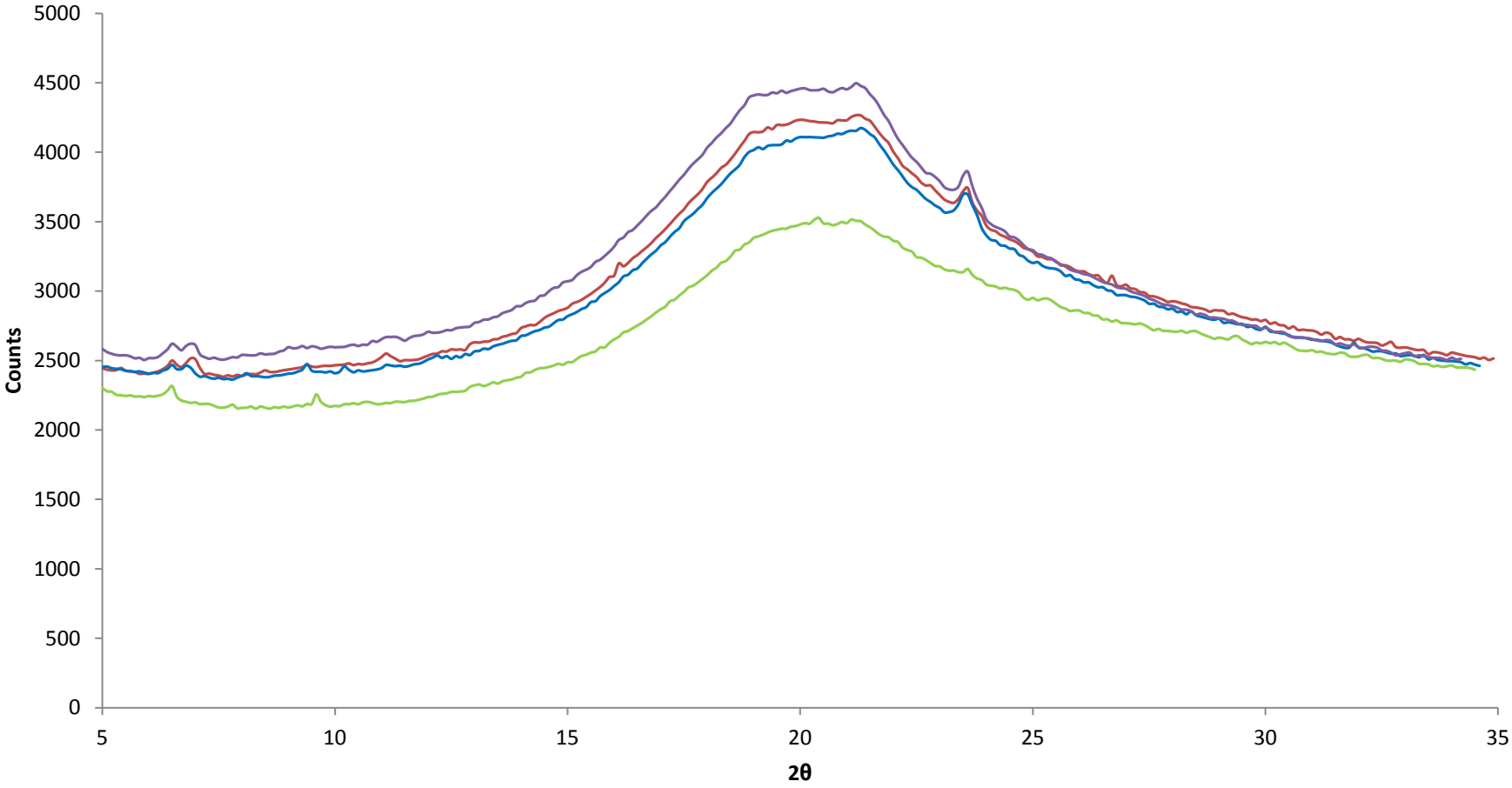

Figure 5.13 – XRD patterns of untreated (green line), CEL treated (red line), GMA treated (blue line) and OPT treated (violet line) *Nannochloropsis* sp. biomass

5.7 SEM characterization

Scanning electron microscope (SEM) was used to observe the cell integrity after the enzymatic pretreatments. In Fig. 5.14 images of intact cells are shown.

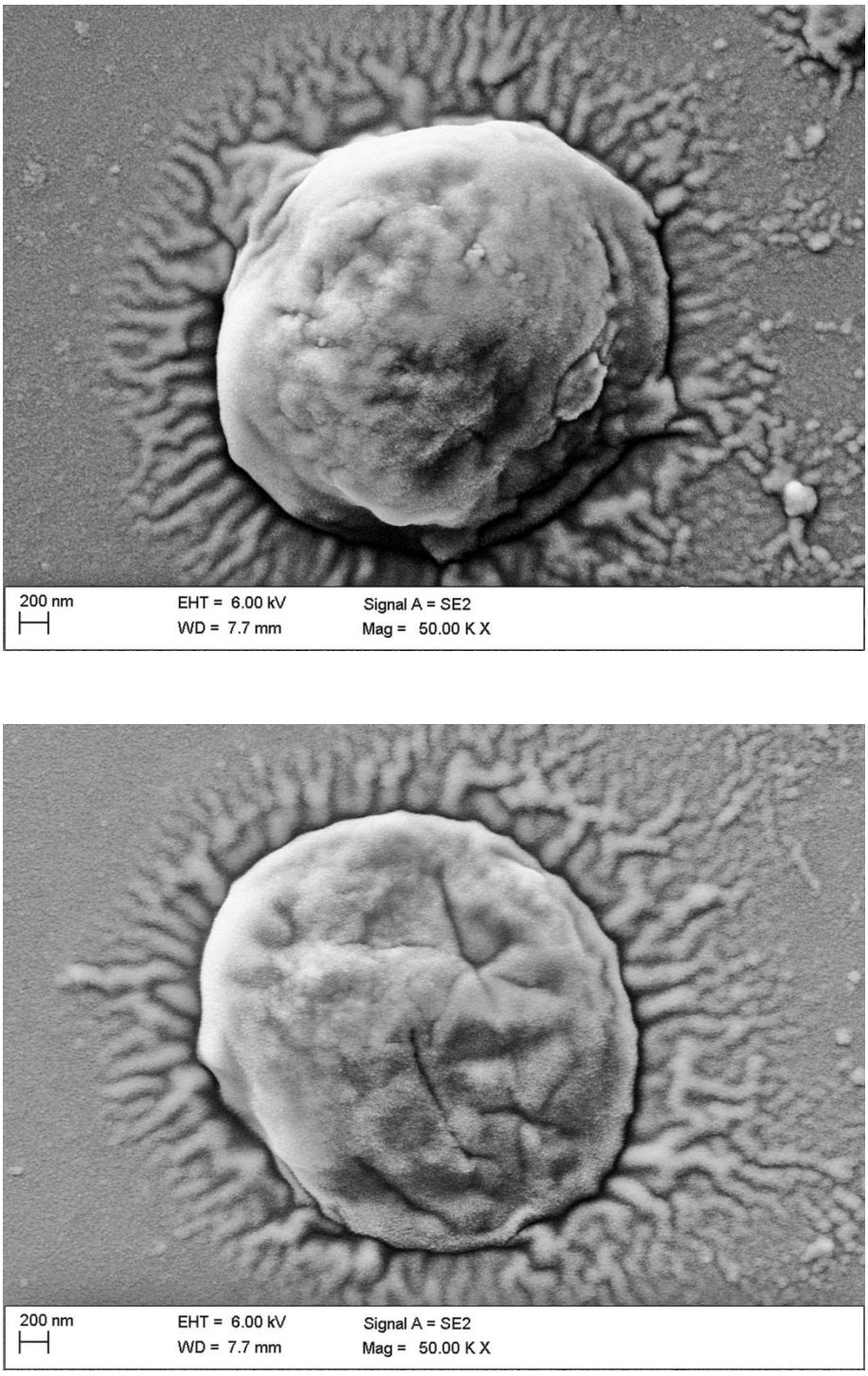

Figure 5.14 – SEM images of intact *Nannochloropsis* sp. cells

In Fig. 5.15-5.17 images of cells after enzymatic hydrolysis respectively with CEL, MAN and OPT are shown.

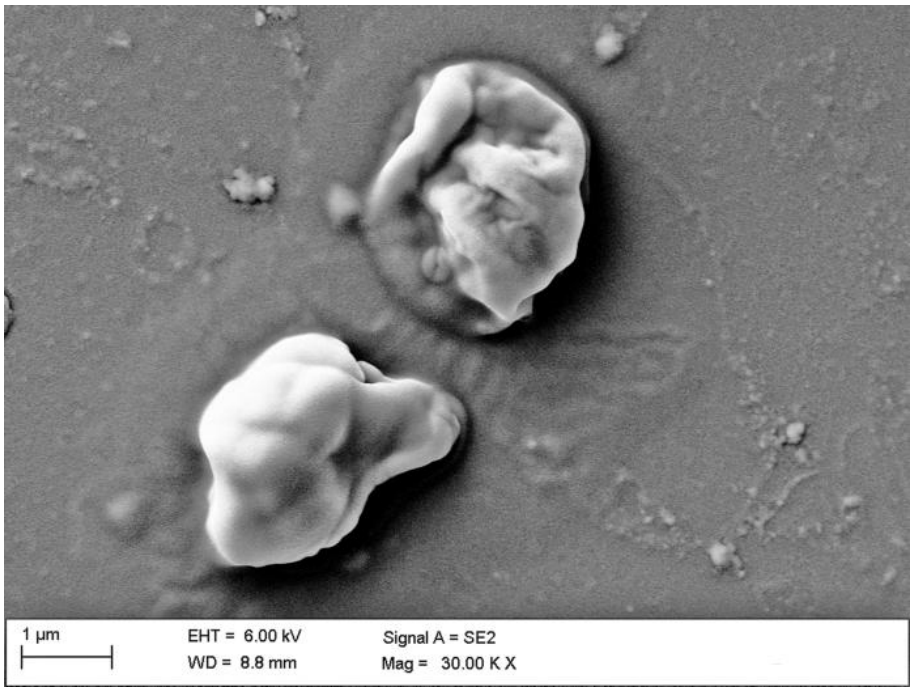

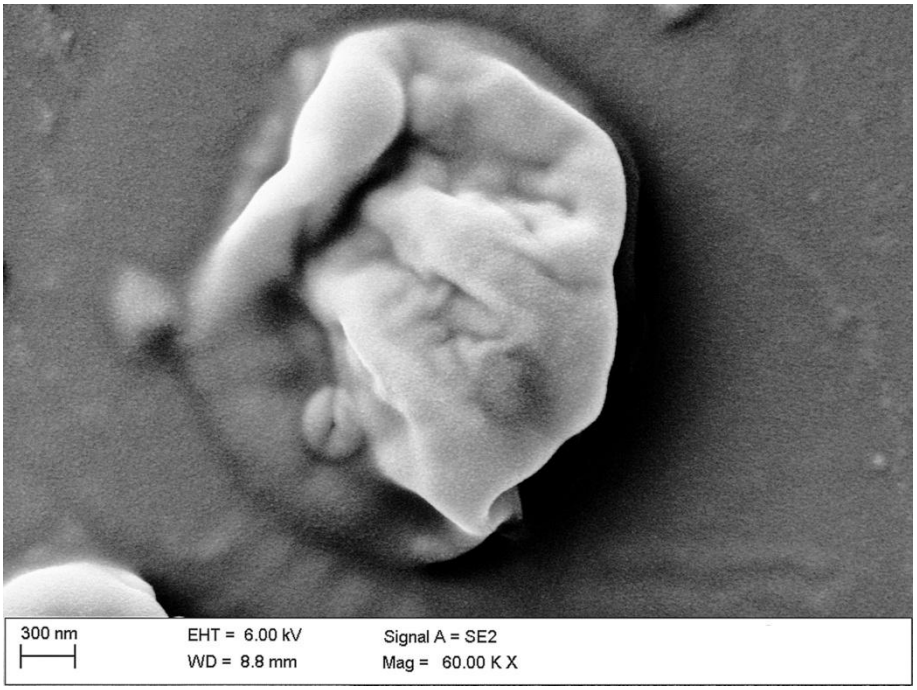

Figure 5.15 – SEM images of CEL treated *Nannochloropsis* sp. cells

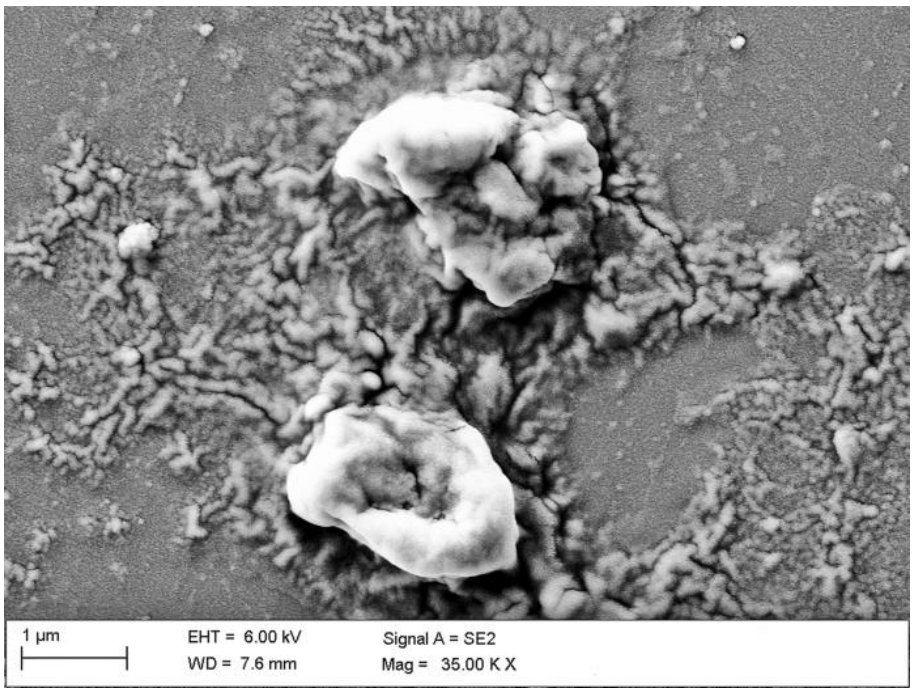

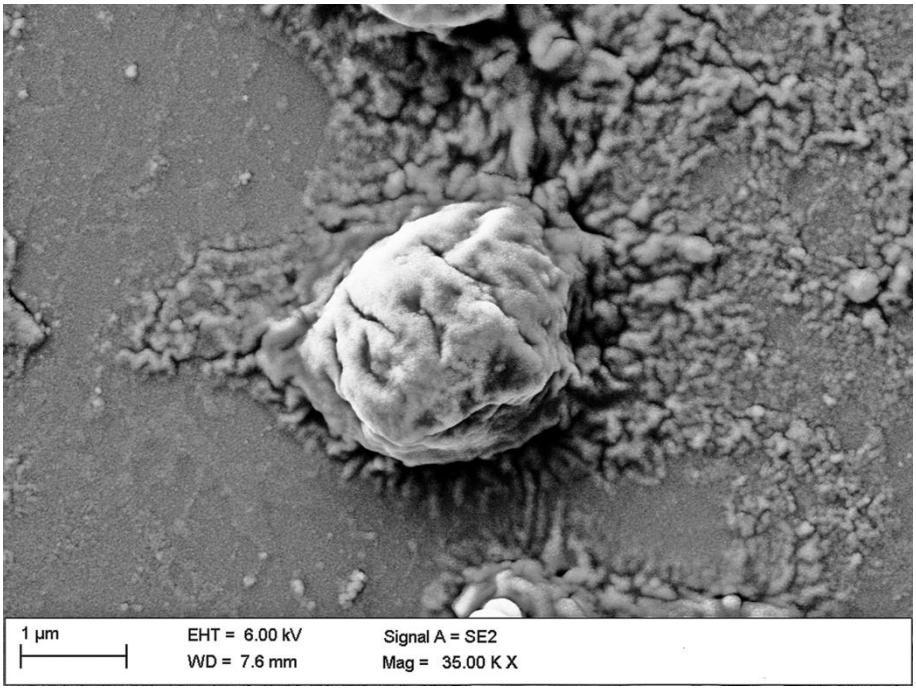

Figure 5.16 – SEM images of GMA treated *Nannochloropsis* sp. cells

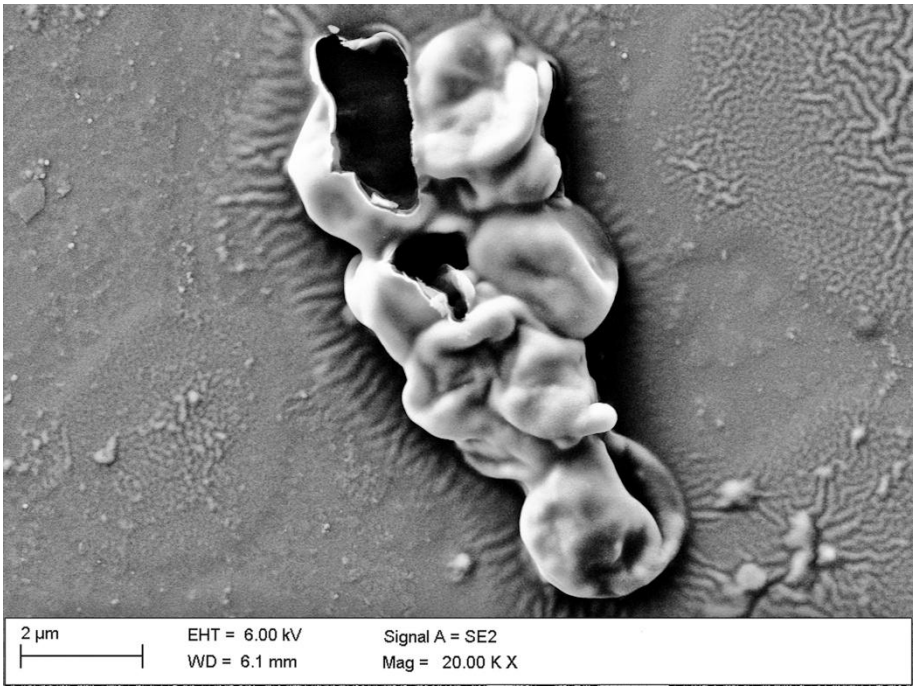

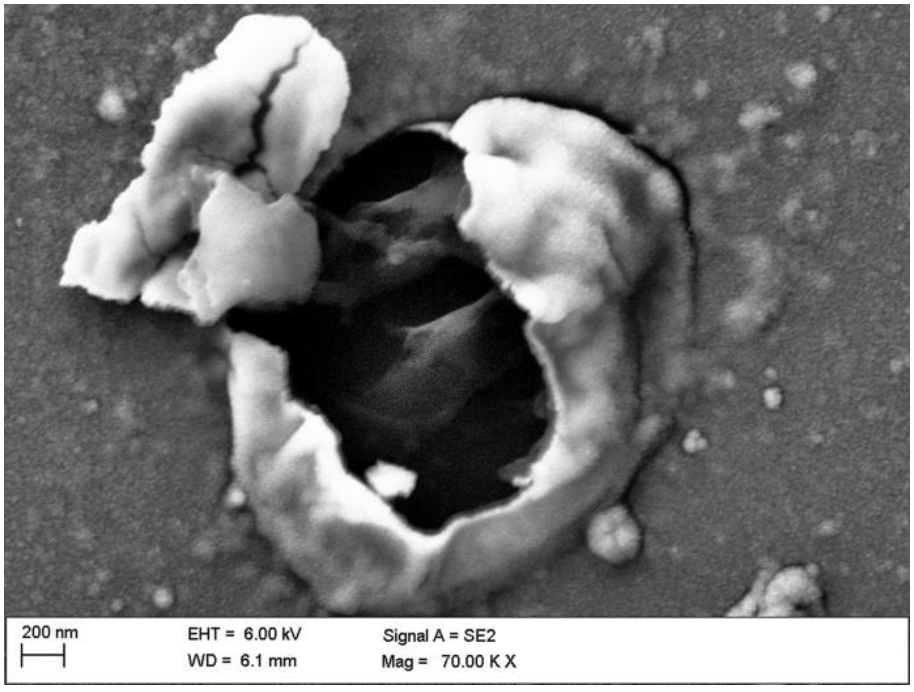

Figure 5.17 – SEM images of OPT treated *Nannochloropsis* sp. cells

These images revealed ultra structural changes after enzymatic hydrolysis. In fact, untreated cells appear to have mainly spheroid shape with dimensions next to 3 µm with smooth and continuous surface, while after treatment they assume an irregular

shape. The treated samples with cellulase appear to remain intact. This situation can be explained by the fact that single enzymatic hydrolyzation partially decomposed the cell wall structure but did not disrupt the cells into pieces. As a result, more cells could keep their intact morphology, but invagination, due to the depolymerization of the macromolecular constituents of the cell wall, can be observed.
Instead, cells treated with GMA lost their regular structure. It can be also noted that the leakage of intracellular material occurred, by assuming the formation of small cracks.
Finally, cells were completely disintegrated after treatment with optimum mix and great fractures can also be observed.

5.8 TEM characterization

TEM images of untreated and enzymatically treated (under optimal conditions) *Nannochloropsis* cells were also taken. Untreated cells had a regular shape, with intact walls and all the components confined inside the cell and in the cytoplasm (Fig. 5.18).
On the contrary, most of the enzymatically treated algal cells underwent major changes, with loss of cell boundaries (Fig. 5.19) and release of intracellular material after solvent extraction (Fig 5.20). This provides a clear evidence of the effectiveness of the enzymatic treatment. As a result of the enzyme action, the mass transfer resistance associated with the cell walls of *Nannochloropsis* can be expected to be greatly reduced, increasing solvent accessibility to lipid bodies and leading to high lipid recovery efficiencies.
Regarding the effects of the enzymatic treatment on the integrity of algal cells, it was found that even under non-optimal process conditions a significant release of intracellular components occurred for a high percentage (> 90%) of the cells. This suggests that the enzymatic hydrolysis of cell wall components following the application of cellulase and mannanase can cause a more or less extensive damage to the algal wall, with the loss of large amounts of intracellular material, including the lipid fraction.

Figure 5.18 – TEM images of intact *Nannochloropsis* sp. cells

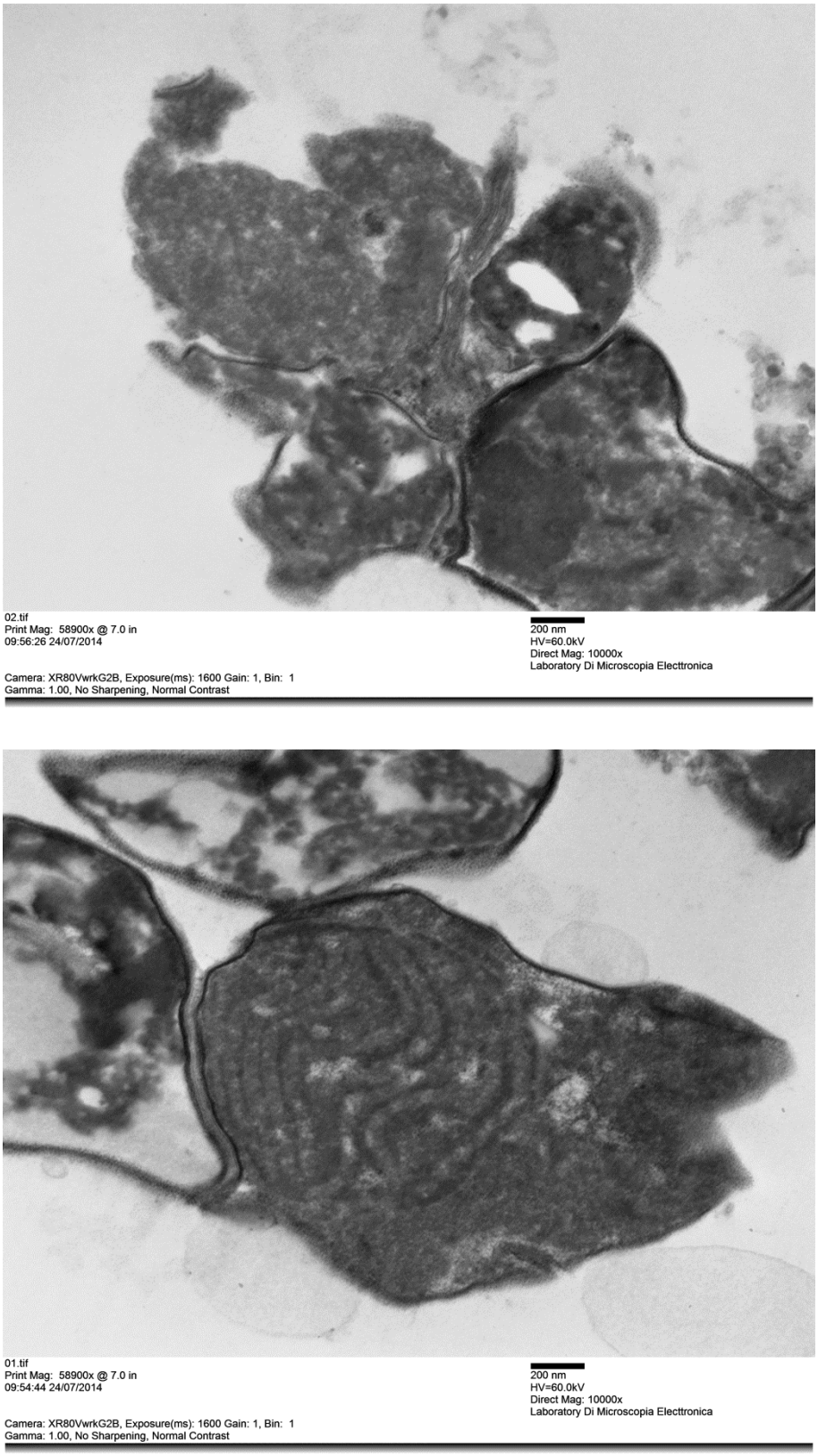

Figure 5.19 – TEM images of OPT treated *Nannochloropsis* sp. cells

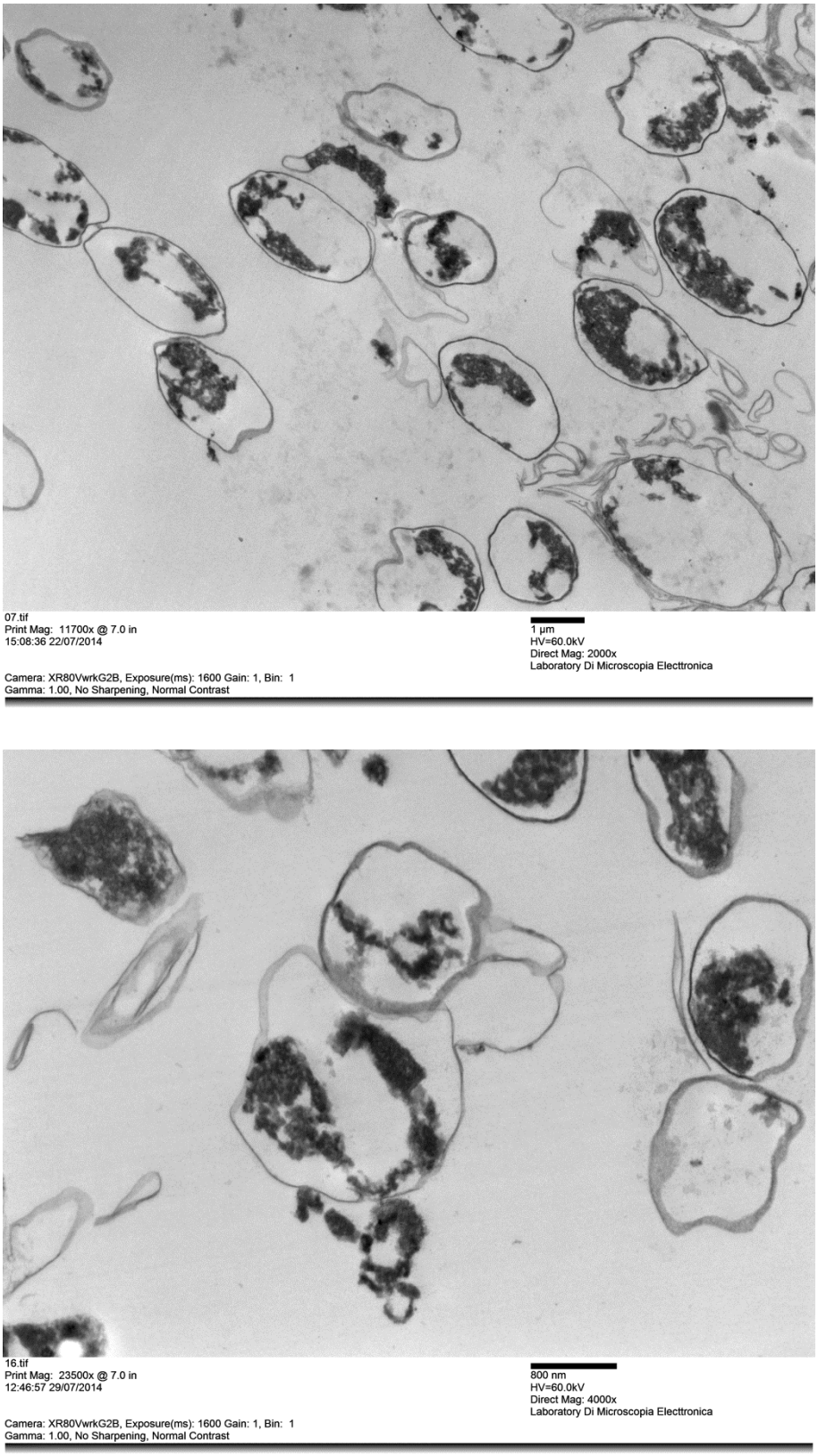

Figure 5.20 – TEM images of OPT treated *Nannochloropsis* sp. cells after solvent extraction

5.9 Discussion of results

These characterizations provided direct evidence of the effectiveness of the enzymatic treatment and give an assessment on the role of each of the enzyme preparation utilized (CEL or GMA).
FTIR spectra in the carbohydrate region, 1250-800 cm^{-1}, gave an important proof of this. In fact, after enzymatic hydrolysis, the bands underwent to significant modifications. In particular the band at 1031 cm^{-1}, due to ν(C–O) stretching of carbohydrates (mainly cellulose), became less pronounced. These changes can be attributed to the degradation of cell wall components. The disappearance of the small peak at 1,197 cm^{-1} also occurred. Moreover, the peak at nearly 1240 cm^{-1}, associated with the stretching of phosphate groups in nucleic acids, became more evident. Also this change can be related to the action of cell wall degrading enzyme.
At the same time, bands associated to lipids and algaenans become more evident due to a relative decrease of carbohydrate content. This was also confirmed by thermal and compositional characterizations.
The thermal degradation of biomass after enzymatic hydrolysis was found to reach its maximum in second stage, observed to be within 290-420 °C temperature range, with a major mass loss between 360 and 420 °C, which indicates that lipids dominates biomass composition.
The hydrolyzed biomass shows an increase in C and H, compared to unhydrolyzed biomass, in particular when the two enzymes were used simultaneously. In fact, after enzymatic treatment carbohydrates content decreased, causing, in the hydrolyzed biomass, a relative increase of lipids, which are richer in carbon and hydrogen.

On the contrary, N content did not change remarkably after single enzyme treatment, while a slight decrease was observed after optimum treatment: a loss of proteins in this sample could have been happened following a more pronounced hydrolysis of the cell wall.
Although the content of protein did not vary, the amide I and amide II bands underwent a significant increase. In addition to this, a strong difference in the shape of the amide I band was clearly visible. This provides information concerning the protein secondary structure. After the enzymatic treatment the band at 1633 cm^{-1}, assigned to intramolecular β-sheets, became significant, while the one at 1649 cm^{-1}, mainly due to α-helix structures (Barth, 2007), was less intense. This is probably due to the fact that β-sheets are more stable than α-helix; so, after the enzymatic hydrolysis, a relative augmentation of the related peak can be found. Similar results are reported in literature. Bamdad et al. (2011) remarked that barley hordein polypeptide chains denaturate with marked changed in secondary structure after pepsin, alcalase and Flavourzyme hydrolysis. Galazka et al. (1995) showed that high pressures have a substantial effect on the secondary structure of bovine serum albumin, suggesting a reduction in α-helix content. Ngarize et al. (2004) showed a

trend toward an increase in β-sheet structure at the expense of α-helix structures in all of the heat-treated samples of ovalbumin and β-lactoglobulin.

From FTIR spectra a shift and flattening of the band at 890 cm^{-1}, related to β-glycosidic bonds between sugar units of cellulose and hemicelluloses, can be also noted. This shift suggests a change in the relative amount of crystalline and amorphous cellulose, which can be explained by considering that the amorphous regions of cellulose are more susceptible to enzymatic attack (Mayers et al., 2013; Wang et al., 2013).
To confirm this, thermal analysis revealed that the cellulose peak at ~350 °C shifted to higher temperature (~360 °C) after enzymatic hydrolysis likely due to an increase crystallinity of the biomass (Cheng et al., 2016). In fact, Kim et al. (2010) stated that initial temperature of thermal decomposition and the peak temperature in the DTG curves shifted to higher temperatures with increasing crystallite size, crystallinity index and degree of polymerization. In particular, the pyrolytic degradation temperature assigned for hemicelluloses shifted from 120-312 °C to 220-290 °C. This indicated that the major components, hemicellulose and cellulose, that were originally bound tightly to each other were subsequently loosened by the pretreatment process, creating a high degree of porosity that allowed easy penetration of enzyme to hydrolyze cellulose leaving behind amorphous parts of biomass (Abraham et al., 2016).
The depolymeriztion was also confirmed by SEM images. Cellulase treated samples appeared to remain intact, but lose the regular shape and invagination seemed to occur, due to the depolymerization of cell wall cellulose.
A direct proof of the action of cellulase is the Crystallinity index. In fact, its value for untreated biomass was 25%, while for CEL treated was 48%. Crystallinity indices increased after enzymatic pretreatment because the crystallites surface corresponding to amorphous region diminished (Kim et al., 2010). Similar results were obtained by Huo et al. (2015) after enzymatic hydrolysis of the microalgae *Scenedesmus* sp. G4. This trend could be related to the fact that amorphous cellulose is attacked first by the action of hydrolytic enzymes, allowing the raise of crystallinity (Yang et al., 2011).

Crystallinity indexes for GMA and OPT treated samples were lower, 40% and 41% respectively. After mannanase treatment, in particular, also less accentuated variations in carbohydrates content were obtained. This is in accordance the results obtained for DOC release. From the experimental design, in fact, it was found that GMA dosage did not affect in a statistically significant manner the process of release of organic carbon. This could be due to the fact that hemicelluloses, although essential in maintaining the architectural integrity of algal cell walls, are present in very low amounts (Razeghifard, 2013). Accordingly, their degradation can be expected to increase the DOC value of the liquid at the end of the treatment only to a limited extent.

However, SEM images showed that cells treated with GMA have lost their regular structure. It can be also noted that the leakage of intracellular material occurred.
So, despite the changes on the wall structure and its crystallinity are minimal, the effect of GMA is decisive for breaking the bonds that hold together the entire structure of the membrane.

Finally, cells were completely disintegrated after treatment with optimum mix and great fractures can also be observed. Moreover, when cell wall was attacked by both cellulase and hemicellulases, it was degraded at a much faster rate (Zhao et al., 2012; Taher et al., 2014; Laothanachareon et al., 2015)..
The evidence of that are the higher lipid yields obtained when the two enzyme preparations were used together. Samples treated with optimum mix reached the highest lipid extraction yield (73.25%), against 56.97% and 54.39% after treatment with mannanase and cellulase, respectively, and 40.81% of untreated samples.
Observing thermal analysis after solvent extraction, a gradual decrease of the peak related to the lipid can be noted, as a confirmation that lipid extraction has actually taken place. As a consequence, there was a relative increase of the peaks assigned to hemicelluloses and cellulose in DTG curves, in particular for OPT treated biomass. For this sample, as happened in all curves of enzymatically treated biomass samples, there was a shift of pyrolytic degradation peak assigned for hemicelluloses towards lower temperatures. Instead, on the contrary to unextracted biomass, also the cellulose shoulder moved to lower temperatures, maybe as a consequence of the fact that also the solvent can enhance the breakage of cellulose (Sathitsuksanoh et al., 2010).
The degradation of large portions of cell walls with the release or exposure of intracellular components to the medium was confirmed also by TEM images and can explain the improvement in lipid extraction for the enzymatically treated biomass. In particular, the high extraction yields observed can be interpreted as the result of the increased accessibility to algal lipids of the extraction solvent due to greater solvent penetration into the cell and/or to the release of lipids into the medium.

CHAPTER 6

Adsorption of textile dyes on unextracted and de-oiled *Nannochloropsis* biomass

In this chapter the evaluation of the reuse of the exhausted biomass after extraction of lipids as a bioadsorbent is studied and reported. In fact, literature studies have shown that microalgae (such as *Chlorella vulgaris*, *Pithophora* sp., *Nostoc linckia*, *Cosmarium* sp., *Caulerpa scalpelliformis*) could be effective solids for the adsorption of dyes. However, despite the high speed of growth and the fact that they do not require agriculture land to be grown, they could be used in the industry of lipids. Lipids are extracted and utilized in the field of alternative fuels, in pharmaceutical industry and as raw material for the production of high value-added compounds. The lipid extraction process produces a large amount of wastes, formed by exhausted algal biomass, which has recently been the subject of study to assess the application as a low cost absorbent material. The main purpose of these experiments was to evaluate, preliminarily, the kinetics and the thermodynamics of

adsorption of Reactive Violet 5 (RV5) of unextracted *Nannochloropsis* microalgae and of the biomass after the extraction of lipids.
As all the reactive dyes, RV5 is hardly biodegradable, because of its complex aromatic structures and synthetic origins, which make it particularly stable. In addition, textile wastewaters have characteristics such as high temperature, varying pH and high chemical oxygen demand (COD), which increase the threatening for aquifers, aquatic basins and life, when dispersed in the environment.
In particular, experimental results and their interpretation and FTIR characterization are presented. Three different isotherms have been taken into account to describe the phenomenon at the equilibrium time. Moreover, a dynamic adsorption model, based on the linear driving force (LDF) approximation, was developed to describe the kinetic adsorption behavior.

6.1 Materials and methods

6.1.1 Chemicals and microalgae

Methanol, chloroform and sodium chloride were purchased from Carlo Erba (Milano, Italy).
Nannochloropsis sp. microalgae were purchased from Archimede Ricerche Srl (Camporosso, Imperia, Italia) in the form of lyophilized powder, and were kept in the freezer at a temperature of -20 ° C. If microalgae were used as raw material for adsorption tests, they were preliminary rehydrated to bring them to the active state.

6.1.2 Reactive Violet 5

The Reactive Violet 5 ($C_{20}H_{16}N_3Na_3O_{15}S_4$, molecular mass 735.58 g/mol), which will be identified as RV5, was purchased from Gammacolor Srl (Seveso, Monza Brianza, Italy). RV5 belongs to the class of azo reactive dyes, i.e. one or more groups chromophores -N = N- (called azo or "azo", Fig. 6.1) are present in the molecule. This gives to RV5, so as to azo dyes in general, properties such as bright colorations and favorable dyeing requirements, even if their stability to light, washing and bleaching is generally less high than that of the dyes of other classes. They are, in general, inexpensive, so they are the most widely used dyes.
A stock solution of RV5 (2000 mg L^{-1}) was prepared and desired concentrations (100–1500 mg L^{-1}) of the dye were obtained by further dilution.

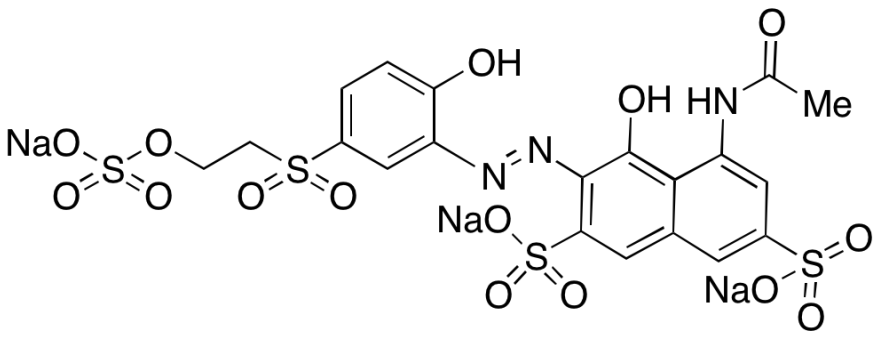

Figure 6.1 – RV5 molecular structure.

The standard calibration curve for RV5 was constructed by measuring the absorbance of known concentration at λ_{max}= 561 nm (Fig. 6.2), through UV-Visible spectrophotometer (Shimadzu UV 2600).
The molar extinction coefficient obtained was ε = 0.0181 L mg^{-1} cm^{-1}.

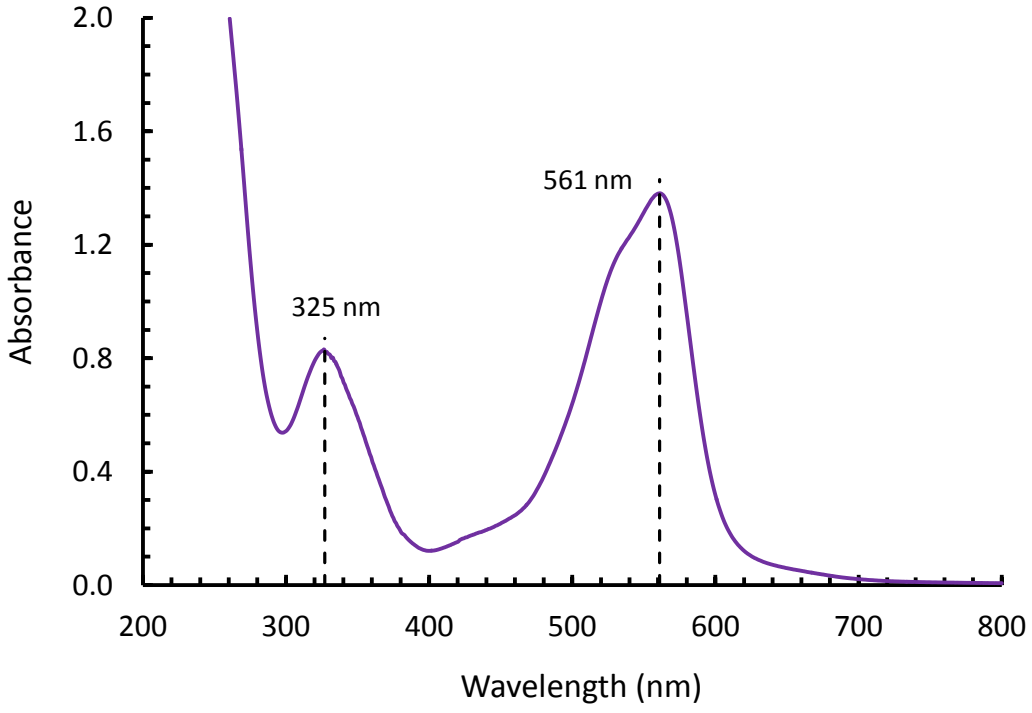

Figure 6.2 – RV5 UV–Vis spectrum.

6.1.3 Microalgae rehydration

50 mg of lyophilized biomass were added to 20 mL of double distillate water in a screw-capped flask.
The flasks were magnetically stirred at room temperature for 5 min. Then, the algal suspension was centrifuged (10,000 ×g, 10 min) and the supernatant removed. Dye solutions at the desired concentration were then added for adsorption tests.

6.1.4 Total lipid extraction and adsorbent preparation

Total lipid extraction of *Nannochloropsis* was performed by the method of Ma et al. (2013) with slight modifications. Specifically, biomass was mixed with chloroform/methanol (2:1, v/v) and stirred at 37 °C for 1 h (Kika Werke 10 power). Then, the mixture was centrifuged at 10,000 ×g for 10 min (Centrifuge MPW 380, Med. Instruments, Poland). The supernatant was collected and the residual biomass was re-extracted more times, under the same conditions until exhaustion of the material. The supernatants were combined and a 1% sodium chloride solution (20% of the total volume) was added. After 10 min stirring at 37 °C, the mixture was centrifuged (10,000 ×g, 10 min), the organic phase was recovered and evaporated under vacuum at 40 °C (Rotavapor R-215, BUCHI Labortechnik AG, Switzerland). The lipid content was calculated from the weight of the residue and expressed as grams of lipids per 100 g of dry biomass.
Total lipid content of *Nannochloropsis* sp. biomass was found to be 29.03 ± 0.35 % (w/w).
The exhausted solid was then dried, grounded and sieved to obtain a powder with uniform particle size.

6.1.5 Adsorption studies

The batch adsorption experiments were carried out with 50 mg of the biosorbent with 20 mL of RV5 dye solutions of desired concentration. The flasks were placed in a water bath thermostated at controlled temperature (10–40 ± 0.1 °C) and magnetically stirred for the appropriate time (3–96 h). Then, the algal suspension was centrifuged (10,000 ×g, 10 min) and the supernatant recovered for analysis. The residual dye concentrations in the solutions were analyzed after centrifugation of the mixtures, by measuring the absorbance of supernatants using a UV–visible spectrophotometer at the maximum wavelength of dye. The concentration of RV5 was calculated by comparing absorbance to the dye calibration curve previously obtained. The adsorption capacity of the adsorbent, q (mg g^{-1}) was calculated as:

$$q = \frac{(c_0 - c_t)}{M} \cdot V$$

where c_o (mg L^{-1}) is the initial dye concentration, c_t (mg L^{-1}) is the residual dye concentration at time t (min), V (L) is the volume of dye solution, and M (g) is the amount of biosorbent used. The q value is equal to q_t at time t and q_e at equilibrium, respectively. In the same way, the c_t value is equal to c_e at equilibrium.

6.1.6 Adsorption isotherms

Langmuir, Freundlich and Temkin models were used to describe the mechanism of adsorption at the equilibrium time. These isotherms describe the distribution of adsorbate molecules in the solid and liquid phases at equilibrium.
The equilibrium experiments were carried out varying the initial dye concentration from 100 to 2000 mg/L for unextracted microalgae and from 500 to 2000 mg/L for de-oiled biomass, keeping the adsorbent dosage (50 mg/20 mL) constant.

Langmuir model is based on the assumption that each adsorbed molecule could occupy only one site, adsorbing surface is homogenous with all sites equivalent undergoing monolayer adsorption with negligible interactions between the dye molecules. Langmuir isotherm can be written according to the following equation:

$$q_e = \frac{q_{max} k_L c_e}{1 + k_L c_e}$$

where q_e (mg/g) is the amount of dye adsorbed at equilibrium, q_{max} (mg/g) is the maximum adsorption capacity, c_e is the adsorbate concentration at equilibrium (mg/L) and k_L is the Langmuir constant.

Freundlich adsorption model is one of the most common isotherms used for dye adsorption assuming heterogeneous surface of adsorbent with multilayer adsorption. This can be expressed by the following equation:

$$q_e = k_F c_e^{1/n}$$

where k_F is the Freundlich constant ($mg^{1-1/n}\ L^{1/n}\ g^{-1}$) related to bonding energy and n is an empirical parameter related to the behavior of the adsorption process. Depending on the value of n the curve has concavity facing downwards if 1/n <1, upwards if 1/n> 1 and is linear if 1/n = 1.

Temkin model was also studied to investigate the adsorption equilibria. This model, unlike the other two, takes into account the effect caused by the indirect interactions among the adsorbent and adsorbate molecules. It assumes that the heat of adsorption (function of temperature) of all molecules on the layer decreases linearly when the coating of the surface of the adsorbent grows. This can be expressed in the following equation:

$$q_e = \frac{RT}{b_T} log(k_T c_e)$$

where k_T is equilibrium binding constant related to the maximum binding energy (L/mg) and b_T (g J mg^{-1} mol^{-1}) is the Temkin isotherm constant related to the heat of adsorption.

6.1.7 Adsorption data evaluation

Each experiment was repeated twice at the same conditions and the arithmetical average values obtained were used. The parameters of isotherm models with statistical evaluation data were defined by nonlinear regressions.
Therefore, to establish the most suitable model the objective function Φ has been calculated. It is defined as the sum of the squares of the differences between the experimental points and those calculated by the different isotherm models. From the minimization of this function, it is possible to evaluate the most suitable model.

6.1.8 Thermodynamic study

From the thermodynamic point of view, the adsorption is a spontaneous phenomenon, accompanied by a decrease in the Gibbs free energy ($\Delta G \leq 0$) of the system. This energy is defined as:

$$\Delta G = \Delta H - T\,\Delta S$$

Using the Vant'Hoff relation, the equation above could be rewritten as:

$$log\, k = \frac{-\Delta H}{RT} + \frac{\Delta S}{R}$$

where k is the adsorption constant that could be derived from the isotherms. This equation represents a line in the semi-logarithmic plane 1/T vs ln(k). Under the simplifying assumption that ΔH and ΔS do not vary with the temperature, it is possible to obtain them from the intercept and the slope of the line.

6.1.9 Adsorption kinetics

The main kinetic models are valid when the equilibrium isotherm is linear. However, this hypothesis is often unsatisfied. In fact, the isotherm models used to describe the equilibrium data are non-linear. Under the hypothesis that the diffusive transport in the adsorbent is the mass transfer controlling resistance, a dynamic, isothermal,

dilute solution adsorption model, based on the linear driving force (LDF) approximation, was developed to describe the kinetic adsorption behavior.

The LDF model is based on a mass transfer model of the adsorbate into the particle, as schematize in Fig. 6.3.

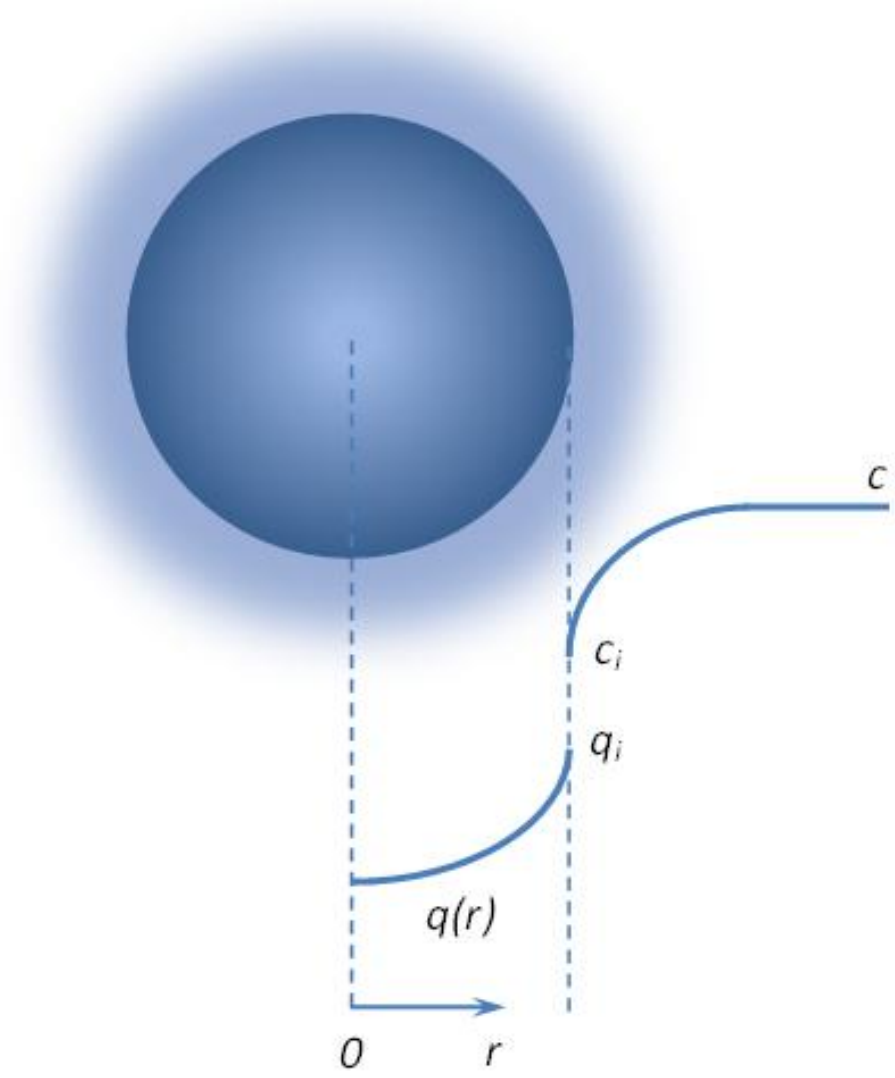

Figure 6.3 – Mass transfer model.

Assuming perfect mixing conditions, a uniform mass transport in the liquid phase can be considered. Taking a constant average value for q(r)= $\bar{q}$, the following differential equation is obtained:

$$\frac{d\bar{q}}{dt} = k_{LDF}(q(c_e) - \bar{q})$$

where $q(c_e)$ is the concentration at the interface q_i, in equilibrium with c_i that could be calculated from the isotherm model, $\bar{q}$ is the dye concentration in the solid and k_{LDF} is a lumped mass transfer coefficient that incorporates the specific surface area. The above equation could be solved when coupled to the mass balance equation:

$$V\frac{dc}{dt} = -M\frac{d\bar{q}}{dt}$$

with the initial conditions $\bar{q}$ (0) = 0 and c(0) = c_o.
The integration of the differential equations was performed numerically through the fourth order Runge-Kutta method.

6.1.10 Fourier transform infrared spectroscopy (FTIR)

Fourier-transform infrared (FTIR) analyses were carried out on dry untreated biomass samples and on their residue after lipid extraction. The samples were grounded and quartered as described by Diniz *et al.* (2014) in order to obtain a representative portion of material from the total amount of biomass. Measurements were performed on a Bruker Vertex 70 spectrometer (Bruker Optics, Billerica, MA, USA) equipped with a Platinum ATR sampling module. FTIR spectra were collected in quadruplicate in the mid infrared region (4000-400 cm^{-1}) with 128 scan at a resolution of 3 cm^{-1}.

6.1.11 Electron microscopy

Scanning electron microscopy (SEM) was used to investigate the morphological changes of microalgal cells after the extraction of lipids.
Small amount of sample was taken from the suspension, placed on silicon substrate, dried, chromium-coated and observed with a High Resolution-Field Emission Scanning Electron Microscope (HR-FESEM_AURIGA Zeiss) at 6kV.

6.2 Adsorption equilibrium on unextracted *Nannochloropsis* sp.

Firstly, the equilibrium time was determined. Assays at different contact time (180-5760 min) were performed at the three temperatures studied (10, 25 and 40 °C), with an initial dye concentration of 200 ppm. Results are reported in Tables 6.1, 6.2 and 6.3.

Table 6.1 – Adsorption of RV5 on unextracted *Nannochloropsis* biomass at different contact times at 10 °C.

T (min)	c_t(mg L^{-1})	q_t(mg g^{-1})
180	177.87	10.26
480	165.09	15.22
900	144.05	23.45
1440	132.91	28.66
1920	128.62	29.36
2880	125.74	31.34
4320	123.21	31.55
5760	122.54	32.00

Table 6.2 – Adsorption of RV5 on unextracted *Nannochloropsis* biomass at different contact times at 25 °C.

T (min)	c_t(mg L^{-1})	q_t(mg g^{-1})
180	146.42	21.55
480	125.84	29.99
900	112.99	34.47
1440	93.54	41.40
1920	81.94	47.60
2880	69.85	52.61
4320	63.95	54.83
5760	62.27	56.28

Table 6.3 – Adsorption of RV5 on unextracted *Nannochloropsis* biomass at different contact times s at 40 °C.

T (min)	c_t(mg L^{-1})	q_t(mg g^{-1})
180	134.16	27.02
480	111.16	34.57
900	89.43	44.52
1440	77.08	48.44
1920	72.56	50.56
2880	64.42	55.26
4320	54.87	58.49
5760	53.09	58.68

As shown in the results, the equilibrium time can be set at 72 hours for all three temperatures. The variations of concentration in the liquid phase and solid for times longer, in fact, appear to be negligible.
Therefore, equilibrium experiments were performed, for all temperatures, with 72 h as contact time, at different initial concentrations: 100, 200, 400, 600, 800, 1000, 1500 and 2000 ppm.

6.2.1 Equilibrium isotherms at 10 °C

Results obtained in equilibrium experiments at 10 °C are listed in Table 6.4.

Table 6.4 – Equilibrium data for the adsorption of RV5 on unextracted *Nannochloropsis* biomass at 10 °C.

Nominal c_o (mg L^{-1})	c_e (mg L^{-1})	q_e (mg g^{-1})
100	49.19	19.20
200	123.21	31.55
400	291.69	42.64
600	480.12	47.34
800	657.87	54.99
1000	843.40	60.75
1500	1318.17	69.85
2000	1811.54	69.66

The statistical results showed in Table 6.5 present that Temkin model was more adequate to represent the data of adsorption equilibrium at 10 °C.

Table 6.5 – Model parameters of adsorption isotherms for unextracted biomass at 10 °C.

Model	Parameters		Φ
Langmuir	k_L (L mg^{-1})	q_{max} (mg g^{-1})	
	0.048	75.97	95.32
Freundlich	k_f ($mg^{1-1/n}g^{-1}L^{1/n}$)	n (–)	
	6.38	0.328	58.17
Temkin	k_T (L g^{-1})	b_T (g J mg^{-1} mol^{-1})	
	0.068	160.55	36.63

Isotherms obtained together with experimental points are represented in Fig. 6.4.

a)

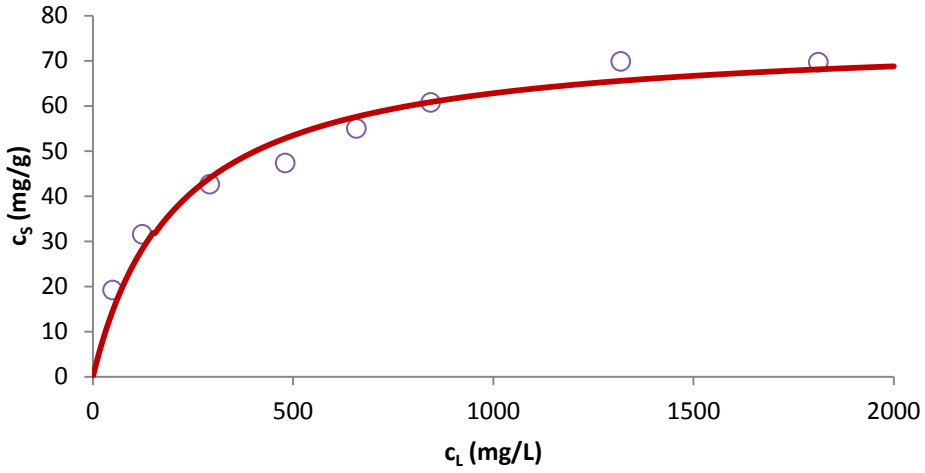

b)

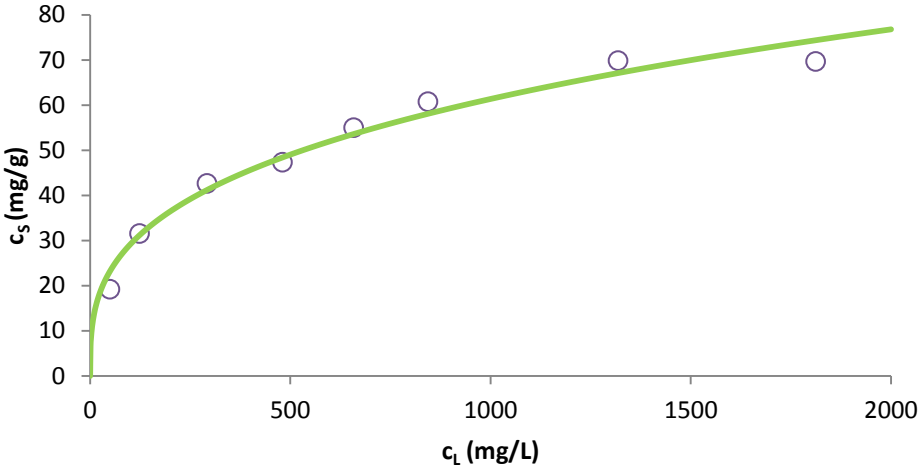

c)

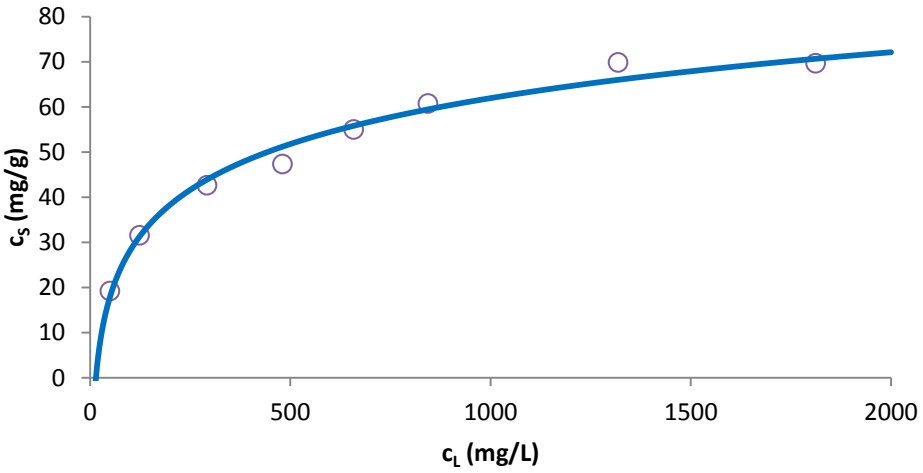

Figure 6.4 – Equilibrium isotherms for unextracted biomass at 10 °C a) Langmuir b) Freundlich c) Temkin.

The Φ values are low for all three models, which, in fact, fit well the experimental data. The value of n of the Freundlich isotherm indicates that the adsorption is positive.

6.2.2 Equilibrium isotherms at 25 °C

Equilibrium data at 25 °C are listed in Tables 6.6.

Table 6.6 – Equilibrium data for the adsorption of RV5 on unextracted *Nannochloropsis* biomass at 25 °C.

Nominal c_o (mg L^{-1})	c_e (mg L^{-1})	q_e (mg g^{-1})
100	23.87	29.49
200	63.95	55.83
400	235.71	66.75
600	409.24	76.00
800	577.58	87.56
1000	772.28	88.82
1500	1254.93	93.40
2000	1751.85	93.73

The statistical results confirmed that Temkin model was found to be the best to describe the equilibrium at 25 °C (Table 6.7).

Table 6.7 – Model parameters of adsorption isotherms at 25 °C.

Model	Parameters		Φ
Langmuir	k_L (L mg^{-1})	q_{max} (mg g^{-1})	
	0.018	93.52	186.94
Freundlich	k_f ($mg^{1-1/n}g^{-1}L^{1/n}$)	n (–)	
	20.97	0.211	288.86
Temkin	k_T (L g^{-1})	b_T (g J mg^{-1} mol^{-1})	
	0.434	166.52	133.37

Isotherms obtained together with experimental points are represented in Fig. 6.5.

a)

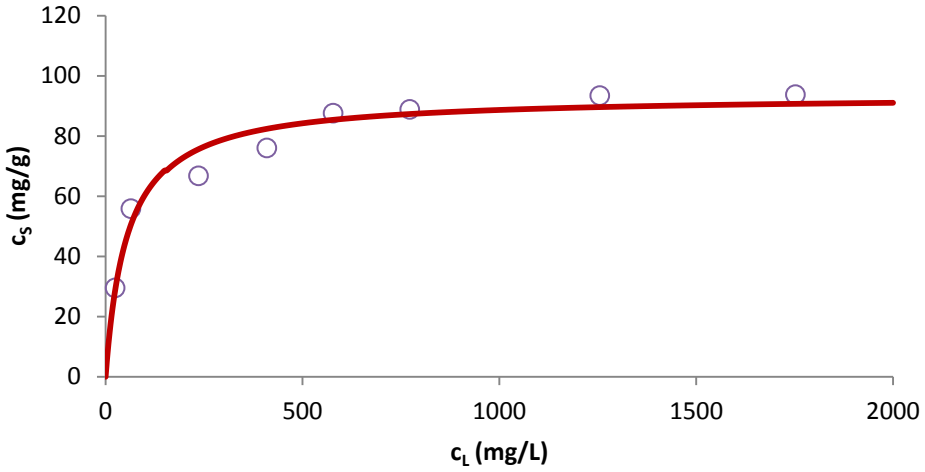

b)

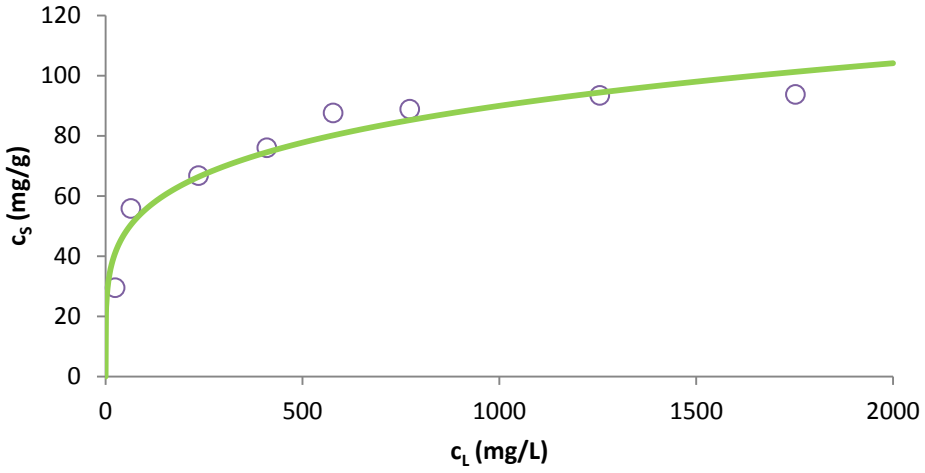

c)

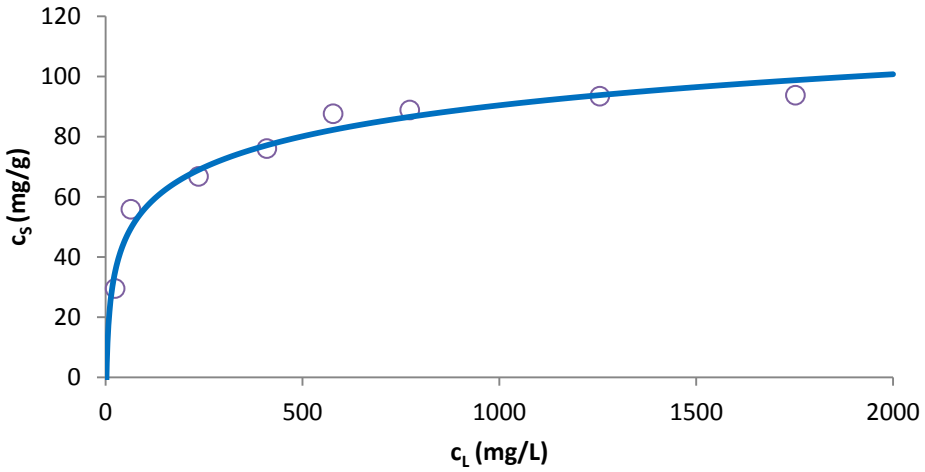

Figure 6.5 – Equilibrium isotherms for unextracted biomass at 25 °C a) Langmuir b) Freundlich c) Temkin

The Φ values are higher than those obtained at 10 °C for all three models. The value of q_{max} of the Langmuir isotherm is higher, indicating that the removal of the dye is favored at higher temperature.

6.2.3 Equilibrium isotherms at 40 °C

Results of equilibrium assays at 40 °C are reported in Tables 6.8.

Table 6.8 – Equilibrium data for the adsorption of RV5 on unextracted *Nannochloropsis* biomass at 40 °C.

Nominal c_o (mg L^{-1})	c_e (mg L^{-1})	q_e (mg g^{-1})
100	16.20	34.19
200	54.87	58.49
400	208.83	76.31
600	373.87	91.67
800	542.07	99.77
1000	724.75	106.48
1500	1203.31	116.22
2000	1683.77	119.18

Even at 40 °C the model that approximate better the experimental point is Temkin isotherm, as shown in Table 6.9.

Table 6.9 – Model parameters of adsorption isotherms at 40 °C.

Model	Parameters		Φ
Langmuir	k_L (L mg^{-1})	q_{max} (mg g^{-1})	
	0.0162	115.05	147.27
Freundlich	k_f ($mg^{1-1/n}g^{-1}L^{1/n}$)	n (–)	
	21.86	0.235	456.25
Temkin	k_T (L g^{-1})	b_T (g J mg^{-1} mol^{-1})	
	0.377	169.63	40.33

Tested models obtained together with experimental points are represented in Fig. 6.6.

a)

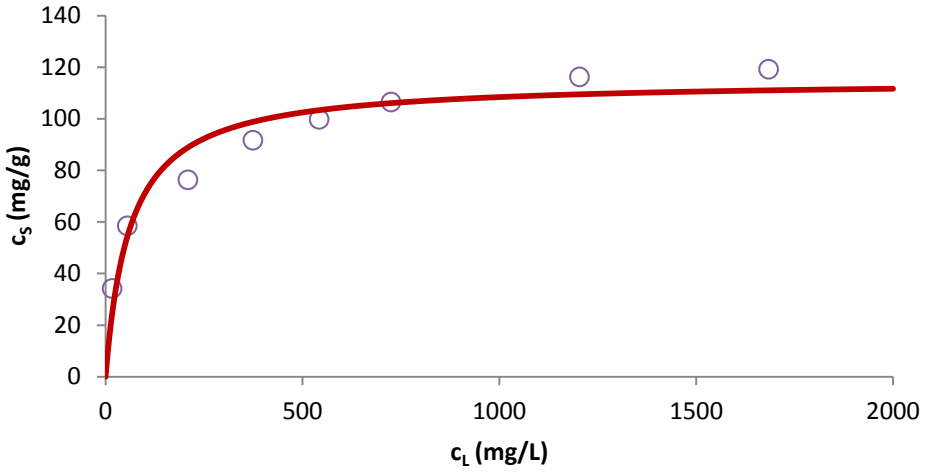

b)

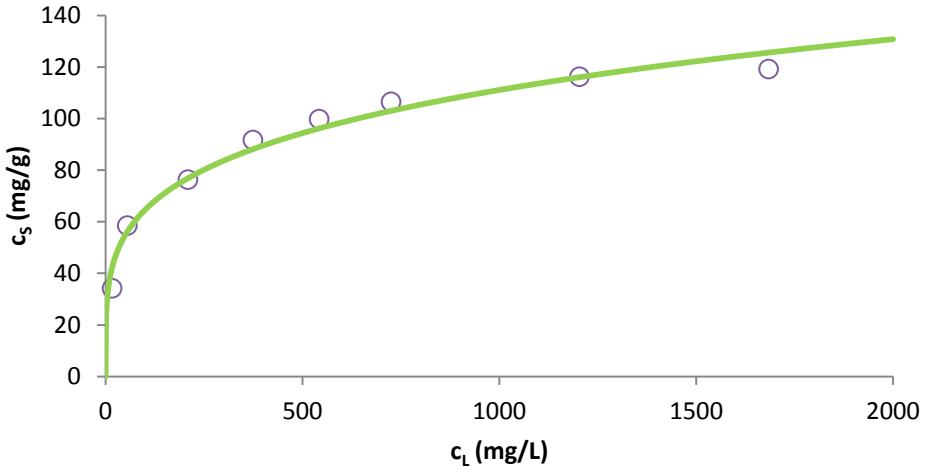

c)

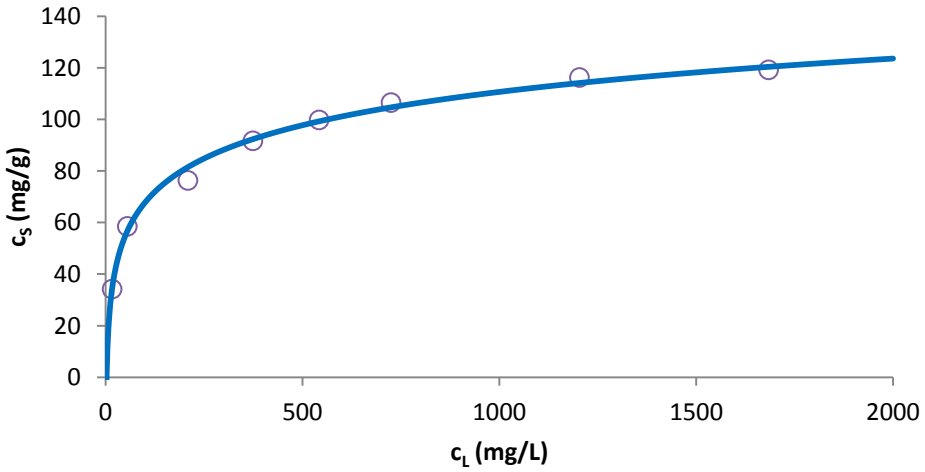

Figure 6.6 – Equilibrium isotherms for unextracted biomass at 40 °C a) Langmuir b) Freundlich c) Temkin

At this temperature the Φ values for Langmuir and Freundlich models are very high. The value of q_{max} of the Langmuir isotherm continues to increase, confirming that the removal of the dye is favored at higher temperature.

6.2.4 Thermodynamic study

The Temkin equilibrium constant k_T values at the studied temperatures were used to determine the Gibbs energy and, therefore, the values of ΔH and ΔS.
These parameters were obtained from the intercept and the slope of the line determined plotting 1/T vs ln(k_T), reported in Fig. 6.7.

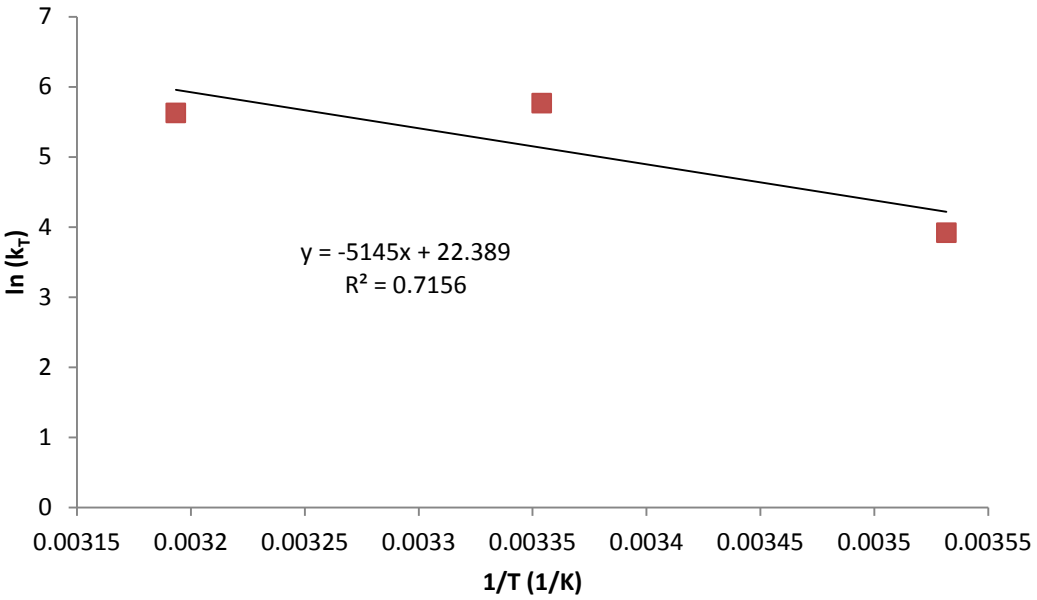

Figure 6.7 – Variation of ln(k_T) with 1/T for unextracted biomass.

The Gibbs energy, enthalpy and entropy of adsorption are reported in Table 6.10.

Table 6.10 – Thermodynamic parameters for the adsorption of RV5 on unextracted *Nannochloropsis* biomass.

Temperature (K)	ΔG (kJ/mol)	ΔH (kJ/mol)	ΔS (kJ/mol K)
10	−9.22		
25	−14.29	42.78	0.186
40	−14.65		

The negative values of ΔG demonstrate that the adsorption of RV5 on unextracted *Nannochloropsis* biomass is a spontaneous process for the range of temperature evaluated. The positive values of enthalpy change (ΔH) show that the adsorption process is endothermic, while any increasing in temperature lead to a higher RV5 amount at equilibrium. The positive value of ΔS obtained reveals the affinity of the dye towards the adsorbent and an increased disorder.

6.3 Adsorption kinetics on unextracted *Nannochloropsis* sp.

A dynamic adsorption model, based on the linear driving force (LDF) approximation, was developed to describe the kinetic adsorption behavior.
According to the results obtained in equilibrium tests, the concentration at the interface was calculated through the Temkin isotherm for all the examined tempertures.
The resulting system of differential equations is the following:

$$\begin{cases} \frac{d\bar{q}}{dt} = k_{LDF}(q(c_e) - \bar{q}) \\ V\frac{dc}{dt} = -M\frac{d\bar{q}}{dt} \\ q(c_e) = B\ln(k_T) + B\ln(c_e) \\ \bar{q}(0) = 0 \\ c(0) = 200 \end{cases}$$

In this system, k_{LDF} is the only unknown parameter. It can be calculated through the minimization of the objective function Φ. As before, this function is defined as the sum of the squares of the differences between the experimental points and those calculated by the linear driving force model.
The integration of the differential equations was performed numerically through the fourth order Runge–Kutta method.
Kinetic tests were performed at the three temperatures studied (10, 25 and 40 °C), with an initial dye concentration of 200 ppm, as reported before in Tables 6.1, 6.2 and 6.3.
The experiments at 96 h were excluded because at this contact time the equilibrium was already reached.
The values of k_{LDF} at different temperatures and the associated Φ are reported in Table 6.11.
The LDF model curves are shown in Fig. 6.8 together with the experimental points.

Table 6.11 – LDF Model parameters for unextracted biomass at 10, 25 and 40 °C.

Temperature (°C)	k_{LDF} (1/min)	Φ
10	1.28E-03	9.59
25	1.18E-03	158.03
40	1.31E-03	199.95

a)

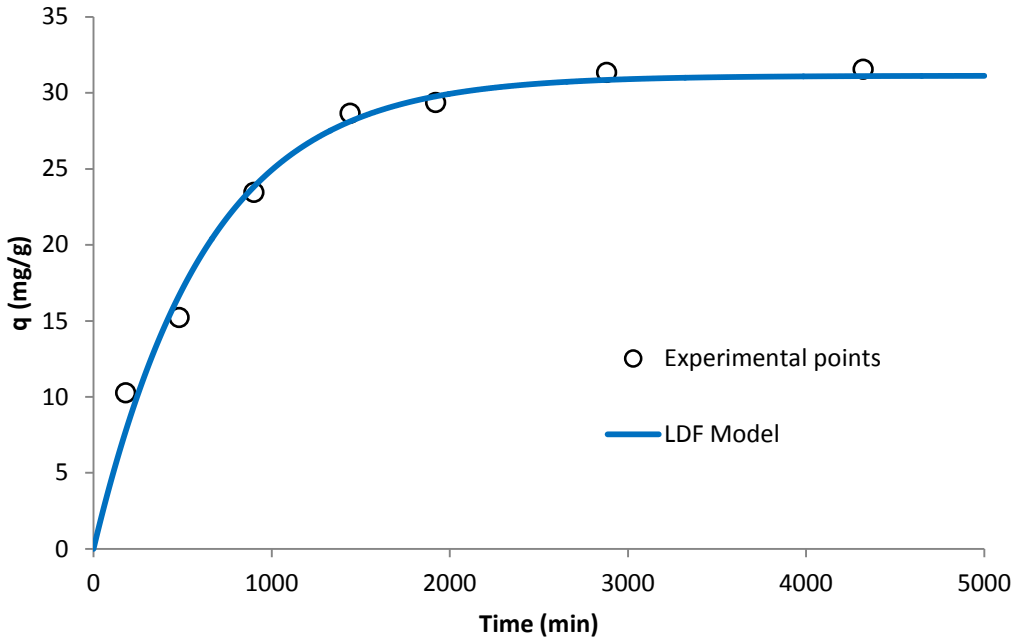

b)

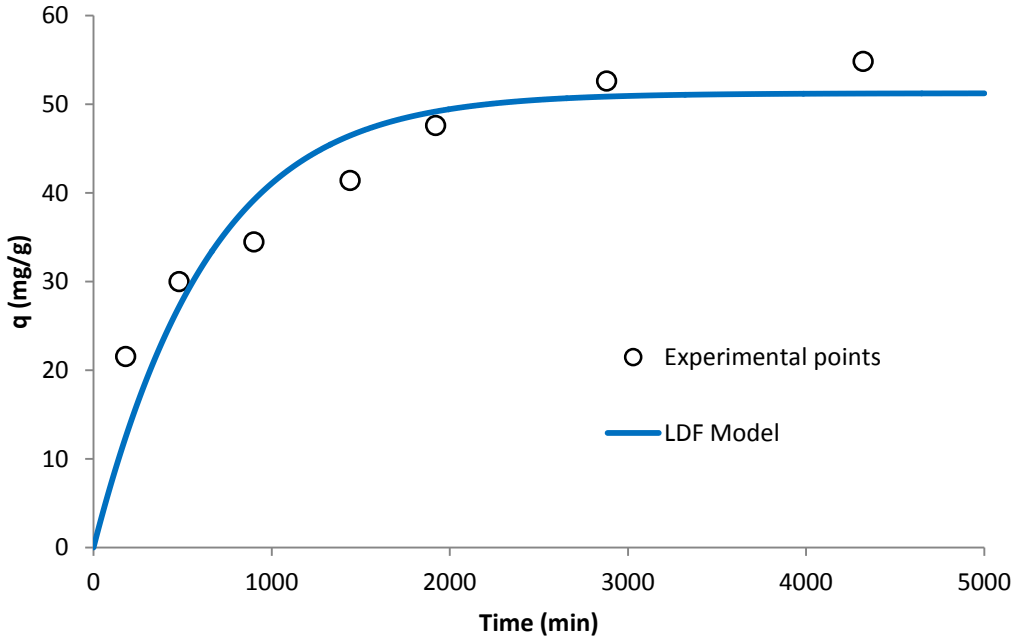

c)

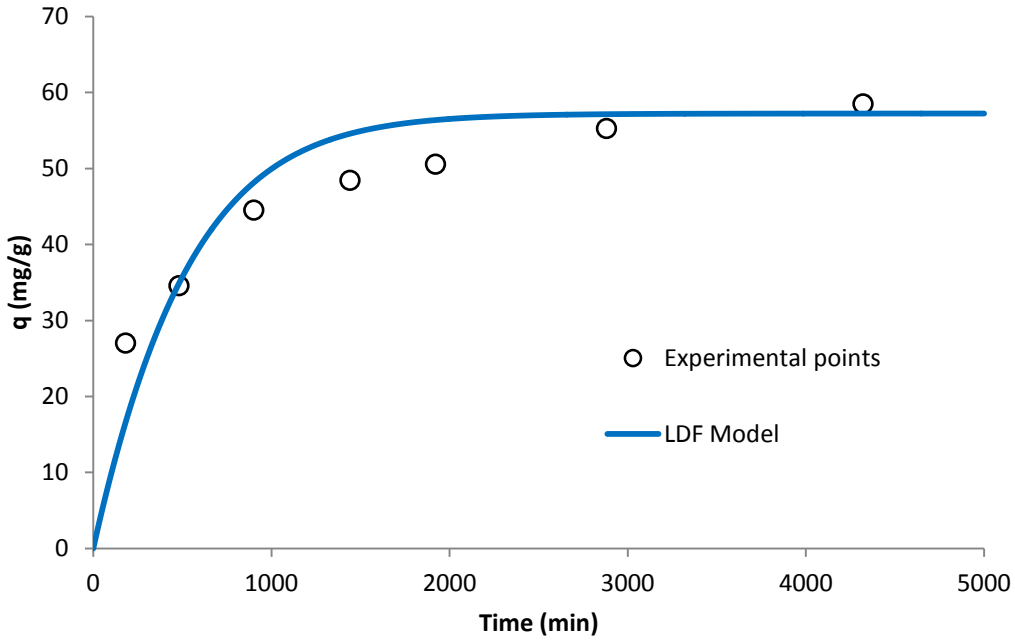

Figure 6.8 – LDF model for unextracted biomass at a) 10 °C, b) 25 °C and c) 40 °C.

The LDF model approximated very well the experimental data at 10 °C, showing that the assumptions made in its construction were correct. At higher temperatures, the values of Φ were higher, but still acceptable.

6.4 Adsorption equilibrium on de-oiled *Nannochloropsis* sp.

As it has been done for unextracted *Nannochloropsis* sp. biomass, the first step was the determination of the equilibrium time. Therefore, the dye removal efficiencies of the de-oiled biomass were evaluated at the three temperatures studied (10, 25 and 40 °C) at different contact time (180–4800 min), with an initial dye concentration of 600 ppm. This value of c_o is higher than the one utilized for unextracted microalgae, because preliminary experiments showed that the adsorption capacity of this solid was higher and the c_o values lower than 400 ppm led to the complete removal of the dye. Results are reported in Tables 6.12, 6.13 and 6.14.

Table 6.12 – Adsorption of RV5 on de-oiled *Nannochloropsis* biomass at different contact times at 10 °C.

T (min)	c_t(mg L^{-1})	q_t(mg g^{-1})
180	550.83	19.72
480	528.20	29.61
900	520.07	31.44
1440	500.08	38.55
2160	497.26	41.77
2880	485.47	45.90
4320	480.12	46.19
4800	479.14	46.77

Table 6.13 – Adsorption of RV5 on de-oiled *Nannochloropsis* biomass at different contact times at 25 °C.

T (min)	c_t(mg L^{-1})	q_t(mg g^{-1})
180	485.02	46.35
480	465.92	54.46
900	455.38	57.47
1440	436.70	63.70
2160	429.67	68.90
2880	422.06	72.16
4320	409.23	76.58
4800	411.60	77.14

Table 6.14 – Adsorption of RV5 on de-oiled *Nannochloropsis* biomass at different contact times at 40 °C.

T (min)	c_t(mg L^{-1})	q_t(mg g^{-1})
180	465.30	55.07
480	429.17	70.88
900	421.02	73.04
1440	390.03	85.09
2160	374.57	89.34
2880	368.72	91.93
4320	361.33	95.60
4800	360.10	95.17

As well as unextracted biomass, for all three different temperatures the equilibrium was reached after 72 hours. In fact, after this time the variations of dye concentration in the liquid and solid phase appear to be negligible.
Therefore, equilibrium tests were performed for 72 h at the three studied temperatures. Eight different experiments at the following initial concentrations were performed in duplicate: 500, 600, 700, 800, 1000, 1250, 1500 and 2000 ppm.

6.4.1 Equilibrium isotherms at 10 °C

Results obtained in equilibrium experiments at 10 °C are listed in Table 6.15.

Table 6.15 – Equilibrium data for the adsorption of RV5 on de-oiled *Nannochloropsis* biomass at 10 °C.

Nominal c_0 (mg L^{-1})	c_e (mg L^{-1})	q_e (mg g^{-1})
500	49.19	19.20
600	123.21	31.55
700	291.69	42.64
800	480.12	47.34
1000	657.87	54.99
1250	843.40	60.75
1500	1318.17	69.85
2000	1811.54	69.66

Model parameters of adsorption isotherms for de-oiled biomass are shown in Table 6.16. Langmuir model was adequate to represent the data of adsorption equilibrium at 10 °C.

Table 6.16 – Model parameters of adsorption isotherms for de-oiled biomass at 10 °C.

Model	Parameters		Φ
Langmuir	k_L (L mg^{-1})	q_{max} (mg g^{-1})	
	0.0144	202.36	81.81
Freundlich	k_f ($mg^{1-1/n}g^{-1}L^{1/n}$)	n (–)	
	75.13	0.134	324.05
Temkin	k_T (L g^{-1})	b_T (g J mg^{-1} mol^{-1})	
	3.09	99.87	254.47

Isotherms obtained together with experimental points are represented in Fig. 6.9.

a)

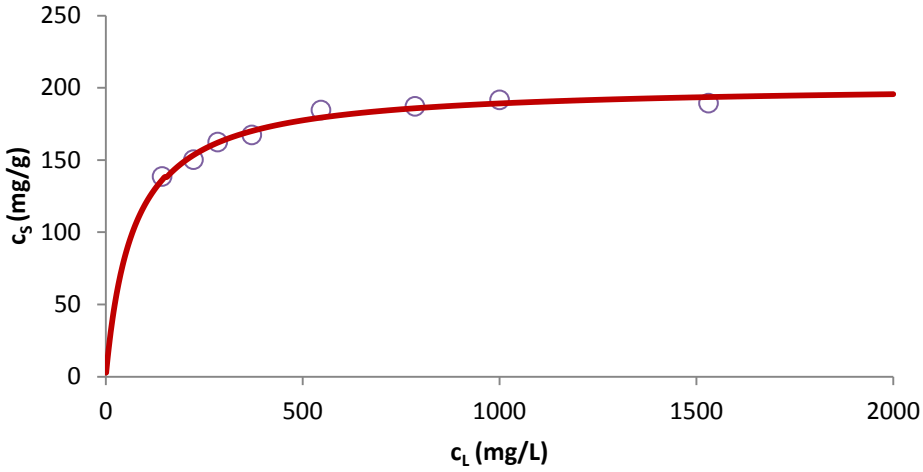

b)

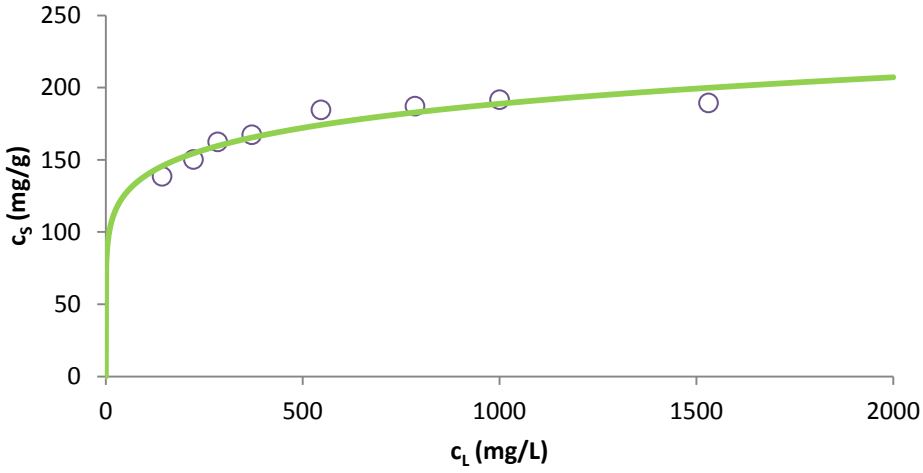

c)

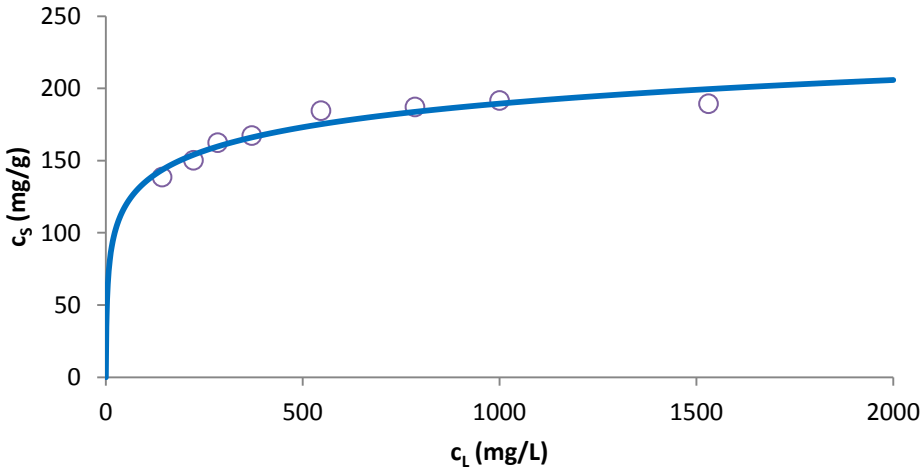

Figure 6.9 – Equilibrium isotherms for de-oiled biomass at 10 °C a) Langmuir b) Freundlich c) Temkin.

The Φ value for Langmuir isotherm is low. In fact, it is the only model which approximates the experimental data accurately. The Φ values of Freundlich and Temkin isotherms are much higher. In any case the adsorption is still positive, as indicate from Freundlich trend, while the adsorption capacity is much greater than that of the unextracted *Nannochloropsis* microalgae.

6.4.2 Equilibrium isotherms at 25 °C

Results obtained in equilibrium tests at 25 °C are listed in Table 6.17.

Table 6.17 – Equilibrium data for the adsorption of RV5 on de-oiled *Nannochloropsis* biomass at 25 °C.

Nominal c_o (mg L^{-1})	c_e (mg L^{-1})	q_e (mg g^{-1})
500	130.81	148.87
600	160.77	179.84
700	219.14	186.76
800	329.59	192.60
1000	491.34	202.24
1250	742.49	204.29
1500	971.34	206.07
2000	1471.08	209.28

The statistical results showed that Langmuir model was found to be the more appropriate to describe the equilibrium of adsorption on RV5 on de-oiled microalgae at 25 °C (Table 6.18).

Table 6.18 – Model parameters of adsorption isotherms for de-oiled biomass at 25 °C.

Model	Parameters		Φ
Langmuir	k_L (L mg^{-1})	q_{max} (mg g^{-1})	
	0.0222	218.03	321.69
Freundlich	k_f ($mg^{1-1/n}g^{-1}L^{1/n}$)	n (–)	
	103.92	0.101	710.45
Temkin	k_T (L g^{-1})	b_T (g J mg^{-1} mol^{-1})	
	36.28	124.52	650.17

Isotherms obtained together with experimental points are represented in Fig. 6.10.

a)

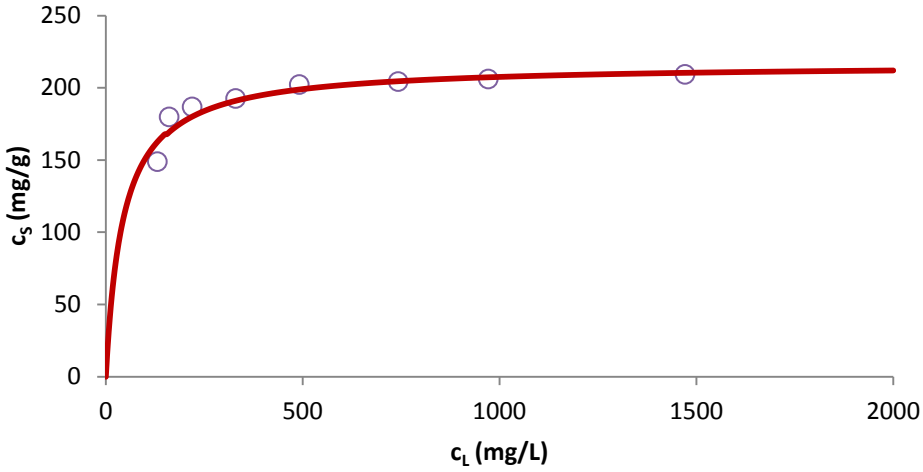

b)

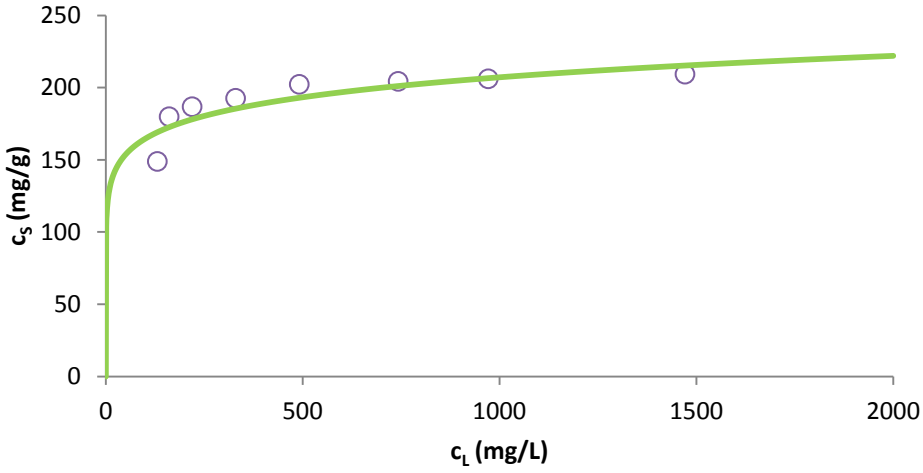

c)

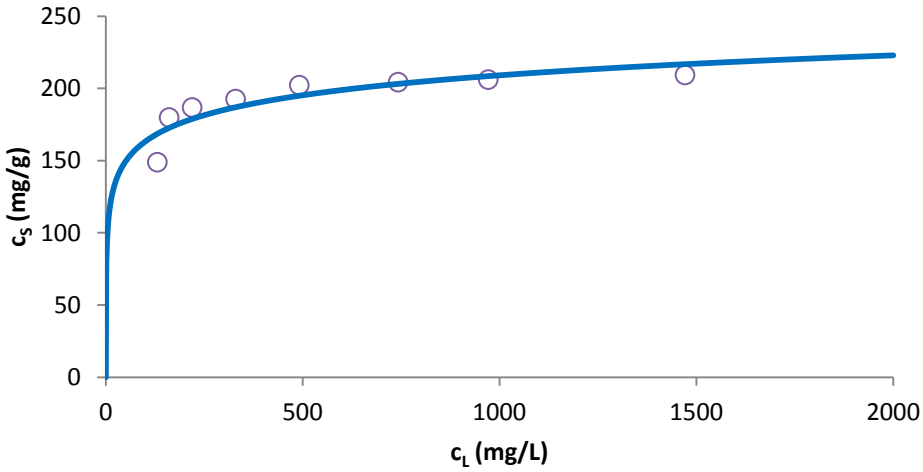

Figure 6.10 – Equilibrium isotherms for de-oiled biomass at 25 °C a) Langmuir b) Freundlich c) Temkin.

The Φ values for all the isotherms are much higher than those determined at 10 °C, as demonstrated by the graphs. In any case the Langmuir model continues to be the more accurate to fit the experimental data. As happened for unextracted biomass, q_{max} of the Langmuir isotherm at 25 °C is higher than the value at 10 °C, confirming that the removal of the dye is favored at higher temperature.

6.4.3 Equilibrium isotherms at 40 °C

Results obtained in equilibrium tests at 40 °C are listed in Table 6.19.

Table 6.19 – Equilibrium data for the adsorption of RV5 on de-oiled *Nannochloropsis* biomass at 40 °C.

Nominal c_o (mg L^{-1})	c_e (mg L^{-1})	q_e (mg g^{-1})
500	30.87	183.44
600	49.34	213.47
700	92.12	242.15
800	188.25	248.69
1000	364.64	262.01
1250	563.23	271.88
1500	776.28	283.53
2000	1276.64	283.63

Even at 40 °C the model that approximate better the experimental point obtained for the adsorption of RV5 on de-oiled *Nannochloropsis* is Langmuir isotherm, as shown in Table 6.20.

Table 6.20 – Model parameters of adsorption isotherms for de-oiled biomass at 40 °C.

Model	Parameters		Φ
Langmuir	k_L (L mg^{-1})	q_{max} (mg g^{-1})	
	0.0607	281.52	271.39
Freundlich	k_f ($mg^{1-1/n}g^{-1}L^{1/n}$)	n (–)	
	143.53	0.101	793.50
Temkin	k_T (L g^{-1})	b_T (g J mg^{-1} mol^{-1})	
	85.54	103.16	604.83

Isotherms obtained together with experimental points are represented in Fig. 6.11.

a)

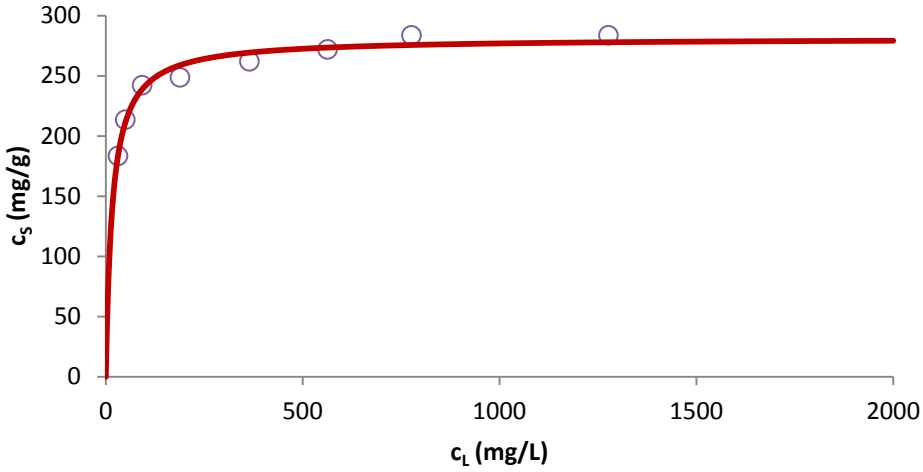

b)

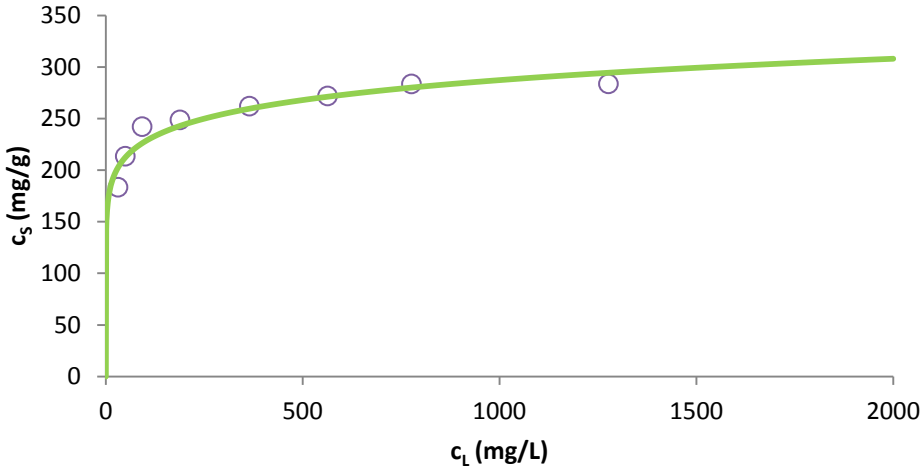

c)

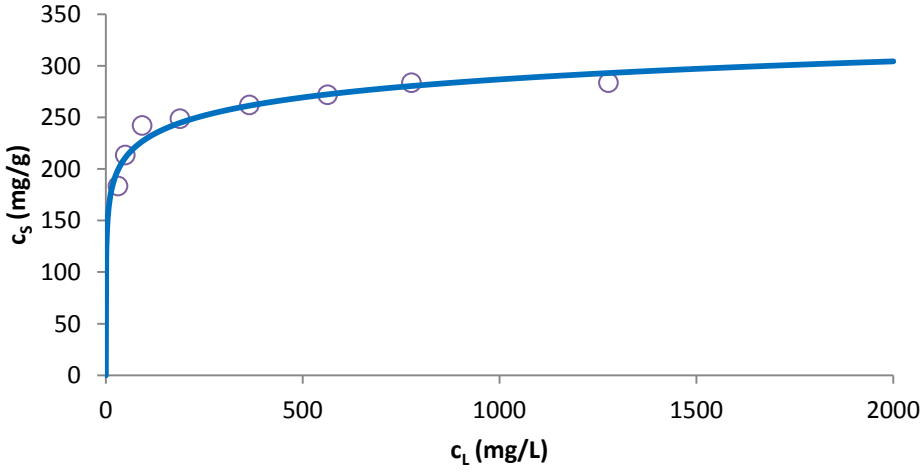

Figure 6.11 – Equilibrium isotherms for de-oiled biomass at 40 °C a) Langmuir b) Freundlich c) Temkin.

Results obtained at 40 °C are very similar to those at 25 °C. The Φ values for all the isotherms are very high, while Langmuir model continues to be the more accurate to fit the experimental data. The value of q_{max} of the Langmuir isotherm continues to increase, confirming that the removal of the dye is favored at higher temperature.

6.4.4 Thermodynamic study

The Langmuir equilibrium constant k_L values at the studied temperatures were used to determine the Gibbs energy at the considered temperature and, therefore, the values of ΔH and ΔS of the process.
These parameters were obtained from the intercept and the slope of the line determined plotting 1/T vs ln(k_L), reported in Fig. 6.12.

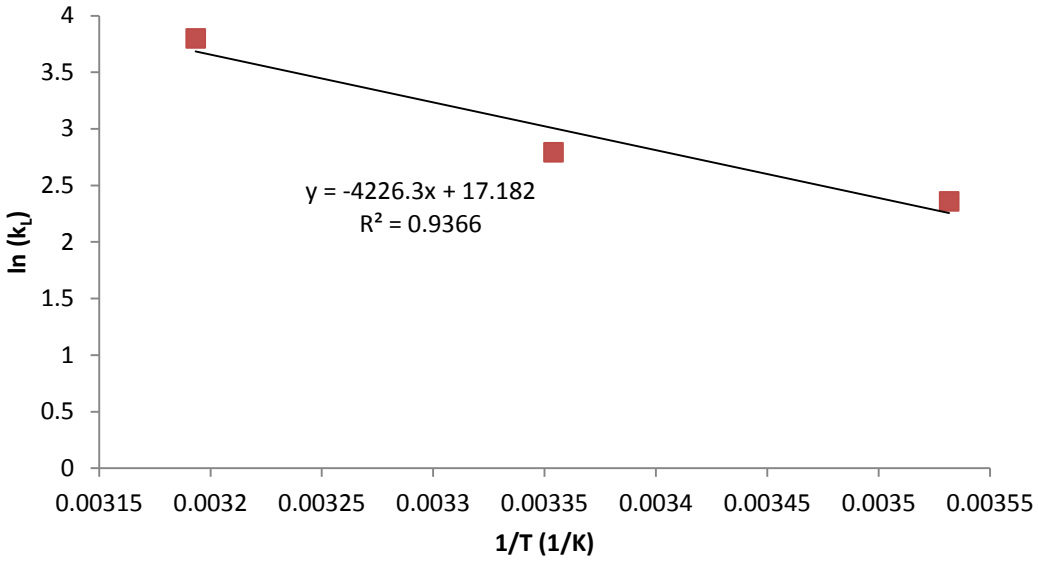

Figure 6.12 – Variation of ln(k_L) with 1/T for de-oiled biomass.

The Gibbs energy, enthalpy and entropy of adsorption are reported in Table 6.21.

Table 6.21 – Thermodynamic parameters for the adsorption of RV5 on de-oiled *Nannochloropsis* biomass.

Temperature (K)	ΔG (kJ/mol)	ΔH (kJ/mol)	ΔS (kJ/mol K)
10	–5.55	35.14	0.14
25	–6.92		
40	–9.89		

The values of ΔG are negative, demonstrating that the adsorption of RV5 on de-oiled *Nannochloropsis* biomass is a spontaneous process for the range of temperature evaluated. The positive enthalpy change (ΔH) values show that the adsorption process is endothermic, while any increasing in temperature lead to a higher RV5 amount uptake at equilibrium. The positive value of ΔS obtained reveals an increased disorder and the affinity of the dye towards the adsorbent.

6.5 Adsorption kinetics on de-oiled *Nannochloropsis* sp.

A dynamic adsorption model, based on the linear driving force (LDF) approximation, was developed to describe the kinetic adsorption behavior at the three different temperature.
According to the results obtained in equilibrium tests, the concentration at the interface was calculated through the Langmuir isotherm for all the examined tempertures.
The resulting system of differential equations is the following:

$$\begin{cases} \frac{d\bar{q}}{dt} = k_{LDF}(q(c_e) - \bar{q}) \\ V\frac{dc}{dt} = -M\frac{d\bar{q}}{dt} \\ q_e = \frac{q_{max}k_L c_e}{1 + k_L c_e} \\ \bar{q}(0) = 0 \\ c(0) = 600 \end{cases}$$

In this system, k_{LDF} is the only unknown parameter. It can be calculated through the minimization of the objective function Φ. As before, this function is defined as the sum of the squares of the differences between the experimental points and those calculated by the linear driving force model.
The integration of the differential equations was performed numerically through the fourth order Runge–Kutta method.
Kinetic test were performed at the three different temperatures studied (10, 25 and 40 °C), with an initial dye concentration of 600 ppm, as reported before in Tables 6.12, 6.13 and 6.14.
The experiments at 80 h were excluded because at this contact time the equilibrium is already reached.
The values of k_{LDF} at different temperatures and the associated Φ are reported in Table 6.22.
The LDF model curves are shown in Fig. 6.13 together with the experimental points.

Table 6.22 – LDF Model parameters for de-oiled biomass at 10, 25 and 40 °C.

Temperature (°C)	k_{LDF} (1/min)	Φ
10	1.83E-03	2612.91
25	2.72E-03	1284.36
40	2.61E-03	5741.74

a)

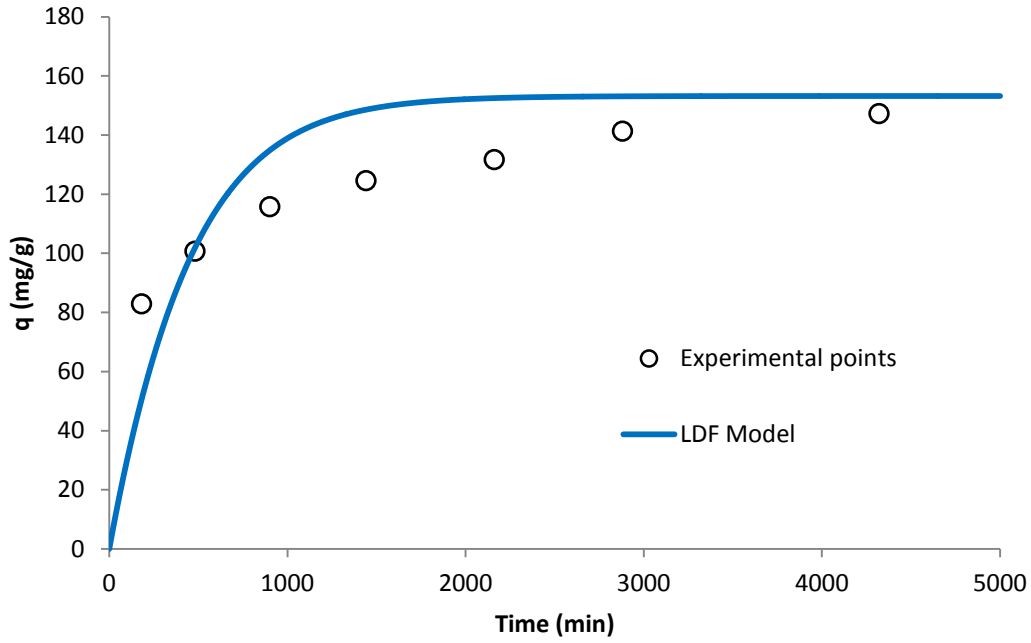

b)

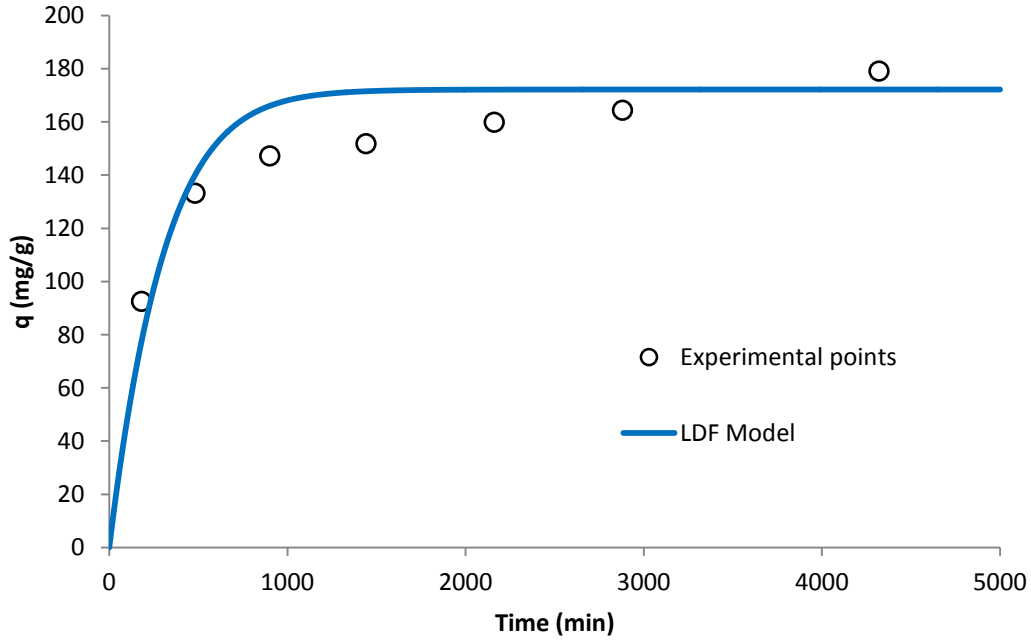

c)

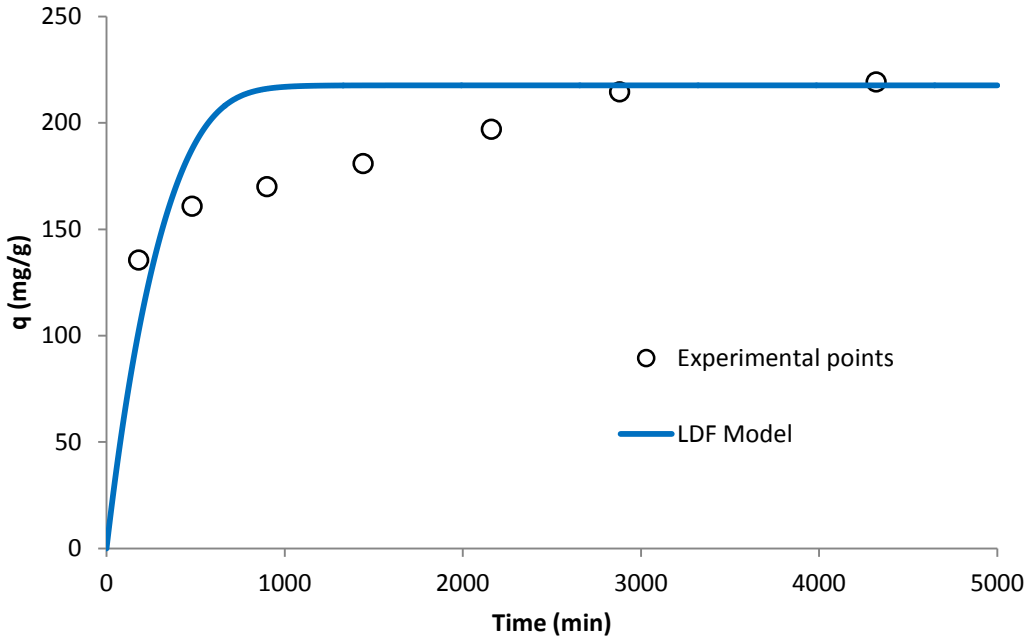

Figure 6.13 – LDF model for de-oiled biomass at a) 10 °C, b) 25 °C and c) 40 °C

The values of Φ for LDF model are very high for all the temperatures taken into account, showing that the assumptions made in its construction are not good for the de-oiled biomass, in contrast to unextracted *Nannochloropsis* microalgae.

6.6 FTIR characterization

The algae cell wall is composed of various compounds with polar functional groups, such as hydroxyl, phenolic, aldehydic, ketonic, carboxylic, etc. behaving as the active binding sites for the dye molecules. FTIR spectra are useful to examine the functional groups present on the surface of the adsorbents responsible for binding RV5 molecules. Figs. 6.14 and 6.15 show the FTIR spectra of unextracted and de-oiled *Nannochloropsis* sp. microalgae, while in Figs. 6.16 and 6.17 spectra of the dye and of the biomass before and after RV5 adsorption are compared. Solids after adsorption were obtained from tests performed at 72 h of contact time and 2000 ppm as c_0.

The spectra of unextracted and de-oiled microalgae are very similar. The main differences are, as might be expected, the disappearance of the peak at 1741 cm^{-1} (ν C=O) and the strong decrease of the peaks at 2919 cm^{-1} (νas CH_2) and 2852 cm^{-1} (ν CH_2), all related to lipids.

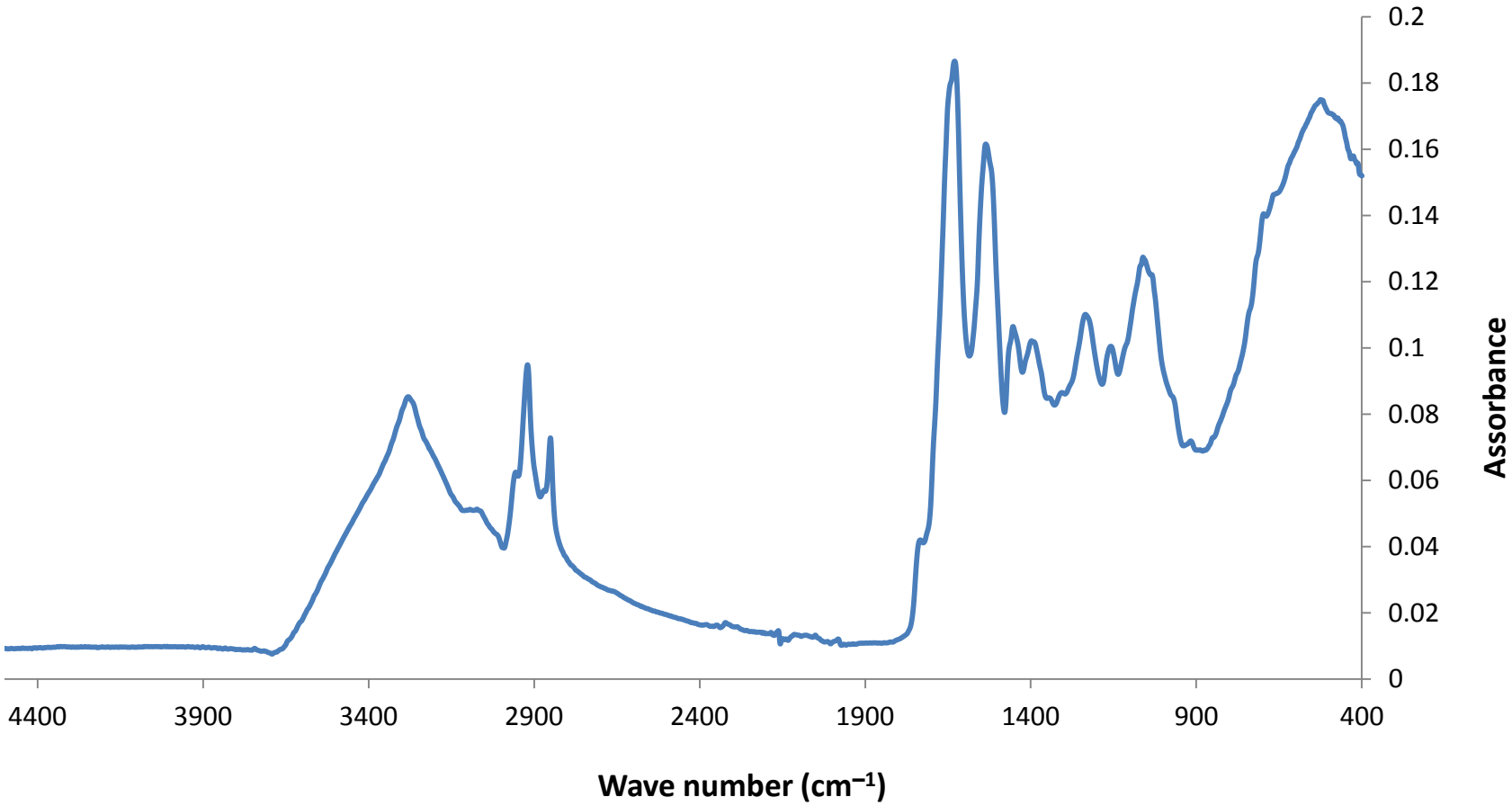

Figure 6.14 – FTIR spectrum of unextracted *Nannochloropsis* biomass.

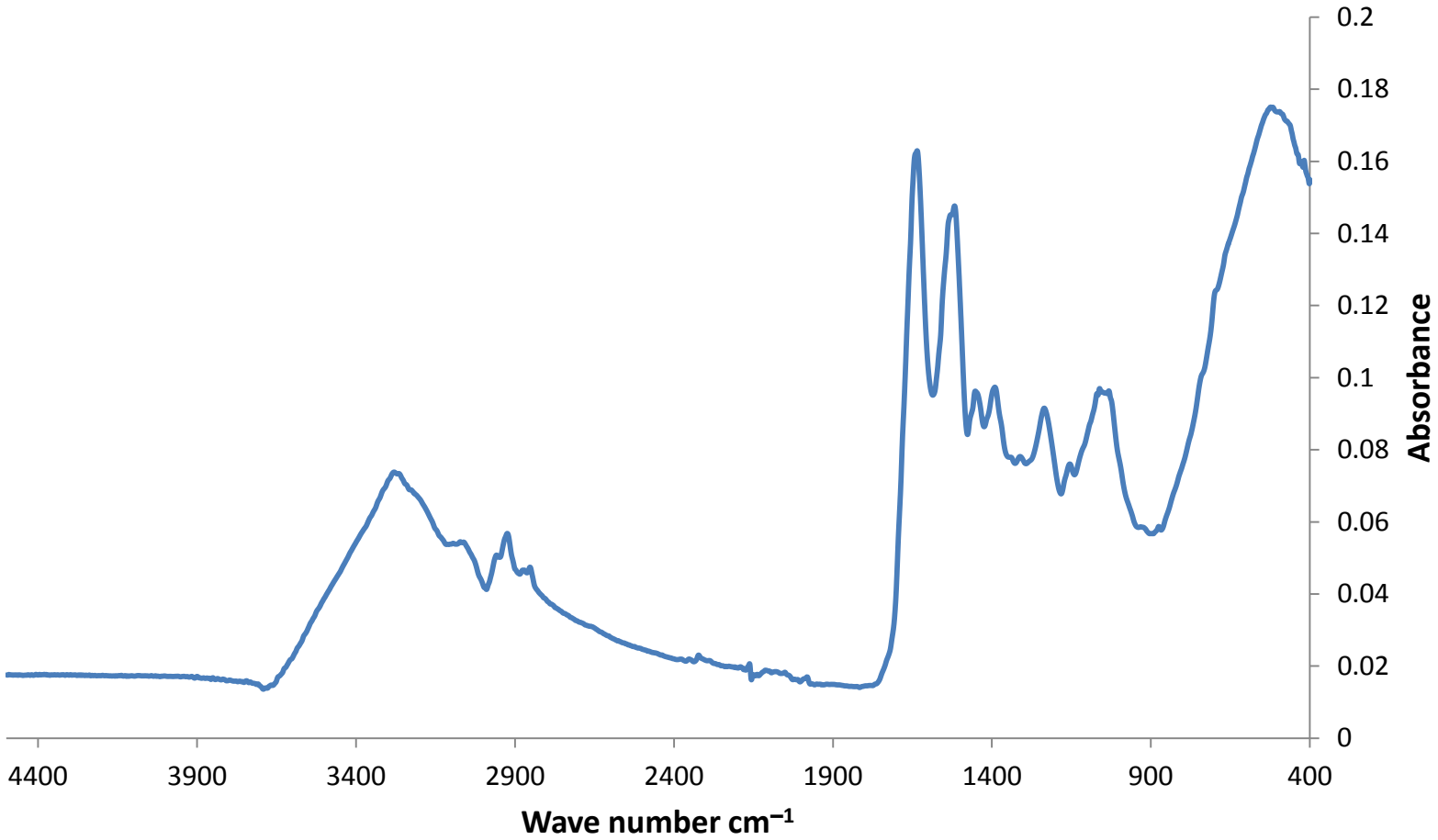

Figure 6.15 – FTIR spectrum of de-oiled *Nannochloropsis* biomass.

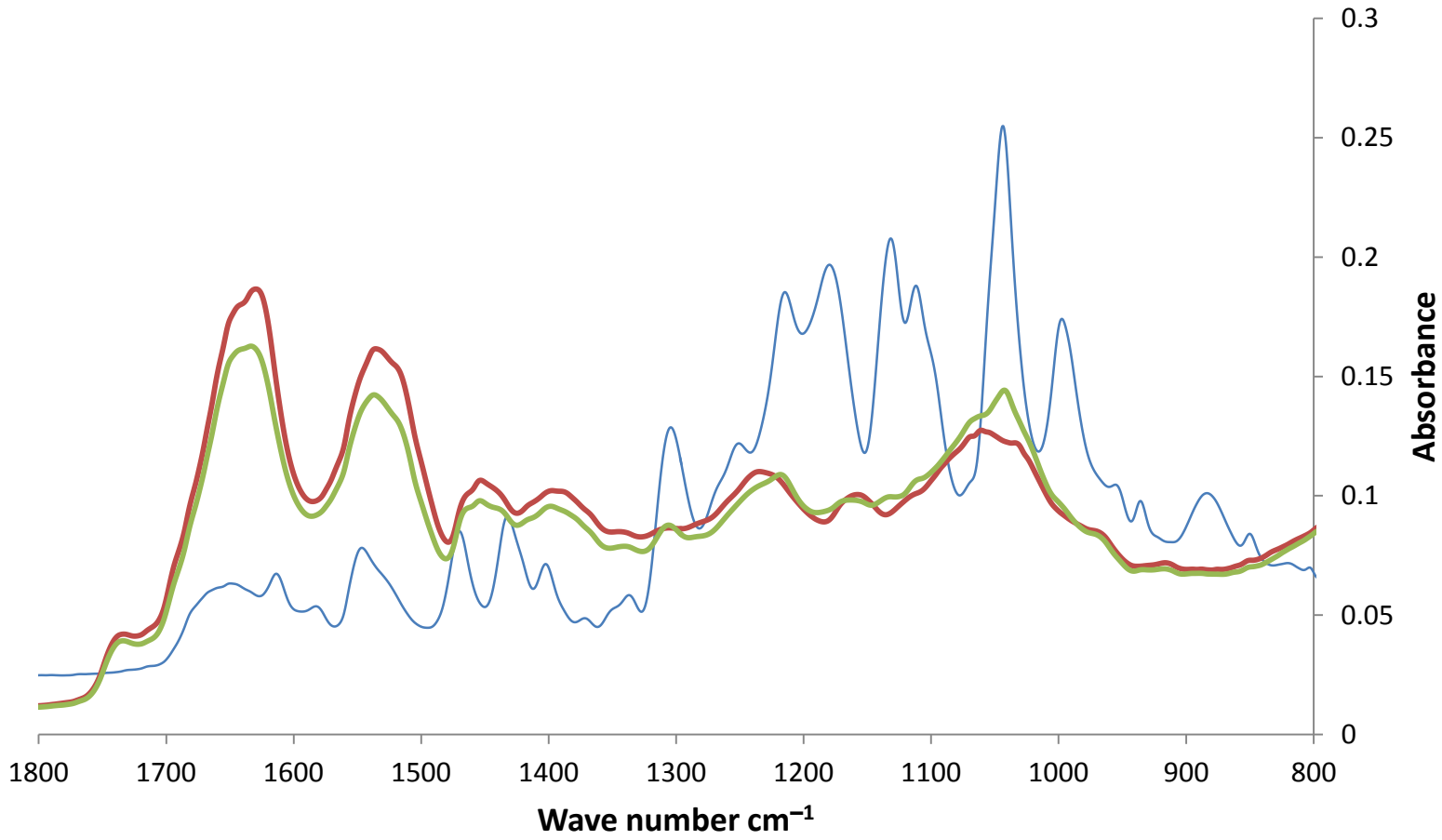

Figure 6.15 – FTIR spectrum of unextracted *Nannochloropsis* biomass before (red line) and after (green line) adsorption of RV5 (blue line).

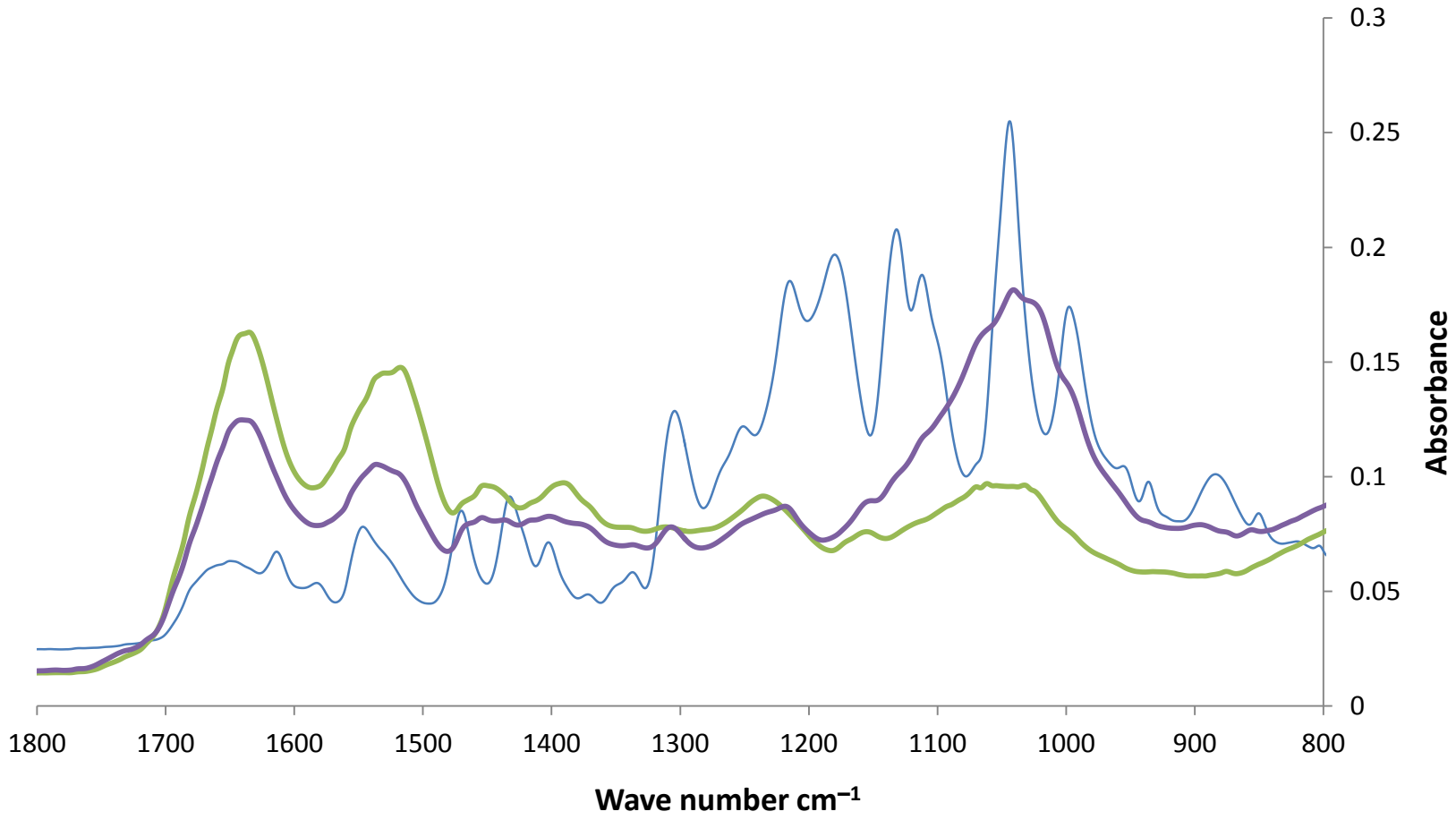

Figure 6.16 – FTIR spectrum of de-oiled *Nannochloropsis* biomass before (red line) and after (green line) adsorption of RV5 (blue line).

After adsorption, the change in intensity and/or shift of some bands and appearance of significant peaks are observed.
The decreasing intensity of peaks at 1,646 cm^{-1} (ν C=O), and 1,540 cm^{-1} (ν N-H/C-N) indicates that amide groups are the main responsible of the adsorption phenomena.
Similarly, the slight decrease in the intensity and shift of peaks at 1031 cm^{-1} (ν C-O) and 1158 cm^{-1} (asν C-O-C) show the co-participation of polysaccharide chains during adsorption.
The shifting of the peak at 1216 cm^{-1} and formation of a new peak at 1305 cm^{-1} in the spectra of microalgae are due to the presence of RV5, as it could be deduced from the dye spectrum.
In the spectrum of de-oiled biomass after adsorption, a strong change is visible in the region 950-1150 cm^{-1}. This could be also due to higher amount of dye adsorbed, as demonstrated by the higher value of q_{max} for de-oiled biomass than unextracted microalga.

6.7 SEM characterization

Figs. 6.18 and 6.19 elucidate the SEM images of *Nannochloropsis* sp. microalgae before and after the extraction of lipids with the solvent mixture.

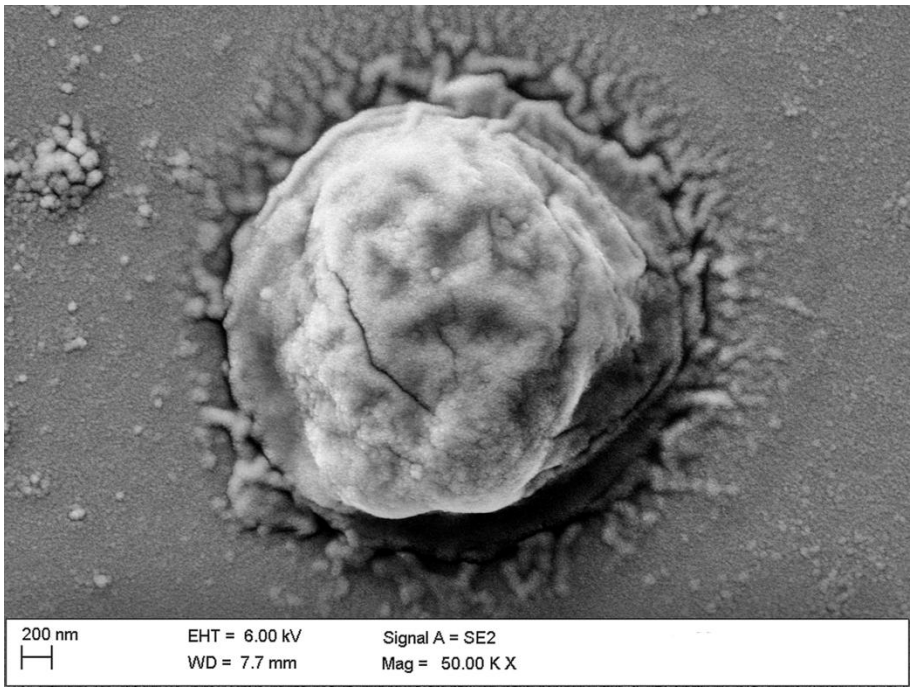

Figure 6.18 – SEM image of unextracted *Nannochloropsis* cell.

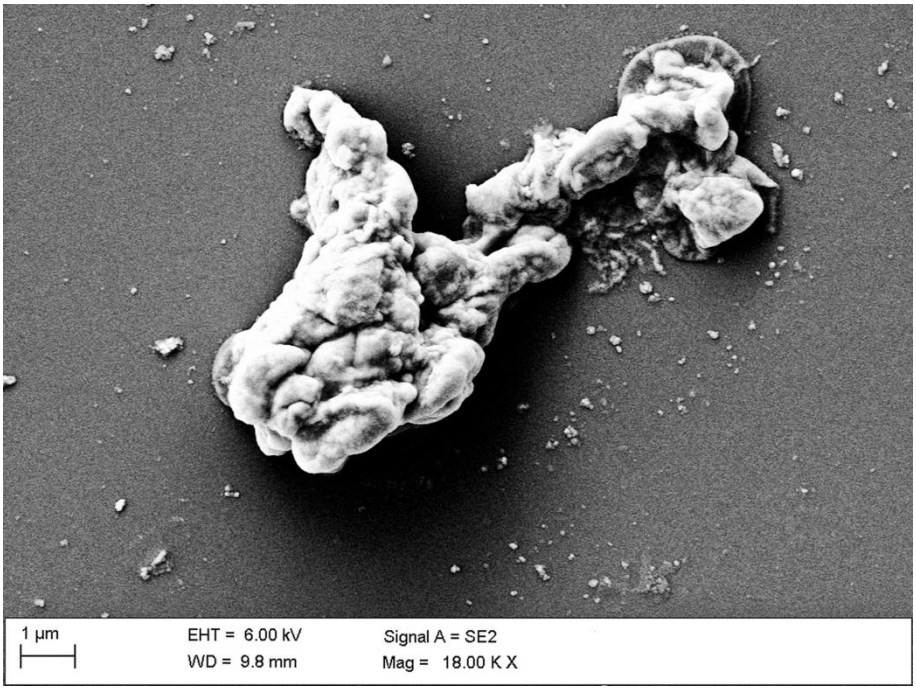

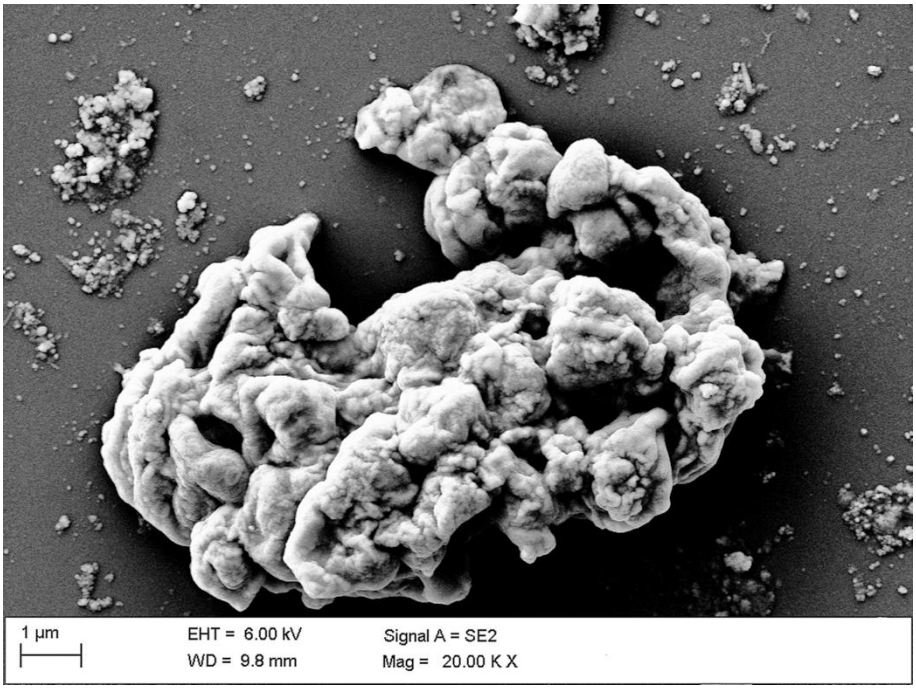

Figure 6.19 – SEM images of de-oiled *Nannochloropsis* cells

The figures clearly show morphological and microstructural differences of the surface. It can be observed that the surface of original cell is relatively smooth, while the residue after lipid extraction is corrugated with pores and cavities that increase the surface area of the biomass and, therefore, enhance its adsorption capacity.

6.8 Discussion of results

Azo-dyes, such as the RV5, are hard to biodegrade; furthermore they are synthetic and complex, since they have aromatic structures origins which make them particularly stable. In fact, they must have high resistance to physical and chemical agents as well as high resistance to coloring, light, perspiration, rubbing, stain removal with solvents and to all the processes of degradation. In the process of tissue staining at the industrial level, a large amount of wastewater is produced, which requires purification treatments (Cardoso et al., 2012). In fact, it is not possible to let these effluents enter into the environment, not only for the aesthetic factor of the coloring, but also because of the high amount of contaminants present in them. In addition, they have characteristics such as high temperatures, different pH values and high chemical oxygen demand (COD), which increase the threatening represented by these effluents for aquatic basins and life (Lim et al., 2010).
Currently, the adsorption is considered the fastest and most efficient way to reduce the concentration of dissolved dyes in the effluents. The most widely used adsorbent material is activated carbon although it is quite expensive and has high regeneration costs, once exhausted (Nautiyal et al., 2016). For this reason, in recent years researchers are attempting to find cheaper and widely available adsorbent materials. These must have high removal efficiency and should be economically advantageous. Byproducts or agroindustrial wastes are among this class of adsorbents, which have no cost, and do not require expensive preliminary treatments for their activation (Rafatullah et al., 2010). An alternative is represented by organic biomass such as bacteria, fungi or microalgae provide numerous advantages, including the fact that produce low quantities of waste and have low environmental impact (Zheng et al., 2016b). Although most of the studies were initially focused on the living biomass, the use of dead biomass or by-products from industrial processes offers exciting new possibilities for the control of pollutants, since such methods are considerably more effective and economic (Tsai et al., 2010).
Numerous studies have shown that microalgae have high potential for nitrogen, phosphorus, heavy metals and dyes removal from industrial waste water. For this reason, they have recently aroused a particular interest, as adsorption agents, for the treatment and purification of waste water. The greatest obstacle to their use is the current cost of production, calculated at around € 5 / kg of dry biomass. This cost is reduced at least 10 times for a use in the biofuel industry, while it is already compatible with the manufacturing of other products, such as food additives, molecules for the fine chemicals, proteins of pharmaceutical interest, animal vaccines.
Moreover, the microalgal biodiesel process would generate huge amounts of de-oiled microalgal biomass, if produced at an industrial scale. After oil extraction, the high cost of biodiesel can be suitably offset by the effective use of biomass residues in further energy recovery and other applications. Precisely to reduce costs, a series of studies have recently been carried out on the exhausted algal biomass, to try to find

a cost-effective use. This residual biomass after lipid extraction has been a subject of numerous studies for their utilization in various fields (Maurya et al., 2016).

Recently, studies focused on the use of such biomass as bio-adsorbent (Rashid et al., 2103). In fact, such material has special surface properties that make it more suitable than unextracted microalgae to adsorb compounds such as heavy metals and dyes, as demonstrated by results of this study. Equilibrium data showed, in fact, that the removal capacity of the de-oiled *Nannochloropsis* sp. microalgae is about 2.5 times higher than the unextracted one.
In literature, there are still few researches about these adsorbent materials, but there are some studies confirming similar results. Chandra et al. (2015) found that the *Scenedesmus dimorphus* after the extraction of lipids was a better adsorbent than the unextracted microalga, with a q_{max} value of 7.73 mg/g, compared to 6 mg/g of the unextracted biomass. Nautiyal et al. (2016) studied the production of biochar through pyrolysis of the microalgae *Spirulina platensis* after lipid extraction. During the experimentation they evaluated the properties of different adsorbents, such as activated carbon, biochar, unextracted and exhausted microalgae. After 30 minutes, the exhausted biomass removed the 73% of the dye, against the 68% removed by the unextracted biomass. Experiments on the adsorption of heavy metals by exhausted microalgae are more numerous. Xie et al. (2014) used *Chlorella vulgaris*, from which the lipids were extracted, for the removal of Cr (IV) from aqueous solutions. They found that the adsorbent capacity of this material is equal to 43.3 mg/g, against 34 mg/g of unextracted *Chlorella*. A further study on the use exhausted *Coelastrum* sp. as adsorbent of Cd reports a q_{max} value of 32.8 mg/g, higher than those obtained with other biosorbents, such as the green alga *Ulva lactuca* (29.2 mg/g), *Gelidium* (18 mg/g) or *Hypnea valentiae* (17 mg/g) seaweeds (Zheng et al., 2016).
An explanation to this phenomenon may be the increase in the surface area after the extraction of lipids. The SEM images, in fact, have shown that the surface of the de-oiled material turns out to be irregular and porous, increasing the possibility of the dye molecules to diffuse inside the structure and therefore to be adsorbed, as also found by Xie et al. (2014) with *Chlorella vulgaris*. Kim et al. (2011) found that the surface area of *Nannochloris oculata* cells significantly increased from 0.89 to 1.87 m^2/g after lipid extraction. This is an index of the potential increase in the adsorption capacity of the biomass.

For both unextracted and exhausted microalgae the removal efficiencies were higher at high temperatures. The adsorption is generally an exothermic phenomenon, but in the case of reactive dyes, the process is often characterized by a positive change of enthalpy. It results in a better dye removal as the temperature increases. This particular feature was also observed for other adsorbent-adsorbate systems, such as for the removal of Acid Green 25 of palm ash activated (Hameed et al., 2007). According to the authors, this may be a result of increase in the mobility of the dye with increasing temperatures. An increasing number of molecules may also acquire

sufficient energy to undergo an interaction with active sites at the surface. Furthermore, increasing temperatures may produce a swelling effect within the internal structure of the adsorbent, enabling dye to penetrate deeper.
Caner et al. (2009) studied the adsorption potential of dried anaerobic sludge for Burazol Blue ED. They found that the adsorption process was favored at higher temperatures. According to them, the increase in the uptake capacity with increasing temperature could be explained by the availability of more binding sites or due to the increasing number of molecules acquiring sufficient energy to undergo particles interactions. Tahir et al. (2017) evaluated the use of peanut waste and composites of polyaniline, starch, polypyrrole, chitosan aniline and chitosan pyrrole for the adsorption of Crystal Violet (CV) dye. They found a favorable effect of moderate temperature on dye adsorption. They attributed this phenomenon to the re-orientation of cell wall components of the adsorbents, to the ionization of chemical moieties on the cell wall, and to increased rate of adsorbate diffusion across the external boundary layer to the pores of the adsorbent particles since liquid viscosity decreases with temperature. However, this study showed that at higher temperature the adsorption was decreased and this decline in adsorption was correlated with damaging of active sites and with the softening of adsorptive forces between active binding sites of the adsorbent and the adsorbate species.
In according to the temperature effect, the analysis of the thermodynamic parameters showed that both the entropy and enthalpy were negative, the ladder confirmed the endothermic nature of the process. These values were determined from the intercept and the slope of the line determined plotting 1/T vs ln(k). The equilibrium constants at different temperatures for the two adsorbents were calculated from the isotherm that fitted better the experimental data.
For the unextracted microalgae, Temkin isotherm was the best model. According to Palamthodi and Lele (2014) this implies that the adsorption heat of all molecules drops linearly with the rise in the adsorbent surface occupancy and that the adsorption is characterized by a uniform distribution of binding energies until a threshold binding energy is achieved. Instead, for Langmuir model was the best for the exhausted microalgae, despite none of the tested models fitted well the experimental data, as demonstrated by the high values of the sum of the squares of the differences between the experimental points and those calculated by the isotherms.

Since the isotherm models used to describe the equilibrium data were non-linear, it was not possible to use the main kinetic models. In fact the ladders are valid when equilibrium isotherm is linear. However, this hypothesis is often far from the reality. Therefore, under the hypothesis that the diffusive transport in the adsorbent is the mass transfer controlling resistance, a dynamic, isothermal, dilute solution adsorption model, based on the linear driving force (LDF) approximation, was developed to describe the kinetic adsorption behavior.
The model fitted very well the experimental data for the unextracted microalgae, while the sum of the squares of the differences between the experimental points and

those calculated by the LDF model were significantly high for de-oiled biomass. This means that the assumptions made in the construction of the model were not valid for this adsorbent. In particular, as shown by SEM images, the hypothesis of spherical particles cannot be made. Another possible explanation is represented by the fact that the adsorption models did not fit well the experimental data, unlike results for the unextracted microalgae.

Conclusions

The work of this PhD thesis focused on the development of an innovative process of enzymatic pretreatment of microalgae cell wall, through unpurified and low cost commercial enzyme preparations, in order to lower the energy related to the extraction of lipids. Microalgal lipid-based biodiesel is still not competitive for its high cost. One of the main bottlenecks is related to the lipid extraction. The cell wall of microalgae is, in fact, well-structured and poorly permeable to solvents. The use of enzyme preparations able to hydrolyze the main components of this wall allowed an increased recovery of the lipids that are present inside the cell.

A literature review confirmed the limits of pre-treatment technologies currently in use and the benefits of the use of enzymes. Their specificity and the fact that the biomass is not subjected to mechanical, thermal or chemical stress can be expected to preserve the activity of easily degradable compounds, such as proteins and carotenoids, which are produced by microalgae and can be co-extracted with lipids. Therefore, the main objective of the study was to increase the extraction yields of lipids from microalgae with a mild method that does not damage lipids and other high added value potentially extractable compounds.

At first, a screening phase of enzyme preparations was done. The selection was made on the basis of the composition of the cell wall of *Nannochloropsis* sp, the microalga used in this work.

Then, the research activity focused on the development of an original method based on the use of multi-component mixtures containing preparations with different main enzymatic activities to induce the complete hydrolysis of the polysaccharides of the cell wall.

The results demonstrated that treating *Nannochloropsis* microalgae with optimized cell wall degrading enzyme mixtures, composed of cellulase and mannanase rich preparation, can significantly improve lipid recovery. Moreover, efficient enzyme cocktails were easily prepared using the *mixture design* methodology.

Subsequently, the study was addressed to the optimization of the enzyme-assisted extraction of lipids from *Nannochloropsis* sp. using the optimized multi-component mixture. A rigorous approach based on *factorial design* and response surface methodology was used to evaluate the effect of the main process variables on lipid recovery, including single enzyme dosages, temperature, pH and pretreatment time.
In particular, extraction yields close to 90% were obtained by a 3.5-h enzymatic treatment at 53 °C followed by a 4-h solvent extraction. The observed enhancement of extraction efficiency can be attributed to increased solvent accessibility to algal lipids resulting from the enzymatic degradation of cell wall components, which was also evidenced by TEM images.
Moreover, a numerical optimization was performed on the model derived from the central composite design by the gradient descent method, maximizing the extraction yield within the factorial region and minimizing the pretreatment cost.
The cost of the economical optimized mixture turned out to be 2.5 times lower than the mixture not optimized economically, with a slight reduction in the extraction yield (lower than 5%). Further reduction of the pre-treatment cost was obtained through the reuse of the multienzymatic mixture for more pre-treatment cycles.
The extraction yield remains high enough for a good number of cycles and decreases more or less linearly losing about 8 percentage points only after 14 reuse cycles.
A characterization of the untreated and enzymatically treated biomass was performed through the use of instrumental methods, such as Fourier transform infrared spectroscopy (FTIR), X-ray diffraction spectrometry (XRD), thermogravimetry (TGA/DTG) and scanning and transmission electron microscopy (SEM and TEM). *Nannochloropsis* sp. cells were treated with the preparations in cellulase and mannanase and with the optimized cocktail in order to understand the action of each enzyme and, consequently, to properly design the process.
Results revealed that after cellulase treatment there was a change in the relative amount of crystalline and amorphous cellulose, which can be explained by considering that the amorphous regions of cellulose are more susceptible to enzymatic attack. On the opposite, differences after treatment with mannanase were less significant, even if SEM images showed that GMA treated cells lost their regular structure. So, despite the changes on the wall structure and its crystallinity are minimal, the effect of GMA is decisive for breaking the bonds that hold together the entire structure of the membrane.
Finally, the exhausted algal biomass after lipid extraction process has been studied to assess its application as a low cost absorbent material for textile azo-dyes. Results showed that the removal capacity of de-oiled residue is about 2.5 times higher compared to unextracted *Nannochloropsis* sp. microalgae. In fact, SEM images have shown that the surface of the extracted material turns out to be irregular and porous, increasing the possibility of the dye molecules to diffuse inside the structure and to come therefore adsorbed. These results confirmed that the microalgal de-oiled residue is a good candidate for the removal of textile dyes. This application could allow a further decrease of the cost of the entire biodiesel production chain from microalgae.

References

Abo-Shady, Mohamed Y.A., Lasheen T., Chemical composition of the cell wall in some green algae species, Biologia Plantarum 35 (1993), 629–632.

Abraham R.E., Vongsvivut J., Barrow C.J., Puri M., Understanding physicochemical changes in pretreated and enzyme hydrolysed hemp (*Cannabis sativa*) biomass for biorefinery development, Biomass Conversion and Biorefinery 6 (2016), 127–138.

Al-Zuhair S., Ashraf S., Hisaindee S., Al Darmaki N., Battah S., Svistunenko D., Reeder B., Stanway G., Chaudhary A., Enzymatic pre–treatment of microalgae cells for enhanced extraction of proteins, Engineering in Life Sciences (2016), 1–11.

Amin S., Review on biofuel oil and gas production processes from microalgae, Energy Conversion Management 50 (2009), 1834–1840.

Arad S.M. and Levy-Ontman O., Red microalgal cell-wall polysaccharides: biotechnological aspects, Current Opinion in Biotechnology 21 (2010), 358–364.

Araujo G.S., Matosb L.J.B.L., Fernandes J.O., Cartaxo S.J.M., Gonçalves L.R.B., Fernandes F.A.N., Farias W.R.L., Extraction of lipids from microalgae by ultrasound application: Prospection of the optimal extraction method, Ultrasonics Sonochemistry 20 (2013), 95–98.

Baldan B., Andolfo P., Navazio L., Tolomio C., Mariani P., Cellulose in algal cell wall: an “in situ” localization, European Journal of Histochemistry 45 (2001), 51–56.

Bamdad F., Wu J., Chen L., Effects of enzymatic hydrolysis on molecular structure and antioxidant activity of barley hordein, Journal of Cereal Science 54 (2011), 20–28.

Banarra N.M., Pereira P.A., Batista I., Vilela M.H., Fatty acids, sterols and α–tocopherol in *Isochrysis galbana,* Journal of Food Lipids 10 Issue 1 (2003), 25–34.

Bar E., Rise M., Vishkautsan M., Arad S., Pigment and structural changes in *Chlorella zofingiensis* upon light and nitrogen stress, Journal of Plant Physiology 146 (1995), 527–534.

Barsanti L, Gualtieri P. Algae: anatomy, biochemistry and biotechnology, Taylors R. Francis Group, USA (2006), 301.

Barth A., Infrared spectroscopy of proteins, Biochimica et Biophysica Acta 1767 (2007), 1073–1101.

Biller P., Friedman C., Ross A.B., Hydrothermal microwave processing of microalgae as a pre–treatment and extraction technique for bio-fuels and bio-products, Bioresource Technology,136 (2013), 188–195.

Blokker P., Schouten S., Van Den Ende H., De Leeuw J.W., Hatcher P.G. Sinnighe Damasté J.S., Chemical structure of algaenans from the fresh water algae *Tetraedron minimum*, *Scenedesmus communis* and *Pediastrum boryanum*, Organic Geochemistry 29 (1998), 1453–1468.

Bondioli P., Della Bella L., Rivolta G., Chini Zittelli G., Bassi N., Rodolfi L., Oil production by the marine microalgae *Nannochloropsis* sp. F&M-M24 and *Tetraselmis suecica* F&M-M33, Bioresource Technology 114 (2012), 567–572.

Bozbas K., Biodiesel as an alternative motor fuel: production and policies in the European Union, Renewable and Sustainable Energy Review 12 (2008), 542–552.

Bradbury J., Docosahexaenoic Acid (DHA): an ancient nutrient for the modern human brain, Nutrients 3 (2011), 529–554.

Brennan L., Owende P., Biofuels from microalgae: a review of technologies for production, processing, and extractions of biofuels and co-products, Renewable and Sustainable Energy Reviews 14 (2009), 557–577.

Brown M.R., The amino-acid and sugar composition of 16 species of microalgae used in mariculture, Journal of Experimental Marine Biology and Ecology 145 (1991), 79–99.

Caner N., Kiran I., Ilhan S., Iscen C.F., Isotherm and kinetic studies of Burazol Blue ED dye biosorption by dried anaerobic sludge, Journal of Hazardous Materials 165 (2009), 279–284.

Cao Y., Tan H., Structural characterization of cellulose with enzymatic treatment, Journal of Molecular Structure 705 (2004), 189–193.

Carballo-Meilan A., Goodman A., Baron M., Gonzalez–Rodriguez J., A specific case in the classification of woods by FTIR and chemometrics: Discrimination of *Fagales* from *Malpighiales*, Cellulose 21 (2014), 261–273.

Cardoso N.F., Lima E.C., Royer B., Bach M.V., Dotto G.L., Pinto L.A.A., Calvete T., Comparison of *Spirulina platensis* microalgae and commercial activated carbon as

adsorbents for the removal of Reactive Red 120 dye from aqueous effluents, Journal of Hazardous Materials 241–242 (2012), 146–153.

Chandra T.S., Mudliar S.N., Vidyashankar S., Mukherji S., Sarada R., Krishnamurthi K., Chauhan V.S., Defatted algal biomass as a non-conventional low-cost adsorbent: Surface characterization and methylene blue adsorption characteristics, Bioresource Technology 184 (2015), 395–404.

Chang Y.T., Chen Y.S., Lin K.T., Lin I.F., Chen Y.F., Yen Y.–H., Liu B.L., Chang Y.N., Characteristics of galactomannanase for degrading konjac gel, Journal of Molecular Catalysis B: Enzymatic 43 (2006), 153–157.

Chen C.Y., Yeh K.L., Aisyah R., Lee D.J., Chang J.S., Cultivation, photobioreactor design and harvesting of microalgae for biodiesel production: A critical review, Bioresource Technology 102 (2011), 71–81.

Chen L., Li R., Ren X., Liu T., Improved aqueous extraction of microalgal lipid by combined enzymatic and thermal lysis from wet biomass of *Nannochloropsis oceanica*, Bioresource Technology 214 (2016), 138–143.

Cheng K., Winter W.T., Stipanovic A.J., A modulated-TGA approach to the kinetics of lignocellulosic biomass pyrolysis/combustion, Polymer Degradation and Stability 97 (2012), 1606–1615.

Cho H.S., Oh Y.K., Park S.C., Lee J.W., Park J.Y., Effects of enzymatic hydrolysis on lipid extraction from *Chlorella vulgaris*, Renewable Energy 54 (2013), 156–160.

Choi S.P., Nguyen M.T., Sim S.J., Enzymatic pretreatment of *Chlamydomonas reinhardtii* biomass for ethanol production, Bioresource Technology 101 (2010), 5330–5336.

Chojnacka K., Marquez–Rocha F.J., Kinetic and stoichiometric relationships of the energy and carbon metabolism in the culture of microalgae, Biotechnology 3 No.1 (2004), 21–34.

Christi Y., Biodiesel from microalgae, Biotechnology Advances 25 (2007), 294–306.

Chu W.L., Biotechnological applications of microalgae, International e–Journal of Science, Medicine & Education 6 Suppl 1 (2012), S24–S37.

Ciudad G., Rubilar O., Azócar L., Toro C., Cea M., Torres Á., Ribera A., Navia R., Performance of an enzymatic extract in *Botrycoccus braunii* cell wall disruption, Journal of Bioscience and Bioengineering 117 (2014), 75–80.

Cornell J.A., Experiments with mixtures: designs, models and the analysis of mixture data. 3rd edition, John Wiley & Sons, New York (2002).

Corteggiani Carpinelli E., Telatin A., Vitulo N., Forcato C., D'Angelo M., Schiavon R., Vezzi A., Giacometti G.M., Morosinotto T., Valle G., Chromosome scale genome

assembly and transcriptome profiling of *Nannochloropsis gaditana* in nitrogen depletion, Molecular Plant 7 No.2 (2014), 323–335.

Concas A., Pisu M., Cao G., Engineering aspects related to use of microalgae for biofuel production and CO_2 capture from flue gas, Current Environmental Issues and Challenges (2014) 73–81.

Cuellar-Bermudez S.P., Aguilar–Hernandez I., Cardenas-Chavez D.L., Ornelas-Soto N., Romero-Ogawa M.A., Parra-Saldivar R., Extraction and purification of high-value metabolites from microalgae: essential lipids, astaxanthin and phycobiliproteins, Microbial Biotechnology 8 No.2 (2015), 190–209.

Dean A.P., Sigee D.C., Estrada B., Pittman J.K., Using FTIR spectroscopy for rapid determination of lipid accumulation in response to nitrogen limitation in freshwater microalgae, Bioresource Technology 101 (2010), 4499–4507.

Del Carmen Rodriguez-Gacio M., Iglesias-Fernandez R., Carbonero P., Matilla A.J., Softening-up mannan-rich cell walls, Journal of Experimental Botany 63 No.11 (2012), 3975–3988.

Dickinson S., Mientus M., Frey D., Amini-Hajibashi A., Ozturk S., Shaikh F., Sengupta D., El-Halwagi M.M., A review of biodiesel production from microalgae, Cleaner Technology and Environmental Policy 18 (2016), 1–32.

Diniz P.H.D.G., Gomes A.A., Pistonesi M.F., Band B.S.F., de Araújo M.C.U., Simultaneous classification of teas according to their varieties and geographical origins by using NIR spectroscopy and SPA-LDA, Food Analytical Methods 7 (2014), 1712–18.

Dong T., Van Wychen S., Nagle N., Pienkos P.T., Laurens L.M.L., Impact of biochemical composition on susceptibility of algal biomass to acid-catalyzed pretreatment for sugar and lipid recovery, Algal Research 18 (2016), 69–77.

Doucha J. and Livansky K., Influence of processing parameters on disintegration of *Chlorella* cells in various types of homogenizers, Biotechnological Products and Process Engineering 81 (2008), 431–440.

Duygu D.Y., Udoh A.U., Ozer T.B., Akbulut A., Erkaya I.A., Yildiz K., Guler D., Fourier transform infrared (FTIR) spectroscopy for identification of *Chlorella vulgaris* Beijerinck 1890 and *Scenedesmus obliquus* (Turpin) Kützing 1833, African Journal of Biotechnology 11 (2012), 3817–3824.

El-Baky H.H.A., El-Baz F.K., El-Baroty G.S., *Spirulina* species as a source of carotenoids and α-tocopherol and its anticarcinoma factors, Biotechnology 2 (2003), 222–240.

El-Baz F.K., Abdoul-Enein A.M., El-Baroty G.S., Youssef A.M., El-Baky H.H.A., Accumulation of antioxidant vitamins in *Dunaliella salina*, Journal of Biological Science 2 (2002), 220–223.

Fabregas, J. and Herrero C.. Vitamin content of four marine microalgae. Potential use as source of vitamins in nutrition, Journal of Industrial Microbiology 5 No.4 (1990), 259–263.

Florentino de Souza Silva A.P., Carantino Costa M., Colzi Lopes A., Abdala Neto E.F., Carrhá Leitão R., Rossas Mota C., Bezerra dos Santos A., Comparison of pretreatment methods for total lipids extraction from mixed microalgae, Renewable Energy 63 (2013), 762–766.

Foston M. and Ragauskas A.J., Biomass characterization: Recent progress in understanding biomass recalcitrance, Industrial Biotechnology 8 No.4 (2012), 191–208.

Fu C.C., Hung T.C., Chen J.Y., Su C.H., Wu W.T., Hydrolysis of microalgae cell walls for production of reducing sugar and lipid extraction, Bioresource Technology 101 (2010), 8750–8754.

Galazka V.B., Sumner I.G., Ledward D.A., Changes in protein-protein and protein-polysaccharide interactions induced by high pressure, Food Chemistry 57 No.3 (1996), 393–398.

Gelin F, Volkman J.K., deLeeuw J.W., Damste J.S.S., Mid-chain hydroxy long-chain fatty acids in microalgae from the genus *Nannochloropsis*, Phytochemistry 45 (1997), 641–646.

Gerardo M.L., Van Den Hende S., Vervaeren H., Coward T., Skill S.C., Harvesting of microalgae within a biorefinery approach: A review of the developments and case studies from pilot-plants, Algal Research 11 (2015), 248–262.

Gerken H.G., Donohoe B., Knoshaug E.P., Enzymatic cell wall degradation of *Chlorella vulgaris* and other microalgae for biofuels production, Planta 237 (2013), 239–253.

Ghosh T., Paliwal C., Maurya R., Mishra S., Microalgal Rainbow Colours for Nutraceutical and Pharmaceutical Applications Plant Biology and Biotechnology: Volume I: Plant Diversity, Organization, Function and Improvement (2015), 777–791.

Ginzberg A., Cohen M., Sod–Moriah U.A., Shany S., Rosenshtrauch A., Arad S.M., Chickens fed with biomass of the red microalga *Porphyridium* sp. have reduced blood cholesterol level and modified fatty acid composition inbegg yolk, Journal of Applied Phycology 12 (2000), 325–330.

Goiris, K., Muylaert, K., Fraeye, I. Imogen Foubert, De Brabanter J., De Cooman L., Antioxidant potential of microalgae in relation to their phenolic and carotenoid content, Journal of Applied Phycology 24 (2012), 1477–1491.

González-Fernández C., Sialve B., Bernet N., Steyer J.P., Impact of microalgae characteristics on their conversion to biofuel Part II: Focus on biomethane production, Biofuels, Bioproducts and Biorefining 6 (2012), 205–218.

Graham L.E., Wilcox L.W., Algae, Prentice-Hall Inc., USA (2000).

Greenwell H. C., Laurens L.M.L., Shields R.J., Lovitt R.W., Flynn K.J., Placing microalgae on the biofuels priority list: a review of the technological challenges Journal of Royal Society Interface 7 (2010), 703–726.

Griffiths M.J., Harrison S.T.L., Lipid productivity as a key characteristic for choosing algal species for biodiesel production, Journal of Applied Phycologu 21 (2009), 493–507.

Halim R., Harun R., Danquah M.K., Webley P.A., Microalgal cell disruption for biofuel development, Applied Energy 91 (2012), 116–21.

Hameed B.H., Ahmad A.A., Aziz N., Isotherms, kinetics and thermodynamics of acid dye adsorption on activated palm ash, Chemical Engineering Journal 133 (2007), 195–203.

Hammed A.M., Jaswir I., Amid A., Alam Z., Asiyanbi H.T.T., Ramli N., Enzymatic hydrolysis of plants and algae for extraction of bioactive compounds, Food Reviews International 29 (2013), 352–370.

Harun R., Danquah M.K., Enzymatic hydrolysis of microalgal biomass for bioethanol production, Chemical Engineering Journal 168 (2011), 1079–1084.

He P.J., Lu F., Shao L.M., Pan X.J., Lee D.J., Enzymatic hydrolysis of polysaccharide-rich particulate organic waste, Biotechnology and Bioengineering, 20 No.93 (2006), 1145–1151.

Horst I., Parker B.M., Dennis J.S., Howe C.J., Scott S.A., Smith A.G., 2012. Treatment of *Phaeodactylum tricornutum* cells with papain facilitates lipid extraction, Journal of Biotechnology 162 (2012), 40–49.

Hu Q., Sommerfeld M., Jarvis E., Ghirardi M., Posewitz M., Seibert M., Darzins A., Microalgal triacylglycerols as feedstocks for biofuel production: perspectives and avances, The Plant Journal 54 (2008), 621–639.

Huo S., Wan Z., Cui F., Zou B., Zhao P., Yuan Z., Enzyme-assisted extraction of oil from wet microalgae *Scenedesmus* sp. G4, Energies 8 (2015), 8165–8174.

Huynh N.T., Smagghe G., Gonzales G.B., Van Camp J., Raes K., Enzyme-assisted extraction enhancing the phenolic release from cauliflower (*Brassica oleracea* L. var. botrytis) outer leaves, Journal of Agricultural Food Chemistry 62 (2014), 7468–7476.

Iwamoto H., Industrial production of microalgal cell-mass and secondary products-major industrial species *Chlorella*, Handbook of Microalgal Culture Biotechnology and Applied Phycology. Edited by Richmond A. Oxford: Blackwell Publishing Ltd (2004), 255–263.

Jiao J., Li Z.G., Gai Q.Y., Li X.J., Wei F.Y., Y.J., Ma W., Microwave-assisted aqueous enzymatic extraction of oil from pumpkin seeds and evaluation of its physicochemical properties, fatty acid compositions and antioxidant activities, Food Chemistry 147 (2014), 17–24.

REFERENCES

Kacurakova M., Capek P., Sasinkova V., Wellner N., Ebringerova A., FT-IR study of plant cell wall model compounds: pectic polysaccharides and hemicelluloses, Carbohydrate Polymers 43 (2000), 195–203.

Kapasakalidis P.G., Rastall R.A., Gordon M.H., Effect of a cellulase treatment on extraction of antioxidant phenols from black currant (*Ribes nigrum* L.) pomace, Journal of Agricultural Food Chemistry 57 (2009), 4342–4351.

Khan S.A., Rashmi, Algal Biorefinery: a Road towards Energy Independence and Sustainable Future, International Review of Chemical Engineering 2 N. 1 (2010), 63–68.

Kim U.J., Eom S.H., Wada M., Thermal decomposition of native cellulose: Influence on crystallite size, Polymer Degradation and Stability 95 (2010), 778–781.

Kim E.J., Park S., Hong H.J., Choi Y.E., Yang J.W., Biosorption of chromium (Cr(III)/Cr(VI)) on the residual microalga *Nannochloris oculata* after lipid extraction for biodiesel production, Bioresource Technology 102 (2011), 11155–11160.

Kim J., Yoo G., Lee H., Lim J., Kim K., Kim C.W., Methods of downstream processing for the production of biodiesel from microalgae, Biotechnology Advances 31 (2013), 862–876.

Kim K.H., Choi I.S., Kim H.M., Wi S.G., Bae H.J., Bioethanol production from the nutrient stress-induced microalga *Chlorella vulgaris* by enzymatic hydrolysis and immobilized yeast fermentation, Bioresource Technology 153 (2014), 47–54.

Kloareg B., Quatrano R.S., Structure of the cell walls of marine algae and ecophysiological functions of the matrix polysaccharides, Oceanography and Marine Biology, An Annual Review 26 (1988), 259–315.

Kruse O., Rupprecht J., Bader K.P., Thomas-Hall S., Schenk P.M., Finazzi G., Hankamer B., Improved photobiological H_2 production in engineered green algal cells Journal of Biological Chemistry 280 (2005), 34170–34177.

Kulshreshtha A., Zacharia A.J., Jarouliya U., Bhadauriya P., Prasad G.B.K.S., Bisen P.S., *Spirulina* in health care management, Current Pharmaceutical Biotechnology 9 (2008), 400–405.

Laothanachareon T., Bunterngsook B., Suwannarangsee S., Eurwilaichitr L., Champreda V., Synergistic action of recombinant accessory hemicellulolytic and pectinolytic enzymes to *Trichoderma reesei* cellulase on rice straw degradation, Bioresource Technology 198 (2015), 682–690.

Lavecchia R, Zuorro A., Improved lycopene extraction from tomato peels using cell–wall degrading enzymes. European Food Research Technology 228 (2008), 153–158.

Lavecchia R., Maffei G., Zuorro A., Evaluation of Dissolved Organic Carbon (DOC) as a measure of cell wall degradation during enzymatic treatment of microalgae, Chemical Engineering Transaction 49 (2016), 373–378.

Lee R.E., Phycology, Cambridge University Press, Cambridge, UK (2008).

Lee A.K., Lewis D.M., Ashman P.J., Disruption of microalgal cells for the extraction of lipids for biofuels: Processes and specific energy requirements, Biomass and Bioenergy 46 (2012), 89–101.

Lee J.L., Yoo C., Jun S.Y., Ahn C.Y., Oh, H.M., Comparison of several methods for effective lipid extraction from microalgae, Bioresource Technology 101 (2010), S75–S77.

Liang K., Zhang Q., Cong W., Enzyme-Assisted Aqueous Extraction of Lipid from Microalgae, Journal of Agrocultural and Food Chemistry 60 (2012), 11771–11776.

Lim S.L., Chu W.L., Phang S.M. , Use of *Chlorella vulgaris* for bioremediation of textile wastewater, Bioresource Technology 101 (2010), 7314–7322.

Liu J., Mukherjee J., Hawkes J.J., Wilkinson S.J., Optimization of lipid production for algal biodiesel in nitrogen stressed cells of *Dunaliella salina* using FTIR analysis, Journal of Chemical Technology and Biotechnology 88 (2013), 1807–1814.

Lourenço S.O., Barbarino E., Lavín P.L., Lanfer Marquez U.M., Aidar E., Distribution of intracellular nitrogen in marine microalgae: calculation of new nitrogen-toprotein conversion factors, European Journal of Phycology 39 (2004), 17–32.

Ma Y., Wang Z., Zhu M., Yu C., Cao Y., Zhang D., Zhou G., Increased lipid productivity and TAG content in *Nannochloropsis* by heavy-ion irradiation mutagenesis, Bioresource Technology 136 (2013), 360–367.

Maddi B., Viamajala S., Varanasi S., Comparative study of pyrolysis of algal biomass from natural lake blooms with lignocellulosic biomass, Bioresource Technology 102 (2011), 11018–11026.

Mahdy A., Mendez L., Ballesteros M., C. González-Fernández, Enhanced methane production of *Chlorella vulgaris* and *Chlamydomonas reinhardtii* by hydrolytic enzymes addition, Energy Conversion Management 85 (2014a), 551–557.

Mahdy A., Mendez L., Blanco S., Ballesteros M., González-Fernández C., Protease cell wall degradation of *Chlorella vulgaris*: effect on methane production, Bioresource Technology 171 (2014b), 421–427.

Marcilla A., Gómez–Siurana A., Gomis C., Chápuli E., Catalá M.C., Valdés F.J., Characterization of microalgal species through TGA/FTIR analysis: Application to *Nannochloropsis* sp., Thermochimica Acta 484 (2009), 41–47.

Mata T.M., Martins A.A., Caetano N.S., Microalgae for biodiesel production and other applications: A review, Renewable and Sustainable Energy Reviews 14 (2010), 217–232.

Maurya R., Paliwal C., Ghosh T., Pancha I., Chokshi K., Mitra M., Ghosh A., Mishra S., Applications of de-oiled microalgal biomass towards development of sustainable biorefinery, Bioresource Technology 214 (2016), 787–796.

Mayers J.J., Flynn K.J., Shields R.J., Rapid determination of bulk microalgal biochemical composition by Fourier–Transform Infrared spectroscopy, Bioresource Technology 148 (2013), 215–220.

McCann A., Benanti G., Knox J.P., Popper Z.A., The occurrence of arabinogalactan proteins in *Charophytes* (stoneworts), Plant Physiology 130 (2007), 125–131.

Mendes–Pinto M.M., Raposo M.F.J., Bowen J., Young A.J., Morais R., Evaluation of different cell disruption processes on encysted cells of *Haematococcus pluvialis*: effects on astaxanthin recovery and implications for bio–availability, Journal of Applied Phycology 13 (2001), 19–24.

Menetrez M.Y., An overview of algae biofuel production and potential environmental impact, Environmental Science and Technology 46 (2012), 7073–7085.

Meng Y., Yao C., Xue S., Yang H., Application of Fourier transform infrared (FT–IR) spectroscopy in determination of microalgal compositions, Bioresource Technology 151 (2014), 347–354.

Mereghetti P., Corsetto P.A., Cremona A., Rizzo A.M., Doglia S.M., Ami D., A Fourier transform infrared spectroscopy study of cell membrane domain modifications induced by docosahexaenoic acid, Biochimica et Biophysica Acta 1840 (2014), 3115–3122.

Minowa T., Yokoya S.Y., Kishimoto M., Okakura T., Oil production from algal cells of *Dunaliella tertiolecta* by direct thermochemical liquefaction, Fuel 74 No. 12 (1995) 1735–1738.

Miranda M.S., Cintra R.G., Barros S.B., Mancini-Filho, J., Antioxidant activity of the microalga *Spirulina maxima*, Brazilian Journal of Medical Biology Resources 31 (1998), 1075–1079.

Miranda J.R., Passarinho P.C., Gouveia L., Pre-treatment optimization of *Scenedesmus obliquus* microalga for bioethanol production, Bioresource Technology 104 (2012), 342–348.

Molina Grima E., Belarbi E.H., Acién Fernández F.G., Robles Medina A., Chisti Y., Recovery of microalgal biomass and metabolites: process options and economics, Biotechnology Advances, 20 (2003), 491–515.

Montgomery D.C., Design and analysis of experiments, 8th Ed., Wiley, New York, USA (2012).

Muñoz C., Hidalgo C., Zapata M., Jeison D., Riquelme C., Rivasa M., Use of cellulolytic marine bacteria for enzymatic pretreatment in microalgal biogas production, Applied and Environmental Microbiology 80 No.14 (2014), 4199–4206.

Na Y.S., Kim W.J., Kim S.M., Park J.K., Lee S.M., Kim S.O., Synytsya A., Park Y., Purification, characterization and immunostimulating activity of water-soluble polysaccharide isolated from *Capsosiphon fulvescens*, International Immunopharmacology 10 (2010), 364–370.

Nautiyal P., Subramanian K.A., Dastidar M.G., Adsorptive removal of dye using biochar derived from residual algae after in-situ transesterification: Alternate use of waste of biodiesel industry, Journal of Environmental Management 182 (2016), 187–197.

Ngarize S., Herman H., Adams A., Howell N., Comparison of changes in the secondary structure of unheated, heated, and high-pressure-treated β-lactoglobulin and ovalbumin proteins using Fourier Transform Raman Spectroscopy and self–deconvolution, Journal of Agriculture and Food Chemistry 52 (2004), 6470–6477.

Nishiyama Y., Structure and properties of the cellulose microfibril, Journal of Wood Science 55 (2009), 241–249.

Norsker M., Bloch L., Adler-Nissen J., Enzymatic degradation of plant cell wall polysaccharides: The kinetic effect of competitive adsorption, Nahrung 43 (1999), 307–310.

Palamthodi S. and Lele S.S., Optimization and evaluation of reactive dye adsorption on bottle gourd peel, Journal of Environmental Chemical Engineering 4 (2016), 4299–4309.

Park J.K., Kim Z–H., Lee C.G., Synytsya A., Jo H.S., Kim S.O., Park J.W., Park Y., Characterization and immunostimulating activity of a water-soluble polysaccharide isolated from *Haematococcus lacustris*, Biotechnology and Bioprocess Engineering 16 (2011), 1090–1098.

Patel A., Mishr S., Pawar R., Ghosh P.K., Purification and characterization of C-phycocyanin from cyanobacterial species of marine and freshwater habitat, Protein Expression and Purification 40 (2005), 248–255.

Peng W.M. and Wu X.Y., Effects of temperature and holding time on production of renewable fuels from pyrolysis of *Chlorella protothecoides*, Journal of Applied Phycology 12 (2000), 147–152.

Pereira S.C., Maehara L., Machado C.M.M., Farinas C.S., Physical-chemical-morphological characterization of the whole sugarcane lignocellulosic biomass used for 2G ethanol production by spectroscopy and microscopy techniques. Renewable Energy 87 (2016), 607–617.

Perin G., Segalla A., Basso S., Simionato D., Meneghesso A., Sforza E., Bertucco A., Morosinotto T., Biotechnological optimization of light use efficiency in *Nannochloropsis* cultures for biodiesel production, Chemical Engineering Transactions 37 (2014), 763–768.

Popper Z., Tuohy M.G., Beyond the Green: Understanding the evolutionary puzzle of plant and algal cell walls; Plant Physiology 153 (2010), 373–383.

Popper Z., Michel G., Hervé C., Domozych D.S., Willats W.G.T., Tuohy M.G., Kloareg B., Stengel D.B., Evolution and diversity of plant cell walls: from algae to flowering plants, Annual Review of Plant Biology 62 (2011), 567–90.

Popper Z.A., Ralet M.C., Domozych D.S., Plant and algal cell walls: diversity and functionality, Annals of Botany 114 (2014), 1043–1048.

Prabakaran P., Ravindran A.D., A comparative study on effective cell disruption methods for lipid extraction from microalgae, Letters in Applied Microbiology 53 (2011), 150–154.

Prajapati S.K., Bhattacharya A., Malik A., Vijay V.K., Pretreatment of algal biomass using fungal crude enzymes, Algal Research 8 (2015), 8–14.

Radakovits R., Jinkerson R.E., Fuerstenberg S.I., Tae H. Settlage R.E., Boore J.L., Posewitz M.C., Draft genome sequence and genetic transformation of the oleaginous alga *Nannochloropsis gaditana*, Nature Communications 3:686 (2014), 1–10.

Rafatullah M., Sulaiman O., Hashim R., Ahmad A., Adsorption of methylene blue on low-cost adsorbents: A review, Journal of Hazardous Materials 177 (2010), 70–80.

Ranjan C., Patil S., Moholkar V., Mechanistic assessment of microalgal lipid extraction, Industrial and Engineering Chemical Research 49 (2010), 2979–2985.

Raposo M.F., De Morais A.M.M.B., De Morais R.M.S.C., Carotenoids from Marine Microalgae: A Valuable Natural Source for the Prevention of Chronic Diseases, Marine Drugs 13 (2015), 5128–5155.

Rashid N., Saif Ur Rehman M., Han J.I., Recycling and reuse of spent microalgal biomass for sustainable biofuels , Biochemical Engineering Journal 75 (2013), 101–107.

Raveendran K., Ganesh A., Khilar K.C., Pyrolysis characteristics of biomass and biomass components, Fuels 75 (1996), 987–998.

Razeghifard R., Algal biofuels, Photosynthesis Research, 117 (2013), 207–219.

Rebolloso Fuentes M.M., Acién Fernández G.G., Sánchez Pérez J.A., Guil Guerrero J.L., Biomass nutrient profiles of the microalga Porphyridium cruentum, Food Chemistry 70 (2000), 345–353.

Ríos S.D., Torres C.M., Torras C., Salvadó J., Mateo-Sanz J.M., Jiménez L., Microalgae-based biodiesel: Economic analysis of downstream process realistic scenarios, Bioresource Technology 136 (2013), 617–625.

Safafar H., Van Wagenen J., Møller P., Jacobsen C., Carotenoids, phenolic compounds and tocopherols contribute to the antioxidative properties of some microalgae species grown on industrial wastewater, Marine Drugs 13 (2015), 7339–7356.

Safi C., Ursu A.V., Laroche C., Zebib B., Merah O., Pontalier P.Y., Vaca-Garcia C., Aqueous extraction of proteins from microalgae: Effect of different cell disruption methods, Algal Research 3 (2014), 61–65.

Salmon E., Behar F., Lorant F., Hatche P.G., Metzge P., Marquaire P.M., Thermal decomposition processes in algaenan of *Botryococcus braunii* race L. Part 1: Experimental data and structural evolution, Organic Geochemistry 40 (2009), 400–415.

Sarada R., Vidhyavathi R., Usha D., Ravishankar G.A., An efficient method for extraction of astaxanthin from green alga *Haematococcus pluvialis*, Journal of Agriculture and Food Chemistry 54 (2006), 7585–7588.

Sarrobert B, Dermoun D Extraction et valorisation de molecules à haute valeur ajoutée chez la microalgae *Porphyridium cruentum*, Biotechnologie des Microalgues et des Cyanobacteries Appliquée au Thermalisme (1991), 109–114.

Sathish A., Sims R.C., Biodiesel from mixed culture algae via a wet lipid extraction procedure, Bioresource Technology 118 (2012), 643–647.

Scheller H.V. and Ulvskov P., Hemicelluloses, Annual Review of Plant Biology 61 (2010), 263–89.

Schenk P.M., Thomas–Hall S.R., Stephens E., Marx U.C., Mussgnug J.H., Poster S., Kruse O., Hankamer B., Second generation biofuels: high-efficiency microalgae for biodiesel production Bioenergy Resource 1 No.1 (2008), 20–43.

Scholz M.J., Weiss T.L., Jinkerson R.E., Jing J., Roth R., Goodenough U., Posewitz C., Gerken H.G., Ultrastructure and composition of the *Nannochloropsis gaditana* cell wall, Eukaryotic Cell 13 (2014), 1450–1464.

Sheng J., Vannela R., Rittmann B.E., Evaluation of methods to extract and quantify lipids from *Synechocystis* PCC 6803, Bioresource Technology 102 (2011), 1697–1703.

Spiridon I., Teaca C.A., Bodirlau R., Structural changes evidenced by FT-IR spectroscopy in cellulosic materials after pre-treatment with ionic liquid and enzymatic hydrolysis, Bioresources 6 (2011), 400–413.

Steinbrenner J., Linden H., Regulation of two carotenoid biosynthesis genes coding for phytoene synthase and carotenoid hydrolase during stress-induced astaxanthin formation in the green alga *Haematococcus pluvialis*, Plant Physiology 125 (2001), 810–817.

Sukarni, Sudjito, Hamidi N., Yanuhar U., Wardana I. N.G., Potential and properties of marine microalgae *Nannochloropsis oculata* as biomass fuel feedstock, International Journal of Energy and Environmental Engineering 5 (2014), 279–290.

Surendhiran D. and Vijay M., Effect of various pretreatment for extracting intracellular lipid from *Nannochloropsis oculata* under nitrogen replete and depleted conditions, Hindawi Publishing Corporation ISRN Chemical Engineering 2014 (2014), 1–9.

Taher H., Al-Zuhair S., Al-Marzouqi A.H., Haik Y., Farid M., Effective extraction of microalgae lipids from wet biomass for biodiesel production, Biomass and Bioenergy 66 (2014), 159–167.

Tahir N., Bhatti H.N., Iqbal M., Noreen S., Biopolymers composites with peanut hull waste biomass and application for Crystal Violet adsorption, International Journal of Biological Macromolecules 94 (2017), 210–220.

Tomaselli L., The microalgal cell, Handbook of Microalgal Culture: Biotechnology and Applied Phycology, Chapter 1 (2004), 3–19.

Tran N.H., Barlett J.R., Kannangara G.S.K., Milev A.S., Volk H., Wilson M.A., Catalytic upgrading of biorefinery oil from micro–algae, Fuel 89 (2010), 265–274.

Tsai W.T., Chen H.R., Kuo K.C., Surface characterization of dead microalgae–based biomass usingmethylene blue adsorption, Surface and Interface Analysis 43 No.6 (2011), 959–963.

Vanegas C.H., Hernon A., Bartlett J., Enzymatic and organic acid pretreatment of seaweed: effect on reducing sugars production and on biogas inhibition, International Journal of Ambient Energy 36 (2015), 2–7.

Varfolomeev S.D. and Wasserman L.A., Microalgae as Source of Biofuel, Food, Fodder, and Medicines, Applied Biochemistry and Microbiology 47 No. 9 (2011) 789–807.

Vieler A., Wu G., Tsai C.H., Bullard B., Cornish A.J., Harvey C., et al. Genome, functional gene annotation, and nuclear transformation of the heterokont oleaginous alga *Nannochloropsis oceanica* CCMP1779, PLoS Genetics 8 (2012), 1–25.

Vílchez C Forján E., Cuaresma M., Bédmar F., Garbayo I., Vega J. M., Marine Carotenoids: Biological Functions and Commercial Applications, Marine Drugs 9 (2011), 319–333.

Volkman J.K., Brown M.R., Dunstan G.A., Jeffrey S.W., The biochemical composition of marine microalgae from the class *Eustigmatophyceae,* Journal of Phycology 29 (1993), 69–78.

Wang S., Jiang X.M., Wang N., Yu L.J., Li Z., He P.M., Research on pyrolysis characteristics of seaweed, Energy & Fuels 21 (2007), 3723–3729.

Wang G. and Wang T., Lipid and biomass distribution and recovery from two microalgae by aqueous and alcohol processing, Journal of American Oil Chemists' Society 89 (2012), 335–345.

Wang M., Liu K., Dai L., Zhang J., Fang X., The structural and biochemical basis for cellulose biodegradation, Journal of Chemical Technology and Biotechnology 88 (2013) 491–500.

Wang D., Li Y., Hu X., Su W., Zhong M., Combined enzymatic and mechanical cell disruption and lipid extraction of green alga *Neochloris oleoabundans*, International Journal of Molecular Science 16 (2015), 7707–7722.

Wang H.M.D., Chen C.C., Huynh P., Chang J.S., Exploring the potential of using algae in cosmetics, Bioresource Technology 184 (2015), 355–362.

Wu C., Xiao Y., Lin W., Li J., Zhang S., Zhu J., Rong J., Aqueous enzymatic process for cell wall degradation and lipid extraction from *Nannochloropsis* sp., Bioresource Technology 223 (2017), 312–316.

Xie Y. , Li H., Wang X., Ng I.S., Lu Y., Jing K., Kinetic simulating of Cr(VI) removal by the waste *Chlorella vulgaris* biomass, Journal of the Taiwan Institute of Chemical Engineers 45 (2014), 1773–1782.

Xu H., Miao X.L., Wu Q.Y., High quality biodiesel production from a microalga *Chlorella protothecoides* by heterotrophic growth in fermenters, Journal of Biotechnology 126 (2006), 499–507.

Yang H., Yan R., Chen H., Lee D.H., Zheng C., Characteristics of hemicellulose, cellulose and lignin pyrolysis, Fuel 86 (2007) 1781–1788.

Yang B., Dai Z., Ding S.Y., Wyman C.E., Enzymatic hydrolysis of cellulosic biomass, Biofuels 2 (2011), 421–450.

Yap B.H.J., Crawford S.A., Dumsday G.J., Scales P.J., Martin G.J.O., A mechanistic study of algal cell disruption and its effect on lipid recovery by solvent extraction, Algal Research 5 (2014), 112–120.

Yin X., You Q., Jiang Z., Optimization of enzyme assisted extraction of polysaccharides from *Tricholoma matsutake* by response surface methodology, Carbohydrate Polymers 86 (2011), 1358–1364.

Yoo G., Park W.K., Kim C.W., Choi Y.E., Yang J.W., Direct lipid extraction from wet *Chlamydomonas reinhardtii* biomass using osmotic shock, Bioresource Technology 123 (2012), 717–722.

Yun Y.M., Kim D.H., Oh Y.K., Shin H.S., Jung K.W., Application of a novel enzymatic pretreatment using crude hydrolytic extracellular enzyme solution to microalgal biomass for dark fermentative hydrogen production, Bioresource Technology 159 (2014), 365–372.

Zamora O. and Richmond A., Microalgae production for aquaculture, Handbook of Microalgal Culture Biotechnology and Applied Phycology, Edited by Richmond A. Oxford: Blackwell Publishing Ltd (2004), 365–379.

Zhao X., Zhang L., Liu D., Biomass recalcitrance. Part I: the chemical compositions and physical structures affecting the enzymatic hydrolysis, Biofuels Bioproducts and Biorefinery 6 (2012), 465–482.

Zheng H., Yin J., Gao Z., Huang H., Ji X., Dou C., Disruption of *Chlorella vulgaris* cells for the release of biodiesel-producing lipids: a comparison of grinding, ultrasonication, bead milling, enzymatic lysis, and microwaves, Applied Biochemistry and Biotechnology 164 (2011), 1215–1224.

Zheng Y., Xiao R., Roberts M., Polymer-enhanced enzymatic microalgal cell disruption for lipid and sugar recovery, Algal Research 14 (2016), 100–108.

REFERENCES

Zheng H., Guo W., Li S., Wu Q., Yin R., Feng X., Du J., Ren N., Chang J.S., Biosorption of cadmium by a lipid extraction residue of lipid-rich microalgae, RSC Advances 6 (2016b), 20051–20057.

Zuorro A., Sviluppo di un processo innovativo per la valorizzazione dei residui solidi dell'industria di trasformazione del pomodoro, PhD Thesis, Sapienza University, Roma, Italy, 2009.

Zuorro A., Lavecchia R., Maffei G., Marra F., Miglietta S., Petrangeli A., Familiari G., Valente T., Enhanced lipid extraction from unbroken microalgal cells using enzymes, Chemical Engineering Transaction 43 (2015), 211–216.

Zuorro A., Maffei G., Lavecchia R., Optimization of enzyme-assisted lipid extraction from *Nannochloropsis* microalgae, Journal of the Taiwan Institute of Chemical Engineers 67 (2016), 106–114.